SANDIA REPORT
SAND2020-1030
Printed January 2020

Sandia National Laboratories

Scan of an Unpublished Report: "Fission Product Behavior During Severe LWR Accidents: Recommendations for the MELCOR Code System"

D.A. Powers, J.L. Sprung (Ed.), and C.D. Leigh

Prepared by
Sandia National Laboratories
Albuquerque, New Mexico
87185 and Livermore,
California 94550

Issued by Sandia National Laboratories, operated for the United States Department of Energy by National Technology & Engineering Solutions of Sandia, LLC.

Available to DOE and DOE contractors from
U.S. Department of Energy
Office of Scientific and Technical Information
P.O. Box 62
Oak Ridge, TN 37831

Telephone: (865) 576-8401
Facsimile: (865) 576-5728
E-Mail: reports@osti.gov
Online ordering: http://www.osti.gov/scitech

Available to the public from
U.S. Department of Commerce
National Technical Information Service
5301 Shawnee Rd
Alexandria, VA 22312

Telephone: (800) 553-6847
Facsimile: (703) 605-6900
E-Mail: orders@ntis.gov
Online order: https://classic.ntis.gov/help/order-methods/

ABSTRACT

This document provides a scanned version of a 1987 SAND report that was never formally published. However, this report was referenced within the MELCOR Reference Manual and, therefore, provides historical information and technical basis for the MELCOR code. This document is being made available to permit users of the MELCOR code access to the information. The title page has been edited to prevent any confusion with regards to the possible documentation identifiers, such as the SAND report number or the intended date of publication. Beyond these modifications, a cover, distribution, and back cover are prepended and appended to the document to conform to modern SAND report style guidelines.

The first four chapters of this report were updated and released under the title "Fission Product Behavior During Severe LWR Accidents: Recommendations for the MELCOR Code System. Volume I" and were made available by the U.S. NRC through the Adams database under accession number ML19227A327. No prior release of the remaining content of this report has occurred.

This page left blank.

FISSION PRODUCT BEHAVIOR DURING SEVERE LWR ACCIDENTS: RECOMMENDATIONS FOR THE MELCOR CODE SYSTEM

D. A. Powers, J. L. Sprung (Ed.), and C. D. Leigh

Sandia National Laboratories
Albuquerque, NM 87185
Operated by
Sandia Corporation
for the
U. S. Department of Energy

Prepared for
Division of Reactor System Safety
Office of Nuclear Regulatory Research
U. S. Nuclear Regulatory Commission
Washington, DC 20555
Under Memorandum of Understanding DOE 40-550-75
NRC FIN No. A-1339

ABSTRACT

TABLE OF CONTENTS

TABLE OF CONTENTS (cont.)

TABLE OF CONTENTS (cont.)

TABLE OF CONTENTS (cont.)

TABLE OF CONTENTS (cont.)

TABLE OF CONTENTS (cont.)

LIST OF ILLUSTRATIONS

LIST OF ILLUSTRATIONS

LIST OF ILLUSTRATIONS

LIST OF ILLUSTRATIONS

LIST OF TABLES

LIST OF TABLES

LIST OF TABLES

Acknowledgments

Executive Summary

CHAPTER 1

INTRODUCTION

J. L. Sprung

Probabilistic Risk Assessment. The probabilistic assessment of the risks of severe core damage accidents at a nuclear power plant is called a PRA. A PRA analysis identifies and delineates those combinations of events which, if they occur, can lead to a core melt accident, and estimates the frequency of occurrence of each such combination of events and of the consequences of each event combination.

The first two nuclear reactor PRAs, those for the Surry and Peach Bottom nuclear power plants, were performed as a part of the Reactor Safety Study [1] using analytical methods which were later implemented in the computer codes, MARCH [2], CORRAL [3], and CRAC [4]. During the last decade user experience and peer reviews have identified serious deficiencies in this series of PRA codes including: (1) inadequate or inconsistent treatments of important phenomena or plant features, (2) coding that does not easily permit the uncertainties associated with predictions obtained using these codes to be estimated, (3) code structures that do not facilitate incorporation of alternative or improved phenomenological representations, (4) interfaces that are poorly matched, and (5) poor documentation.

To overcome these deficiencies the Nuclear Regulatory Commission (NRC) initiated in 1982 a major multi-year program called MELCOR that has as its objective the development of a new system of risk assessment codes, the MELCOR Code System, which (1) models appropriately all phenomena essential to the description of severe Light Water Reactor (LWR) accidents, (2) provides credible predictions of the consequences of severe accidents, (3) permits meaningful estimates of the uncertainties associated with those predictions to be made, and (4) has a structure that facilitates the incorporation of new or alternative phenomenological models.

Architecture of the MELCOR Code System. The MELCOR code system will be structured, modular, integrated (matched interfaces), and portable (coded in ANSI FORTRAN 77). Discrete phenomena or groups of of closely coupled phenomena will be coded in separate modules. This will facilitate modification or replacement of phenomenological representations. Modules will be variably dimensioned, which will allow system nodalization (compartmentalization) and the size of sets of ordinary differential equations (ODEs) to be easily changed. Because all parameter values will be externally accessible, sensitivity and uncertainty studies will be relatively convenient to perform withthe MELCOR code system (at least by comparison to other PRA codes).

The MELCOR code system will have four structural levels: Level 1, executive control; Level 2, data management; Level 3, phenomenological representations; and Level 4, numerical implementations. Levels 3 and 4 are likely to be closely coupled. Ex-plant consequences (i.e., health effects and economic consequences) will be solved wholly separately from in-plant thermal-hydraulic processes and fission product behavior, which will be closely coupled but solved separately. For each time step, the solution for the thermal-hydraulic equations will be developed simultaneously for all control volumes (~15 for the reactor coolant system, ~10 for the containment building, ~1 for the auxiliary building). Then, using the thermal-hydraulic solution as input, the fission product behavior equations will be solved, one control volume at a time. Where necessary, the solution for fission product behavior from the previous time step will be used to support solution of the thermal-hydraulic equations during the current time step.

Phenomenological Assessments. In order to identify those phenomena essential to the description of severe LWR accidents (i.e., the set of phenomena that should be treated by the MELCOR Code System), a series of phenomenological reviews have been performed as part of (or in support of) the MELCOR Program. Reviews of thermal-hydraulic processes [5, 6] and ex-plant consequence phenomena [7-10] are reported elsewhere. This report presents the results of the review of fission product behavior conducted as a part of the MELCOR Program.

Fission Product Behavior. During the analysis of hypothetical severe accidents at Light Water Reactors , Fission Product Behavior is modeled in order to develop realistic source terms as a starting point for the prediction of the ex-plant consequences of the accident. The essential features of an ex-plant source term are the masses and identities of the radioisotopes released from the failed LWR containment, their chemical and physical forms, and the heat and moisture content and release time and duration of the plume that contains them.

Specification of the masses, identities, and forms of the radioisotopes released to the environment upon containment failure requires (1) calculation of the rates of release of radioactive materials from overheated or molten fuel, (2) specification of the chemical and physical forms of the released radioactive materials (e.g., CsI vapor, aerosol of a given chemical composition), (3) calculation of their rates of transport through and deposition and resuspension within the primary system and the containment, and (4) specification of changes in their chemical and physical forms during transport, deposition, or resuspension. Accordingly, this report will discuss the

processes (agglomeration, deposition, resuspension), species (vapors, aerosols), and physical states (gas borne, deposited or condensed on surfaces, suspended or dissolved in water), that must be treated in order to develop source terms adequate for the calculation of ex-plant consequences. Determination of the heat and moisture content and the release time and duration of the radioactive plume will not be discussed, since these quantities are generally not calculated by the fission product behavior portions of severe accident risk analysis codes.

Processes. Review of pertinent literature including documentation for published fission product behavior codes suggests that the processes listed in Table 1 should be treated by the fission product behavior modules of the MELCOR code system. When a process listed in Table 1 can take place by different mechanisms, Table 1 also lists those mechanisms that make significant contributions to its rate. This review concluded that adequate mathematical representations are available for each mechanism and process that should be treated by the MELCOR code system.

Species and States. Because the rate of change with time of the mass of a species (vapor or aerosol) in a state (location within a control volume) can be appropriately represented by an ordinary differential equation comprised of terms which give the contribution of individual rate processes to the total rate of change of the species, the MELCOR fission product behavior equations will consist of a set of ordinary differential equations. Since a separate ODE is required to describe each species in each state in which it can exist, detailed descriptions of fission product behavior (descriptions that involve many species and many states) can easily produce fission product behavior ODE sets that are very large (~500 ODEs). Since routine MELCOR calculations probably will be unacceptably slow if the fission product ODE set can not be held to something like 50 ODEs, this report will also present the technical basis for adequately modeling fission product behavior using a number of species and states that produces an ODE set of approximately 50 ODEs (as few as 25 for scoping calculations; as many as 100 for sensitivity calculations).

Report Organization. Reduction of the size of the MELCOR fission product ODE set to a computationally tractable size, by limiting the number of species and states modeled by the MELCOR code system, is examined in Chapters 2 and 7 of this report. Chapters 3 through 6 review the rate processes that significantly influence fission product behavior and recommend a representation for each process.

TABLE 1 : FISSION PRODUCT PROCESSES

Species	Process
Fission Product Vapors	Chemical Reactions
	Gas Phase (gas borne)
	Solution Phase (dissolved in water)
	Solid Phase (on surfaces)
	Condensation on Aerosols and Surfaces
	Brownian Diffusion
	Turbulent Diffusion
	Evaporation from Aerosols and Surfaces
	Release from Fuel
	Intercompartment Flow
	Removal by Engineered Safety Features
	Sprays
	Ice Condensers
	Suppressions Pools
	Filters
	Fans
	Decay Heat
Aerosols	Agglomeration
	Brownian Coagulation
	Turbulent Coagulation
	Gravitational Coagulation
	Deposition on Surfaces (walls, equipment)
	Brownian Diffusion
	Turbulent Diffusion
	Gravitational Settling
	Thermophoresis
	Diffusiophoresis
	Resuspension from Surfaces
	Release from Fuel
	Intercompartment Flow
	Removal by Engineered Safety Features
	Sprays
	Ice Condensers
	Suppression Pools
	Filters
	Fans
	Decay Heat
Steam	Condensation on Aerosols
	Evaporation from Aerosols

Chapter 2 begins with an examination of radioactive decay and isotope effects, then develops the case for reducing the number of species modeled by neglecting isotope effects and grouping chemical elements into classes, and finally recommends a set of element classes for use in the modeling of in- and ex-vessel release processes. In-vessel release processes are then discussed in Chapter 3 and ex-vessel processes in Chapter 4. Chemical reactions of vapors and natural vapor deposition processes, and natural deposition processes for aerosols and aerosol agglomeration mechanisms are reviewed in chapter 5. Removal of gas borne species by Engineered Safety Features (ESFs) is discussed in Chapter 6. Chapter 7 examines methods for modeling aerosol agglomeration and recommends a method for use in the MELCOR code system, discusses the number of aerosol species required by the recommended agglomeration method, and then presents the technical basis for reduction of the fission product behavior ODE set to a tractable size by limiting the number of states modeled and by further reduction of the number of species modeled by combination of the chemical classes developed in Chapter 2 into components.

REFERENCES

1. U. S. Nuclear Regulatory Commission, Reactor Safety Study - An Assessment of Accident Risks in U.S. Commercial Nuclear Power Plants, WASH-1400 (NUREG-75/014), October 1975.

2. R. O. Wooton and H. I. Avci, MARCH (Meltdown Accident Response Characteristics) Code Description and User's Manual, BMI-2064 NUREG/CR-1711 Battelle Columbus Laboratories, Columbus, OH, October, 1980.

3. P. C. Owzarski and A. K. Postma, CORRAL Code User's Guide Addendum to Appendix J of Appendix VII of the Reactor Safety Study - An Assessment of Accident Risks in U. S. Commercial Nuclear Power Plants, WASH-1400 (NUREG-75/014), October 1975.

4. L. T. Ritchie, J. D. Johnson, and R. M. Blond, Calculations of Reactor Accident Consequences, Version 2 (CRAC2): Computer Code User's Guide, NUREG/CR-2326, SAND81-1994, Sandia National Laboratories, Albuquerque, NM, February 1983.

5. G. G. Weigand et al., Thermal-Hydraulic Process Modeling in Risk Analysis: An Assessment of the Relevant Systems, Structures, and Phenomena, NUREG/CR-3986, SAND-1219, Sandia National Laboratories, Albuquerque, NM, August 1984.

6. S. R. Greene, Realistic Simulation of Severe Accidents in BWRs -- Computer Modeling Requirements, NUREG/CR-2940, ORNL/TM-8517, Oak Ridge National Laboratories, Oak Ridge, TN, April 1984.

7. R. M. Ostmeyer and J. C. Helton, Exposure Pathways Models for Accidental Radiological Releases, Sandia National Laboratories, Albuquerque, NM (in preparation).

8. G. E. Runkle et al., An Assessment of Dosimetry Data for Accidental Radionuclide Releases, Sandia National Laboratories, Albuquerque, NM (in preparation).

9. D. W. Moeller et al., Improved Radiological Health Effect Model, Sandia National Laboratories, Albuquerque, NM (in preparation).

10. R. P. Burke et al., Economic Risks of Nuclear Power Reactor Accidents, NUREG/CR-3673, Sandia National Laboratories, Albuquerque, NM, April 1984.

CHAPTER 2

ISOTOPES, ELEMENTS, AND CHEMICAL CLASSES

D. A. Powers

2.1. An Introductory Description of Severe Accident Source Terms and This Document

Severe accidents at commercial nuclear power plants would involve damage to the reactor fuel, emissions of radioactivity, and general plant conditions more drastic than those considered in the design and safety analysis of the plants. Great interest has developed in severe reactor accidents since the publication of the Reactor Safety Study [1] and the mild, but still beyond-design-basis, accident at the Three Mile Island Generating Station [2]. The interest arises because there is the possibility the severe reactor accidents could lead to the uncontrolled release of radioactivity from a nuclear power plant which would have life-threatening consequences and produce long-term property damage. Because of this possibility, severe reactor accidents make the largest contribution to the risk that must be associated with the use of nuclear power [3].

Accidents of sufficient severity to produce dire consequences have never occurred in U.S. commercial nuclear power plants. The progression and consequences of these accidents can only be estimated in analytic studies.

Analytic studies of severe reactor accidents consist of several key elements:

1. The probability that a severe reactor accident might be initiated is estimated.

2. The phenomena that arise in a severe accident are described and calculations made to determine if and when uncontrolled release of radioactivity will occur.

3. The amount of radioactive material that might escape the plant is calculated.

4. The consequences of exposing people and property to the radioactivity expelled from the plant is estimated.

The lack of experience with severe reactor accidents has made exercises of this type difficult and the results uncertain. Strong biases have been built into the analytic studies so that any errors in the analyses will accrue toward overpredicting the severity of accidents that go beyond the design basis of the plants.

Past analyses of severe accidents have come under substantial criticism because of feelings that the conservatism of the analyses to error on the side of overpredicting accident severity has been carried too far. There is a perception that modern nuclear power plants may be better able to cope with even the severest accidents than has been admitted in the past. The relatively inconsequential events associated with the accident at Three Mile Island Unit #2 have bolstered the confidence that natural processes have been neglected which will substantially reduce the amount of radioactive material inflicted on the environment, even if accident phenomena lead to containment failure.

The assessments of accident phenomena and the estimates of radioactivity release are the elements of severe accident analyses that appear to embody the greatest conservatism that can be removed by further, more careful study. The further studies of these elements may allow engineering bounds on the calculations to be replaced by realistic evaluations based on mechanistic, physical processes. Many research programs are now underway to provide the greater understanding of severe accident phenomena and the behavior of radioactivity necessary to conduct more realistic analyses.

This document addresses the subject of radioactivity behavior during severe accidents. Analysis of the behavior of radioactive materials during severe accidents begins by dividing the behavior into several elements:

1. Release of radioactive material from the reactor fuel so it can be transported.

2. Transport of the radioactive material to locations where it can escape the confines of a reactor plant.

3. Behavior of the radioactive material while it awaits development of a pathway out of the plant or the chance to follow such a pathway.

The first of these elements of severe accident analysis, release of radioactive materials from the reactor fuel, can be further classified in terms of (a) release from fuel within the reactor vessel, and (b) release from fuel that has escaped the reactor vessel. The processes that lead to "in-vessel" and "ex-vessel" release are discussed in Chapters III and IV of this document.

Before delving into the release and transport processes, it is useful to establish what materials are released and how much of each material might be present during a reactor accident. Establishing the inventories of materials that might be released in a reactor accident is the first objective of this chapter. It is found that there are many radionuclides whose release ought

to be of interest. Further, nonradioactive species from structural materials, control rods, fuel cladding, and the like may be vaporized during an accident. Since vapors of these nonradioactive species should affect behavior of the radionuclides, their release, too, is of interest. Quite clearly, the number of releasable materials that could be of interest gets quite large. Tracking the behavior of all these materials could strain the capacity of even the largest computer models. Consequently, definition of a basis for categorizing and simplifying the materials released during a severe accident is a second objective of this chapter.

2.2 Definitions of Radioactive Materials

Radioactive materials are produced by a variety of processes during normal operations of nuclear power plants:

A. Fission

Unstable nuclei can spontaneously fragment to produce, usually, two daughter isotopes that may also have unstable nuclei. Some important isotopes and their half-lives for spontaneous fissioning are:

Isotope	Half-Life for Spontaneous Fissioning*
$^{236}_{92}U$	73.6 y
$^{238}_{92}U$	8×10^{15} y
$^{240}_{94}Pu$	1.2×10^{11} y
$^{244}_{96}Cm$	1.4×10^{7} y
$^{252}_{98}Cf$	66 y
$^{256}_{100}Fm$	2.4 h

* Abbreviations used in this report in connection with half-lives are: year = y; days = d;, hours = h; minutes = m; seconds = s

Far more important than spontaneous fissioning is the fissioning of unstable nuclei brought on by neutron bombardment. Fissile nuclei in commercial light water reactors are:

$$^{235}_{92}U,\ ^{239}_{94}Pu,\ ^{241}_{94}Pu,\ \text{and}\ ^{233}_{92}U$$

Normally, fissioning of a nucleus is thought to be a "binary" process that produces two daughter nuclei. But, once in about 200-500 normal, binary, fission events a third particle is formed [6-8]. More rarely, four or more nuclei are formed during fissioning. Alpha particles are the most common additional nuclei formed in higher order fission processes. But, other nuclei can be formed. Comparitive yields (normalized to the ^{4}He yield set equal to 100) of nuclei for higher order fissioning of ^{252}Cf are listed below [8]:

^{1}H	1.1
^{2}H	0.63
^{3}H	6.42
^{3}He	0.008
^{4}He	100
^{6}He	1.95
^{8}He	0.06
Li	0.126
Be	0.156

Ternary fissioning is such a rare event it is normally neglected. But, it is obvious ternary fissioning can be a source of tritium.

Products of fissioning are not simply described. These products will be discussed in the section below dealing with inventories.

B. BETA DECAY

The nuclei produced by fissioning are typically quite unstable and radioactively decay. The most important decay process involves emission of an electron ($^{0}_{-1}e \equiv \beta^{-}$), a neutrino.

and often a gamma ray.This is called beta decay and it results in increasing the atomic number of the decaying isotope by one, with no change in the mass number. Some of the important decay chains initiated by nuclear fissioning in light water reactor fuels are shown in Figure 2.1. Beta decay chains initiated by processes other than fissioning are shown in Figure 2.2. Note that naturally occurring isotopes can undergo beta decay. Some of these processes are listed in Figure 2.2.

C. OTHER DECAY PROCESSES

Other nuclear decay reactions are (a) emission of a gamma ray (γ), (b) emission of a positron ($\beta+$) and an antineutrino, and (c) emission of an alpha particle ($\alpha = {}^{4}_{2}He$). Four decay chains of importance to light water reactor safety are shown in Figures 2.3-2.6. These are the (a) uranium decay chain, (b) the thorium decay chain, (c) the actinide decay chain, and (d) the synthetic neptunium decay chain.

Decay processes of various natures are continually being discovered. For instance, in 1983 a two proton decay reaction was first discovered [4]:

$$ {}^{22}_{13}Al \xrightarrow[\beta+]{} {}^{22}_{12}Mg \xrightarrow[2p]{} {}^{20}_{10}Ne $$

D. NEUTRON CAPTURE

Absorption of a neutron does not necessarily lead to fissioning of a nucleus. The unstable isotope created by absorption of a neutron can instead decay by other processes.

Within light water reactor fuel, neutron capture is responsible for formation of transuranic elements. Some example reactions and the decay processes set off by these reactions are:

$$ {}^{239}_{94}Pu + n \rightarrow {}^{240}_{94}Pu + \gamma $$

$$ {}^{238}_{92}U + n \rightarrow {}^{239}_{92}U + \gamma $$

$$ {}^{240}_{94}Pu + n \rightarrow {}^{241}_{94}Pu + \gamma \xrightarrow{\beta-} {}^{241}_{95}Am $$

$$ {}^{241}_{95}Am + n \rightarrow {}^{242}_{95}Am + \gamma \xrightarrow{\beta-} {}^{242}_{96}Cm $$

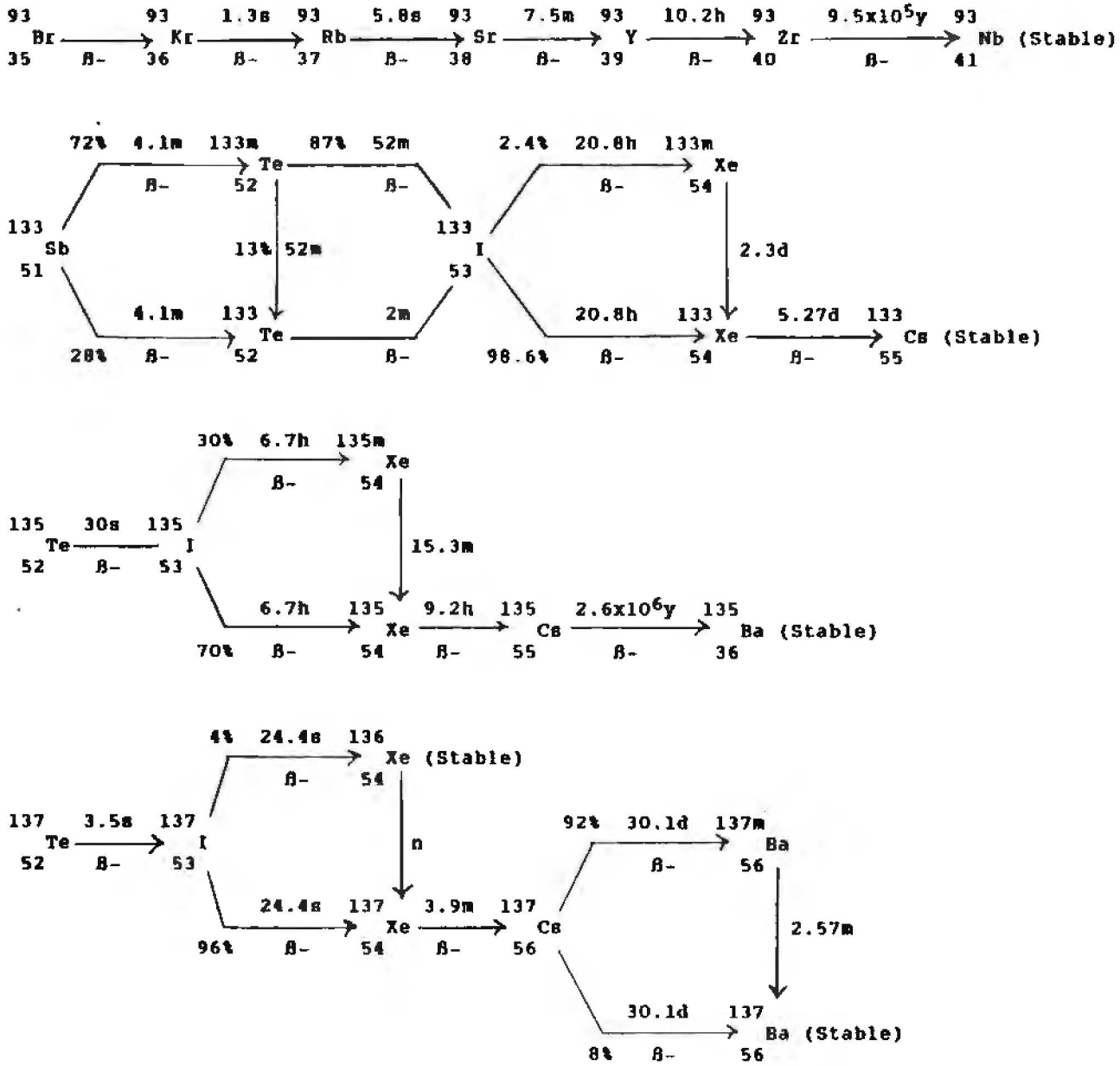

Figure 1. Some Important Beta Decay Reactions (Half-Lives Indicated Above Arrows to Products)

A. Neutron Capture Initiation

$$^{239}_{92}U \xrightarrow[\beta-]{23m} {}^{239}_{93}Np \xrightarrow[\beta-]{2.3d} {}^{239}_{94}Pu$$

$$^{241}_{94}Pu \xrightarrow[\beta-]{15y} {}^{241}_{95}Am$$

$$^{242}_{95}Am \xrightarrow[\beta-]{} {}^{242}_{96}Cm$$

$$^{234}_{90}Th \xrightarrow[\beta-]{24d} {}^{234}_{91}Pa \xrightarrow[\beta-]{1.1m} {}^{234}_{92}U$$

$$^{94}_{40}Zr \xrightarrow{n} {}^{95}_{40}Zr \xrightarrow[\beta-]{65d} {}^{95}_{41}Nb \xrightarrow[\beta-]{35d} {}^{95}_{42}Mo \text{ (Stable)}$$

B. Naturally Occurring Isotopes

$$^{14}_{6}C \xrightarrow[\beta-]{5770y} {}^{14}_{7}N \text{ (Stable)}$$

$$^{40}_{19}K \text{ (nat'l. abund. = 0.0118\%)} \xrightarrow[\beta-]{1.3\times10^{9}y} {}^{40}_{20}Ca \text{ (Stable)}$$

$$^{48}_{2}Ca \text{ (nat'l. abund. = 0.18\%)} \xrightarrow[\beta-]{2\times10^{16}y} {}^{48}_{21}Sc \xrightarrow[\beta-]{41h} {}^{48}_{22}Ti \text{ (Stable)}$$

$$^{87}_{37}Rb \text{ (nat'l. abund. = 27.85\%)} \xrightarrow[\beta-]{4.7\times10^{10}y} {}^{87}_{38}Sr \text{ (Stable)}$$

Figure 2. Beta Decay Chains Initiated by Processes Other Than Fissioning

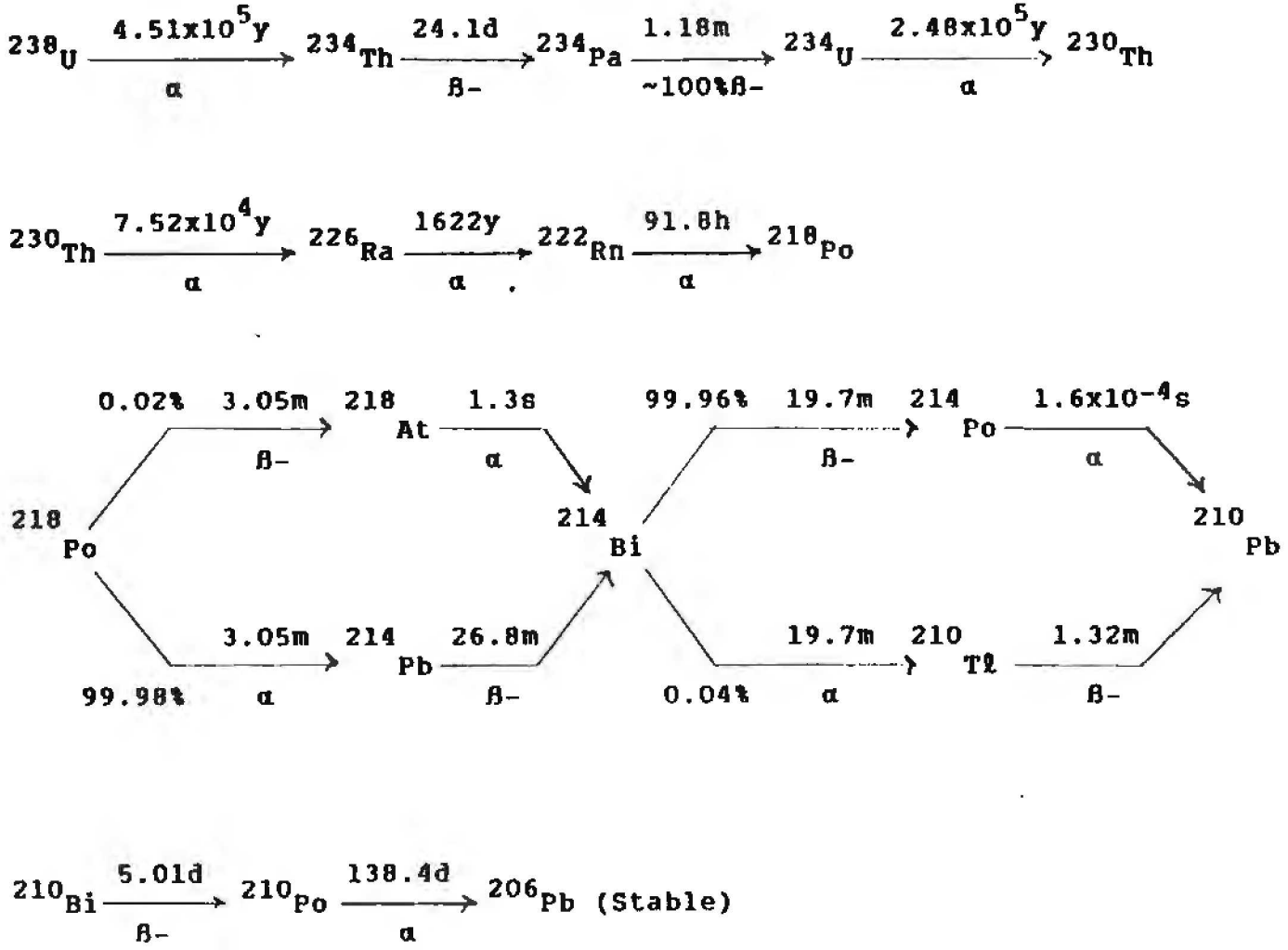

Figure 3. The Uranium Decay Series

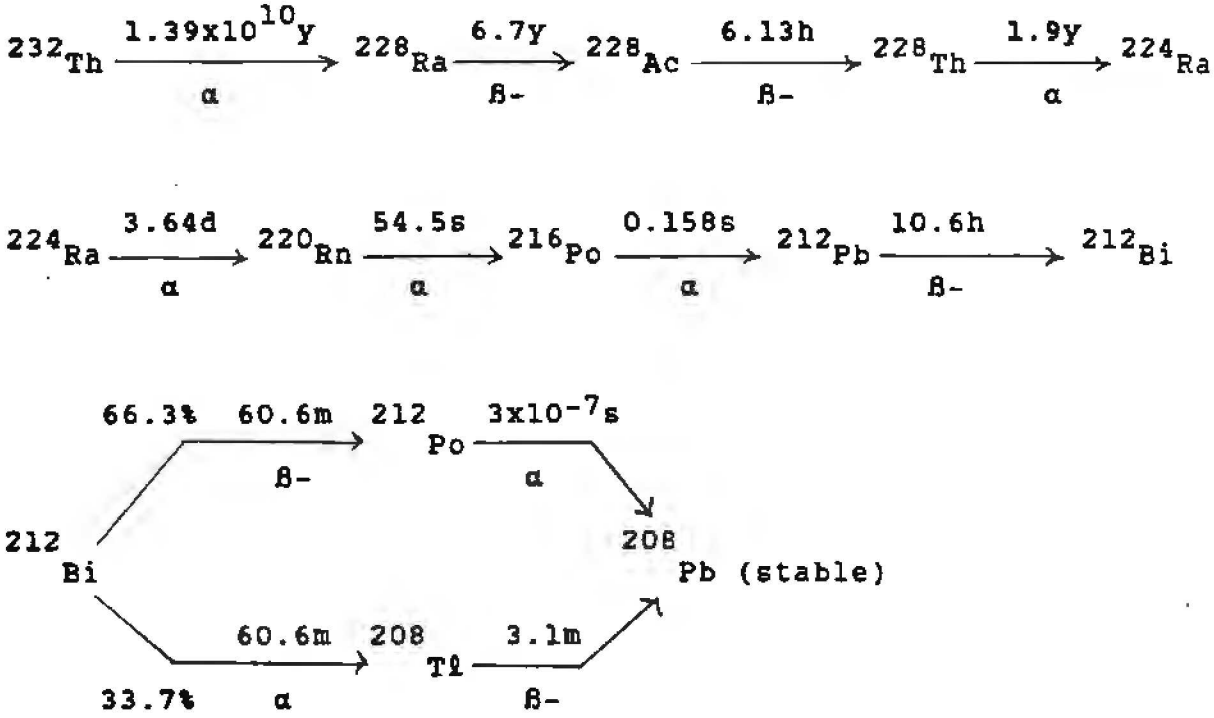

Figure 4. The Thorium Decay Series

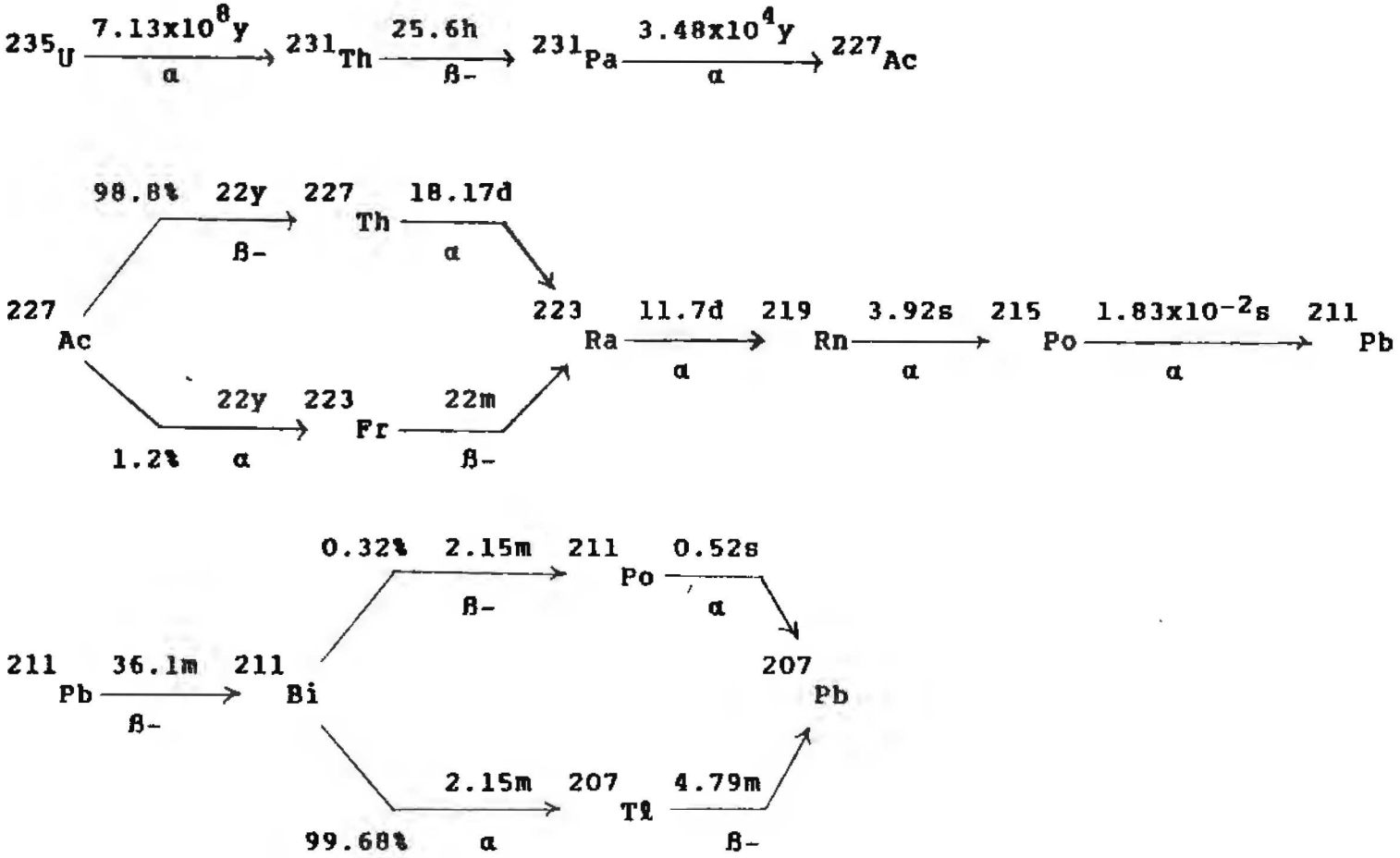

Figure 5. The Actinium Decay Series

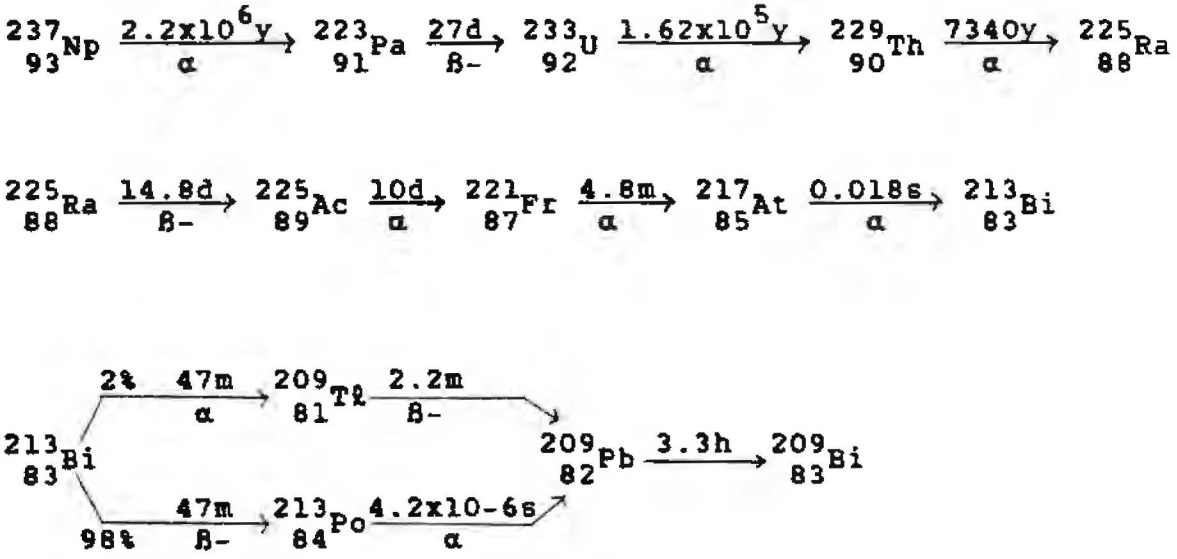

Figure 6. Neptunium Decay Chain

Neutron capture is responsible for making structural materials in a reactor radioactive. The ability of structural materials to capture a neutron depends on the "neutron capture cross section" of isotopes in the material. These cross sections depend on the energy of the neutron. For light water reactors, so-called thermal neutrons--energies on the order of kT, where k is the Boltzman constant and T is the absolute temperature--are of greatest interest. Thermal neutron capture cross sections for isotopes of structural materials in light water reactors are listed in Table 2.1.

Absorption of neutrons by structural elements can produce unstable nuclei. Some of the radioactive products of neutron capture by structural materials are also shown in Table 1 along with the half-lives and decay processes of these product isotopes.

Generation of radioactive species in structures by neutron capture is probably not important for severe accident analyses. At shutdown radioactive species in structures in a PWR core with a fuel burnup of 33,500 MWd/ton will decay at a rate of about 3×10^7 curies. Fission products and actinides in the fuel will decay at a rate of about 2×10^{10} curies.

Most of the radioactivity of structures comes from the isotopes [5]:

^{51}Cr	19% of curies at shutdown
^{56}Mn	39% of curies at shutdown
^{55}Fe	4% of curies at shutdown
^{60m}Co	12% of curies at shutdown
^{95}Zr	9% of curies at shutdown
^{95}Nb	8% of curies at shutdown
^{117m}Sn	5% of curies at shutdown

Activation products produced in some types of concrete that could be of interest are $^{63}Ni(t_{1/2} = 100y)$, $^{54}Mn(t_{1/2} = 0.85y)$, $^{152}Eu(t_{1/2} = 13y)$, $^{41}Ca(t_{1/2} = 10^5y)$, $^{39}Ar(t_{1/2} = 270y)$, and $^{14}C(t_{1/2} = 5700Y)$.

E. OTHER CAPTURE REACTIONS

Besides neutrons, capture of alpha particles and electrons can produce new unstable isotopes. Some example reactions are:

$$^{238}_{92}U + \alpha \rightarrow {}^{241}_{94}Pu + n$$

$$^{239}_{94}Pu + \alpha \rightarrow {}^{242}_{96}Cm + n$$

$$^{195}_{79}Au + {}^{0}_{-}e \rightarrow {}^{195}_{78}Pt$$

Precisely speaking, the term fission product should be reserved for the daughter isotopes produced during fissioning and possibly the isotopes produced by the beta decay chains initiated by the fissioning. Here, however, the term "fission product" will be used to mean any radioactive material, regardless of how or where it was produced.

2.3. Inventories

A. Radioactive Materials

The first step in estimating the release of fission products is to determine the inventory of fission products available for release. It will be shown in later sections that inventory does, in fact, affect the release rate. Fortunately, calculation of the fission product inventory has become a well-developed technology.

If fissioning of the ^{235}U isotope were a homolytic process, the nuclear reaction would be

$$^{235}_{92}U + n \rightarrow 2\ {}^{118}_{46}Pd$$

Rather than yielding two palladium isotopes, the ^{235}U fissioning yields a wide variety of isotopes. The probability that fissioning will yield a particular isotope is bimodally distributed with repect to the atomic mass number of the isotope. Peaks in the distribution occur for atomic mass numbers of 137 and 97. The distribution does depend slightly on the energy of the neutrons causing the fissioning. The fissioning yields for ^{235}U subjected to thermal neutrons are plotted against the mass number of the product isotope in Figure 2.7.

Fission yield also depends on the fissile isotope. The fission yields for ^{235}U and ^{239}Pu are compared in Table 2.2. Entries in the table are the probabilities in percent that fission will yield the indicated material. Since each fission

Table 1

Thermal Neutron Capture Cross Sections for Elements Found in Reactor Structures

Isotope	Natural Abundance (%)	Cross Section* (Barns)	Product Isotope	Half-Life	Decay Process
^{50}V	0.24	~200	^{51}V		
^{51}V	99.76	4.5	^{52}V	3.77m	ß-
^{50}Cr	4.31	17	^{51}Cr	27.8d	ß-
^{52}Cr	83.76	0.8	^{53}Cr		
^{53}Cr	9.55	18	^{54}Cr		
^{54}Cr	2.38	0.38	^{55}Cr	3.5m	ß-
^{55}Mn	100	13.3	^{56}Mn	2.58h	ß-
^{54}Fe	5.82	2.5	^{55}Fe	2.7y	Electron capture
^{56}Fe	91.66	2.7	^{57}Fe		
^{57}Fe	2.19	2.5	^{58}Fe		
^{58}Fe	0.33	1.0	^{59}Fe	45d	ß-
^{59}Co	100	18	^{60}Co	5.27y	ß-, γ
^{58}Ni	67.88	4.4	^{59}Ni	$8x10^{4}y$	Electron capture
^{60}Ni	26.23	2.6	^{61}Ni		
^{61}Ni	1.19	2	^{62}Ni		
^{62}Ni	3.66	15	^{63}Ni	92y	ß-
^{64}Ni	1.08	1.6	^{65}Ni	2.56h	ß-, γ
^{107}Ag	51.82	40	^{108}Ag	2.4m	ß-, Electron capture
^{109}Ag	48.18	84	^{110}Ag	249d	ß-
^{110}Cd	12.39	0.2	^{111m}Cd	49m	γ
^{111}Cd	12.75	?	^{12}Cd		
^{112}Cd	24.07	0.03	^{113m}Cd	14y	ß-, γ
^{113}Cd	12.26	27,000	^{114m}Cd		
^{114}Cd	28.86	1.24	^{115}Cd	43d	ß-, γ
^{116}Cd	7.58	1.4	^{117}Cd	3.2h	ß-
^{113}In	4.28	63	^{114}In	50d	γ
^{115}In	95.72	200	^{116m}In	54m	ß-
^{112}Sn	0.96	1.3	^{113}Sn	113d	Electron Capture
^{116}Sn	14.3	0.006	^{117m}Sn	14d	γ
^{118}Sn	24.03	0.01	^{119m}Sn	250d	γ
^{120}Sn	32.85	0.14	^{121}Sn	75y	ß-
^{122}Sn	4.92	0.2	^{123}Sn	40m	ß-
^{124}Sn	5.94	0.204	^{125m}Sn	9.4m	ß-
^{90}Zr	51.46	0.1	^{91}Zr		
^{91}Zr	11.23	1	^{92}Zr		
^{92}Zr	17.11	0.2	^{93}Zr	$9.5x10^{5}y$	ß-
^{94}Zr	17.40	0.1	^{95}Zr	65d	ß-, γ
^{96}Zr	2.80	0.1	^{97}Zr	17h	ß-

* These cross-sections do not take into account resonance adsorption. Such resonances are approximately accounted for by increasing the cross-sections by 45%.

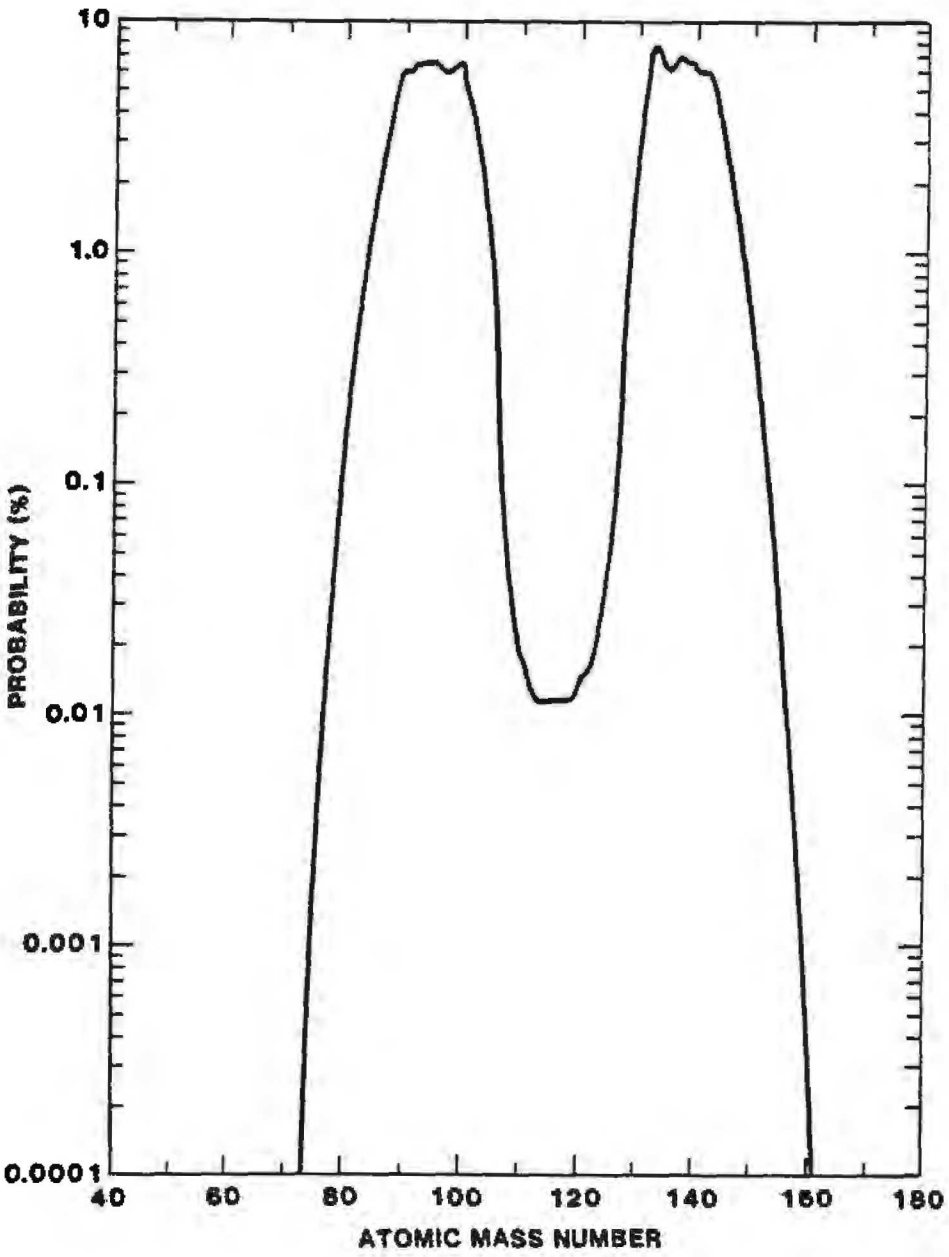

Figure 2.7. Fission Yields for ^{235}U

Table 2.2.

Comparison of Fission Yields From $^{235}_{92}U$ and $^{239}_{94}Pu$ [9].

Fission Product Group	Yield (%) from $^{235}_{92}U$	Yield (%) from $^{239}_{94}Pu$
Zr, Nb	29.8	20.4
Y, La, Ce, Pr, Nd, Po, Sm, Eu, Ga	53.4	47.1
Ba, Sr	14.9	9.6
Mo	24.0	20.3
Ru, Te, Rh, Pd	26.3	51.6
Cs, Rb	22.6	18.9
I, Te	1.2	7.0
Xe, Kr	25.1	24.8

event yields two daughter products, the columns in Table 2.2 each sum to 200 percent. Notable features of the comparison of ^{235}U and ^{239}Pu fissioning are (1) the higher yield of noble metals (Pu, Te, Rh, Pd) in ^{239}Pu fissioning and (2) lower yields of both the Ba,Sr and the Zr,Nb groups.

To determine the absolute amounts of fission products in a reactor core requires:

1. The extent of fissioning and capture that has taken place.

2. The enrichment of the fuel in fissile isotopes.

3. The time and power history over which fissioning took place.

The need to know how much fissioning took place is obvious since the absolute isotope yield is the product of the probability a fission event will produce the isotope times the number of fission events. The irradiation history of fuel is usually reported in terms of "burnup," which includes both fissioning and capture.* Unfortunately, the fuel in reactor cores does not burn up uniformly. The burnup history of fuel assemblies in the Three Mile Island Core just prior to the accident are shown in Figure 2.8 (only one quarter of the core is shown in this figure; the rest of the core and the burnup histories of fuel assemblies in the rest of the core are symmetrically related about the centerlines shown in figure).

As a rough rule, burnup decreases with distance from the center of the core. This is because neutrons that would have been captured or would have continued the nuclear chain reaction if they were generated deep within the core have more of a chance to escape unproductively when they are generated near the perimeter of the core. Fission product inventories would of course vary, approximately, as do the burnups throughout the core.

---

* There are two conventional units of burnup. Percent burnup is the amount of fuel atoms destroyed by both capture and fission. Thus 1 percent burnup means that 10 kg of uranium have been converted in 1 metric tonne of fuel metal atoms. The other unit is megawatt days thermal per metric tonne of uranium. Conversion between the units is difficult because capture creates fissile plutonium which can act as a fuel. A 1 percent burnup corresponds to 6760 MWdth/t U, if credit for the plutonium is not taken and 7765 MWdth/t U if credit is taken.

4008	3512	3091	3187	2513	3206	3675	2479
3511	3234	3316	2965	2988	2927	2885	2107
3099	3280	3026	2974	2471	2835	3074	1713
3185	2971	2996	2675	2729	2395	2281	
2511	2991	2502	2736	2349	2129	1404	
3204	2902	2808	2410	2128	1494		
3672	2911	3048	2280	1403			
2478	2106	1711					

Figure 2.8. Burnup of TMI Fuel Rods in Megawatt Days per Metric Tonne Uranium [10]

The variations in burnup are not smooth functions of distance from the center of the core because the fuel is not uniformly enriched in fissile ^{235}U. The initial enrichment of fuel assemblies in the Three Mile Island Core are shown in Figure 2.9. (Again, only one quarter of the core is shown.) The fueling pattern consists of an outer ring of highly enriched material (2.96 percent ^{235}U). Within this ring there are alternating assemblies of medium enrichment (2.64 percent ^{235}U) and low enrichment (1.98 percent ^{235}U) fuel assemblies. The isotopic distributions of fission products in these fuel elements will be different even if burnup were the same. Powers [11] has used these differences in isotopic abundances in both uranium and plutonium to infer from samples of released material the damage pattern to the TMI core.

The time duration over which a level of burnup occurs affects the fission product inventories because the daughter isotopes of fissioning and the products of neutron capture are unstable and radioactively decay. Progress along the decay chains described above is a strong function of time and so, too, is the isotopic mix of fission products.

Reinspection of the decay chains described above and the complicated nature of products of the fission process, as well as the complexities described above concerning irradiation history and enrichment, should be enough to persuade even the most dogged that calculations of inventories is a complicated activity. Fortunately, the problem has been avidly pursued and is particularly susceptible to computer solution. Within the United States, the computer code ORIGEN has become an especially popular tool for solving the fission product inventory problem [12]. The basic algorithm solves systems of coupled, moderately stiff differential equations. A typical version of ORIGEN tracks the evolution of 1064 isotopes with half-lives greater than 1 second [5]. It is backed by an extensive library of nuclear data concerning half-lives, branch decay probabilities, and capture cross sections. Output is provided in terms of gram atoms, curies, and thermal power.

Other codes besides ORIGEN exist to solve the same problem. The CINDER code has been mentioned in the literature [13]. The British codes RICE and FISPIN are also available. Proprietary codes of reputably outstanding sophistication are apparently held by reactor vendors.

These computer models do not explicitly treat the radial distribution problem described above. Nor do they consider axial variations in fission product inventories which should parallel the axial power distribution in the core.

2.64%	1.98%	1.98%	2.64%	1.98%	2.64%	2.64%	2.96%
1.98%	1.98%	2.64%	1.98%	2.64%	1.98%	2.64%	2.96%
1.98%	2.64%	1.98%	2.64%	1.98%	2.64%	2.96%	2.96%
2.64%	1.98%	2.64%	2.96%	2.64%	1.98%	2.96%	
1.98%	2.64%	1.98%	2.64%	1.98%	2.96%	2.96%	
2.64%	1.98%	2.64%	1.98%	2.96%	2.96%		
2.64%	2.64%	2.96%	2.96%	2.96%			
2.96%	2.96%	2.96%					

Figure 2.9. Enrichment Pattern of Fuel in the TMI Unit 2 Core [10]

B. Justification of Elemental Phenomenological Source Terms

The same considerations that demonstrate the complexities of calculating the fission product inventories also demonstrate that there are a lot of fission products. The fission products are isotopes of a much smaller number of elements. It has become traditional to analyze the severe accident source term in terms of the behavior of the elements rather than the isotopes. When analyses progress to the point radiological concerns need to be adressed, the isotopic abundances in the elements released from the fuel are assumed to be the same as they would have been in the fuel were there no release. That is, the assumption is made that there are no effects on release or behavior, save inventory changes by radioactive decay, that arise because of different isotopes.

An alternative to this traditional approach would be to develop models of release and behavior that are peculiar to each isotope. This alternative would increase, of course, the labor involved in the development of severe accident source term models.

Isotopic difference could affect the behavior of fission products in three ways:

1. Isotopic differences could affect the chemical processes in which fission products engage by altering chemical equilibria.

2. Isotopic differences could affect the rates of chemical reaction.

3. Transmutation of the elements by radioactive decay could alter the release rates or behavior of fission products.

A definitive proof that none of the effects are important would be difficult to formulate. Below, evidence is presented that the first two effects are likely to be insignificant. The third effect, transmutation, is shown to be considerable only for a few particular cases. Because of these occasional transmutation effects, the traditional approach to source term modeling in terms of elements rather than isotopes may not be universally acceptable. But, because the transmutation effects are rare and because neither the thermodynamics nor kinetics of different isotopes are significantly different, it may not be necessary to adopt the alternative of isotopically based source term models.

The chemical processes that affect fission product release and behavior can be identified by systematically examining chemical equilibria. Are these chemical equilibria significantly different for the isotopes of a given element?

Consider two general equilibrium reactions, one involving the isotope A and the other the isotope A*:

$$AB + C \rightleftarrows AC + B \qquad K = \frac{[AC]\,[B]}{[AB]\,[C]}$$

$$A^*B + C \rightleftarrows A^*C + B \qquad K^* = \frac{[A^*C]\,[B]}{[A^*B]\,[C]}$$

The isotopic distortion of the equilibrium is shown by the ratio of the equilibrium constants:

$$K/K^* = \frac{[AC]\,[A^*B]}{[A^*C]\,[AB]}$$

But this ratio is just the equilibrium constant for the isotopic exchange reaction:

$$A^*C + AB \rightleftarrows A^*B + AC$$

This equilibrium constant is given by

$$K_{ex} = \frac{F_{A^*B}\,F_{AC}}{F_{A^*C}\,F_{AB}}$$

where F_i = the partition function of the species i. The partition function of the i^{th} species is given by:[14]

$$F_i = \frac{g_{el}^{(i)} g_{nucl}^{(i)}}{S_i} \left[\frac{(2\pi m_i kT)^{3/2}}{h^3}\right] \left[\frac{22.627\pi^{7/2} I_i^{1/2} (kT)^{3/2}}{h^3}\right] f_{vib}^{(i)}$$

where $g_{el}^{(i)}$ = electronic contribution to the partition function

$g_{nucl}^{(i)}$ = contribution to the partition function from nuclear spins

m_i = mass of the i^{th} species

I_i = moment of inertia of the i^{th} species

k = Boltzmann's constant

h = Plank's constant

$$f_{vib}^{(i)} = \prod_j \left[\frac{\exp(-h\nu_j/2kT)}{1 - \exp(-h\nu_j/kT)} \right]$$

ν_j = frequency of the j^{th} vibration

s_i = symmetry number of the i^{th} species.

Isotopic substitution of one element in the i^{th} species will leave, of course, the symmetry of the species unaltered. Similarly, isotopic substitution does not alter $g_{el}^{(i)}$. Nuclear masses are so much greater than electronic masses for the isotopes of interest in reactor accident analyses that electronic motions are little altered when the nuclear mass is changed by one or two atomic mass units (amu).

The partition function for nuclear spin in the species AB can be cast in the form

$$g_{nucl}^{AB} = g_{nucl}^{(A)} \, g_{nucl}^{(B)}$$

Similar expressions can be written for the species A*B, AC, and A*C. Chemical process can almost never affect nuclear spin so the term $g_{nucl}^{(A)}$ is the same whether the atom A is in the species AB or the species AC.

If the species AB is considered a diatomic species composed of atom A and molecular fragment B, then

$$I_{AB} = \left(\frac{M_A M_B}{M_A + M_B} \right) \left(r_{eq}^{(AB)} \right)^2$$

where $r_{eq}^{(AB)}$ = equilibrium bond length between A and B. Since electronic motions are unaffected by isotopic substitution,

$$r_{eq}^{(AB)} = r_{eq}^{(A*B)}$$

Then, the equilibrium constant for the isotopic exchange reaction is given by

$$\frac{K}{K^*} = \left(\frac{M_{A^*B}}{MAB}\right)^{3/2}\left(\frac{M_{AC}}{M_{A^*C}}\right)^{3/2}\left(\frac{I_{A^*B}I_{AC}}{I_{AB}I_{A^*C}}\right)^{1/2}\left(\frac{f_{vib}^{A^*B}}{f_{vib}^{AB}}\,\frac{f_{vib}^{AC}}{f_{vib}^{A^*C}}\right)$$

$$= \frac{M_{A^*B}}{M_{AB}}\,\frac{M_{AC}}{M_{A^*C}}\,\frac{f_{vib}^{A^*B}}{f_{vib}^{AB}}\,\frac{f_{vib}^{AC}}{f_{vib}^{A^*C}}$$

If the diatomic approximation for the species is again assumed, then there will be but one vibration for each species. The frequency of that vibration is given by

$$\nu_i = \sqrt{\frac{f_i}{m_i}}$$

where f_i is the force constant. Since the force constant is dictated by the chemical bonding, the force constant is essentially unaffected by isotopic substitution. Quite clearly a 1 to 2 percent change in m_i makes a very modest change in the vibrational frequency if m_i is large. At elevated temperatures the exponential terms in the vibrational contribution to the partition function can be linearized. Then,

$$\frac{K^*}{K} = \left(\frac{M_{A^*B}}{M_{AB}}\right)^{3/2}\left(\frac{M_{AC}}{M_{A^*C}}\right)^{3/2}$$

Clearly, for massive isotopes K*/K deviates little from unity. That is, equilibria are little affected by isotopic abundances.

The next question is whether the approach to equilibrium is sensitive to isotope effects. Melander [15] has presented an extensive review of isotope effects on chemical reaction rates. Nearly all analyses of these effects evolve from H. Eyring's [16] transition state theory of elementary chemical reaction rates.*

* Elementary chemical reactions are the actual microscopic, molecular transformations that take place in a chemical process. They are nearly never known except for simple systems that have attracted academic interest. Elementary reactions seldom bear much resemblance to the reactions defined from the stoichiometry of the process.

In this theory, molecular collisions give rise to an energetic, but metastable, transition complex:

$$AB + C \rightleftarrows [ABC] \rightarrow AC + B$$

After a brief induction period, the reactants AB and C come into dynamic equilibrium with the transition complex:

$$AB + C \rightleftarrows [ABC]$$

The rate at which products are produced depends on the concentration of the transition complex ABC. Analysis of the change in concentration brought on by isotopic substitution is just an equilibrium analysis much like that above. The reaction rate, given the concentration of ABC or A*BC, is a vibrational analysis. As the temperatures increase the ratio of the rates of reaction of A*B and AB approaches:

$$\frac{R_{A*B}}{R_{AB}} = \left(\frac{\frac{1}{M_{A*B}} + \frac{1}{M_{A*C}}}{\frac{1}{M_{AB}} + \frac{1}{M_{AC}}} \right)^{1/2}$$

It is apparent that for atomic masses on the order of 100, the ratio of rate constants will vary little with changes in mass of one or two units in comparison to the general uncertainty of the elementary reaction rate constant.

Thus, isotopes should participate in similar chemical reactions at similar rates. The existence of isotopes need not lead to formulation of isotopically based source term models.

Transmutation by radioactive decay does depend on the isotope in question, in terms both of the rate and the nature of the product. It is easy to imagine situations in which an isotope decays to an element with radically different chemical character and consequently radically different behavior during a severe accident. For instance, consider these situations:

1. The isotope of interest is the product of radioactive decay of a noble gas. The isotope of interest is released from the fuel at a rate much slower than the rate of release of the noble gas. Nevertheless, this isotope will appear in the emissions from the core during an accident to an extent dictated by the radioactive decay of released noble gas.

2. The element of interest is quite volatile and is expected to be released quite rapidly from the fuel. But, a fraction of the element is produced by decay of a fairly refractory species that is not released from the fuel. Then, release of the element of interest may persist long after conditions of the fuel are well beyond those expected to lead to quantitative release. The persistent release is the result of decay of the refractory species and prompt release of the decay products.

Though these situations can be imagined, it is important to ascertain their significance before investing in the labor of developing isotopically based source term models.

At first blush, the situations in which radioactive decay might affect fission product behavior mostly involve highly volatile species--the noble gases and, perhaps, iodine. The most important decay processes involving the noble gases and iodine are the ß-decay chains.

For radioactive decay to have a significant bearing on the source term, three conditions must be met:

1. The inventory of the decaying isotope must be high enough to have a perceptible effect.

2. The decay proccess must occur to a significant extent during the time frame of interest.

3. The decay process must not be so rapid that it is largely complete before any significant release can take place.

Let G be the inventory of the decaying element and H the inventory of the element that is the product of the decay process of interest. Let Co be the inventory of the decaying isotope and $t_{1/2}$ be the half-life of this isotope. Co'is the inventory of the product of decay, were decay to go instantaneously to completion. Assume that an error of E in the release fraction of an isotope is barely tolerable. Then, decay processes need to be considered to avoid an excessive error, when

$$Co/G > E$$

and

$$\frac{0.693\ t(min)}{-\ln\left(1-\frac{EG}{Co}\right)} \leq t_{1/2} \leq \frac{0.693\ t(max)}{-\ln\left(1-\frac{EG}{Co}\right)}$$

or

$$Co'/H > E$$

and

$$t_{1/2} \leq \frac{0.693\ t(max)}{-\ln\ 1-\frac{EH}{Co'}}$$

where t(max) is the maximum time of interest and t(min) is the time from reactor scram to the onset of significant fission product release.

Isotopes in the portion of the β-decay chain involving Te, I, Xe, and Cs are shown in Table 2.3. The half-lives of the isotopes and typical inventories in fuel irradiated to about 33,000 MWd/t are also shown in the table. The inventories in this table are provided in the form of decay rates. Any other unit, such as thermal power, dose, or moles, might be used. To scan these isotopes for instances of transmutation effects that might have a significant impact on source term behavior, it was assumed that

$$E = 0.1$$

$$t(min) = 1200$$

$$t(max) = 80,000$$

The isotopes ^{132}Te and ^{134}Te meet the criterion for concern over radioactive decay effects in source term models. Williams [17] has discussed the effect of ^{132}Te and the ex-vessel source term. If Te is not released in-vessel because it has bound chemically to unoxidized zircaloy clad, it is available for release ex-vessel. Ex-vessel release of Te is slow because of the low chemical activity of the element when dissolved in metals. Iodine release ex-vessel is expected to be quite rapid. Because of the decay of ^{132}Te, there is the potential of prolonged ex-vessel iodine release into the containment atmosphere. This release rate is essentially the rate of Te decay since iodine is so promptly purged from the fuel ex-vessel.

Similarly, protracted release of iodine can occur in-vessel if ^{134}Te binds to clad or structures within the reactor vessel. As the tellurium isotope decays, iodine is produced and possibly released even if conditions have long been established that should have allowed rapid, quantitative expulsion of all iodine.

Table 3

The B-Decay Series Involving Te, I, Xe, and Cs Isotopes

Tellurium			Iodine			Xenon			Cesium		
Atomic Mass (amu)	$t_{1/2}$ (s)	Co (10^5Ci)	Atomic Mass (amu)	$t_{1/2}$ (s)	Co (10^5Ci)	Atomic Mass (amu)	$t_{1/2}$ (s)	Co (10^5Ci)	Atomic Mass (amu)	$t_{1/2}$ (s)	Co (10^5Ci)
127	3.3×10^4	72.8	127	Stable							
127m[a]	9×10^6	0.2									
129	4038	250	129	5×10^{14}	2×10^{-5}	129m[c]	6.9×10^5	7×10^{-3}			
						129	Stable				
131	1500	761	131	7×10^5	867	131m	1×10^6	5.4			
						131	Stable				
131m[b]	1×10^5	65.5									
132	2.8×10^5	1259	132	8280	1277						
133	120	1044	133	7.5×10^4	1832	133	4.6×10^5	1833	133	Stable	
133m	3780	692									
134	2520	1514	134	3180	2011	134	Stable		134	6.9×10^7	116.9
135	18	792	135	2.4×10^4	1728	135	3.3×10^4	344	135	6×10^{13}	1.9×10^{-4}
136	21	445	136	86	810	136	Stable		136	$1\times1\times10^6$	35.6
			137	24	837	137	234	1681	137	9.5×10^8	65.3
						138	1020	1579	138	1932	1670
						139	41	1246	139	570	1645
						140	17	866	140	66	1510

a. Only 2 percent of the ^{127m}Te decays by B- emission. The rest decays by emission of a γ ray to yield ^{127}Te.

b. 52 percent of the ^{131m}Te decays by B- emission. The rest decays by emission of a γ ray to yield ^{131}Te.

Several iodine isotopes meet the criterion for consideration. But, there seem to be no no radical consequences of iodine transmutation to xenon. This transmutation can probably be adequately handled by inventory adjustments with time.

Decay of ^{133}Xe and ^{135}Xe meet the criterion for consideration. The decay of ^{133}Xe is to the stable cesium isotope and so can be treated simply by inventory adjustment. Decay of ^{135}Xe does yield a radioactive cesium isotope. Because of the decay, there will always be some cesium suspended in the reactor atmosphere if there was xenon release from the fuel. But, because the half-life of xenon is very long, the amount of cesium wil not be large.

Within the decay series examined here only the ^{132}Te and perhaps the ^{134}Te isotopes seem to deserve attention that could not be supplied by source term models based on the chemistry of the element and neglecting transmutation. A few other examples of significant transmutation effects in radioactive source term behavior are known. Decay of ^{140}Ba to ^{140}La and its effect on ex-vessel release is such an example.

So few instances of transmutation effects make it difficult to consider going to the difficulty of developing isotopically-based source term models. Better would be to treat in an ad hoc manner the instances where transmutation effects are important and do so within the context of source term models based on the elements.

C. Elemental Inventories of Fission Products

Inventories of fission products for a pressurized water reactor with end-of-life fuel are shown in Table 2.4. Inventories for 30 minutes, 1 hour, 4 hours, and 1 day after scram of the reactor are listed in the table. These inventories are just examples to provide an indication of the order of magnitude of the inventories likely to be encountered in reactor accident analyses. The reactor core for the example was assumed to consist of 89.1 metric tons of uranium. The burnup of the fuel was 33,500 MWd/ton uranium produced over 3 years on an 80 percent duty cycle. For more details on the calculations see Reference 5.

D. Need to Consider Nonradioactive Inventories

The consideration of inventories would stop after the amounts of radioactive materials were defined if the classic pathways to defining source term were followed. This is acceptable in bounding estimates, in which mitigation of the phenomenological source term is not mechanistically evaluated. As outlined in the introductory material, this is not now an acceptable procedure. Source terms developed now and in the future will have to meet

Table 4

Fission Product Inventories* for a PWR Core

Element	Amount (gram moles) After Decaying for 30 Min	1 Hour	4 Hours	1 Day
Tritium	1.123	1.123	1.123	1.122
Ge	0.321	0.321	0.321	0.321
As	0.105	0.105	0.105	0.104
Se	45.13	45.13	45.13	45.14
Br	17.50	17.50	17.49	17.48
Kr	294.1	294.1	294.0	294.0
Rb	272.0	272.0	272.0	272.0
Sr	717.6	717.6	717.4	716.8
Y	366.3	366.3	366.2	365.9
Zr	2439	2349	2439	2439
Nb	37.4	37.4	37.4	37.4
Mo	1995	1995	1996	1996
Tc	510.3	510.3	510.4	511.0
Ru	1265	1265	1265	1265
Rh	230.5	230.5	230.6	231.0
Pd	545.4	545.4	545.4	545.7
Ag	27.38	27.39	27.39	27.42
Cd	32.04	32.04	32.04	32.06
In	0.751	0.751	0.752	0.754
Sn	21.71	21.71	21.70	21.70
Sb	7.852	7.844	7.825	7.778
Te	203.5	203.5	203.3	202.8
I	103.6	103.6	103.3	102.3
Xe	2380	2380	2380	2381
Cs	1237	1237	1237	1238
Ba	629.2	629.1	629.0	628.4
La	548.8	548.8	548.7	548.6
Ce	1276	1276	1276	1276
Pr	477.0	477.0	477.1	477.5
Nd	1532	1532	1532	1533
Pm	67.59	67.60	67.61	67.68
Sm	179.5	179.5	179.5	179.6
Eu	53.35	53.35	53.36	53.42
Gd	23.67	23.67	23.68	23.73
Tb	0.565	0.565	0.566	0.566
Dy	0.276	0.276	0.276	0.277
Ho	0.021	0.021	0.021	0.021
Er	0.004	0.004	0.004	0.004
Np	126.3	126.1	125.1	118.7
Pu	2333	2334	2335	2341
Am	16.81	16.82	16.82	16.85
Cm	5.277	5.278	5.278	5.278

*Inventories in this table were taken from Reference 5.

the needs of mechanistic calculations of fission product behavior after the fission products have escaped the fuel. The detailed description of the behavior of fission products released from the fuel are to be found in Chapter 5 of this document. Two of the most important features of the behavior are:

1. Fission product vapors can condense to form aerosols which can subsequently grow, sediment, or deposit on primary system structures and not escape either into containment or into the environment.

2. Fission product vapors can react with structural materials and be bound so they cannot escape into the containment or the environment.

Both of these processes have the potential of substantially reducing the fraction of the phenomenological source term that becomes the radiological source term.

Temperatures and conditions in the reactor core conducive to the vaporization of fission products are equally conducive to the vaporization of nonradioactive materials from the core. The extent of vaporization of nonradioactive materials that occurs while fission products are being vaporized directly affects the post-release behavior of the fission products. In particular, vaporization of nonradioactive materials will have a direct bearing on the efficacy of the two source term mitigation processes mentioned above.

Consider a situation in which a well-stirred atmosphere initially contains 10 g/m^3 of radioactive particles. These particles will be lost from the atmosphere by a variety of processes--diffusion to the walls, settling, etc. At the relatively high concentrations considered here and the relatively high concentrations of interest for reactor accident analyses, gravitational settling of the particles is the dominant mechanism of particle loss from the atmosphere. Settling is an especially efficient process because the particles agglomerate. In a well-stirred atmosphere the particles settle more rapidly with increasing particle size. The rate of loss of particles depends on a variety of factors such as the particle shape and density. A typical example of the variation in the concentration of material in the atmosphere with time is shown as a dashed line in Figure 10. After about 2 hours the mass concentration in the atmosphere has fallen to 1 g/m^3. After about 34 hours the concentration is only 0.01 g/m^3.

Now consider a situation in which the well-stirred atmosphere initially contains 10 g/m^3 of nonradioactive aerosol in addition to 10 g/m^3 of radionuclides. Though interest focuses on the radionuclides, the nonradioactive particles also agglomerate both with other nonradioactive particles and with radionuclide

particles. The rate of agglomeration varies with nearly the square of the particle number concentration irrespective of the radioactivity of the particles [18]. More rapid loss of radionuclides from the atmosphere would be expected. This is, in fact, what occurs. The solid line in Figure 2.10 is the time dependence of radioactive material concentration in the atmosphere when the nonradioactive particles are present. In this case the concentration of radioactive species falls to 1 g/m^3 after only 1.5 hours. The concentration is less than 0.01 g m^3 after only 25 hours.

In reactor accident situations, the effects of nonradioactive particles may be even more severe than depicted in the hypothetical example described above. The inventory of nonradioactive species available for release during an accident will be shown, below, to be very large. Particle concentrations in the atmosphere from these nonradioactive sources can be several times the concentrations of particles formed from radionuclides. The dotted line in Figure 10 is for a situation in which the initial mass concentration in the atmosphere is 100 g/m^3 of which 10 g/m^3 is radionuclides. In this case, it takes only 0.5 hours to reduce the suspended radioactivity by a factor of 10 and only 2.5 hours to reduce it by a factor of 100.

Clearly, to take into account mitigation of radionuclide release by aerosol processes, it is necessary to know the release of nonradioactive species. Because nonradioactive species come from sources other than the fuel, release models distinct from those used for radionuclides may be needed. The generation of aerosols from non-radioactive materials can exceed aerosol generation from radionuclides by well over an order of magnitude.

Next, consider an example of fission product vapors reacting with structures. Elrick and Sallach [19] have found that tellurium vapors react rapidly with structural steel such as type 304 stainless steel. They have also found that Te vapors will react rapidly with silver, which might be present in the primary system atmosphere because precious metal control rod alloys are vaporizing. Clearly, a competition for Te vapors can exist. The Te vapors can react with structural metals, and consequently, not become part of the radiological source term. Or, the Te vapors can react with silver aerosols and remain part of the source term provided aerosol processes are neglected.

The fate of Te vapors depends on the availability of surfaces --either structural or aerosol--for reaction. In Figure 2.11, the fraction of Te that has reacted with silver aerosol rather than structural steel, and consequently, remains a part of the source term, is shown as a function of the silver aerosol concentration. For this calculation the aerosol was assumed to consist of 1 μm particles and the steel was assumed to be present as the walls of an 18-inch diameter pipe. This figure shows that the

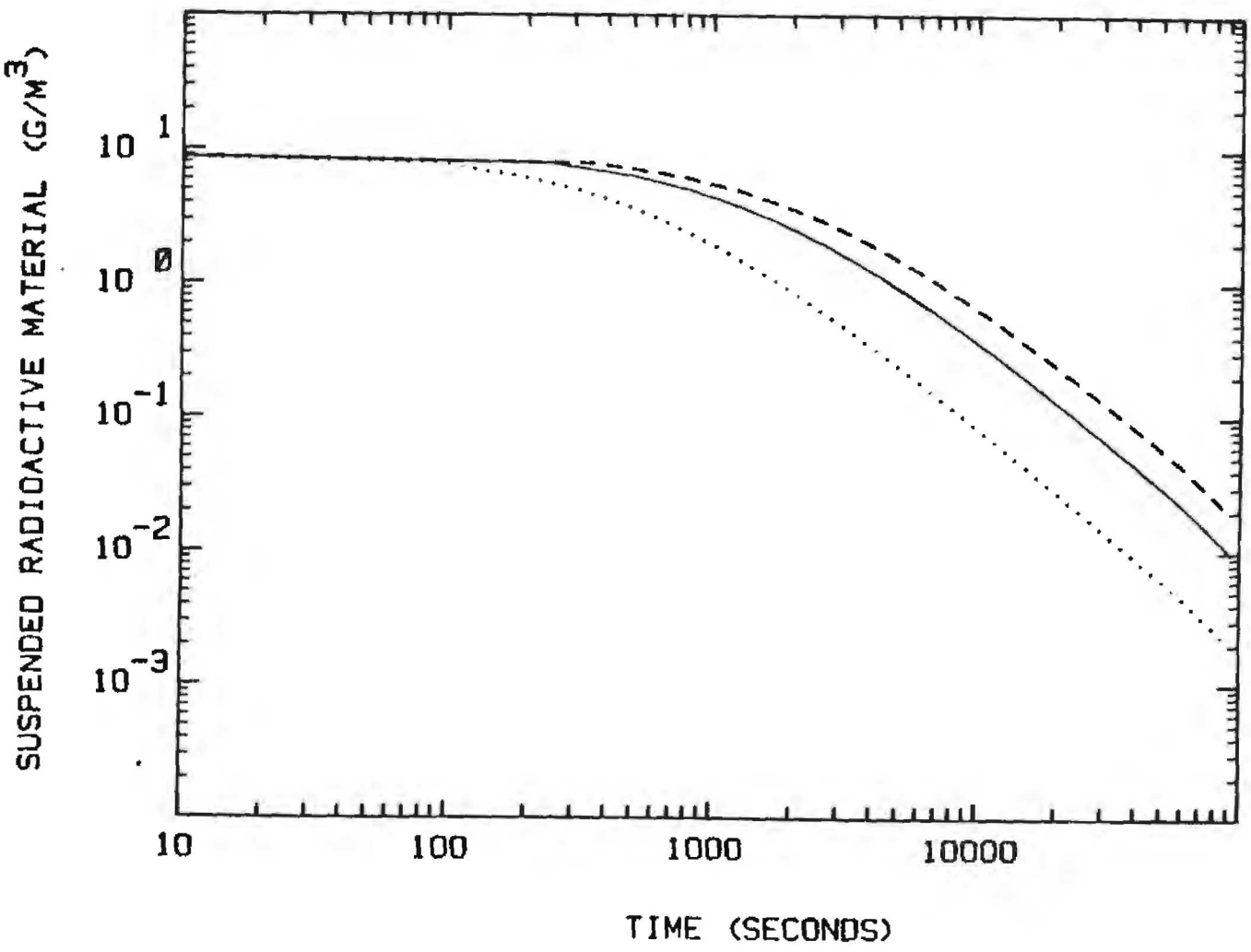

Figure 10. Effect of Nonradioactive Aerosols on the Time Dependence of the Concentration of Radioactive Aerosols. Dashed line is for radionuclides only. Solid line is for radionuclides and an equal amount of non-radioactive material. Dotted line is for a case in which radionuclides make up only 10% of the initial aerosol mass.

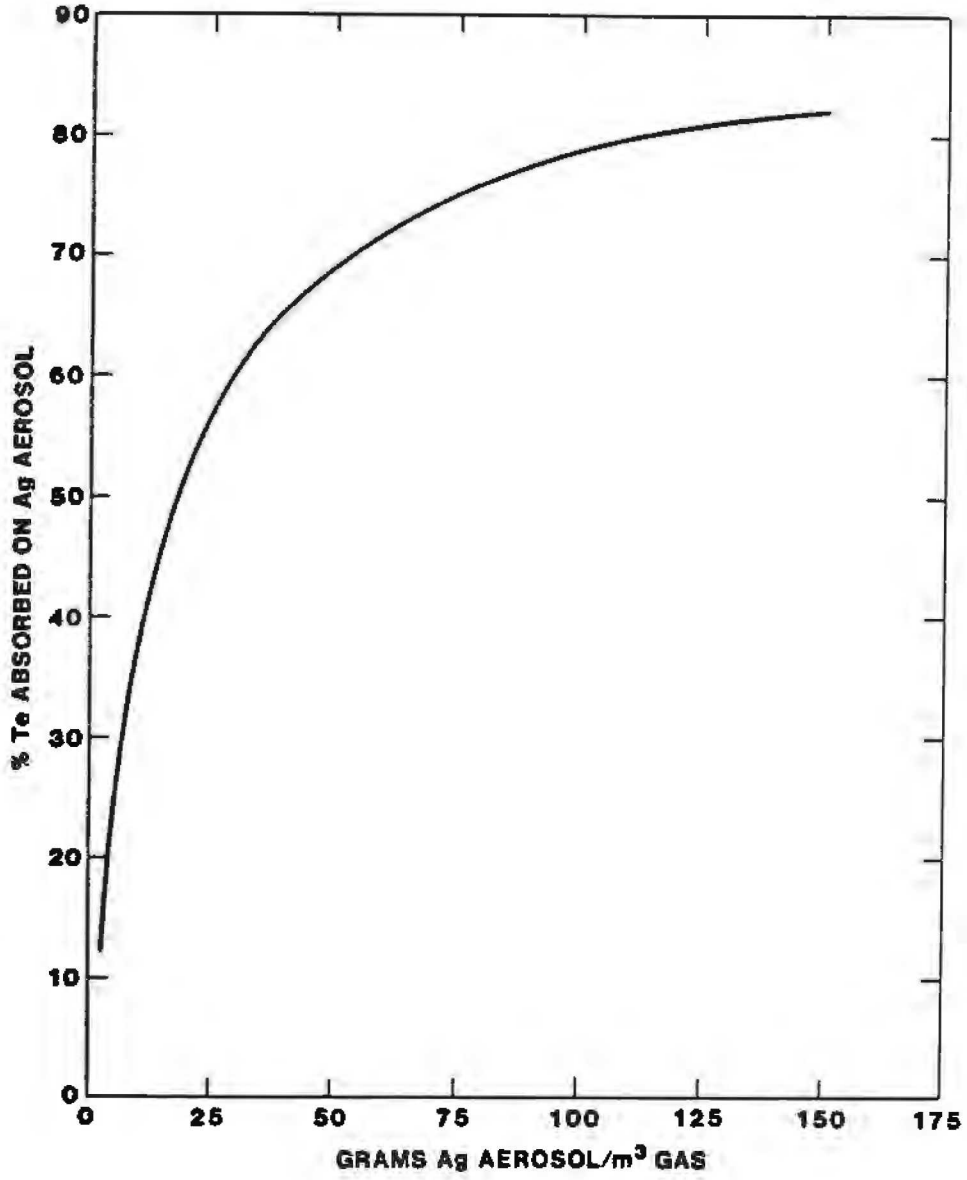

Figure 11. Competition Between Reaction of Te with Steel and Reaction of Te with Silver Aerosols

mitigative effect of fission product release caused by fission product reactions with structures can be prevented to a significant extent if reactive aerosols are present along with the fission products. Since the aerosols produced by vaporization of nonradioactive materials can be chemically quite reactive toward fission products, the magnitude and timing of the vaporization must be known if the fate of the fission products is to be properly described.

E. Inventories of Nonradioactive Materials

The arguments made above demonstrate how important it is to develop source terms for nonradioactive species likely to be vaporized from the reactor core. There are some essential differences between the fission product source term and the nonradioactive source term. The most important of these is that the nonradioactive sources are not intimately associated with a heat source. The attentions concerning the nonradioactive sources should then focus on the most volatile constituents since it is likely that the host matrix for these constituents will be cool, at least relative to fuel. Some care must be exercised in making this discrimination among nonradioactive materials in the core since materials that might appear refractory readily react in the high temperature, high pressure steam environment of a reactor to yield volatile products.

Because the nonradioactive materials are not typically associated with a heat source, the contribution of these materials to the aerosol emissions from a reactor core during an accident are difficult to define. Inventories of volatile materials that can make these contributions are not defined simply by the masses of nonradioactive host materials in and adjacent to the core. Some other means, preferably mechanistic calculation, must be found to determine if the host material gets hot enough for its volatile constituents to contribute to the aerosol emissions. Whether and how much of the host materials participate in the vaporization process will depend on the heat up and melting of the reactor fuel. The behavior of the fuel, in turn, will depend on the nature of the particular accident in question.

Considerations made to date indicate that the nonradioactive materials most likely to be vaporized from the core are:

1. Alloying agents in the fuel cladding.

2. Precious metal control rod alloys.

3. Products of steam reaction with boron carbide or borosilicate glass control rod materials.

4. Volatile alloy constituents or impurities in the structural steels of the reactor.

Fuel cladding in nearly all light water reactors is either Zircaloy 2 or Zircaloy 4 (stainless steel cladding on the fuel in San Onofre Unit 1 is a well-known exception). The compositions of these alloys are:

Weight Percent of Trace Elements in Zircaloy 2 and 4

Element[a]	Zircaloy 2	Zircaloy 4
Sn	1.5	1.5
Fe	0.12	0.2
Cr	0.10	0.10
Ni	0.05	-

[a] Balance of alloy mass is Zr and < 150 ppm Hf.

Tin is the most volatile constituent of the clad. In a typical pressurized water reactor there will be 250 kg of tin. In a boiling water reactor there might be as much as 905 kg of tin that can participate in the vaporization process. Other constituents of the clad could contribute only about 1/10 as much to the aerosol as tin. Chromium is moderately volatile when in the metallic state (boiling point = 2938 K) or in the highly oxidized hexavalent state (boiling point of CrO_3 = 600 K). The volatility of chromium is significantly depressed when the trivalent state of chromium is stable.

Iron is not especially volatile, except at quite high temperatures. In oxygen both Fe(g) and FeO(g) are important gas species. In steam FeOH(g) and $Fe(OH)_2$(g) can form. The gas species FeO(OH)(g) has been hypothesized.

Nickel vaporizes primarily as a metal.

Many pressurized water reactors use an alloy of silver, indium, and cadmium as a control rod material. A typical inventory of this control rod alloy in a large pressurized water reactor is:

Silver (Ag)	2365 kg
Indium (In)	442 kg
Cadmium (Cd)	147 kg

All constituents of this alloy are volatile. A rather thorough thermochemical analysis of the vaporization of this alloy has been done recently [20]. As the alloy is heated within the control rod sheath, quite high partial pressures of Cd are reached:

Temperature (K)	Cadmium Partial Pressure (atm)
1000	0.015
1200	0.129
1400	0.598
1600	1.898
1800	4.671
2000	9.634

Pressure from the cadmium as well as pressurization of the helium fill gas in the rod can cause the control rod clad to rupture [21, 22]. Once evaporation can take place the cadmium is preferentially distilled from the alloy. Subsequent evaporation from the Ag-In alloy requires higher temperatures and is not congruent. The rate of vaporization may be controlled in a reactor accident by heat input to the alloy.

Both pressurized water reactors and boiling water reactors use B_4C control rod materials or borosilicate glass burnable poisons. The predominant neutron absorption reaction is

$$^{10}_{5}B + n \rightarrow {}^{7}_{3}Li + \alpha$$

so that after some period of operation, the rods contain lithium. A typical boiling water reactor would contain 530 kg of boron. A pressurized water reactor might contain 82 kg boron and 137 kg SiO_2.

In steam, boron reacts according to the stoichiometry [23]:

$$B_4C + 6H_2O \rightarrow 2B_2O_3 + C + 6H_2$$

The product B_2O_3 will also react with steam to produce boric acid vapors (H_2BO_2 and H_3BO_3). Reactions of these boric acids with fission products are of concern. For instance, the reaction

$$HBO_2 + CsI \rightarrow HI + CsBO_2$$

is suspected as a means of creating vapor phase iodine in the primary system.

Silicates will also vaporize at high temperatures. The vaporization process can be described by the reactions such as:

$$SiO_2(c) + H_2 \rightarrow H_2O + SiO(g)$$

$$SiO_2(c) + 2H_2O \rightarrow Si(OH)_4(g) \quad .$$

Silica, too, is reactive toward CsI, yielding a silicate and free iodine [23].

Compositions of important structural alloys found in nuclear reactors are listed in Table 2.5. It is not possible a priori to say how much of a contribution constituents of these alloys could make to aerosol emissions during a severe accident. The contribution depends on the heating of the steel, which in turn depends on the nature of the core meltdown process. The vaporization of Mn, Mo, Si, S, and P will make the earliest contributions. Vaporization of the major alloy constituents has been discussed above. If reactive vaporization is neglected, then the vapor pressure of 304 stainless steel is given by [24]:

$$\log P(\text{atms}) = 6.1210 - 18,836/T(K)$$

and the vapor pressure of 316 stainless steel is given by:

$$\log P(\text{atms}) = 6.1127 - 18,868/T(K) \quad .$$

The vaporization of neither alloy is congruent.

F. Chemical Classification of the Elements for Source Term Models

There are about 1000 isotopes that are of interest for severe accident source term models. From the preceding discussions it is apparent that the source term models need not be constructed to explicitly predict release and behavior of so many isotopes. Rather, the models can be constructed to predict the behavior of some 100 elements. This factor of 10 reduction in the effort needed to develop source term models is important. The effort needed to describe release and behavior of 100 elements may still be too much for many applications. Even if the list of elements to be explicitly treated were pared of elements with low inventories in the reactor core, only about a factor of two reduction in the source term modeling effort would be achieved.

Table 2.5

Compositions of Important Structural Alloys (weight percent)

Alloy	Fe	Cr	Ni	Mn	Mo	Other Elements
304 Stainless	bal	18-20	8-10.5	2	-	0.08 C; 0.045 P; 0.03 S; 1 Si
308 Stainless	bal	19-21	10-12	2	-	0.08 C; 0.045 P; 0.03 S; 1 Si
309 Stainless	bal	22-24	12-15	2	-	0.2 C; 0.045 P; 0.03 S; 1 Si
316 Stainless	bal	16-18	10-14	2	2-3	0.08 C; 0.045 P; 0.03 S; 1 Si
Inconel 600	8	15.5	76	0.5		0.08 C; 0.008 S 0.25 Cu

To further reduce the magnitude of the source term model development effort, another approximation must be introduced. Historically, the additional approximation is to group the elements into chemically similar categories and explicitly treat only one element from each category in the source term model. This is exactly the type of approximation used in the Reactor Safety Study [1]. Seven chemical categories were defined as listed below:

1. Noble Gases: Xe, Kr
2. Halogens: I, Br
3. Alkali metals: Cs, Rb
4. Alkaline earths: Sr, Ba
5. Tellurium group: Te, Se, Sb
6. Transitional metal group: Ru, Mo, Pd, Rh, Tc
7. Lanthanides: La, Nd, Eu, Y, Ce, Pr, Pm, Sm, Np, Pu, Zr, Nb, U, Th

The underlined element in each of the above groups was taken to be the representative of that group. It was this representative element that was actually treated in the Reactor Safety Study source term model. The behaviors of other elements were assumed to be similar to that of the group representative.

All chemical categorizations of the elements require some subjective discrimination between the similarities and differences in the chemistries of the elements. The chemistries of all elements are indeed different. The differences can be amplified or muted depending on the chemical environment and the process of interest.

Consider, as an example of the difficulties of chemical categorization of the elements, the noble gases. The very, very weak chemical interactions of Xe and Kr leads nearly all analysts to group these elements and treat them as one species. Certainly for the purposes of estimating the behavior of noble gases at very high temperatures this is an acceptable approximation. Were the attentions switched to the consideration of filtered vents with activated charcoal trapping of the noble gases, grouping of the noble gases Xe and Kr would not be acceptable. Xenon will absorb efficiently on activated charcoal even at surprisingly high temperatures. Krypton, on the other hand, absorbs on charcoal only at low temperatures that would be difficult to maintain in an environment expected to develop during a severe reactor accident. Most schemes for filtered venting with noble gas trapping are found wanting because of the chemical differences between Krypton and Xenon which in other contexts are negligible.

It is apparent then that any categorization of the elements will be specific to a given process and will reflect only some subset of the properties of the elements. As a broader base of information and analysis develops, it will not be surprising if exceptions are found or paradoxes develop from the categorizations.

The groupings for the noble gases, halogens, and alkali metals developed for the Reactor Safety Study are defensible. As noted above, grouping of the noble gases can fail for situations radically different than the high temperature environments usually of interest in source term modeling. Chemical bonding of bromine and iodine are somewhat different but these differences are usually manifest at only low temperatures or in an aqueous medium. Grouping of the alkali metals is particularly acceptable. Even in sophisticated chemical studies Cs and Rb are considered to have nearly identical chemistries.

Difficulties with the Reactor Safety Study categorization begin to appear in the alkaline earth group. Barium and strontium have qualitatively similar chemistries. But, in quantitative features they are somewhat different. Barium is more easily

reduced from the oxide to the metal than strontium. Barium typically exhibits higher vapor pressures than does strontium. The Reactor Safety Study authors recognized these quantitative differences, apparently, and in many cases explicitly treated both elements. For most purposes the quantitative differences between the behavior of Sr and the behavior of Ba may not be of sufficient significance to warrant separate treatment of the elements. For situations involving release of the elements from fuel some conservatism can be introduced by selecting barium rather than strontium as the group representative.

The remaining chemical categories defined in the Reactor Safety Study (the Tellurium, Transition Metal, and Lanthanides Groups) are most difficult to rationalize. These categorizations ignore both quantitative and qualitative differences in chemistry. Tellurium and certainly selenium are essentially nonmetals. Antimony, on the other hand, is a main group metal. Te and Se will react with metals much as does sulfur to form covalent compounds. Antimony will alloy with metals. When antimony does form a compound with a metal compound, it is typically an intermetallic with metal-metal bonding. There seems to be little reason to expect release of antimony to parallel the release of tellurium and selenium in all of the wide variety of chemical circumstances created by severe reactor accidents. The differences in chemistry during transport of antimony and tellurium released from the fuel ought to be even more obvious.

Ruthenium, palladium, and rhodium are platinoids, notably for their lack of reactivity and refractory qualities. Molybdenum and technitium are early transition elements with a rich oxide chemistry that can develop at the oxygen potentials liable to be present around reactor fuel during a severe accident. There seems to be no reason to expect all these elements to behave similarly during release from the fuel or during transport.

Actinides, lanthanides, and early transition metals, Nb and Zr, are lumped into the Reactor Safety Study's "Lanthanide" Group. Thereby, the release of practically nonvolatile zirconium is presumed similar to uranium despite the fact uranium can form quite volatile hexavalent species such as UO_3 and $UO_2(OH)_2$.

The conservative approach utilized in the Reactor Safety Study focused on release of radionuclides and largely neglected natural processes that might mitigate this release. Consequently, there was little need in the Reactor Safety Study to consider release of nonradioactive species. As noted above, modern source term analyses do not neglect mitigation and consequently cannot neglect release of the nonradioactive species during a severe accident. These nonradioactive species must then be included in any categorization of the elements.

An alternative to the chemical categorization of elements used in the Reactor Safety Study is shown in Tables 2.6 and 2.7. This 13 category scheme incorporates the more important nonradioactive species likely to be vaporized during a severe accident. It repairs some, but by no means all, of the chemistry approximations made in the Reactor Safety Study.

The categorization of the noble gases, alkali metals, alkaline earths, and halogens done in the Reactor Safety Study is retained in this alternate scheme. The only change has been to declare barium the representative of the alkaline earth group. Were the categorization to be used for purposes other than release from the fuel, the representative of the alkaline earth group might be selected to be strontium because of the decay of ^{140}Ba.

Explicit addition of sodium and potassium to the alkali metals has been noted. Also, calcium and magnesium have been added to the alkaline earth groups. These additions have been made to accommodate the release from concrete during ex-vessel interactions of core debris.

Tellurium and selenium constitute a single group in the scheme. Antimony has been incorporated into one of the two Main Group categories.

The Main Group categories are added to accommodate releases of control rod alloy species and tin from the Zircaloy clad. The Main Group elements exhibit a wide range of volatilities. For instance, cadmium boils at 1040K whereas tin boils at 2543K. Consequently, the Main Group elements have been split into two categories. Cadmium is taken as the representative of the more volatile Main Group category. Tin, rather than silver, is taken as the representative of the less volatile Main Group elements.

The choices for representatives of the two Main Group categories have been made based on expectations concerning accident analyses. It would be expected that during severe accidents in pressurized water reactors that the control rods would rupture and expel cadmium. There is so much cadmium, and it would be released so suddenly, it will be important to consider explicitly in accident analyses. Silver, too, might be released from the control rod alloy. But, the alloy will be quite fluid and should promptly drain from the heated core regions so releases will be minimized. Tin from the fuel clad will be present in both pressurized and boiling water reactors. The tin will remain intimately associated with degrading fuel. It will then be necessary to explicitly consider tin release.

The platinoids are grouped. Ruthenium is taken to be the representative of this group because of its radiological consequences if it appears in the radiological source term.

Table 2.6

Classification of the Elements into Chemically Similar Groups

Group Name	Representative Element	Elements in the Group
Noble gases	Xe	He, Ne, Ar, Kr, Xe, Rn, He, Ne
Alkali metals	Cs	Li, Na, K, Rb, Cs, Fr, Cu, Ag
Alkaline earths	Ba	Be, Mg, Ca, Sr, Ba, Ra
Halogens	I	F, Cl, Br, I, At
Chalcogens	Te	O, S, Se, Te, Po
Platinoids	Ru	Ru, Rh, Pd, Re, Os, Ir, Pt, Au
Transition Metals I	Mo	V, Cr, Fe, Co, Mn, Nb, Mo, Te, Ta, W
Tetravalents	Ce	Ti, Zr, Hf, Ce, Th, Pa, U, Np, Pu
Trivalents	La	Al, Sc, Y, La, Ac, Pr, Nd, Pm, Sm, Eu, Gd, Tb, Dy, Ho, Er, Tm, Yb, Lu, Am, Cm, Bk, Cf
Uranium	U	U
Main Group I	Cd	Cd, Hg, Zn, As, Sb, Pb, Tl, Bi
Main Group II	Sn	Ga, Ge, In, Sn, Ag
Boron	B	B, Si, P

Table 2.7

Alphabetical Listing of the Elements
and Their Classification

Element	Group	Representative
Actinium	Trivalents	La
Aluminum	Trivalents	La
Americium	Trivalents	La
Antimony	Main Group I	Cd
Argon	Noble Gases	Xe
Arsenic	Main Group I	Cd
Astatine	Halogens	I
Barium	Alkaline Earths	Ba
Berkelum	Trivalents	La
Berylium	Alkaline Earths	Ba
Bismuth	Main Group I	Cd
Boron	Boron	B
Bromine	Halogens	I
Cadmium	Main Group I	Cd
Calcium	Alkaline Earths	Ba
Californium	Trivalents	La
Carbon	Tetravalents	Ce
Cerium	Tetravalents	Ce
Cesium	Alkali Metals	Cs
Chlorine	Halogens	I
Chromium	Transition Metals	Mo
Cobalt	Transition Metals	Mo
Copper	Alkali Metals	Cs
Curium	Trivalents	La
Dysprosium	Trivalents	La
Einsteinium	Alkaline Earths	Ba
Erbium	Trivalents	La
Europium	Trivalents	La
Fermium	Alkaline Earths	Ba
Fluorine	Halogens	I
Francium	Alkali Metals	Cs
Gadolinium	Trivalents	La
Gallium	Main Group II	Sn
Germanium	Main Group II	Sn
Gold	Platinoids	Ru
Hafnium	Tetravalents	Ce
Helium	Noble Gases	Xe
Holmium	Trivalents	La
Hydrogen	Noble Gases	Xe

Table 2.7 (continued)

Alphabetical Listing of the Elements
and Their Classification

Element	Group	Representative
Indium	Main Group II	Sn
Iodine	Halogens	I
Iridium	Platinoids	Ru
Iron	Transition Metals	Mo
Krypton	Noble Gases	Xe
Lanthanum	Trivalents	La
Lithium	Alkali Metals	Cs
Lead	Main Group I	Cd
Lutetium	Trivalents	La
Magnesium	Alkaline Earths	Ba
Manganese	Transition Metals	Mo
Mercury	Main Group I	Cd
Molybdenum	Transition Metals	Mo
Neodymium	Trivalents	La
Neon	Noble Gases	Xe
Neptunium	Tetravalents	Ce
Nickel	Platinoids	Ru
Niobium	Transition Metals	Mo
Nitrogen	Noble Gases	Xe
Osmium	Platinoids	Ru
Oxygen	Chalcogens	Te
Palladium	Platinoids	Ru
Phosphorus	Boron	B
Platinum	Platinoids	Ru
Plutonium	Tetravalents	Ce
Polonium	Chalcogens	Te
Potassium	Alkali Metals	Cs
Prasedymium	Trivalents	La
Promethium	Trivalents	La
Protactinium	Tetravalents	Ce
Radium	Alkaline Earths	Ba
Radon	Noble Gases	Xe
Rhenium	Platinoids	Ru
Rhodium	Platinoids	Ru
Rubidium	Alkali Metals	Cs
Ruthenium	Platinoids	Ru

Table 2.7 (continued)

Alphabetical Listing of the Elements
and Their Classification

Element	Group	Representative
Samarium	Trivalents	La
Scandium	Trivalents	La
Selenium	Chalcogens	Te
Silicon	Boron	B
Silver	Main Group II	Sn
Sodium	Alkali Metals	Cs
Strontium	Alkaline Earths	Ba
Sulfur	Chalcogens	Te
Tantalum	Transition Metals	Mo
Technetium	Transition Metals	Mo
Tellurium	Chalcogens	Te
Terbium	Trivalents	La
Thallium	Main Group I	Ca
Thorium	Tetravalents	Ce
Thulium	Trivalents	La
Tin	Main Group II	Sn
Titanium	Tetravalents	Ce
Tungsten	Transition Metals	Mo
Uranium	Uranium	U
Vanadium	Transition Metals	Mo
Xenon	Noble Gases	Xe
Ytterbium	Trivalents	La
Yttrium	Trivalents	La
Zinc	Main Group I	Cd
Zirconium	Tetravalents	Ce

Some caution is necessary in the use of this representative. Rhodium can have greater volatility than ruthenium in the steam/hydrogen environment of the primary system during a severe accident. Nickel is included in the platinoid group because of this element's low volatility in steam and hydrogen atmospheres.

A new group is formulated of the early transition elements. There elements are readily oxidized in steam and hydrogen environments. The oxidized forms of these elements tend to be volatile. Molybdenum is chosen to be the representative of the group because of the diversity of its chemistry and the radiological importance of this element. Structural elements iron and manganese are included in the group, though it would not be difficult to rationalize a separate category for these elements. The structural element chromium is included in the group because of the similarity of its chemistry to that of the representative of the group, Mo.

Uranium could easily be incorporated in the early transition metal group. Because of the actinide contraction, uranium exhibits chemistry quite similar to that of molybdenum. In particular, the hexavalent state of uranium is quite volatile. But, because of the obvious importance of distinct, explicit, treatment of uranium during severe reactor accidents, a separate category is reserved for this element.

The lanthanides and actinides are split into two categories, the trivalent elements and the tetravalent elements. The tetravalents favor, even at high temperatures, the cubic fluorite structure of UO_2. Consequently, the activity and volatility of these elements dissolved in UO_2 remains low.

The trivalent elements favor the various hexagonal structures and dissolve in UO_2 only at the expense of some loss of stability. This loss of stability is reflected by somewhat higher than expected volatility. Yttrium is included with the trivalents though it is assuredly a transition element. Because of the lanthanide contraction, the chemistry of yttrium is amazingly similar to that of lanthanum.

At first glance, it might seem unreasonable to place plutonium among the trivalents. It is, after all, present as tetravalent PuO_2 in-reactor fuel. But at elevated temperatures plutonium exhibits a distinct tendency to reduce to the trivalent state.

Finally, a separate group is set aside for boron. This category is important only if large amounts of boron or borosilicate glass are present in the core. Silicon and phosphorous are included in the group because these elements too reactively vaporize in steam.

Because of its subjective nature and its dependence on chemical circumstances which are poorly known, chemical categorization will never be an entirely satisfactory approximation. Categorizations, and certainly the selection of the representative element from each group, ought to change as more knowledge develops concerning severe accidents.

Alternatives to chemical categorization have been suggested. Powers [25] has developed a procedure for allocating scarce research resources to the study of fission products that is based on the attributes of the fission products rather than the similarities of their chemistries. The elements are rank-ordered in terms of several attributes. Powers chose (1) inventory, (2) decay rate, (3) thermal power, (4) melting point, and (5) radiological consequences. Ties are allowed in the ranking to account for uncertainty. The ranks within each attribute group are summed for each element. These sums can be multiplied by penalty functions to account for risk adverse or cost adverse tastes. The rank sums are themselves ranked in rank order until (1) resources are exhausted, (2) the marginal rate of return has fallen to a sufficient level that greater utility is obtained by turning to the next lower rank, or (3) attentions have gone to ranks low enough that the elements are known to be unimportant. An example of this type of rank ordering is shown in Table 2.8.

The rank-ordering procedure has not received universal endorsement and has not been adopted here.

Another procedure that has been suggested is to assume various releases of elements, use the CRAC code [26] to determine the consequences of the release, and from these consequences determine which fission products are most important. Unfortunately, this procedure is exceptionally laborious. It requires a great deal more knowledge concerning chemical form and nature of the release than is typically available. Finally, the results change with different assumptions concerning the consequence code.

2.4 Recommendations for MELCOR

From the preceding discussions the following recommendations for the development of MELCOR are formulated:

1. Radionuclide inventories ought not be calculated within MELCOR. Rather, these inventories should be calculated with one of the specialized codes such as ORIGEN. A set of default values should be included in MELCOR.

2. It is desirable that provision be made in MELCOR to have radical and axial variations in the inventories of the radionuclides.

3. Elemental release models rather than isotopic release models can be used in MELCOR. It is possible that one exception to this general rule is the release of ^{132}I and ^{132}Te.

4. Release of nonradioactive species as well as release of radionuclides will have to be considered in MELCOR. This may necessitate separate release models for fuel, cladding, structural materials, and control rods.

5. The many elements susceptible to release during a severe accident may be grouped into 13 categories. The release and behavior of members of a given category is then described by the release and behavior of a single representative element in the category. The categorization recommended here is shown in Table 6 and an alphabetical cross index is provided in Table 7.

Table 2.8

Importance Ranking of Radionuclides
in Terms of Inventory, Dose Curies, and Mobility

Rank	Element at Indicated Time After Scram		
	1 Hour	1 Day	100 Days
1	Cs	I	Zr
2	I	Te	U
3	Te	Cs	Pr
4	Rb	Xe	Nb
5	Ba	Ba	Cs
6	Mo	Pr	Ce
7	Pr	Mo	Rh
8	La	Ce	Y
9	Np	Zr	Sr
10	Xe	Nb	Fe
11	Sn	Np	Ru
12	Sr	La	Te
13	Nb	Sn	Ba
14	Y	Rh	Ni
15	U	Tc	Cr
16	Tc	Sr	Xe
17	Ce	Nd	^{3}H
18	Zr	Y	Kr
19	Sb	U	Sn
20	Br	Ru	Pm
21	Kr	Sm	Cm
22	Rh	Sb	Se
23	Nd	Pd	Rb
24	Ru	Cr	Cd
25	Mn	Ag	Zn

References

1. USNRC, Reactor Safety Study: An Assessment of Accident Risks in US Commercial Nuclear Power Plants, WASH 1400, NUREG 75/04, October 1975.

2. J. G. Kemeny, Chairman, Report of the President's Commission on The Accident at Three Mile Island, and L. Jaffe, Head, Reports of the Technical Assessment Task Force, Vol. 1, October 1975.

3. R. S. Denning, "Reduction in Reactor Risk by the Mitigation of Accident Consequences," Proc. ANS/ENS Topic Meeting on Thermal Reactor Safety, Knoxville, TN, April 1980, CONF-8 00403, Vol. 1, p. 189.

4. M. D. Cable, J. Honkanen, E. C. Schloemer, M. Ahmed, J. W. Ewidd, Z. Y. Chou and J. Cerny, Phys. Rev. C 30 (1984) 1276.

5. D. E. Bennett, NUREG/CR-0987, SAND79-0299, Sandia National Laboratories, Albuquerque, NM, October 1979.

6. N. Feather, "Ternary Fission--a Review," Proc., 2nd IAEA Symposium on the Physics and Chemistry of Fission, Vienna, 28 July-1 August 1969, International Atomic Energy Agency, 1969.

7. R. A. Nobles, Phys. Rev. 126 (1962) 1508.

8. S. W. Cooper, et al., Phys. Rev. 154 (1967) 1193.

9. D. R. Olander, Fundamental Aspects of Nuclear Reactor Fuel Elements, UC-796, TID 26711, 1975.

10. Personal Communication to D. A. Powers from T. P. Suchocki (GPU) dated 6 June 1978.

11. D. A. Powers, "Plausible Conditions of the TMI-2 Core," Transactions ANS 34 (1980) 563.

12. A. G. Croff, ORNL-5621, Oak Ridge National Laboratory, 1980.

13. "Radionuclide Release and Transport," Chapter 8 in PRA Procedures Guide, Volume 1, NUREG/CR-2300, January 1983.

14. T. L. Hill, An Introduction to Statistical Thermodynamics, Addison Wesley Pub. Co., 1960.

15. L. Melander, Isotope Effects on Reaction Rates, The Ronald Press Co., NY, 1960.

16. S. Gladstone, K. J. Lalder, and H. Eyring, The Theory of Rate Processes, McGraw-Hill Book Co., 1961.

17. D. Williams, "Effects of Radioactive Decay Chains on Source Terms," Appendix C in R. J. Lipinski, et al., Uncertainty in Radionuclide Release Under Specific LWR Accident Conditions Volume II: Analyses, SAND84-0410/2, Sandia National Laboratories, Albuquerque, NM, October 1984.

18. L. D. Reed, J. A. Gieseke, and H. Jordan, Effects of Radiation on Aerosol Behavior, BMI-NUREG-1943, Battelle Columbus Laboratory, Columbus, Ohio, December 1975.

19. R. L. Sallach, C. J. Greenholt, and A. R. Taig, Chemical Interactions of Tellurium Vapors with Reactor Materials, NUREG/CR-2921, SAND82-1145, Sandia National Laboratories, Albuquerque, NM, March 1984.

20. D. A. Powers, Behavior of Control Rods During Core Degradation I: Pressurization of Silver-Indium-Cadmium Control Rods, Sandia National Laboratory, Albuquerque, NM.

21. S. Hagan, KfK 2750, pp. 4300-4362, Kernforschungszentrum Karlsruhe, November 1978.

22. G. W. Parker, G. E. Creek, and A. L. Sutton, Jr., "Influence of Variable Physical Process Assumptions on Core Melt Aerosol Release," Proc. Int'l Mtg. on Thermal Reactor Safety, Chicago, IL, NUREG/CP-0027, Vol. 2, p. 1078, 1983.

23. R. M. Elrick and R. A. Sallach, Quarterly Report for The Advanced Reactor Safety Research Program, SAND82-0904, NUREG/CR-2679, Sandia National Laboratories, Albuquerque, NM.

24. C. S. Kim, Thermophysical Properties of Stainless Steels, ANL-75-55, Argonne National Laboratory, September 1975.

25. D. A. Powers, unpublished results.

26. L. T. Ritchie, D. C. Aldrich, and R. M. Blond, Calculation of Reactor Accident Consequences, Version 2, NUREG/CR-2324, SAND81-1984, Sandia National Laboratories, Albuquerque, NM, 1981.

CHAPTER 3

RELEASE OF FISSION PRODUCTS AND GENERATION OF AEROSOLS DURING THE IN-VESSEL PHASES OF A SEVERE REACTOR ACCIDENT

D. A. Powers

3.1 An Introduction to the In-Vessel Source Term and the Objectives of this Chapter.

Severe reactor accidents are, by definition, accidents in which the reactor fuel and clad are heated to the point that they suffer significant damage. Typically, this damage is presumed to progress through complete melting of the core and extensive reaction of the fuel cladding with steam.

The cladding on the fuel is often considered to be the first, and in some respects, the most important barrier to release of radionuclides from the reactor core. As soon as the cladding is damaged, radionuclide release begins. Volatile radionuclides such as Xe, Kr, Cs and I can be nearly quantitatively expelled from the fuel during core degradation within the reactor vessel. Once radionuclides have escaped the fuel there is at least the possibility that they may escape the power plant. The volatile radionuclides, so extensively released during core degradation, are also among the most radiologically consequential. A great deal of the attentions in severe reactor accident analyses is devoted to determining the release and behavior of these volatile radionuclides. Over 70% of the discussion of severe accident source terms presented in the Reactor Safety Study [1] is devoted to the escape of volatile fission products from degrading reactor fuel. In some very simplified discussions of severe reactor accidents, there has been the implication that release of cesium and iodine from degrading reactor fuel is indeed the entire, substantive source term of radioactivity. Though this simplification is grossly in error, it is true the release of Cs and I from degrading reactor fuel is an important aspect of severe accidents.

The approach toward the severe accident source term taken in the Reactor Safety Study was intended to be "conservative." That is, errors in the analysis were to accrue on the side of over-estimating the extent of fission product release - especially the release of volatile radionuclide both from the fuel and from the plant. Recently, and especially since the accident involving fuel degradation at Three Mile Island, the treatment of radionuclide release presented in the Reactor Safety Study has been questioned [2,3]. Most of the criticism has suggested that the models developed for the Reactor Safety Study may have been too conservative. These models may, incorrectly, neglect natural phenomena that would reduce the

amount of radioactive material escaping the fuel that could escape the plant. Criticism that the Reactor Safety Study may have been nonconservative has also appeared. Criticisms of the analyses done for the Reactor Safety Study have focused on release of radioactivity from the plant. But, in every case, the alternate considerations have been based on different portrayals of radionuclide release from the reactor fuel.

Criticisms of the Reactor Safety Study have prompted the initiation or continuation of many analytic and experimental research programs. A recent survey [4] identified 15 major programs to characterize release of radionuclides from reactor fuel as well as several programs to define the behavior of these radionuclides after release. Several analytic efforts that utilize results of the research to define new severe accident source terms have appeared [5-8]. A consistent thrust in all of the recent work has been to relate in a more mechanistic manner the release of radioactive species from the fuel to phenomena taking place during core degradation. That is, generic release estimates applicable to a wide variety of accidents at a wide variety of plants are being abandoned. In the place of these generic releases are models that are sensitive to features specific to the plant and the accident in question.

Development of mechanistic models of release is a formidable task. The diversity of radionuclides and non-radioactive species that are of interest has been discussed in the preceding chapter. Release of these species is an inherently chemical process. So, release models ought to be sensitive to those features of severe reactor accidents that ought to affect chemistry -- notable temperature, pressure, and atmosphere composition. Release is also a transport process so release models ought also to be sensitive to those features of severe accidents that affect transport -- such a gas flow velocities, core geometry, fuel microstructure and clad state.

The definition of severe reactor accidents has progressed considerably since the time of the Reactor Safety Study. Small-break accidents and accidents initiated by power transients have been found to be much greater contributors to the potential risks of nuclear power plants (see, for example, references 9 and 10). Further, it has been found desirable to know not just the potential release of radioactivity, but also how the release varies from one type of accident to another. An indication of the range of variation of accident features that ought to affect release during accidents of interest today is provided in Table 3.1. Flow velocities through the core can vary by 2-3 orders of magnitude. Pressures can vary by 2 orders of magnitude. Fuel burn-up can vary by an order of magnitude. Local gas compositions can vary by several orders of magnitude. These wide variations in accident features ought then cause variations in release of some significant nature.

Table 3.1

Features of Severe Reactor Accidents that Ought to Affect Release

Feature	Typical Range
System Pressure	2 - 170 atmosphere
Maximum Core Temperature	2200 - 3100 K
Heatup rate of core	~ 0 - 50 K/s
Flow velocities through the core	1 - 200 cm/s
Extent of clad oxidation	20 - 100%
Ratio of Hydrogen to Steam in the atmosphere	0 - 10^{10}
Fuel Burnup	1000 - 33000 MWd/ton
Time from SCRAM to core melting	1 - 32 hours

Developments have taken place since the time of the Reactor Safety Study in the analyses of radionuclide behavior after release from the fuel as well as in the description of the release process. Some of these developments are described in Chapters 5 and 6 of this report. A key input to the tools for analysis of radionuclide behavior is the timing of radionuclide release. That is, it is no longer adequate to know what is released and how much is released. It is also necessary to know when radioactive and non-radioactive species are released and how fast they are released.

It is clear, then, that models of radionuclide release must be much more sophisticated than those adequate for the Reactor Safety. Essential aspects of modern release models are:

(1) The models must be sensitive to those features of plants and accidents that make various accidents different. Generic tables of release are inadequate.

(2) Release models must be of mechanistic sophistication compatible with descriptions of subsequent phases of severe accident analyses. That is, seldom will it be adequate to simply assert an integral release fraction without defining the timing and chemical form of the release.

(3) Both radioactive species and non-radioactive species must be considered in the definition of release models.

The objective of this chapter is first to describe the technology available for developing models of release from reactor fuel during core degradation. Meeting this objective will require reviewing some of the fundamental aspects of the release process. The second objective of the chapter is to discuss models that have been developed and used to describe release from the reactor fuel. An attempt is made to critically review these models in light of the discussions of the fundamentals of release. Finally, an objective of the chapter is to specify a release model for the MELCOR code that is at once of sufficient sophistication to meet the essential needs for modern reactor accident analyses yet simple enough to fit within the space and execution requirements of a systems code.

3.2 Nomenclature

Despite criticisms of the work, the framework created for the Reactor Safety Study is useful for describing release of radionuclides and non-radioactive species during in-vessel phases of an accident. As set down in the Reactor Safety Study and subsequently modified (11) release in-vessel can be divided into four regimes:

(1) Gap Release
(2) Diffusion Release
(3) Meltdown Release
(4) Fragmentation and Oxidation Release

Some sense of the magnitudes in each of these release stages is provided in Table 3.2.

As fuel heats, gases within the fuel rod pressurize. At the same time the clad itself weakens. If the ambient atmosphere is at low pressure, the clad will balloon and rupture. Even if this does not occur, eventually the clad ruptures. During normal operation and during early phases of the accident, radionuclides escape the fuel and collect between the fuel pellet and the fuel clad. When the clad ruptures this collected material can suddenly escape the fuel rod. This gap release of radioactivity can itself be divided into two steps -- sudden release during depressurization of the rod and slower release as vapors in the fuel/clad gap diffuse to the point of clad rupture. This release was explicitly considered in the Reactor Safety Study. It is given only limited discussion here. Quite frankly this release is small. It is so rapid that it probably does not require detailed modelling. Uncertainty in gap release pales in comparison to uncertainties in release during subsequent stages of a reactor accident.

Table 3.2

Estimates Made in the Reactor Safety Study [1] of Radioactivity Release During In-Vessel Stages of a Severe Accident

Element	Fraction of the Core Inventory That Escapes the Fuel During [a]			
	Gap Release	Diffusion Release[b]	Meltdown Release	Fragmentation Release[c]
Xe, Kr	0.030	-	0.870	0.9
I, Br	0.017	-	0.883	0.9
Cs, Rb	0.050	-	0.760	-
Te, Se, Sb	0.0001	-	0.150	0.6
Sr, Ba	1×10^{-6}	-	0.100	-
Ru, Mo, Pd, Rh, Tc	-	-	0.030	0.9
Nd, La, Eu, Y, Ce, Pr, Pm, Sm, Np, Pu, Zr, Nb	-	-	0.003	-

(a) Leach release in-vessel was not considered.

(b) Diffusion release estimates were split between Gap release and Meltdown release.

(c) Indicates fraction of the inventory remaining in fragmented fraction of the fuel that is released. Release was presumed in the Reactor Safety Study to be due to oxidation of dispersed debris.

The fuel continues to heat following clad rupture. During this stage radionuclides migrate to the surfaces of the fuel and can escape into the fuel/clad gap. From this gap, the radionuclides can escape the fuel rod. This phase of release was not explicitly included in the Reactor Safety Study analyses. It was defined shortly after the study was published [11]. It has been a regime of great interest and is discussed here.

Further heating of the fuel can lead to melting. Formation of a liquid phase can take place in two ways. Clearly, the fuel or the products of fuel interaction with ZrO_2 produced by steam oxidation of the clad can melt. Nominal temperatures for melting of fuel and UO_2/ZrO_2 mixtures are 3140 K and 2800 K, respectively. Also the clad can melt. But, it has been found that melting clad can interact strongly with the fuel to form materials that start to melt at temperatures as low as 2170 K [12]. Melting of mixtures of ZrO_2, Zr, and UO_2 is often called "liquefaction" to distinguish it from melting of the fuel itself. For most purposes this distinction is useful only for specifying temperature and timing. An attempt is made here to retain this distinction.

Liquefaction of the $ZrO_2/Zr/UO_2$ mixture has also been called "eutectic formation." Since it manifestly is not the "formation of a eutectic," this nomenclature is avoided.

It is possible during the course of an accident that high temperature core debris will interact with liquid water. This might occur if molten or fragmented fuel fell from the core region of the reactor into the water-filled lower plenum of the reactor. It might also occur if water were deliberately injected into the vessel in an attempt to terminate an accident.

The interaction of molten fuel with water can lead to a steam explosion. In the Reactor Safety Study steam explosions were thought to expel finely fragmented debris into oxidant-rich atmospheres. Vigorous oxidation of the debris was estimated to cause extensive radionuclide release. This oxidation release is discussed extensively in Chapter 4 in connection with ex-vessel release and is not treated here.

Fuel/coolant interactions can be benign in the sense that fragmentation of the fuel is not violent and does not involve broad dispersal of the debris. Still this fragmentation can affect fission product release. A very high surface area is created. Rapid flows of steam across the surfaces take place. These conditions are conducive to rapid radionuclide release especially if the debris is still quite hot. Some discussion of release from fragmented fuel is presented in this chapter.

If the fuel is fragmented but not completely quenched by interaction with water, continued release of radionuclides can occur. Until the bed of debris begins to melt, release during

this stage of the accident is similar to the diffusion release defined above though the geometry is quite different. This situation of release from a debris bed can be reached by means other than fuel/coolant interactions. The differences in geometry of debris beds and intact fuel rods lead to differences in the methods for predicting release which are discussed here.

Finally, if the fuel is quenched radionuclide release can occur by leaching into the surrounding liquid water. This type of release has not been a serious concern in accident analyses in the past and is not discussed here. The interested reader is referred to the discussion of ex-vessel leaching release in Chapter 4 and the relevant literature [13-16].

One other note on nomenclature refers to the use of the terms "fission product" and "radionuclide." As stated in Chapter 2 these terms are used interchangeably here even though it is known that not all the radioactive material available in a reactor is produced as a result of fissioning of uranium or plutonium nuclei. The terms are also used to refer to the stable isotopes formed in the decay chains of some important isotopes. This nomenclature ought not cause confusion.

3.3 Fundamentals of the Release Process

Release during core degradation is just the conversion of a material in the core to an airborne material (leaching is ignored here). This process can occur by either mechanical means or as a result of chemical processes that convert a condensed species into a vapor species.

Mechanical aerosol formation does occur during core degradation. Lorenz et al. [17] have observed that a small amount of "dust" is expelled from fuel rods when the clad balloons and ruptures. Analyses show this material to be fuel with particle sizes between 5 and 50 μm. Brockmann and Stalker [18] have observed that coarse particulate is evolved when zircaloy clad is burned in air. The sizes and shapes of these particles could be rationalized only in terms of mechanical comminution of the condensed products of Zr oxidation. It is not difficult to imagine that rapid oxidation of cladding by steam could also produce coarse particulate. Parker et al. [19] have observed that when pressurized control rods rupture an alloy of silver and indium is sprayed about. Mitchell et al. [20] have shown these alloy droplets can have aerosol dimensions. Finally, violent fuel/coolant interactions could produce aerosol-sized particles of water and core debris (see Chapter 4).

In general, release by mechanical mechanisms of aerosol formation are of a sudden, transitory nature during core degradation. The products of the mechanical processes are

coarse and would remain airborne for only short periods of time. Compositions of the mechanically-produced particulate reflect the bulk composition of the parent material. That is, they are neither enriched nor depleted of radionuclides.

Continuing release of material from the core comes from vaporization -- that is, from condensed-to-vapor phase transitions. Vaporization is responsible for most of the radionuclide release during core degradation and may be responsible for most of the total mass release. Vapors, when they condense, form very fine particles which can remain suspended for long periods of time. These particles can be quite enriched relative to the parent material in radionuclides.

Vaporization can be a simple unary process such as:

$$[AB]_{UO_2} \rightarrow AB\ (gas)$$

or

$$[AB]_{UO_2} \rightarrow A\ (gas) + B\ (gas)$$

where the symbol $[\ ]_{UO_2}$ means the condensed species is in the fuel lattice. Vaporization can also be a complex process involving reactions of the condensed species with ambient gases (predominantly H_2 and H_2O) to form a volatile species. Examples of these more complex vaporization processes are:

$$UO_2(c) + 2H_2O \rightarrow UO_2(OH)_2(gas)$$

$$BaZrO_3(c) + H_2O \rightarrow Ba(OH)_2(gas) + ZrO_2(c)$$

$$[CeO_2]_{UO_2} + 2H_2 \rightarrow Ce(gas) + 2H_2O$$

Regardless of their natures, all vaporization processes have some features in common. The driving force for vaporization and the maximum extent of vaporization are specified by difference between existing conditions and thermochemical equilibrium conditions. The rate of vaporization or, equivalently, the rate of approach to equilibrium is limited by kinetic or mass transport factors. The thermochemistry and kinetic factors of release are described in the subsections below.

A. Thermodynamics of Vaporization

Consider the vaporization of a species A from a host lattice. A particular vaporization process might be

$$[A]_{host} \rightarrow A_i(gas)$$

where A_i is some vapor form which may be distinct from the chemical form A dissolved in the host lattice. The driving force for this process is proportional to the difference between the equilibrium partial pressure of A_i in the ambient atmosphere and the actual partial pressure:

$$i^{th} \text{ driving force} \propto [P_i(eq) - P_i(t)]$$

$P_i(eq)$ = equilibrium partial pressure of A_i

$P_i(t)$ = actual partial pressure of A_i

Since $[A]_{host}$ can vaporize by a variety of processes, the total driving force for vaporization of $[A]_{host}$ is given by:

$$\text{driving for release of } [A]_{host} = \sum_{j=1}^{N} [P_j(eq) - P_j(t)]\, K_j$$

where the K_js are proportionality factors and the summation is over all vapor species formed by A.

As a specific example, the vaporization of barium oxide dissolved in a UO_2 lattice is examined. Some vaporization reactions of barium oxide into an atmosphere of steam and hydrogen are:

$$[BaO]_{UO_2} \rightarrow BaO(gas)$$

$$[BaO]_{UO_2} + H_2 \rightarrow Ba(gas) + H_2O$$

$$[BaO]_{UO_2} + 1/2\ H_2 \rightarrow BaOH(gas)$$

$$[BaO]_{UO_2} + H_2O \rightarrow Ba(OH)_2(gas)$$

Then the driving force for barium oxide vaporization is:

$$K_{BaO}\,[P_{BaO}(eq) - P_{BaO}(t)] + K_{Ba}\,[P_{Ba}(eq) - P_{Ba}(t)]$$

$$+ K_{BaOH}\,[P_{BaOH}(eq) - P_{BaOH}(t)]$$

$$+ K_{Ba(OH)_2}[P_{Ba(OH)_2}(eq) - P_{Ba(OH)_2}(t)]$$

There are several features of vaporization processes that are revealed by examining the driving force expression. First, the driving force varies with time. As the actual concentration of the vapor forms approaches the equilibrium concentration (concentrations are related to partial pressures), the driving force, and consequently, the rate of vaporization go to zero. In a flowing system, such as steam/hydrogen mixtures flowing through a reactor core, the driving force for vaporization is spatially dependent. The driving force can be high at the flow entrance where the ambient vapor concentration of species is low. The driving force falls then along the flow path as the ambient concentration of the vapor species builds up toward equilibrium.

A second obvious feature of vaporization is that the driving force for vaporization increases with the number of vapor species that can form. Analyses that omit species with high equilibrium partial pressures can error badly.

Finally, it is essential, obviously, to know the equilibrium partial pressures. The equilibrium partial pressures determine the maximum extent of vaporization as well as figuring in the driving force for vaporization.

Consider again the vaporization of the hypothetical species $[A]_{host}$. The equilibrium partial pressure of A_i is given by:

$$\Delta G_i(T) = -RT \ln [\phi_i P_i(eq)/\gamma_A X_A]$$

where $\Delta G_i(T)$ = standard state free-energy change for the vaporization process

T = absolute temperature

ϕ_i = fugacity coefficient of the i^{th} vapor species

γ_A = activity coefficient of A in the host material

X_A = mole fraction of A in the host material

R = gas constant

The values of $\Delta G_i(T)$ are typically available for most species of interest for reactor accident analyses [21]. If A can be present in only one host material, then X_A can be determined from inventories. When A can partition among several condensed host materials there is an additional problem of determining X_A in each phase. Discussion of this problem is deferred until later in this section.

The activity and fugacity coefficients that appear in the equilibrium are seldom known. There are limited data available for the activity coefficients of binary systems which show the activity coefficients can be functions of the system temperature, composition and pressure. Similarly, data for well-known gases show the fugacity coefficients are dependent on temperature, pressure, and properties of the vapor species.

The dichotomy between the simple elegance of the thermodynamic description of vaporization and the difficulty of implementing this description has been known for a long time. There has been quite a lot of effort expended to model the activity and fugacity coefficients for complicated systems. The experience gleaned from the use of these models provides a data base on their applicable range. These models will be the subject of discussion in the balance of this subsection.

Activity and fugacity coefficients as used above are measures of the deviation from ideality of condensed and vapor phases, respectively. These deviations from ideality arise because the molecular interactions, whether repulsive or attractive, are not the same in mixtures as they are in some pure reference state. It would seem obvious, intuitively, that since interactions among molecules are weak in the gas phase, that deviations from ideality would also be small in the gas phase. Extensive studies over the last 100 years have allowed descriptions to be formulated of even these small deviations from ideality in gases. It is conventional to express the descriptions in the form of an equation of state. Most of the popular models can be expressed in the form:

$$Z = \frac{PV}{RT} = \frac{V}{RT}\left\{\frac{RT}{(V - b)} - \frac{\theta\,(v - \eta)}{(V - b)\,(V^2 + \delta V + \epsilon)}\right\}$$

where $\theta = RT(\delta - \alpha)$

$\eta = (\beta - \epsilon)/(\delta - \epsilon)$

The value of Z, often called the "compressibility factor," for an ideal system would be one for all pressures and temperatures. When the system deviates from ideality, Z becomes a function of both pressure and temperature. Values for the parameters in various forms of the equation of state shown above are listed in Table 3.3. To make the models as useful as possible for the widest varieties of fluids, it has been traditional to express functional forms of the models in terms of the so-called "reduced variables":

$$T_r = T/T_c \text{ and } P_r = P/P_c$$

where T_c = critical temperature

P_c = critical pressure

This is quite useful for well-characterized gases. Unfortunately, most of the gaseous species of interest for the purposes of reactor safety are not well-characterized and the critical temperatures and pressures have never been measured. Even methods to estimate these critical constants require data about the gases that are not known, in general. With the critical constants known, the equation of state must be fit to data to determine quantitative values for the parameters. Usually adequate data for the species of interest in severe accident analyses are not available.

Another popular equation of state is the Virial Expansion:

$$Z = 1 + B/V + C/V^2 + D/V^3 + \ldots$$

In the nomenclature of Table 3.3, the parametric values in this equation of state can be written as:

$$B = b - \theta/RT \qquad C = b^2 - \theta b/RT + \theta\,(\delta + \eta)/RT$$

$$D = b^3 - \theta b^2/RT + \theta b(\delta + \eta)/RT - \theta(\delta^2 - \varepsilon + \eta\delta)/RT$$

The Virial Expansion is of particular interest since it, unlike the empirical equations of state in Table 3.3, has some theoretical significance. The relationship between the parameter B and molecular interactions is well-known [32]. Whereas the detailed molecular properties are seldom known, they can sometimes be guessed. A Virial equation of state truncated after the B/V term is often quite accurate until:

$$P > [T/2]\,[\Sigma\, y_i P_c(i)/\Sigma\, y_i T_c(i)]$$

Table 3.3

Popular Equations of State

Model Name and Year It Was First Suggested	PARAMETERS			
	θ	η	δ	ε
Van der Waals (1873)	a	b	o	o
Berthelot (1900)	a/T	b	o	o
Clausius (1880)	a/T	b	2C	C^2
Redlich-Kwong (1949)	$a/T^{1/2}$	b	b	o
Wilson[1]	$\theta_w(T)$	b	b	o
Peng-Robinson[2] (1976)	$\theta_{PR}(T)$	b	2b	$-b^2$
Lee-Erbar-Edminster[3] (1973)	$\theta_L(T)$	(T)	b	o

1. $P_c\theta_w(T)/R^2T_c^2 = 0.4275[1 + (1.57 + 1.62\ \omega)\ (T_r^{-1} - 1)\ T_r]$

2. $P_c\theta_{PR}(T)/R^2T_c^2 = 0.4275[1 + (0.480+1.574\omega-0.776\omega^2)(1 - T_r^{1/2})]^2$

3. $P_c\theta_L(T)/R^2T_c^2 = 0.45725[1 + (0.37464+1.542266\omega-0.2699\omega^2)(1 - T_r^{1/2})]^2$

where Y_i = mole fraction of the species i in the gas phase. Once an equation of state is known, the fugacity coefficients can be calculated from:

$$\Phi_i = \exp\left[\frac{1}{RT}\int_V^{\infty}\left[\frac{\partial P}{\partial n_i}\right]_{T,V,n_{j\neq i}} - \frac{RT}{V}dV - \ln Z\right]$$

Again, what is simple in concept is difficult to implement, and the lack of appropriate data can make it impossible. Fortunately, the deviations from ideality do become small at high temperatures if the system is far from the critical point and pressures are low. The assumptions of ideality become questionable for fission product vapors only near the upper limit of pressures encountered in reactor accidents ~150 atmospheres.

Theoretically, an equation of state should provide the information necessary to correct nonidealities in the condensed phase as well as the gas phase. Even in the simplest systems, this is difficult to achieve. Consequently, an entirely different formalism has developed for dealing with the condensed phase.

Activity coefficients for the condensed phase are not confidently rationalized away as can be fugacity coefficients. Thermodynamic laws do show that the pressure dependence of the activity coefficients can be separated from the compositional and temperature dependencies. A general expression of the pressure-dependence of condensed phase activity coefficients is:

$$\gamma_i(P) = \gamma_i(P_{REF}) \exp\left[\int_{P_{REF}}^{P} \frac{V_i}{RT}\, dP\right]$$

where P = pressure of interest

P_{REF} = reference pressure where the activity coefficient is known

V_i = partial molar volume of the species i in the mixture

The reference pressure is usually 1 atmosphere. Partial molar volumes of species in a mixture are seldom known. It has become common to assume partial molar volumes are equal to the molar volumes of the pure species and that the partial molar volumes

are independent of pressure. This assumption can only be made if conditions are well-removed from the critical point.

With these assumptions the pressure dependeance of activity coefficients is given by

$$\gamma_i(P) = \gamma_i(P_{REF}) \exp [V_i(P-P_{REF})/RT]$$

This expression shows that activity coefficients increase with pressure. The factor of increase is called the Poynting correction factor. Poynting correction factors for a species with a partial molar volume of 50 cm^3/mole at temperatures of 1000, 2000, and 3000 K are plotted against pressure in Figure 3.1. Most species of interest here would have even smaller partial molar volumes and, consequently, smaller correction factors. Clearly, for systems of interest for reactor safety analyses, the pressure correction of activity coefficients is not especially important.

Quite a variety of models have been developed to describe the compositional and temperature dependence of activity coefficient. The simplest model is, of course, that of the ideal mixture:

$$\gamma_i(P_{REF}) = 1 \quad \text{for all i and T}$$

This model should represent the asymptote that mixtures approach as temperatures increase.

More exotic models to describe activity coefficients at lower temperatures are summarized in Table 3.4. It is not difficult to reach a point at which these empirical models cannot be used because of the lack of data. Models that are based on binary interactions are attractive because the necessary parametric data can be extracted from binary phase diagrams which are far more abundant than detailed activity data. Powers [22] has used the Wilson equation to describe activities in the Ag-In-Cd mixture. Powers and Brockmann [23] have used regular solution models in their model of fission product release during core debris interactions with concrete.

Return now to the example of barium oxide vaporization. Some insight into the vaporization of this species can be obtained by examining the quantity:

$$\Sigma = P_{BaO}(eq) + P_{Ba}(eq) + P_{BaOH}(eq) + P_{Ba(OH)_2}(eq)$$

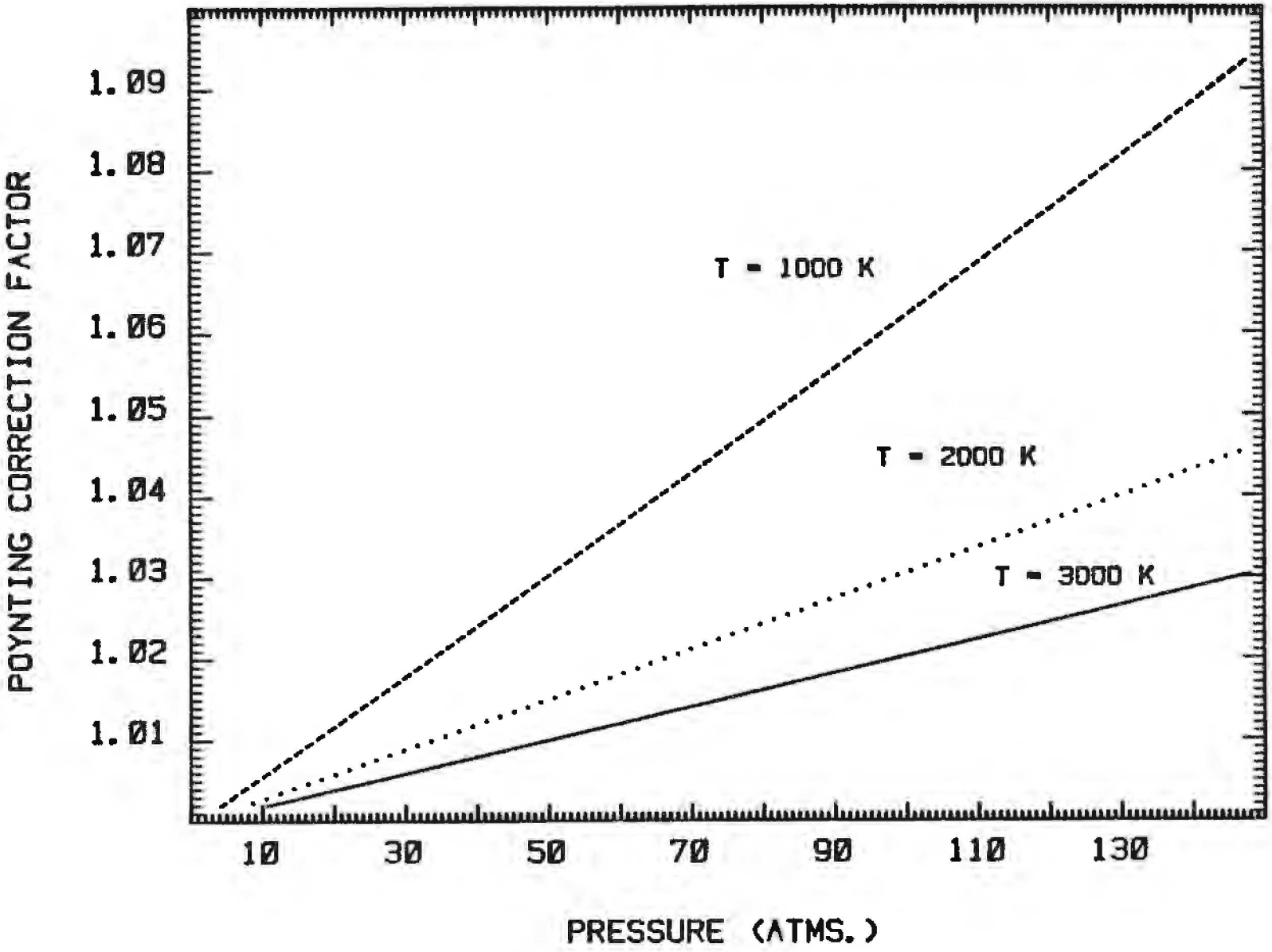

Figure 3.1 Poynting correction factors for several temperatures as a function of pressure

From the discussions above, it is apparent that when ideality is assumed in both the gas and condensed phases then:

$$\Delta G_{BaO}(T) = - RT \ln \left[\frac{P_{BaO}(eq)}{X_{BaO}} \right]$$

$$\Delta G_{Ba}(T) = - RT \ln \left[\frac{P_{Ba} \, P_{H_2}}{X_{BaO} \, P_{H_2O}} \right]$$

$$\Delta G_{BaOH}(T) = - RT \ln \left[\frac{P^2_{BaOH}}{X_{BaO} \, P_{H_2}} \right]$$

$$\Delta G_{Ba(OH)_2}(T) = - RT \ln \left[\frac{P_{Ba(OH)_2}}{X_{BaO} \, P_{H_2O}} \right]$$

Thus,

$$S = X_{BaO} \left\{ K_{BaO} + K_{Ba} \left[\frac{P_{H_2O}}{P_{H_2}} \right] + K_{BaOH} \, P^{1/2}_{H_2} + K_{Ba(OH)_2} P_{H_2O} \right\}$$

where K_i are proportionality factors that are functions of temperature. It is obvious that the vaporization of barium oxide will depend on its concentration in the host material. It also depends on the composition of the ambient gas. The variations in partial pressures of the various barium-bearing species as a function of the P_{H_2}/P_{H_2O} ratio at 2000 K and a total pressure of 10 atmospheres are shown in Figure 3.2. In preparing this figure the chemistry of water and hydrogen at high temperatures was also recognized:

$$H_2 \rightleftarrows 2H$$

$$H_2O \rightleftarrows H_2 + 1/2 \, O_2$$

Table 3.4

Popular Models for Activity Coefficients

Model	$RT \ln [\gamma_k (P_{REF})]$
Ideal	0
Regular Binary	$B (1 - X_k)^2$

Wilson

$$RT \left\{ 1 - \ln \left[\sum_{j=1}^{N} X_j A_{kj} \right] - \sum_{i=1}^{N} \left[\frac{X_i A_{ik}}{\sum_{j=1}^{N} X_j A_{ij}} \right] \right\}$$

where

$$A_{ij} = \exp [-(\lambda_{ij} - \lambda_{ii})/RT] (V_j/V_i) \text{ and } \lambda_{ij} = \lambda_{ji}$$

NRTL

$$RT \left\{ \sum_{j=1}^{N} \left[\frac{X_j \tau_{jk} A_{jk}}{\sum_{\ell=1}^{N} X_\ell A_{\ell k}} \right] + \sum_{i=1}^{N} \left[\frac{X_i A_{ki}}{\sum_{\ell=1}^{N} X_\ell A_{\ell i}} \right] \left[\tau_{ki} - \sum_{j=1}^{N} \left[\frac{X_j \tau_{ji} A_{ji}}{\sum_{\ell=1}^{N} X_\ell A_{\ell i}} \right] \right] \right\}$$

$$\tau_{ji} = (\lambda_{ji} - \lambda_{ii})/RT \qquad A_{ji} = \exp (-\alpha_{ji} \tau_{ji}) \qquad \alpha_{ij} = \alpha_{ji}$$

UNIQUAC

$$RT (\ln \gamma_k^C + \ln \gamma_k^R)$$

where

$$\ln \gamma_k^C = 1 - \phi_k/X_k + \ln [\phi_k/X_k] - \frac{Z}{2} q_k \left(1 - \frac{\phi_k}{\theta_k} + \ln \left(\frac{\phi_k}{\theta_k}\right)\right)$$

$$\ln \lambda_k^R = q_k \left[1 - \ln \left(\sum_{j=1}^{N} \theta_j A_{jk} \right) - \sum_{i=1}^{N} \left(\frac{\theta_i A_{ki}}{\sum_{j=1}^{N} \theta_j A_{ji}} \right) \right]$$

$$A_{ji} = \exp \left[- \frac{(\lambda_{ji} - \lambda_{ii})}{RT} \right] \qquad \phi_i = \frac{X_i r_i}{\sum_{j=1}^{N} X_j r_j} \qquad \theta_i = X_i q_i / \sum_{j=1}^{N} X_j q_i$$

$$O_2 \rightleftarrows 2O$$

$$H_2O \rightleftarrows 1/2\ H_2 + OH$$

$$2H_2O \overset{\rightarrow}{\leftarrow} HO_2 + 3/4\ H_2$$

The results in Figure 3.2 make it apparent that tabulated values of vapor pressures as functions of temperature only are of little value in the analysis of severe accident source terms. The vaporization should be a function of the ambient gas composition. It should also be apparent that within a reactor core the driving force for vaporization may change since the gas composition changes due to reactions such as the steam oxidation of the zircaloy clad on the fuel.

The analyses done for the Reactor Safety Study did consider effects of gas composition on vaporization though the final release fractions were independent of these considerations. However, the analyses done for the Reactor Safety Study restricted attention to oxidation reduction reactions of the type

$$MO_X(gas) + X\ H_2 \rightleftarrows M(gas) + X\ H_2O$$

Thus, for the barium oxide example the formalism of the Reactor Safety Study would yield:

$$\Sigma_{RSS} = [K_{BaO}P_{BaO}(eq) + K_{Ba}P_{Ba}(eq)]\ X_{BaO}$$

A comparison f Σ and Σ_{RSS} is presented in Figure 3.3. The comparison shows that a more complete description of the chemistry can yield higher driving forces for the vaporization of species than might be anticipated from the analyses done in the Reactor Safety Study. Higher driving forces do not necessarily translate into higher extents of release. But, the potential certainly exists for releases much higher than those predicted in the Reactor Safety Study. This possibility, if realized, would be, of course, quite contrary to the "conventional wisdom" that releases predicted in the Reactor Safety Study conservatively bound the actual releases during severe accidents.

The difficulty with the approach used in the Reactor Safety Study is that important vapor phase species were neglected. Vapor phase hydroxides figured prominently in the discussion above for BaO vaporization. The vaporization of many other species can be enhanced by vapor phase hydroxide formation. A general reaction expression for vapor phase hydroxide formation can be:

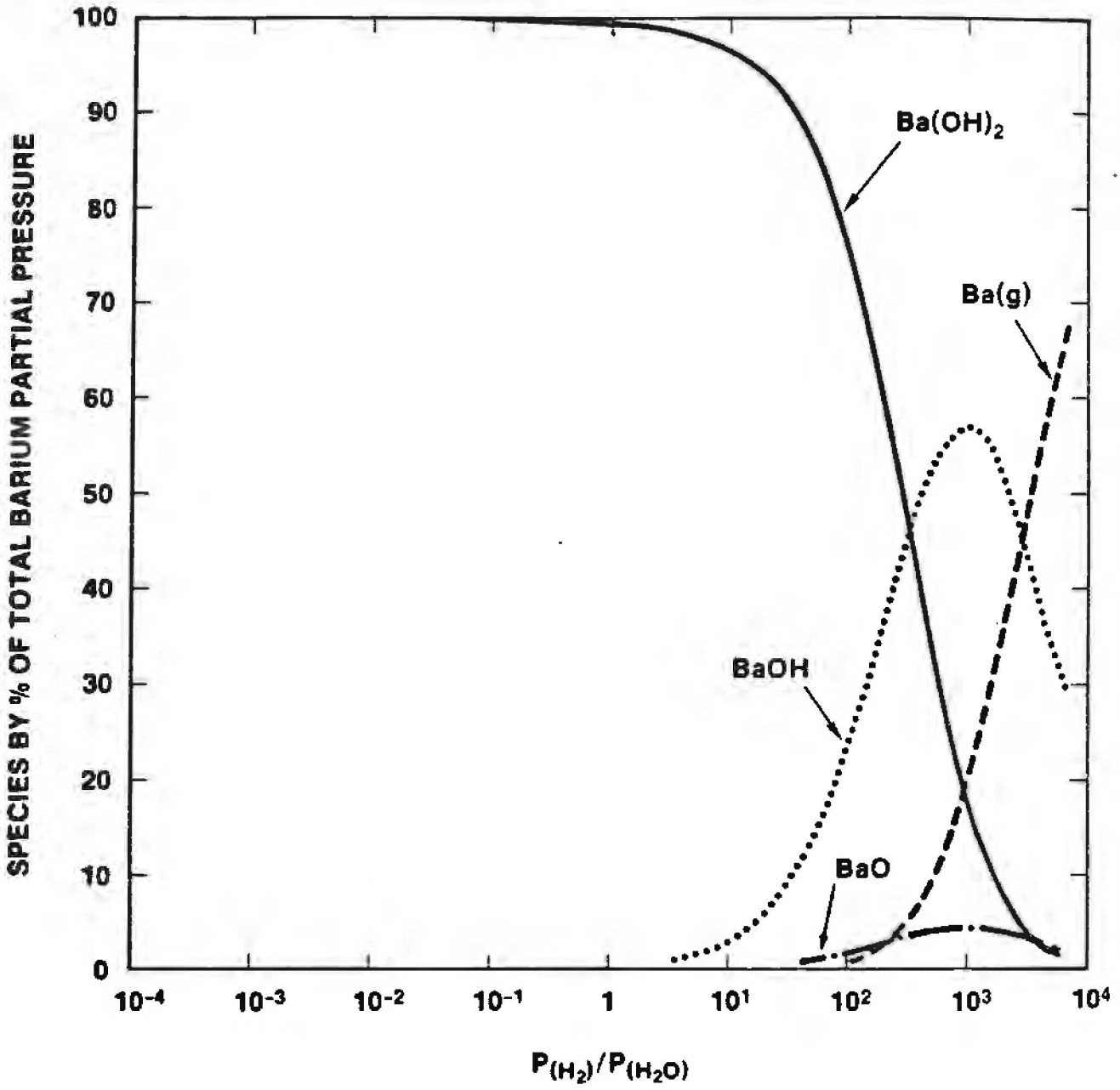

Figure 3.2 Vapor species produced by barium oxide vaporization as a function of P_{H_2}/P_{H_2O} at 2000 K and a total pressure of 10 atmospheres.

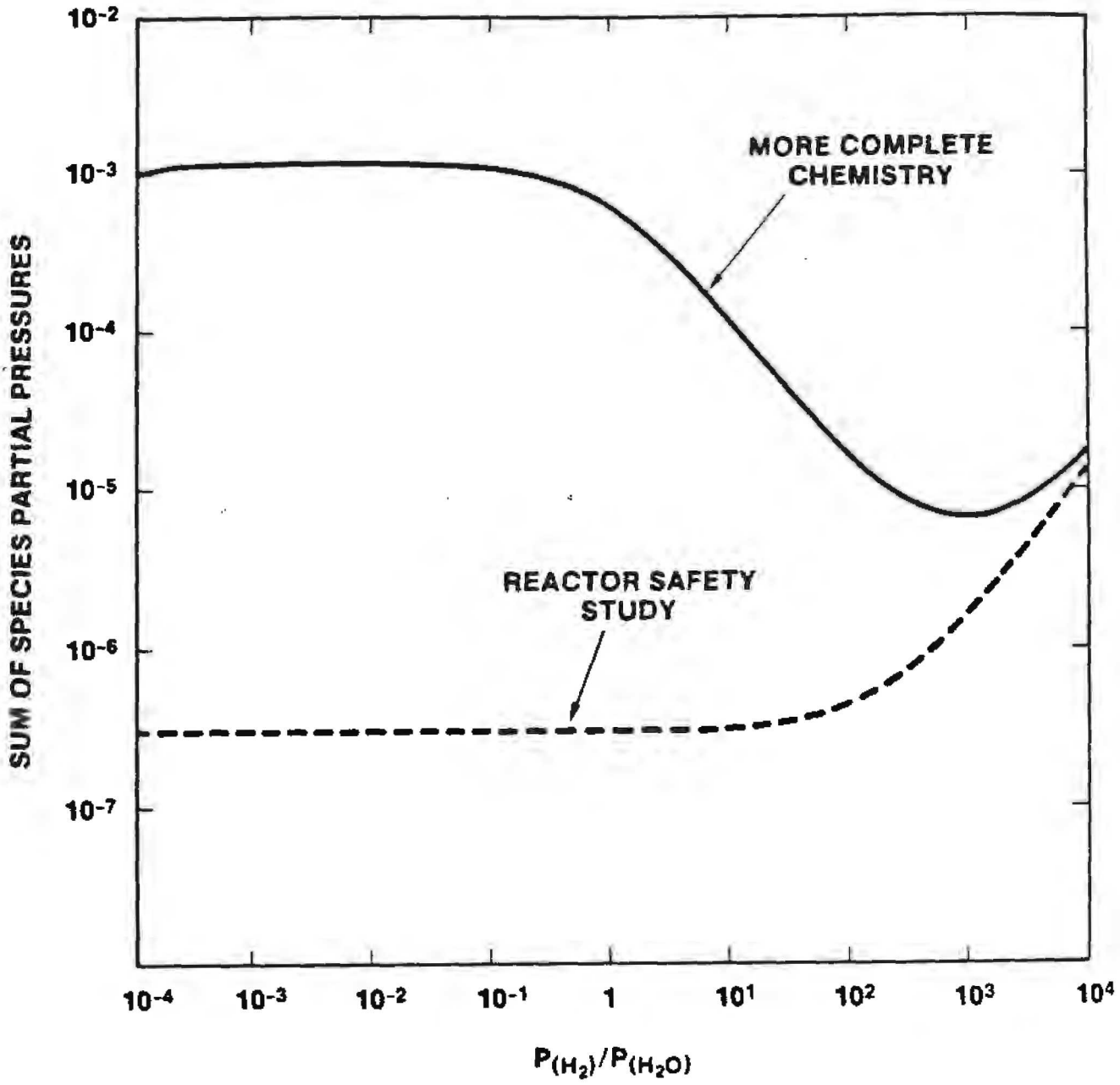

Figure 3.3 Σ and Σ_{RSS} for barium oxide vaporization as a function of P_{H_2}/P_{H_2O} at 2000 K and a total pressure of 10 atmospheres. Σ is shown as the solid line. Σ_{RSS} is shown as a dashed line.

$$MO_y^{(c)} + n\ H_2O \rightleftarrows MO_{(y-n)}(OH)_{2n}(g)$$

and the corresponding equilibrium expression is:

$$\Delta G(T) = - RT\ \ln \left[\frac{P_{MO_{(y-n)}(OH)_{2n}}}{X_{MO_y} P_{H_2O}^n} \right]$$

Consideration of vapor-phase hydroxides is hampered by lack of data. High-temperature chemical studies are usually done in refractory metal furnaces. Because these refractory metals are easily oxidized, the conditions conducive to vapor-phase hydroxide formation have been carefully avoided. By far, the greatest amount of work on vapor-phase hydroxides has been done in the geologic field and in the study of nuclear fallout. What studies have been done show that vapor-phase hydroxides will be important for many of the species of interest for source term development. A list of known vapor-phase hydroxides is presented in Table 3.5. Attempts have been made to predict the existence of vapor phase hydroxides for elements that have not been studied experimentally [21i].

Two other classes of vapor species that were not considered extensively in the development of the source terms for the Reactor Safety Study are the vapor phase hydrides and mixed-vapor species. A general reaction for the formation of vapor-phase hydrides is

$$MO_y(g) + (y + z/2)\ H_2 \rightleftarrows MH_z(g) + y\ H_2O$$

$$\Delta G(t) = - RT\ \ln \left[\frac{P_{MH_2}}{P_{MO_y}} \frac{P_{H_2O}^y}{P_{H_2}^{(y+z/2)}} \right]$$

Hydride formation clearly depends on temperature and the absolute pressures of both steam and hydrogen. The importance of vapor-phase hydrides has not been explored in any significant way to date. Based on inspection of the terms in the free-energy equation above, it would be expected that the contributions to the gas phase made by hydrides would vary markedly over the course of an accident as well as among various accident sequences.

Table 3.5

Some Vapor Species that Were Not Considered in the Reactor Safety Study

Fission Produce Category	Representative Element	Significant Vapor-Phase Hydroxide	Suspected Vapor-Phase Hydride
Alkali Metals	Cs	CsOH, $(CsOH)_2$	
Alkaline Earths	Ba	BaOH, $Ba(OH)_2$	BaH, SrH
Halogens	I		HI
Chalcogens	Te	TeO(OH)	H_2Te
Platinoids	Ru	RhO(OH)	
Early Transition Elements	Mo	$MoO_2(OH)_2$ $CrO_2(OH)_2$	
Tetravalents	Ce		
Trivalents	La	LaO(OH) $La(OH)_2$	
Uranium	U	$UO_2(OH)_2$	
Main Group Metals	Cd, Sn	InOH, $In(OH)_2$	SnH, SbH_3
		SnOH, $Sn(OH)_2$	
Boron	B	H_3BO_3, HBO_2	

Mixed-vapor species are those made of two or more atoms whose vaporization is of interest. These species have not been extensively studied. CsI(g) is the only well-recognized example. Vapor-phase tellurides such as AgTe, SnTe, and SbTe are known but seldom have been taken into consideration in the formulation of source terms. The efficiency with which mixed-vapor species transport fission products will lead to greater interest in these species as results of integral fission product release tests become available and attempts are made to rationalize these results.

Another class of species that has not been considered in the past is ions. Thermal ionization of vapors seldom is a major consideration in typical thermochemical analyses at temperatures less than 2800 K. Ionization would not be important in accident analyses, except that chemistry is taking place in the reactor in an intense radiation field. Though ions formed by the intense radiation are unstable, the continuing exposure to radiation assures that ions are reformed. Thus, a meta-stable equilibrium concentration of ions may well exist in the ambient atmosphere.

Insufficient analyses of the effects of ionizing radiation on chemistry have been undertaken to know if it is an effect of importance. What data are available show that it may be important for iodine and CsI chemistry [33].

Several chemical processes important to the analysis of fission product vaporization have been mentioned to this point. It is useful to examine how well these processes can be analyzed given that the data available are uncertain. The quantitative expression of the equilibria mentioned above can be written in the general form:

$$f = \frac{P_{H_2}^{a}}{P_{H_2O}^{b}} \exp\left(-\Delta G/RT\right)$$

where f is the quantity to be calculated and the partial pressures of hydrogen and steam are provided, but are uncertain, as is the temperature. The quantity ΔG is derived from tabulations and also may be uncertain. The uncertainty in the quantity f derived from these uncertain data, if cross-terms are neglected, is given by:

$$\left[\frac{\delta f}{f}\right]^2 = a^2\left[\frac{\delta P_{H_2}}{P_{H_2}}\right] + b^2\left[\frac{\delta P_{H_2O}}{P_{H_2O}}\right]^2 + \left[\frac{\Delta G}{RT}\right]^2\left[\left[\frac{\delta \Delta G}{\Delta G^2}\right]^2 + \left[\frac{\delta T}{T}\right]^2\right]$$

It can be assumed that partial pressures calculated for severe accident scenarios might be 100 percent in error and temperatures might be 10 percent in error. Then

$$\left[\frac{\delta f}{f}\right]^2 \cong a^2 + b^2 + \left(\frac{\delta \Delta G}{RT}\right)^2 + \frac{(\Delta G)^2}{(RT)} + 10^{-2}$$

Rather high quality free-energy data from the various tabulations will be uncertain to about $\pm RT$ and a typical value of ΔG might be ηRT. Then

$$\left[\frac{\delta f}{f}\right]^2 \cong a^2 + b^2 + 1 + 10^{-2}\,\eta^2$$

where η is a small integer as are a and b.

This derivation illustrates several points:

(1) Uncertainties in even the best thermodynamic data place a constraint on the accuracy of calculated vapor-phase speciation of about ±100%.

(2) Temperatures produced by even crude thermal analyses of the core meltdown process do not have a tremendous influence on the relative uncertainty in calculated speciation of the vapor.

(3) By far and away the greatest source of uncertainty in the vapor-phase speciation comes from the uncertainties in steam and hydrogen partial pressures.

Because the equilibrium speciation of the gas phase plays such an important role in determining the driving force for vaporization, the quality of steam and hydrogen partial pressure calculations is of essential concern. The current state-of-the-art in making these calculations places a very big constraint on the quality of fission product source term calculations. Even so, neglect of these vapor phase speciation issues can lead to errors in the vapor pressures on the order of 10^3 to 10^5 percent, as illustrated by the discussion of Ba vaporization.

To this point, the analysis of thermochemistry has been done by explicitly stating the chemical reactions of interest and evaluating each of these reactions. A key point in the discussions has been the importance of including all the major species. Such a procedure can easily become overwhelming as the number of elements and species grows. A somewhat more formalized procedure is obviously needed.

A variety of procedures for analyses of multicomponent chemical equilibria have been developed over the past years [24-30]. These procedures often are based on minimizing the total free-energy, G, of a system where

$$G = \Sigma\, n_i \mu_i$$

$$\mu_i = G_f(i) + RT\, \ell n\, X_i \gamma_i \quad \text{for condensed phases}$$

$$\mu_i = G_f(i) + RT\, \ell n\, P_i \phi_i \quad \text{for vapors}$$

n_i = moles of the ith species

subject to mass balance constraints:

$$\sum_{\text{all species}} n_i a_{i,e} = B_e \qquad \text{for } e = 1 \text{ to } E$$

where $a_{i,e}$ = number of atoms of element e in the ith species

B_e = moles of element e in the system

and non-negativity constraints:

$$n_i \geq 0 \qquad \text{for all i.}$$

The problem as stated is an N dimensional constrained optimization with linear equality and inequality constraints. A little manipulation of the equations can reduce the dimensionality to E+1. This nearly always has to be done. Practical methods for solving nonlinear optimization problems rarely are feasible for dimensions greater than 100. Species of importance in calculation of phenomenological source terms can easily exceed 300 in number [23].

Direct search and sequential linear programming techniques have been used to solve the optimization problem in the past. Descent techniques are now almost exclusively used. Some of the more popular descent methods are:

(1) STEEPEST DESCENT: Approach to a solution is guaranteed by the first order steepest descent method. The method is not widely used in specialized codes because the rate of convergence to a solution becomes infinitely

slow as the solution is approached. Conservation of mass to any specified accuracy is possible at the expense of increasing number of iterations. The method is attractive because it is robust with respect to initial solutions for the iterative procedure and the programming is simple. The method is used in the PUFF code [31]. Muir has used a modification of the steepest descent method in the CORCON model of core debris interactions with concrete [24]. The method must be programmed with an arbitrary criterion for terminating the iterations and it will yield only approximate answers. The answers can be thermodynamically incorrect because they do not conform necessarily to the Gibbs Phase Rule.

(2) SECOND ORDER STEEPEST DESCENT: Many of the problems of the first order steepest descent method are solved by the second order, or Newtonian, steepest descent method. Convergence to an exact solution that does obey the Gibbs Phase Rule is theoretically possible. In practice, however, the second order method has its own set of problems. Some of these have been described in a recent review [25]. The most germane is that convergence to a solution is guaranteed only if the initial solution for the iterative procedure is within a prescribed neighborhood of the exact solution. With increasing complexity of the problem, the allowed neighborhood can become quite small. This is a serious problem even for stand-alone implementations of the method and would be catastrophic for systems codes using equilibria calculations. Programming of the method is very complicated.

Second order methods are widely used. Second order steepest descent is the basis of the RAND Code [26]. The most up-to-date implementations of the method are the FLUEQU code [27] and the SOLGASMIX Code [28,29]. The implementation in FLUEQU is of particular interest since this code provides a steepest descent routine to generate an acceptable initial solution for the second order iterations. SOLGASMIX has been used in the release estimates done for the IDCOR program [8,32]

(3) OTHER DESCENT METHODS: Conjugate gradient, variable metric, and projected gradient methods are all being researched as methods to solve equilibrium problems. Results to date suggest that only the projected gradient method offers great advantages over the more conventional descent techniques. The advantage of the projected gradient method lies in its ability to

handle mixtures that deviate significantly from ideality. This may not be a tremendously important feature for source term calculations since data necessary to describe strongly nonideal mixtures are not available and ideal mixtures are usually assumed.

An alternative to descent methods for solving complex chemical equilibria problems is the so-called "equilibrium constant method" developed by Brinkley [30]. This method involves converting the optimization problem into a set of coupled nonlinear equations. To reduce the dimensionality of the problem, the nonlinear equations are formulated in terms of a set of "basis" species which are nearly always the most abundant species in the system. The equations are usually solved by a Newton-Raphson method.

This method has lost popularity because of the complexity of programming necessary to define suitable basis species for arbitrary problems. This may not be a severe restriction in codes used to repetitively solve a single problem. The equilibrium constant method is used in the VANESA model of aerosol generation during core debris/concrete interations [23]. For in-vessel phases of an accident, the conditions of the system change enough and are different enough from accident scenario to accident scenario that coding for basis state definition may be needed.

Regardless of the equilibrium calculation method used there are several well-characterized test problems that can be used to assure the validity of the modeling [31]. A completely gas phase problem (pyrolysis of propane) and a heterogeneous problem (iron ore reduction) are particularly useful tests.

The thermodynamic nature of vaporization defines the maximum extent of vapor formation that could occur if time were allowed for the system to equilibrate. A simple method of using this thermodynamic formulation of the vaporization problem could be developed. Steam and hydrogen gases flowing past the melting core could be assumed to equilibrate with the core. These gases would then emerge from the core saturated with the vaporizing species. Simply knowing the saturation partial pressures of the vapor species and the flow rate of steam and hydrogen would be enough to determine estimates of release rates of fission products and nonradioactive materials from the core. Integration of the release rate would yield release fractions.

The saturated gases emerging from the core would produce the maximum amount of aerosol when they cooled sufficiently to initiate condensation of vapor. This in turn would maximize the

natural mitigation of the release by aerosol processes of sedimentation and deposition. Saturated gases would maximize the rate of vapor reactions with structural materials. Large quantities of non-radioactive materials will, of course, accentuate deposition of radionuclide in the reactor coolant system and the reactor containment.

There is no reason to believe that maximizing the estimates of vapor release from the reactor core by relying on thermodynamic calculations of vaporization will lead to an upper bound on the radiological source term. There are, in fact, good reasons to believe the assumption of saturation is not conservative.

The approach to equilibrium is, then, an essential aspect of the problem of fission-product vaporization, even when only bounding approximations are sought. Since the approach to equilibrium is always from below, real gases emerging from the core will not be saturated in vapor. Condensation of this vapor will not lead to maximum aerosol production and natural mitigation of the releases by aerosol processes will not be maximized.

B. Phase Distribution of Fission Products

The composition of condensed phases play important roles in both the thermodynamics and kinetics of vaporization. Were there a single, condensed phase present during reactor accidents, the effects of composition would be easily handled. The initial composition would be known from the inventories and the time evolution of the condensed phase would be a direct consequence of the release process. When more than one phase is present, then volatile materials could exchange between phases as well as vaporize. This too would pose no major difficulty if the condensed phases and the gas phase were all in mutual equilibrium. At equilibrium, the equilibrium partial pressures of vaporous species are the same over all condensed phases. Condensed phase equilibrium is harder to achieve, unfortunately, than is equilibrium between a condensed and a vapor phase. Equilibrium is achieved by movement of species from regions of excessive concentration to regions of deficient concentration (Note that this does not mean movement from regions of high to regions of low concentration. The terms of "excessive" and "deficient" refer to free-energies of the species, not their concentrations). Quite clearly, this movement is slower when it is from one condensed phase to another than when it is to or from a gas phase over a condensed phase.

There are situations in a reactor accident when the duration of condensed phase disequilibrium is the item of principle interest. The process of core melting is a prime example. Equilibrium has not been achieved during this melting process else progression of the melting would cease.

Because condensed phase composition plays such an important role in vaporization, it is necessary to include analysis of the variations in phase composition even when equilibrium has not been achieved. A generally useful assumption to make in multi-phase, dynamic, vaporization problems is that gas phases will equilibrate with condensed phases even when the condensed phases are not in equilibrium with each other. This assumption was made to good use in the CORCON model of core-debris interactions with concrete [24] and the VANESA model of ex-vessel aerosol generation [23].

During severe reactor accidents there are several points at which compositional relationships between several condensed phases, and possible disequilibrium in these compositions, are of great interest for the vaporization problem:

(1) The fuel itself can be composed of several phases

(2) The cladding and the fuel are not necessarily in equilibrium

(3) The fuel melting stage, by definition, involves liquid and solid phases

(4) Once melting is complete there are at least two phases present--a metallic liquid and an oxidic liquid.

If the disequilibrium produced by the fission process is negligible, then reactor fuel during normal operation is probably an equilibrium* system. The fuel has been hot for a long time during normal reactor operations so there has been an opportunity for disequilibrium features to anneal. This may not be entirely true for such things as grain growth and fuel sintering which are slow because of the refractory nature of reactor fuel. But, for chemical mixture effects that are important to the issues of vaporization, the assumption of equilibration of the fuel is probably accurate.

Equilibration of the fuel does not make that fuel single phase. The possible presence of fission gas bubbles entrapped in the fuel has been mentioned and is discussed further below. The fission products of a condensed nature may also cluster together and not dissolve in the fuel. Postirradiation examinations of the fuel show that there are at least three distinct phases in the fuel:

---

* Equilibrium fuel here is used in a chemical thermodynamics sense. "Equilibrium" fuel is a term that also arises in the discussion of the extent of fuel irradiation. This alternate definition ought not be confused with the chemical equilibrium discussed here.

(1) A METALLIC PHASE: This phase is composed of the more noble metals. Some compositions of the metallic inclusions, which are typically a few hundred micrometers in size, in UO_2 fuel are [50,51]:

(a) 60 a/o Mo; 24 a/o Ru; 16 a/o Tc
(b) 55 a/o Mo; 22 a/o Ru; 17 a/o Tc; 6 a/o Rh
where a/o means atom percent.

The elemental yields of the above fission products would typically be: 50 a/o Mo; 30.6 a/o Ru; 12.8 a/o Tc; 6.4 a/o Rh.

(2) AN ALKALINE EARTH PHASE: This phase contains Ba, Sr, and Zr and probably is an alkaline earth zirconate. The phase may exist at low operating temperatures because of the low solubility of Ba and Sr ions in UO_2. At high temperatures of accident transients, this phase may be absorbed into the fuel lattice.

(3) THE FLUORITE PHASE: This is the phase with the fuel and most of the fission products.

In addition to these phases, there have been reports of CsI crystals and Te on the surface of spent fuel [3]. A UPd_3 phase has been reported [52].

This phase partitioning of the fuel does not affect the thermodynamics of vaporization from the fuel since it is an equilibrium system. Quite obviously, it may affect the kinetics of vaporization if the rate-controlling factor is condensed phase mass transport.

An interesting problem that seems not to have been examined systematically is how the phase partitioning of the fuel varies with temperatures. The most obvious species to undergo changes with temperature is molybdenum. If at elevated temperatures it can be stabilized in the fuel matrix as MoO_2, the molybdenum might be extracted from the metallic inclusions.

The clad on the reactor fuel and the fuel are usually separated by a very narrow physical gap. This can prevent the clad from chemically equilibrating with the fuel which, in fact, is probably desirable. But this disequilibrium can affect fission product release. Fission products rejected from the fuel can react and bind with the clad. The release of Te may be particularly sensitive to this type of reaction with the clad.

The disequilibrium between the fuel and the clad becomes a far more serious problem when temperatures reach the point the cladding can melt. Zirconium can reduce UO_2 and even dissolve it. There is evidence that the process can occur in the solid

state [54] but it becomes most dramatic when the clad melts. The process of fuel attack dramatically lowers the temperature at which fuel "melts," and dramatically alters the chemical environment of fission products. The essential features of the process have been studied in some depth by workers at the Kernforschungszentrum Karlsruhe. The essential steps of the process are [55].

(1) As Zr(ℓ) extracts oxygen from the fuel, the wetting of fuel by clad improves and the extraction process accelerates.

(2) When the local oxygen concentration in the fuel has reached the lower phase boundary of the UO_{2-x}/U system, the formation of liquid uranium causes the fuel matrix to desinter.

(3) Fuel particles become entrained in the melt and are rapidly consumed to form a homogeneous (U,Zr)O melt.

This process is discussed in much greater detail elsewhere in this document. Unfortunately, no experimental investigations of the process have examined the behavior of fission products during the attack. Though phase diagrams of the U-O-Zr system have been developed [56], they have not been reduced to a thermochemical characterization that would permit analytic examinations of fission product behavior.

The simple formation of liquid in contact with its solid form may not at first appear to cause phase partitioning of trace impurities such as fission products. In fact, it does, and is the basis of "zone refining" of materials. Consider a simple binary system in which both the solid and the liquid are ideal mixtures. Then the partitioning of the impurity between the solid and the liquid phases is given by:

$$\Delta H_m (1 - T/T_m) + RT \ln (y/x) = 0$$

where ΔH_m = heat of fusion of the impurity

T_m = melting point (K) of the impurity

T = absolute temperature

y = mole fraction of the impurity in the liquid phase

x = mole fraction of the impurity in the solid phase

This simple model allows some conclusions of the effects of species properties on the phase partitioning:

(1) partitioning increases with decreasing heat of fusion

(2) partitioning increases with the temperature and decreases with increasing melting point of the species of interest.

Partitioning between a liquid and a solid phase will have its greatest effect on the rate rather than the ultimate extent of vaporization if that rate is controlled by condensed phase mass transport. The analysis above suggests that those species most susceptible to phase partitioning are the less refractory and usually more volatile species. Analysis with models that do not require ideal mixture behavior shows that some refractory species such as Ba and Sr are quite sensitive to phase partitioning.

As melting of the core progresses to completion, substantial amount of structural steel is melted. The precise ratio of steel and fuel in the resulting melt depends very much on the nature of the core meltdown process. Some bounding estimates have been made [57]. Since steel and molten fuel are largely immiscible, there is the possibility of fission products partitioning between the two phases.

The partitioning of fission products between molten steel and molten UO_2 has been studied experimentally [58]. Results of these studies are shown in Table 3.6. Unfortunately, the partitioning experiments were done in an inert environment. The partitioning would be expected to be a strong function of the oxygen potential of the ambient atmosphere.

The effects of atmosphere composition and pressure of phase partitioning between steel and UO_2 can be estimated at least qualitatively by considering the exchange reactor between the phases to be

$$[MO_x]_{oxide} + xH_2 \rightleftarrows [M]_{metal} + xH_2O$$

where MO_x is a fission product in the oxide form dissolved in the fuel melt and M is the fission product in the metallic state dissolved in the steel melt. Then the partitioning is given by:

$$-\Delta G_f(MO_x) + x\Delta G_f(H_2O) = RT \ln\left[\frac{P_{H_2}}{P_{H_2O}}\right] - RT \ln\left[\frac{\gamma_m X_m}{\gamma_o Y_o}\right]$$

where $\Delta G_f(i)$ = free-energy of formation of the ith species

P_j = partial pressure of species j

γ_m = Activity coefficient of the metallic fission product in the metal

X_m = mole fraction of the metallic fission product in the metal

γ_o = activity coefficient of the oxidic form of fission product in the fuel melt

Y_o = mole fraction of the oxidic fission product in the fuel melt.

C. Kinetics of Vaporization

The need to consider the kinetics of the vaporization process introduces substantial complications in the analysis of radionuclide release. The data requirements expand considerably and the sources of data become quite sparse. But, even an approximate treatment of vaporization kinetics is more realistic than a priori assumption of equilibrium.

The rate limitations to vaporization are due to:

(1) Transport of vaporizing species in the condensed phase to a free surface.

(2) The time required for the condensed-to-vapor phase change of a surface species.

(3) The transport of vapors away from the surface.

The potential always exists for one or more of these three processes to limit the rate of vaporization. Two other processes can be rate controlling for some vaporization processes:

(4) Transport of reactants such as H_2 or H_2O to the free surface where they convert the condensed species into a volatile chemical form.

(5) The rate of heterogeneous reaction at the surface.

Table 3.6

Experimental Partition Coefficients
For Species Between UO_2 and Iron

Species	Wt % in UO_2	Wt % in Fe
Zr*	93.8 - 95.6	6.2 - 4.4
ZrO_2	93.6 - 97.3	6.4 - 2.7
Y_2O_3	93.8 - 97.4	6.2 - 2.6
La_2O_3	100	$\sim 10^{-4}$
CeO_2	97.1	2.9
PrO_2	92.4 - 96.5	7.6 - 3.5
SrO	99.4 - 99.5	0.6 - 0.5
BaO	97.8 - 98.6	2.2 - 1.4
Ru	8.7 - 5.9	91.3 - 94.1
Mo	6.2 - 7.7	93.8 - 92.3
Nb_2O_5	98.9 - 76.9	1.1 - 23.1
Nb	36.4 - 55.7	63.6 - 44.3

* time dependent

The discussions below concentrate on the first three of the rate controlling processes. (The second two are more specialized and all information to date suggests they proceed rapidly during release from reactor fuel.) These rate limitations operate in series, so the slowest will control the overall rate of vaporization. Some simplification of the analysis is possible if one of the above limitations can be selected as rate controlling. Though this is frequently done, it is not a wise procedure. The range of conditions that develop in a given reactor accident scenario or among different accident scenarios is sufficiently broad that it is very likely the rate-controlling step varies.

The first rate-controlling step cited above alludes to one very important feature of the kinetics of vaporization--it depends on the amount of free surface area that is available. The amount of free surface area that can participate in the vaporization process depends, of course, on the nature of core degradation processes. These processes are beyond the scope of this chapter. But, it must be emphasized that data on the variation in the available free surface area is essential input to any kinetic analysis.

To further define the information needs that must be met to conduct a kinetic analysis of vaporization, a simple development is carried out below.

Consider a host material, say UO_2, containing a vaporizing species at an initial concentration of X_b mole fraction. For the species to vaporize, it must be at a free surface. In UO_2, there are a variety of means for a species to get to a free surface. Obviously it can diffuse. It might also nucleate as a bubble in the UO_2 grains or be part of a bubble. This bubble can diffuse to a free-surface. The determination of how species migrate in UO_2 grains has been an area of active research for many years. This topic is discussed at greater length below in connection with the GRASS, FASTGRASS and similar models. For the moment assume that the migration of a species to a free surface can be characterized by a mass-transport coefficient, K_ℓ. Then, the rate at which the species migrate to a free-surface is given by:

$$\frac{1}{A}\frac{dn_s}{dt} = k_\ell (X_b - X_s)$$

where A = free surface area

n_s = moles of vaporizing species transported to the free surface

X_s = the concentration of vaporizing species at the surface

k_ℓ = mass transport coefficient.

Estimating the mass transport coefficient, k_ℓ, is beyond the intent of the simple discussions here. It is determined in reactor accident situations by the behavior of the fuel during the core meltdown process. There are several useful correlations for estimating k_ℓ and others can be derived by analogy with heat transport to the surface.

Quite clearly, the rate of condensed phase mass transport can limit the rate of vaporization. Since the rate is proportional to concentration, at low concentrations this rate can become slow-approaching infinitely slow. Thus, especially for those species released to a significant extent, condensed phase mass transport must be recognized as a limit to the vaporization process.

At the surface, vaporization is driven by a force proportional to the difference between the partial pressure in equilibrium with a mixture of the surface composition, $P_s(eq)$, and the actual partial pressure, P_g. The quantitative expression of the rate of phase change at the surface is often given as:

$$\frac{1}{A}\frac{dn_v}{dt} = \frac{44.33}{(MT)^{1/2}}\left[P_s(eq) - P_g\right]$$

where n_v = moles of species vaporized

M = molecular weight of the vapor species

This is just the Hertz-Knudsen vaporization rate expression. Derivation of this expression requires the assumption that a surface species is nearly gaslike. This might seem a severe assumption. Certainly, evaporation rates from single crystals are often slower than would be expected from the Langmuir expression by factors of 0.1 to 10^{-6} [34]. Metals seem to obey the Langmuir vaporization expression well [35]. Other surfaces with pores and cracks or crystals with high defect concentrations approach to within a factor of 2 the Langmuir expression [34]. Even this deviation can be attributed to failure to properly account for back pressure from vaporized species.

A somewhat superior expression for the rate of surface vaporization that takes into account the necessary difference between the surface temperature, T_s, and the gas temperature, T_g, is [36]:

$$\frac{1}{A}\frac{dn_v}{dt} = \frac{2\alpha}{2-\alpha}(4-\pi)\frac{1}{(2\pi M)^{1/2}}\left[\frac{P_s(eq)}{(RT_s)^{1/2}} - \frac{P_g(T_s)^{1/2}}{(RT_g)^{1/2}}\right]$$

where α is a correction factor that is often near unity though it can become quite small. For the simple derivation here, the Hertz-Knudsen expression will be used. It has been found adequate for a number of systems analogous to release during core degradation. For instance, Ward [37] found it adequate for analyzing vaporization of Mn, Cu, and Cr from iron at 1850 K.

Continued vaporization will occur only if vapor species are swept away from the surface. The rate at which this occurs is given by:

$$\frac{1}{A}\frac{dn_g}{dt} = \frac{k_g}{RT}(P_g - P_b)$$

where n_g = moles of vapor species removed

k_g = gas phase mass transport coefficient

P_g = partial pressure of the vapor above the vaporization surface

P_b = partial pressure of the vapor in the bulk gas

R = gas constant.

Again, the estimation of the mass transport coefficient k_g is beyond the scope of this work. Providing the information necessary to calculate this mass transport coefficient is an essential product of calculations of the core degradation process. There are many correlations from which approximate mass transport coefficients can be derived. For instance, natural convection above a flat plate in laminar flow conditions gives a mass transport coefficient of [38]:

$$k_g = \frac{0.14}{M} \frac{\rho^{7/6} D_{AB}^{2/3}}{P} \left[\frac{K}{c_p}\right]^{1/12} \left[g\beta\frac{\Delta T}{L}\right]^{1/4}$$

where M = molecular weight of the gas

ρ = density of the gas

P = total pressure of the gas

D_{AB} = diffusion coefficient of the vapor in the gas phase

K = thermal conductivity of the gas

c_p = heat capacity of the gas

g = gravitational force

L = length of surface

μ = viscosity of the gas

β = $1/T$

When mass transport in the gas phase is through the pore structure of the UO_2 pellets, then an approximate expression for k_g is

$$kg = \frac{D_{AK}}{rP}$$

where D_{AK} = Knudsen diffusion coefficient for the vapor species

$$= \frac{4}{3}\left[\frac{8RT}{\pi M_A}\right]^{1/2} K_o$$

r = radius of the pellet

Two common expressions for K_o are available:

(1) $K_o = \varepsilon(d/4)$

where ε = porosity of the pellet

d = diameter of the pores

(2) $\frac{1}{K_o} = \frac{128}{9} n_d \frac{\tau}{\varepsilon} r_{gr}^2 (1 + \pi/8)$

where $n_d = 3(1-\varepsilon)/4\pi r_{gr}^3$

$\tau/\varepsilon = D_{AB}/D_{AB}(eff)$

$D_{AB}(eff) = D_{AB}^{-1} + D_{AK}^{-1}$

D_{AB} = diffusion coefficient of the vapor in the ambient gas.

r_{gr} = grain radius

τ = tortuosity of pathway

All correlations of a suitable type involve the diffusion coefficient of the vapor in the gas phase. This diffusion coefficient has not been measured for most of the vapors of interest to the discussions here. Fortunately, the diffusion of gases is far better understood than diffusion in condensed phases. Theories have been developed that relate the diffusion coefficients of gases to the molecular properties of these gases [40]. Unfortunately, these theories require data that are not usually available for vapors of interest here. Some useful approximate descriptions of the gas phase diffusion coefficients include the Gilliland equation [41]

$$D_{AB} = \frac{0.0043T^{3/2}}{P\left[V_A^{1/3} + V_B^{1/3}\right]^2}\left[\frac{1}{M_A} + \frac{1}{M_B}\right]^{1/2}$$

where V_i = the molar volume of the ith gas phase species when condensed,

Recently, Singh and Singh suggested [42]:

$$D_{AB} = \frac{1.79x10^{-3}T^{1.622}}{P\left[V_A^{1/3} + V_B^{1/3}\right]^2}\left[\frac{1}{M_A} + \frac{1}{M_B}\right]^{1/2}$$

At steady state, the rates at which a vaporizing species is transported to the surface, vaporized, and swept away must all be equal:

$$\frac{dn_s}{dt} = \frac{dn_v}{dt} = \frac{dn_g}{dt} = \dot{N}$$

Then, with a little manipulation, the rate of vaporization, $\dot{N}$, is given by:

$$\frac{\dot{N}}{A}\left[\frac{(MT)^{1/2}}{44.33} + \frac{RT}{k_g} + \frac{P_b(eq)}{X_b k_\ell}\right] = P_b(eq) - P_g$$

where $P_b(eq)$ = the equilibrium partial pressure of vapor over a mixture of composition X_b.

This simple development of the kinetics of vaporization was carried out to illustrate the features of a system that affect its vaporization. In summary, these factors are:

(1) temperature

(2) absolute pressure

(3) flow conditions both in the melt and in the gas phase

(4) surface area

(5) condensed phase composition

(6) equilibrium behavior of the system.

Notice that the first four of these essential quantities are not, in general, determined by the vaporizing system. These factors must be supplied. Condensed-phase composition is an essential feature that is, after being initialized, affected by vaporization. If there is but one condensed phase, then the composition of that phase is determined by vaporization. If there are several condensed phases then the equilibrium among these phases and the kinetics of approach for this equilibrium also affect the phase compositions. Finally, the equilibrium thermodynamics of the condensed-to-vapor phase transition, which has to appear in the kinetics because it defines the driving force for vaporization, is an essential part of the vaporization problem.

This simple development of vaporization kinetics also serves to show how rate control of the process can be affected by the conditions of the system. The first term within the brackets of the above rate expression refers to surface vaporization. The form of the term shows that when temperatures are very high and the vaporizing species have large molecular weights, surface vaporization becomes rate controlling. This situation could be expected late in an accident, when meltdown has advanced quite far and temperatures have reached the point where high molecular weight species such as the second row transition metals, actinides, and lanthanides are volatile.

Finally, the explicit appearance of composition in the third term shows that as vaporization progresses, mass transport in the condensed phase becomes increasingly important as a rate-controlling process. Condensed phase mass transport must eventually always become the rate controlling step if the vaporization process continues long enough.

Quite clearly, it is not possible to "legislate" a single rate-controlling step for vaporization.

The rate-controlling processes discussed above do not exhaust the possible sources of rate control. For instance, vaporization is an endothermic process. The heat required to produce a mole of vapor can vary from about 9 kcal to more than 130 kcal. Due to an inability to supply heat to the structures, structural materials in a reactor core can be subject to vaporization rate control. It has been suggested that heat supply may be the rate controlling step in vaporization of silver and indium from control rod materials [22].

D. Condensation and Nucleation

The condensation of vapors is an essential part of radionuclide transport through the reactor coolant system. As such, it is treated in greater detail elsewhere in this document (see Chapter 5). A brief discussion of the condensation of vapors to form aerosols is included here because this process can affect the rates of vaporization from a condensed phase. For the purposes of this discussion, the interest is focused on the homogeneous nucleation of particles from the vapor. For these discussions only species that condense congruently will be considered. Where condensation involves decomposition or reaction of the vapor, the problems of analyzing nucleation are much harder. Unfortunately, incongruent nucleation is also important in reactor safety analyses.

As a gas is cooled or chemical conditions are altered, a point is reached where the vapor is saturated with respect to the pure condensed phase. At this point the vapor can begin to heterogeneously condense on other condensed phases--particularly solid, structural materials. If the gas is cooled at such a fast rate that the condensation rate cannot keep the gas saturated, the gas becomes supersaturated. It is possible then the condensed species could homogeneously nucleate to form aerosols. But, since the free-energy of tiny particles produced by nucleation is increased by surface effects, some high level of supersaturation is necessary before spontaneous nucleation can begin. Even when this level of supersaturation is achieved, there are kinetic barriers that must be crossed to relieve the supersaturated condition. Once nucleation begins, then the vapors in the gas are presented additional surface area for condensation. A competition for the excess vapor in the gas is set up between condensation on structures and condensation on the nuclei.

It is immediately obvious why the issue of homogeneous nucleation is important for the analysis of severe accident source terms. Condensation of vapors on solid surfaces removes these vapors at least temporarily from the inventory of vapors that will contribute to any radiological source term. Vapors that nucleate and vapors that condense on the nuclei remain, at least temporarily, potential contributors to the radiological source term. The questions to be addressed in this section concerning homogeneous nucleation are:

(1) what level of supersaturation must be achieved before nucleation can begin?

(2) what size are the nuclei?

(3) how fast do the nuclei grow?

The thermodynamic condition for equilibrium between a vapor and a condensed phase is equality of the respective free-energies. When the condensed phase is present as a perfectly flat, deep pool, this condition defines the equilibrium vapor pressure. When the condensed phase is present as a finite body such as a small droplet, the curvature of the surface decreases the free-energy of the condensed phase. Consequently, a vapor pressure higher than the equilibrium vapor pressure is necessary to establish a metastable equilibrium with the condensed phase. If the effects of pressure-volume work can be ignored--they are usually small--the partial pressure of vapor, P, in equilibrium with a small droplet of radius r is:

$$\ell n\ (P/P_{eq}) = \ell n\ (S) = \frac{2V\sigma}{rRT}$$

where P_{eq} = normal equilibrium vapor pressure

V = molar value of the condensed vapor

σ = surface tension of the condensed vapor

R = gas constant = 82.06 cm^3/mole-K

The equilibrium defined here is clearly unstable toward fluctuations in either P or r.

This thermodynamic criterion is not enough to characterize the nucleation problem. It is necessary to also know the rate at which nuclei of radius r form. The problem is solved by defining conditions for which the rate of nucleation is detectably large.

Two important theories of nucleation exist. The rate of nucleation of particles of size r in both theories is given by

$$\frac{dn(r)}{dt} = Z\left[\frac{PN_A}{RT}\right]^2 \left[\frac{2\sigma}{\pi}\frac{MW}{N_A}\right]^{1/2} V \exp\ [-\xi]$$

where MW = molecular weight of condensed species

N_A = Avogadro's number

$$\xi = \frac{16}{3}\left[\frac{V_{molar}}{N_A}\right]^2\left[\frac{\sigma}{kT}\right]^3 \frac{1}{[\ell n(S)]^2}$$

k = Boltzmann's constant

Z = parametric discussed below

For practical purposes, it is convenient to assume the nucleating droplets are monodisperse with a radius given by

$$r = \frac{2V\sigma}{RT\ \ell n(S)}$$

Also, the practical, observable, nucleation rate is usually taken to be 1 nuclei per cubic centimeter per second. This definition of a critical nucleation rate closes the problem. The definition is arbitrary, but nucleation rates are so sensitive to the supersaturation ratio, S, that selection of the critical rate is not especially important [46].

The two theories for the homogeneous nucleation rate differ in their treatment of the parameter Z in the above rate expression. In the classic Becker-Doring theory [47], the parameter Z is taken to be 1. This theory has proved quite successful in the analysis of water nucleation and the nucleation of other species that hydrogen bond in the condensed phase.

A more recent development of homogeneous nucleation, the Lothe-Pound theory, takes Z = 10^{17} [48] of 10^{12} [46]. Nucleation of species that do not hydrogen bond typically fall between the predictions of the Becker-Doring and Lothe-Pound.

A parametric difference of 10^{17} or 10^{12} in two theories might seem of serious consequence. In fact, the only significant difference between the two theories is the prediction of the critical supersaturation which are typically different by a factor of 3 or 4 in the two theories. This deamplification of the effect of the value of Z is because of the sensitivity of the nucleation rate expression. This same difference in the predicted supersaturation would be caused by about a 20 percent change in the value of σ, the surface tension of the condensed material. Uncertainties of 20% in surface tension are quite possible since the surface tensions of core materials have not been definitely measured.

Whether a condensing species behaves according to the Becker-Doring theory or the Lothe-Pound theory seems to depend on the surface structure of the condensate. Those species that can orient themselves on the surface to minimize the unsatisfied bonding potential behave in accordance to the Becker-Doring theory. Hydrogen bonding species-such as water or alcohols-are especially good examples of Becker-Doring condensates. Condensing species that cannot, by optimal orientation on the condensate surface, minimize unsatisfied bonding potentials follow the Lothe-Pound theory. Intuitively, there seems to be an extra energy driving force for condensation for these species that is brought on by the advantages of utilizing the unsatisfied bonding potential of species on the surface. Consequently, lower supersaturations are required to initiate nucleation of Lothe-Pound condensate.

Metal vapors cannot, by orientation on the surface of a condensate, relieve unsatisfied bonding potentials. Consequently, condensation of metallic vapors such as Ag, Te, and Cd would be expected to follow the Lothe-Pound theory quite closely.

Condensation of compounds is not as easily predicted. Strongly ionic compounds such as CsI would retain long-range bonding potentials at the surface of a condensate regardless of the orientation of the surface molecules. Condensation of these strongly ionic compounds would be expected to more closely follow the Lothe-Pound theory than the Becker-Doring theory. Covalent compounds, such as Ag_2Te, could, by orientation, relieve some unsatisfied bonding potential. Similarly, vapor-phase hydroxides could achieve some stability by orientation to take advantage of hydrogen-bonding interactions. These species may approach the Becker-Doring model of condensation.

It appears, then, that for reactor safety analyses, condensation properties of vapors produced during heat up and melting of the core could span the entire range bounded by the Becker-Doring and Lothe-Pound theories. In the absence of definitive information on the condensation of particular species or obvious behavior expecting, such as for metal vapors, the two bounds must be recognized. The most apparent difference between the bounds is that the Lothe-Pound theory predicts that lower supersaturations are required to initiate nucleation than does the Becker-Doring theory.

Fortunately, the question of the condensation behavior of vapors during nuclear reactor accidents will probably not be too severe. The rate at which vapors are carried out of the hot core region into cooler environments is fast enough for most accident scenarios that supersaturations high enough to satisfy the more stringent requirements of the Becker-Doring theory are quickly achieved. When this is not the case, the competitive

process of condensation on structures will probably dominate and the homogeneous nucleation questions becomes mute.

The description of nucleation presented here is for homogeneous nucleation and neglects the presence of any foreign bodies. In the environment created during a nuclear reactor accident, foreign bodies that will affect nucleation processes will be present in abundance. Notably, gaseous ions created by the intense flux of radiation can be important nucleation sites. Russel [53] has discussed the theories of nucleation in the presence of gaseous ions. Again, the effects are of theoretical importance but these effects are not overwhelmingly large in comparison to the effects of uncertainties in surface tension, or uncertainties caused by co-condensation of vapors.

The treatment of nucleation has also neglected thermal effects associated with condensation. Clement [125] has shown that the heat liberated during condensation can have an important effect on the competition between nucleation of vapors and condensation of vapors on structures.

Once the nuclei form, if supersaturation has not been relieved, the nuclei grow either by condensation of vapor or by agglomeration. The rate of growth by vapor condensation is given by

$$\frac{dm(r)}{dt} = \frac{4\pi r^2 P}{(2\pi MRT)^{1/2}} (M/N_A)$$

where m(r) is the mass of nuclei of radius r. Growth by agglomeration of nuclei is a more complex problem. While small, the nuclei can be treated as a pseudo-gas. When the nuclei become macroscopic in size ($r \sim 10^{-2}$ μm), then the growth process is probably more accurately described by models of aerosol agglomeration.

The preceding development of homogeneous nucleation was restricted to pure vapors and condensed phases. The problem of mixed condensation involving two or more vapor species is a good deal more complex. Camp [49] is currently developing descriptions of this process.

Even without detailed results for multi-component condensation several important points can be seen. First, from the analyses for pure vapors, it is obvious that surface tension of the condensed phase is an important parameter in determining when a species will nucleate. Since surface tensions do not correlate in a simple way with vapor compositions, there is no reason to suspect that the composition of aerosols will reflect

the composition of the vapors. This is especially true when speciation of vapors and aerosols are of interest. Some species that are quite stable in the gas phase are quite unstable in the condensed phase. Gaseous hydroxides such as $Ba(OH)_2$ and LaOH are good examples of this.

Second, the onset of condensation is brought about by supersaturation of the vapor. Supersaturation can arise from changes in temperature. It can also arise when there is a sudden change in the chemical conditions. Consider the barium oxide vapor pressures discussed above. Suppose vaporization of barium oxide were taking place in a hydrogen rich gas brought about by steam reacting with zircaloy. In hydrogen, the barium partial pressure over barium oxide is quite high. As barium-bearing vapors passed across the boundary layer, they would encounter more oxidizing conditions as steam constitutes more of the gas phase. The equilibrium partial pressure over barium oxide is much lower in the steam-hydrogen mixtures than in nearly pure hydrogen. Consequently, the vapors could be supersaturated and could condense in the boundary layer.

This phenomenon of vapor condensation in the boundary layer is commonly encountered in the ferrous metallurgy [43]. A "fog line" is frequently observed a few millimeters above steel melts. This fog line is created by the condensation of alloy constituents vaporized from the melt. The vaporization of these alloy constituents increases sharply when a fog line appears and exacts a fairly stiff economic penalty, since alloy constituents lost by vaporization are usually quite expensive relative to iron.

Hills and Szekely [44] have found that if the concentration of the vapor is low so it is negligible in the bulk fluid, then the factor of enhancement of the vaporization accompanying fog line formation is approximately:

$$\frac{\Delta H_v}{RT_s}\left[1 - (T_b/T_s)\right]$$

where ΔH_v = heat of vaporization

T_s = temperature of the vaporizing surface

T_b = bulk gas temperature.

When these conditions are not met a more accurate expression, that compares well with data [45] for the factor of vaporization enhancement is [44]:

$$\frac{\frac{\Delta H_v}{C_p}\left[\frac{P_s(eq)}{RT_s} - \frac{P_b(eq)}{RT_b}\right] + (T_s - T_b)}{\frac{\Delta H_v}{c_p} + \frac{RT_s^3}{\xi\, P_s(eq)}\left[\frac{P_s(eq)}{RT_s} - \frac{P_b(eq)}{RT_b}\right]}$$

where

$P_b(eq)$ = equilibrium partial pressure of the vapor (pure) at the bulk temperature

c_p = heat capacity

$$\xi = -T_s \ln[P_s(eq)] + T_s \frac{\Delta S_v}{R}$$

ΔS_v = entropy of vaporization.

E. Summary of the Fundamentals of Vaporization Processes.

The preceding review of the fundamentals of vaporization ought to convince anyone that there are significant complications in estimating the release of radioactive and non-radioactive species during core degradation. A model that pursued each of the topics raised in the review to any depth would be an imposing creation - far too large to be accommodated in a systems code such as MELCOR. No such extensive model has yet been devised. The MELCOR development effort will adopt, in all probability, one of the simplified models of radionuclide release that is now available. The review then provides a framework for ascertaining what features are included and what features are omitted from the available models.

Calculations produced by the MELCOR model should be, of course, as accurate as is feasible. But, equally important, the model should be capable of examining the sensitivity of the calculated results to assumptions concerning the nature of the plant and the accident in question. The review of the fundamentals of vaporization processes defines several features of release processes that ought to be available in the model used in MELCOR:

(1) Release should be constrained by the limits imposed by the thermochemistry of the volatile element.

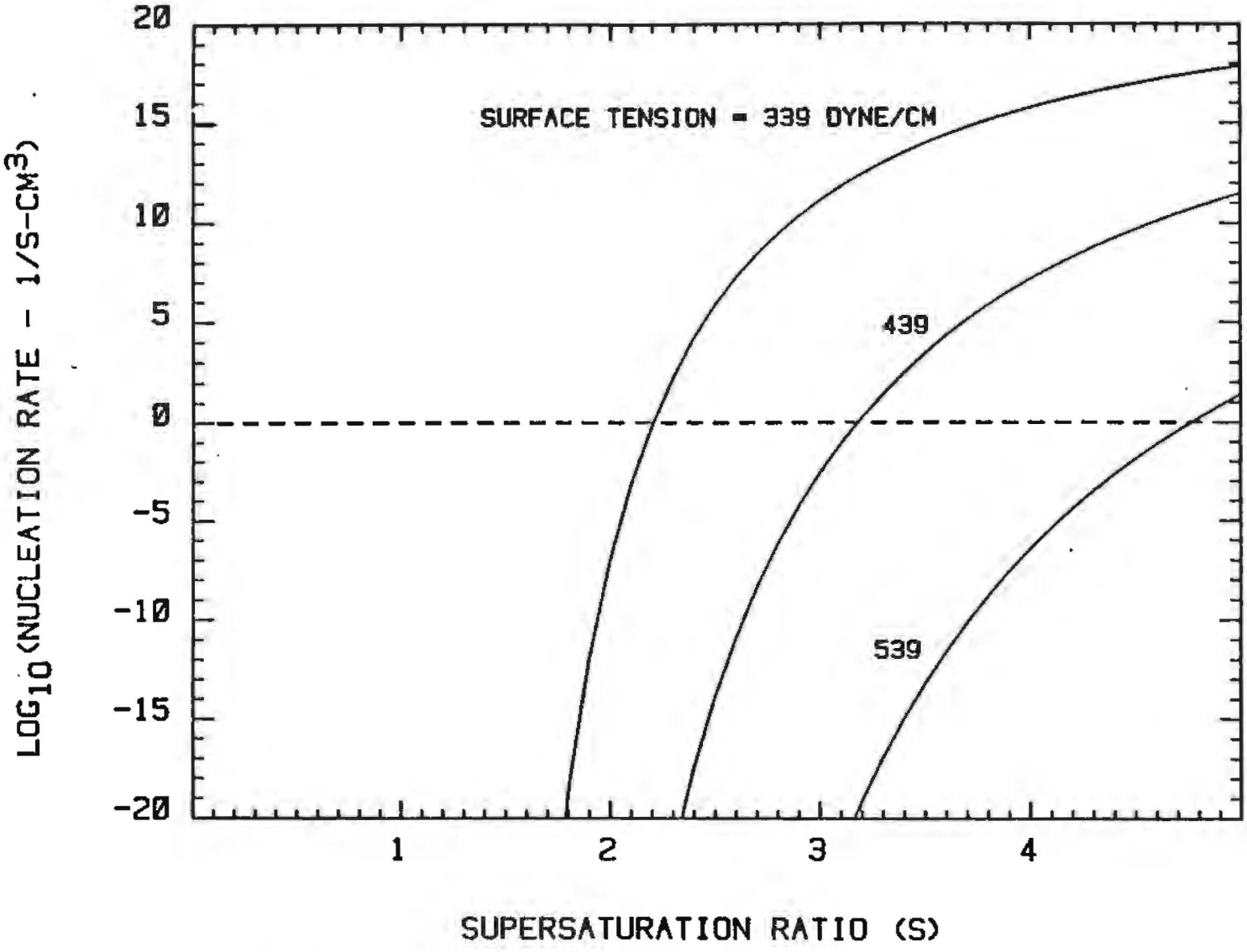

3-4

Figure 48. Nucleation Rate of Tin at 2000 K as a Function of the Supersaturation of the Vapor. Curves are marked by the assumed surface tension of liquid tin.

(2) Release rates ought to be sensitive to pressure, flow velocity, gas composition as well as time and temperature.

(3) Release rates should be sensitive to the melting and slumping of reactor fuel.

(4) Release rates should be dependent on location in the core.

(5) The release model should consider various rate limiting processes such as condensed phase mass transport, surface reactions, and gas phase mass transport rather assuming one of these processes is rate limiting.

3.4 Extant Models of In-Vessel Release

In this section the various models of fission product release that have been used in reactor accident analyses are described. Some attempt is made to comment on how well these models fit with the framework of fundamental properties of vaporization processes outline above.

The organization of the section is along the lines of the description of the in-vessel source term developed in the Reactor Safety Study. That is, the discussions are divided into sections dealing with:

A) Gap Release

B) Diffusion Release

C) Meltdown Release

D) Fragmentation Release

Release of materials from the core is a continuous process. The categorization is done merely to mark major phenomenological events in the core degradation process.

A. Gap Release

The first dramatic event in a reactor core following loss of adequate cooling is the pressurization, expansion (called ballooning), and rupture of the fuel cladding. More detailed accounts of this process are to be found elsewhere [126]. Suffice it here to say that cladding on the fuel can be expected to rupture when the clad temperature is between 700 and 1100°C. The precise temperature of clad rupture depends on the rate the clad is heated, the system pressure, and the gas inventory of the fuel rods.

When the clad ruptures there is a rapid expulsion of fission products as the internals of the fuel rod pressure equilibrate with the primary system atmosphere. Estimation of the release of fission products that occurs during this period might at first appear to be fairly simple annular flow problem with serious wall friction. It must be remembered though that a substantial portion of the void structure in a fuel rod is produced by cracks, gaps, and pores in the fuel itself. Fission products in these crevices can also contribute to the release.

Experimental studies of gap release have been conducted at Oak Ridge National Laboratory [59]. Results of these studies have been used to develop empirical descriptions of the gap release. The entire process is divided into two steps. The first step, called burst release, is due to the pressure equilibration with the primary system atmosphere. This step occurs very quickly, so time resolution of release by this process is not necessary for severe reactor accidents. The mass of the i^{th} radionuclide released during the pressure equalization was found to be:

$$M_i = \alpha_i V \left[\frac{M_o(i)}{A}\right]^{\alpha_i} \exp\left(-C_i/T\right)$$

where

M_i = mass of the i^{th} radionuclide released (g)

V = volume of gas expelled (cm^3) calculated at the system pressure and 273 K

$M_o(i)$ = mass of i^{th} radionuclide in the fuel-to-cladding gap.

A = internal surface area of the cladding

T = absolute temperature at the clad rupture location.

Parametric values, α_i, a_i, C_i, were obtained by fitting the model to data. These values are listed in Table 3.7. The second step in the gap release can be treated as part of the diffusion release discussed next.

Table 3.7

Parameters for the Gap Release Model Developed at Oak Ridge

Parameter	Cesium	Iodine
α	3.49	0.163
∂	0.8	0.8
e	7420	3770
σ	1900	122
γ	19800	14800

Recommended Gap Inventories

Element	% of Total inventory in the Gap*		
	Reference 7	Reference 1	Reference 59
Xe	3	8	1.27
Kr	3	8	1.27
Cs	5	5	0.025
I	1.7	3.3	0.053
Te	0.01		
Sb	0.01		
Ba	0.0001		
Sr	0.0001		

* Note these are the % at the entire rod inventory, not just the node adjacent to the breach.

In addition to parametric values, the model also requires that gap inventories of the radionuclides be provided. Gap inventories are not especially certain. Some values recommended in various investigations are shown in Table 3.7.

B. Diffusion Release

During the time between clad rupture and fuel melting, fission products are slowly released from the fuel. They must be conducted along the cladding fuel gap to a site of clad rupture. Early in the accident, the only opening in the clad that will allow fission products to enter the primary system atmosphere is that created by clad ballooning and rupture. As the accident progresses, multiple openings in the clad may develop. It would be expected that release of fission products during this time period would accelerate, not only because of the temperature increases, but also because continued rupture of the cladding would provide some relief to rate-limiting transport of released fission products to a single rupture site.

The early phases of fission product release by diffusion have been described by the empirical model [53]:

$$M(i) = M_o(i) \quad 1 - \exp\left[-R_o(i)t/M_o\right]$$

where $M(i)$ = mass (g) of the $i^{\underline{th}}$ fission product released at time t (hrs).

$$R_o(i) = \sigma_i[W/P][M_o(i)/A]^{a_i} \exp\left[-\gamma_i/t\right]$$

W = width of the fuel-to-cladding gap (μm)

P = system pressure (MPa)

Again, the model parameters σ_i, γ_i, and a_i were found by fitting the model to experimental data. Some values of these parameters are shown in Table 3.7.

When this and the gap release model have been used for accident analysis, the results are lower than those estimated in the Reactor Safety Study. For a 10-minute transient to 1200°C, the predicted releases of cesium, iodine, and the fission gases

were 0.025 percent, 0.053 percent, and 1.27 percent of the respective inventories. The Reactor Safety Study suggests gap releases of 3, 1.7, and 3 percent of the cesium, iodine, and fission gas inventories, respectively. It should be remembered, however, that the Reactor Safety Study definition of gap release continued longer and to higher temperatures than the above diffusion release model and the preceeding gap release model.

It is clear from the model predictions that diffusion release at temperatures less than 1000°C is small, and this is not the release that is the source of greatest concern in severe reactor accidents. Diffusion release at higher temperatures is faster and more important for accident analyses.

Another empirical model, based again largely on correlation of experimental data, is the CORSOR model [60]. This model was first described in conjunction with the U.S. Nuclear Regulatory Commission's "NUREG-0772" effort to assess the technical basis for changing the source term descriptions in the Reactor Safety Study [5]. It has subsequently been used with the MARCH code for accident analyses. The CORSOR model is intended to treat the entire process of fission product release from the time of clad rupture through rapid diffusion release to gross core slumping and release from molten fuel. A more complete discussion of this model is presented in the subsection dealing with Meltdown Release.

Based on the attempts to describe the process empirically, it might be concluded that the state of knowledge concerning fission product release from hot, but still solid fuel is poor. Within the fast reactor safety and development fields, there has, however, been a considerable effort to develop detailed mechanistic understanding of the process. Models developed in the fast reactor field are now being applied to light water reactor severe accident analysis. For the most part, these models were designed for normal operating conditions and must be extrapolated to severe reactor accident conditions.

The earliest mechanistic models of fission product release were dedicated to determining the release of fission gases Xe and Kr from the fuel and have come to be known as "Booth-type" diffusion models [61,62]. These models consider the fuel pellets to consist of grains that are treated as spheres. Each sphere is isothermal, though a pattern of spheres across the fuel pellet can be used to mimic a thermal gradient. Self-consistent temperature profiles can be calculated with the models given a description of the thermal conductivity of the fuel/cladding gap. None of the Booth-type diffusion models appear to have considered heat input to the fuel from clad oxidation, since for fast breeder reactors, this is not a serious problem.

In the simplest models, transport of fission gases to the grain boundaries is assumed to occur by simple diffusion through a homogeneous medium. If fission gas production can be neglected, as would be the case following SCRAM of a light water reactor, then an approximate solution to the diffusion problem for a grain is:

$$J_i = D_o(i) \exp [-E(i)/RT] \frac{C_o(i)}{a} \{[\pi\tau(i)]^{-1/2} - 1\}$$

where J_i = flux of the ith fission gas out of the grain pores

$D_o(i)$, $E_o(i)$ = parameters characterizing the diffusion coefficient of the i^{th} fission product gas in the fuel

$C_o(i)$ = initial concentration of fission gas in the fuel grain

$\tau_{(i)} = D_o(i)[t/a^2] \exp[- E(i)/RT]$

a = the radius of the sphere that has the same surface to volume ratio as the grain.

This solution is usually applicable up to releases of 80-90 percent.

The models can be used by fitting the model to release data to determine the parameters that characterize the diffusion coefficient of the species in question. Some values of the diffusion coefficient parameters are listed in Table 3.8.

Very early in the use of the Booth diffusion models, it was found that diffusion coefficients determined by different methods were not in good agreement. Quite an extensive base of literature exists showing how corrections to the general diffusion model would yield a more correct description of the release process. The possibility that defects introduced by the fission process trap diffusing species is an especially popular explanation of this problem with the simple diffusion models. Models have been formulated to account for these defects [62] and typically involve two additional parameters.

TABLE 3.8

Parameters for Booth Diffusion Model [65]

Fission Product	$D_o(i)$ (cm/s)	E(i) (Kcal/mole)	Temp Range (°C)
Xe	$3x10^{-6}$ to $8x10^{-3}$	61 to 92	800-1600
Xe	$1.1x10^{-5}$	72	1500-2000
Xe	$1.6x10^{-4}$	67	1500-2000
Xe	$3x10^{-3}$	63	600-2400
I	50	110	900-1500
I	$1.9x10^{-3}$	68	900-1500
I	$3.5x10^{-3}$	87	1500-2000
I	$1.5x10^{-5}$	53.5	1500-2000
I	$1.5x10^{-3}$	59	1400-2500
Te	90	120	1000-1500
Te	0.56	84	1000-1500
Te	$1.5x10^{-3}$	78	1500-2000
Te	$4.2x10^{-5}$	58	1500-2000
Te	$6.6x10^{-3}$	70	1400-2500
Cs	0.04	100	1000-1500
Cs	$4.5x10^{-7}$	40	1000-1500
Cs	$3.8x10^{-3}$	97	1500-2000
Cs	$1.9x10^{-5}$	52	1500-2000
Cs	$8.5x10^{-9}$	6.1	1400-2500
Sr	1600	160	1300-1500
Sr	86	140	1500-2000
Sr	86	140	1500-2000

TABLE 3.8

Parameters for Booth Diffusion Model (Cont.)

Fission Product	$D_o(i)$ (cm/s)	E(i) (Kcal/mole)	Temp Range (°C)
Sr	4.5×10^{-7}	24.4	1400-2500
Ru	4.2	95	800-970
Ru	5.0×10^{-7}	175	1200-1500
Ru	0.08	110	1500-2000
Ru	0.09	110	1500-2000
Ru	8.6×10^{-8}	19.2	1400-2500
Zr	1.2×10^{-9}	45.6	800-950
Zr	1.6×0^{-6}	59.2	1120-1410
Zr,Nb	0.167	104	1400-2500
Ce	7.2×10^{-6}	37	1400-2500
La	2.2×10^{-6}	35	1400-2500
Y	6.8×10^{-8}	46.4	1150-1450
Pr	3.5×10^{-6}	56.8	1120-1420
Mo	3.9×10^{-4}	54	1400-2500
Am	0.03	92	1200-1500
Np	2.9	109	1200-1500
Pa	2.5	107.6	1200-1500
Pm	3.5×10^{-6}	56.8	1120-1410
Pu	0.34	97.3	1200-1500
Tn	0.16	98	1200-1500

Booth diffusion type models probably reached their zenith with the publication of the ANS 6.5 Standard Fission Product Release Model [64]. This model took an empirical approach to diffusion by using release data to define "effective" diffusion coefficients. It also took an important step of including a correction term for the effects of irradiation on the diffusion coefficients. Diffusion coefficients for Cs, I, and Te were determined relative to those found for Xe and Kr. The diffusion coefficients specified by the model are:

$$D_{Kr} = D_{Xe} = \frac{D_o}{a^2} \exp(-Q/RT)\ 100^{(Bu/B)}$$

$$D_I/D_{Xe} = 0.575 \exp(8900/RT)$$

$$D_{Cs}/D_{Xe} = 0.078 \exp(12100/RT)$$

$$D_{Te}/D_{Xe} = 1100 \exp(-12500/RT)$$

where $D_o/a^2 = 0.61\ sec^{-1}$

$Q = 72300$ cal/mole

$B = 28000$ MWd/t

R = gas constant = 1.987 cal/mole-K

Bu = fuel burn up in MWd/t

To summarize, Booth diffusion type models assume the release rate is limited by condensed phase mass transport. No rate limitation arising because vapors must migrate through the pore structure of the pellets or along the fuel-to-cladding gap is recognized. Diffusion coefficients are peculiar to each element and are functions of temperature and, in the case of the ANS 5.4 model, fuel burnup. The operative geometry is the fuel grain which is assumed to be fixed in size.

The difficulties with simple diffusion models of fission gas release prompted a considerable amount of experimental investigation into fission product behavior within the fuel. Improved data led to the definition of "deep" traps and "shallow" traps for fission gases that affected the diffusion process. Eventually, the deep traps were identified as gas bubbles about 10-50 Å diameter.

The more modern of the mechanistic models of fission gas release take into account the behavior of bubbles as well as atomic diffusion, the behavior of grains, and the behavior of bulk fuel. The best known of the modern fission gas release codes is GRASS-SST [63] developed at Argonne National Laboratories. GRASS-SST has been the basis of two other codes that deserve mention:

(1) FASTGRASS: A faster running version of GRASS-SST. Speed was achieved largely by using a single, average but time varying, fission gas bubble size.

(2) PARAGRASS: A correlational model based on an extensive library of computations with either GRASS-SST or FASTGRASS.

Several other models of the same general type as GRASS-SST have been developed [66].

Much of the modeling in both GRASS-SST and FASTGRASS has been included to describe the dynamic behavior occurring during the fission process. This modeling is, of course, not important for severe light water reactor accidents. In the brief description that follows, the discussions focus on the phenomena germane to accidents in which the reactor has been neutronically shut off.

The grains in the fuel are viewed as polyhedra with faces and edges rather than as spheres. Fission gases can migrate in the grain both as atomic species and as bubbles. The diffusivities of atomic species and gas bubbles are:

$$D_{atomic} = 2.1 \times 10^{-4} \exp(-91000/kT)$$

$$D_{bubble} = D_{atomic} (r_{atom}/r_{bubble})^{1.62} Q$$

where

r_{atom} = radius of the atomic species

r_{bubble} = radius of the bubble

Q = correction factor to account for lattice distortion by the bubble.

The correction factor Q is a function of the bubble size, pressure and UO_2 material properties.

Bubbles collect at the faces of the grains, move about, and coalesce. The surface diffusivity of the bubbles is

$$D_i = (2.4 \times 10^{-25}/r_{bubble}) \exp(-10800/RT)$$

The migration of bubbles on the surface of the grains can lead the bubbles to the grain edges which lead to the interconnected network of porosity in the fuel. Bubble density can saturate at the grain surface [$N(max) = 6 \times 10^{12}$ bubbles/m^2], which opens the grain surfaces to the network of porosity. The release can also be accelerated by microcracking of the fuel. All three of these processes are considered in the model.

Obviously, GRASS-SST and FASTGRASS are very sophisticated and very complex codes. When compared to experimental data involving normal operating conditions or relatively mixed transient heating conditions, these codes yield high-quality predictions. Among these predictions is the nature of burnup on release. Burnup is found to increase the rate of release for burnups up to about 10000 MWd/t. At higher burnups the effects are less dramatic. At about 30000 MWd/t, all the effects of burnup on release have been realized.

Accentuation in the release caused by fuel burnup is the result of two processes in the GRASS-type models. As the inventory of fission gases builds with burnup, it becomes easier for bubbles of the fission gases to collect and coalesce to form an interconnected network of porosity that provides release pathways from the pellet. Coalescence is enhanced by grain growth which sweeps bubbles from the interior of grains to the grain boundary. But, grain growth is inhibited by impurities such as radionuclides. Thus, with increasing burnup, it becomes harder for grains to grow. At sufficiently high burnups, a complete network of interconnected porosity may exist in the fuel before an excursion in fuel temperature during an accident begins. Further irradiation will not add to this network of porosity. But, further irradiation will inhibit fission products reaching the porosity because of inhibition to the grain growth process. Thus, there is a limit to the accentuation of release brought on by irradiation.

The severe failing of FASTGRASS, that it only treats fission gases, is being corrected at least to the extent that Cs and I are being included. The way these species are being incorporated is fairly elegant. Both Cs and I are allowed to migrate in the fuel as atomic species:

$$D_I = 2.1 \times 10^{-4} \exp(-91000/RT)$$

$$D_{Cs} = 8.53 \times 10^{-9} \exp(-61000/RT)$$

It is also recognized that these species will tend to vaporize into gas bubbles at the fuel temperatures during accident transients [68]. The partial pressures of these species present in the vapor state as Cs(g), I(g), and CsI(g) are calculated. The condensed form of Cs is taken to be Cs_2UO_4 or Cs_2MoO_4, as dictated by the oxygen-partial pressure of UO_{2+x} calculated with the Blackburn model [67]. The gaseous forms of Cs and I are assumed to saturate the fission gas bubbles and to migrate with these bubbles. It should be noted that there are some questions about the vapor equilibration with gases in bubbles.

The chemistry being added to the GRASS-type models is assumed to be dictated by the fuel. Thus, oxygen potential is created by hyperstoichiometric urania. Condensed forms of cesium are uranates and molybdates. Vapor forms of iodine are I(gas) and CsI(gas). In this regard, two experimental observations are noteworthy. Kleykamp [69] has found cesium in the fuel-to-cladding gap to be in an oxide mixture which contains Zr and Sn but neither U nor Mo. Also, a variety of evidence from studies of Zircaloy stress corrosion cracking suggests that iodine reacts with zirconium probably to for ZrI_2 [70]. The iodides of zirconium appear stable in radiation fields - unlike CsI [71]. Thus, to complete the chemistry in these models may require that clad chemistry as well as fuel chemistry be included.

The GRASS and similar type models assume rate control lies within the condensed phase mass transport to a free surface. The barrier to release caused by transport through the pore structure or along the fuel-to-cladding gap is assumed negligible. The operative geometry for release is, as in the Booth diffusion models, the fuel grain. Unlike the Booth diffusion models grains are allowed to grow. Also, not all grains are equal. Surfaces of the grain must be adjacent to the network of interconnected porosity of the fuel pellet for release to occur. Some chemistry is being incorporated into the models. But, this is chemistry dictated by the fuel and is unrelated to the chemical environment created by the steam and hydrogen atmosphere surrounding the core.

C. Meltdown Release

Meltdown release presumably begins with liquefication of the fuel. Distinguishing this stage of release from release while the fuel is solid makes good physical sense. Mass transport in

the condensed phase should greatly accelerate with the formation of liquid. The nonideality of liquid mixtures is typically much less than in solid mixtures so significant changes in the thermodynamic driving force for release would be expected. Finally, the cladding should have lost its integrity by the time of fuel melting so any rate limitation posed by transport of vapor species to a rupture in the clad has disappeared.

As noted in the discussion of phases present during an accident, there is some ambiguity about when meltdown release should start because of liquified clad attack on the fuel pellets. There is presumably some transient period in which there is the potential of rate limitation by both diffusion from an eroding solid to the liquid phase, and through liquid phase to a free surface.

Clad attack on the fuel could result in chemical transformations of the radionuclides that could effect release. For instance, noble metals such as Ru, Rh and Pd present in the fuel as isolated nodules might dissolve in the molten clad. Dissolution, as noted in section III-A, ought to reduce the driving force for vaporization of these species. Refractory oxides such as BaO might be reduced to the metallic state by clad attack. Since the metal is more volatile than oxide, release of barium might be accentuated by liquefication.

Experimental evidence on the effect of liquefication is mixed. Apparently, out-of-pile tests with highly irradiated fuel rods reveal no dramatic change in release when liquification occurs [86]. In-pile tests with low irradiation fuel rods show a dramatic effect [87].

Modeling of the meltdown release has been attempted many times. Only a few of these attempts are described here.

The Reactor Safety Study Model. To assess the magnitude of fission product release during the melting phase of a severe reactor accident, a series of thermochemical calculations were done in the Reactor Safety Study to determine the equilibrium partial pressure of fission-product-bearing vapors. The vapor-phase chemistry of the fission products was restricted to simple oxidation-reduction:

$$MO_x + H_2O \rightleftarrows MO_{x+1} + H_2$$

Activity coefficients were taken to be unity and pressure invariant (ideal mixture assumption). Temperatures were fixed at 3100 K. An unlimited supply of 1000 psia steam was assumed.

Rate control was assumed to be due to the limitations of surface vaporization, so:

$$R_i \ (g/cm^2\text{-}s) = 0.01 \ P_i(eq) \ [M_i]^{1/2}$$

where M_i = molecular weight of the dominant vapor species of element i

R_i = release rate of element i

P_i = equilibrium partial pressure of the vaporizing species.

The results of these analyses tempered with some laboratory data, were used in an undetermined way to define release fractions for elements during the meltdown process. Time resolution of the release was obtained by determining with the antecedent of the MARCH code when a node within the core melted. Upon melting, this node was assumed to release the entire proportion of the meltdown release fraction that could be ascribed to the node.

The Reactor Safety Study model of release was intended to yield an upper bound. Since behavior of the released material as it passed through the primary system into containment was not carefully treated, release rates were not of great concern. The restrictions on the vapor phase chemistry imposed on this model raise questions as to whether an upper bound release was really determined by this model. Neglect of non-radioactive materials also makes the model useless for modern source term analyses.

The Light Bulb Model. The "Light Bulb" Model of fission product release is mechanistic in the sense that it assumes gas phase mass transport is the rate-controlling process in release [72]. The model could be called semiempirical, in that it does require one experimentally determined release parameter. The rate of release is given by the expression for gas phase mass transport rate control into a bulk gas with negligible fission product content:

$$\frac{1}{A}\frac{dn(i)}{dt} = \frac{K_i P_i(eq)}{RT}$$

where $n(i)$ = moles of the i^{th} species released

A = surface area

$P_i(eq)$ = equilibrium partial pressure of the i^{th} species.

The rate parameter is specified to be

$$K_i = D_{ig}/\delta$$

$$D_{ig} = \frac{0.001858\ T^{3/2}\ (1/M_i + 1/M_g)^{1/2}}{P[(\sigma_i + \sigma_g)/2]^2}$$

P = total pressure

M_i = molecular weight of the vapor phase fission product

M_g = molecular weight of the ambient gas

σ_i and σ_g = collision parameters for the gaseous molecules

δ = parameter determined from experimental release data.

The empirical parameter is theoretically dependent on the temperature, gas composition and pressure, and the nature of the released species. In practice, δ is determined from one data point in a data set of interest. When this parameter is determined, the model does quite a good job correlating experimental data (see Figure 3.5).

The "light bulb model" presents an alternative to all the previously discussed models. Rate control lies in the gas phase mass transport away from the free-surface rather than condensed phase mass transport to the free-surface.

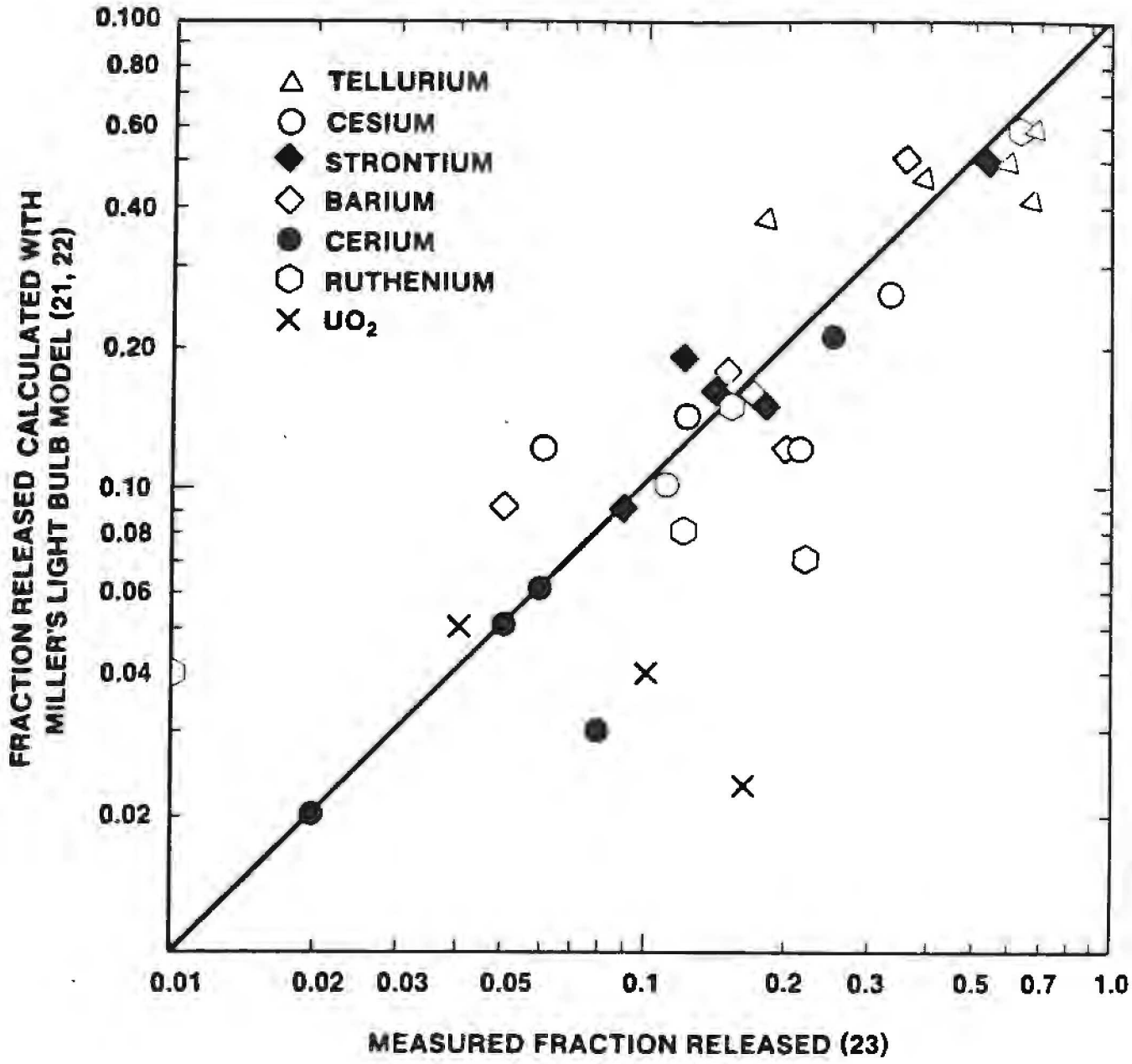

Figure 3.5. Comparison of Observed Releases of Fission Products from UO_2 at Temperatures between 2273 and 2473K with those calculated with the Light Bulb Model.

The IDCOR Model. IDCOR [32] has developed a release model based on a suggestion by Cubicciotti [73] that fission product release is controlled by sintering of UO_2. Sintering of UO_2 is accelerated in steam [74, 75]. Cubicciotti argues that the rate of sintering in steam is correlated with the rate of UO_2 oxidation by steam. He then used oxidation rate data by Bittel et al. [76] and Jain's short-cylinder diffusion model [77] to derive a release expression for fuel pellets in steam:

$$F_i(t) = 1 - [1 - 4(\tau_H/\pi)^{1/2}][1 - 4(\tau_\rho/\pi)^{1/2} + \tau_\rho]$$

where $F_i(t)$ = released fraction of the i^{th} species

$\tau_H = Dt/H^2$

$\tau_\rho = Dt/r^2$

$D = 0.0099 \exp(-28000/T)$ m^2/s

T = absolute temperature (K)

H = length of a fuel pellet ~ 13×10^{-3} m

r = radius of a fuel pellet ~ 6.4×10^{-3} m

t = time (s)

When the ambient atmosphere is inert or reducing, Cubiciotti favored use of Malen's UO_2 grain growth model [78] to predict release:

$$F_i(t) = 1 - [1 + 2kt/d_o]^{-3/2}$$

where $k = 1.46 \times 10^{-8} \exp(-32100/T)$

d_o = initial grain size ~ 1×10^{-5} m

Cubiciotti does not provide an indication of how he would alter the grain growth rates with fuel burnup.

A comparison of releases obtained with Cubiciotti's inert and steam atmosphere models is provided in Figure 3.6. The presence of steam accelerates release by about a factor of 100 at temperatures of 1300-1700K. Steam has a decreasing effect on release as temperatures rise.

As written, the models by Cubiciotti really apply only to fission gases. For more refractory species, the release fractions are reduced by a factor of

$$1 - \exp(-P_i/P_T)$$

where P_T = total pressure

P_i = equilibrium partial pressure of the pure species at temperature T.

For the IDCOR implementation of Cubicciotti's model, SOLGASMIX [28,29] was used to calculate the equilibrium partial pressures of the refractory species.

The IDCOR model presents yet another approach to kinetics of vaporization. Here rate control is limited by the diffusion of a reactant into the host material. Release is then independent of the radionuclide in question except for the dependence of the equilibrium partial pressure. The analysis of the equilibrium partial pressure is completely different than that used in connection with the GRASS code. The partial pressure is independent of the fuel and very dependent on the ambient atmosphere composition. The IDCOR model does not provide an explanation of how cladding affects the release.

The IDCOR model ought to be considered a mere hypothesis. When compared to data, the model at best provides an upper bound on these data. Examination of data in detail shows release has not proceeded as has been hypothesized in the model.

3.5 The CORSOR Model

The CORSOR model [5,7] is part of the U.S. NRC's current Accident Source Term Reassessment effort. CORSOR is used in conjunction with the MARCH model of core degradation [78] and an ad hoc model of gap release to predict both radionuclide and non-radioactive species release within the reactor vessel during a severe accident. As currently used, release predictions with CORSOR are made only when the core is intact, though it may be melting or liquefying. Once core material slumps, release calculations are usually terminated. However, in some cases, the release calculations have been continued up to the point of melt penetration of the reactor vessel.

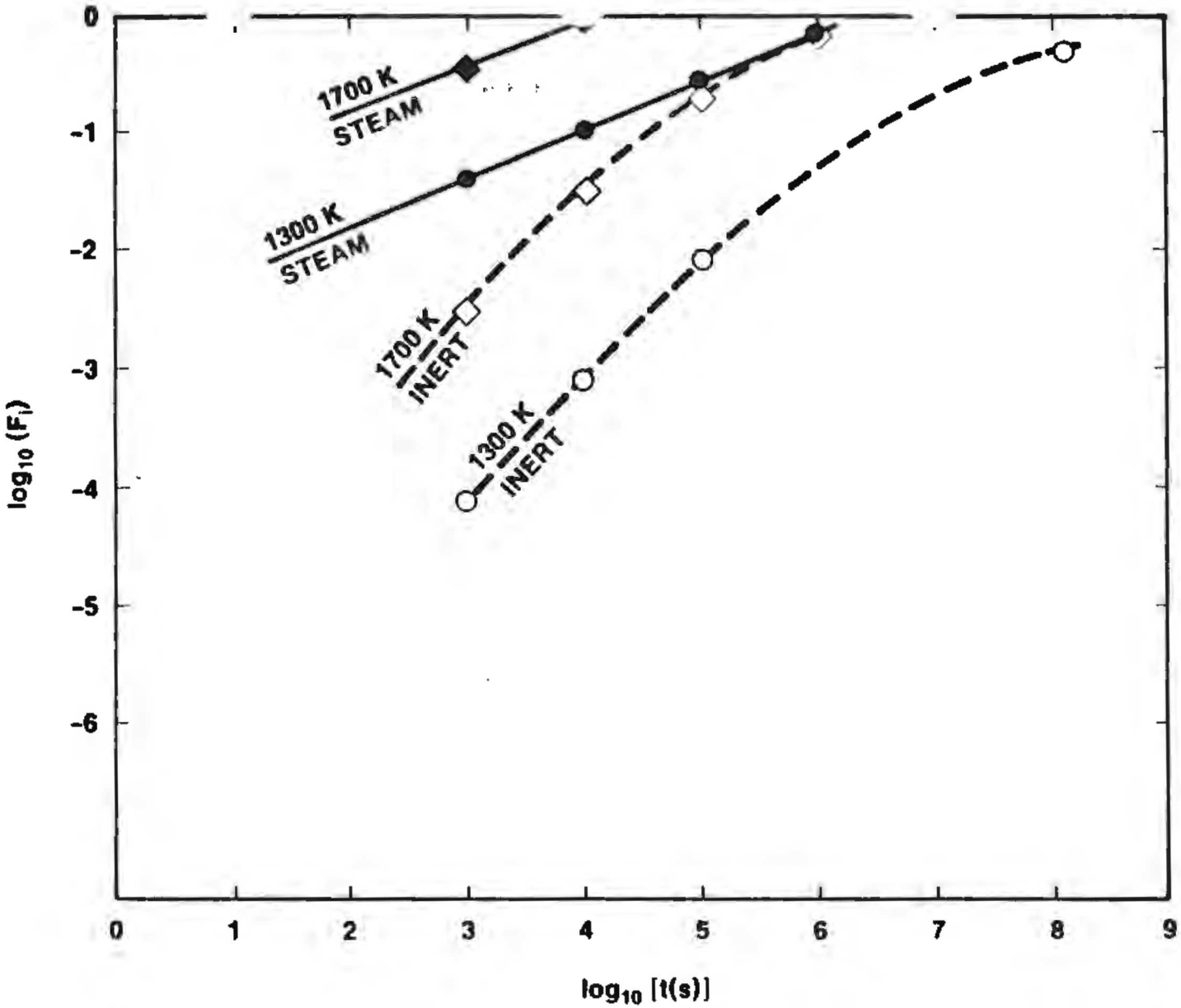

Figure 3.6 Comparison of Cubicciotti's Models of Fission Gas Release in Steam and Inert Environments.

The CORSOR model is an empirical correlation of a variety of experimentally determined release fractions. Most of the data that are the basis for the CORSOR model come from the SASCHA tests at the Kernforschungszentrum in Karlsruhe, West Germany [79-85] and the hot cell tests (HI and HT Series) done at Oak Ridge National Laboratory [86-89,91,92]. The SASCHA tests used simulated fuel doped with fission products to a level expected for fuel with a burnup of 44000 MWd/t. The samples were heated under a variety of atmospheres at pressures up to 2 bars. The Oak Ridge tests used irradiated fuel rods heated in atmospheres initially composed of steam and an inert carrier at a pressure of about 1 atmosphere.

To derive the model it was assumed that release could be described by the first-order rate expression

$$\frac{dF_i}{dt} = - K_i(T)\ F_i(T)$$

where

$K_i(T)$ = temperature-dependent release rate coefficient for the $i^{\underline{th}}$ element

$F_i(T)$ = fraction of the $i^{\underline{th}}$ element remaining in the fuel at time t.

The temperature dependence of the release rate coefficient was assumed to be:

$$K_i(T) = A_{ij} \exp(B_{ij}T)$$

where T = temperature in Celsius

A_{ij} and B_{ij} = release rate parameters for the $i^{\underline{th}}$ species in the $j^{\underline{th}}$ temperature regime.

Temperature regimes used in CORSOR are:

(1) 900 - 1400 °C
(2) 1400 - 2200 °C
(3) > 2200 °C

The parameters in the release expression were evaluated by comparison to experimental data. These data are, in all cases, the integral release achieved after a protracted exposure of a sample to elevated temperatures. Consequently, it is necessary to integrate the release rate to make the comparison to the data. Where temperature changes are involved in the sample's history, these changes were assumed to proceed at a linear rate:

$$T = \alpha + \beta t$$

Then the release rate expression is easily integrated to:

$$\frac{F_i(0) - F_i(t)}{F_i(0)} = 1 - \exp\{(H_{ij}/G_{ij})(1 - \exp[G_{ij}t])\}$$

where $H_{ij} = A_{ij} \exp(\alpha B_{ij})$

$$G_{ij} = \beta B_{ij}$$

The unusual form of the temperature dependence of the release rate coefficient in the CORSOR model was chosen obviously to facilitate the integration during changes in temperature.

A set of parameter values for the CORSOR model is shown in Table 3.9. CORSOR is being maintained. As new experimental data are obtained, improved parametric values are derived. Consequently, the values listed in Table 3.9 may not be the latest version of the parameter set for CORSOR. One recent modification of the CORSOR model has been made to accommodate the possibility that Te released from the fuel may bind to unoxidized Zr metal and not escape the core. To accommodate this possibility, the release rate coefficient of Te is reduced by a factor of 40 whenever 5% or more of the Zircaloy clad has not been oxidized [94].

CORSOR is the only release model that treats all the diverse elements of interest for reactor accident analyses. It is also the only model other than the Reactor Safety Study model that treats release over the entire temperature range of interest. The close relationship between the model and experimental data also provides an attraction. By empirically correlating data, the need to identify and to describe a host of detailed mechanisms is avoided. At the same time the coupling to experimental data makes the applicability of CORSOR without

extrapolation quite limited. For instance, all data that are the basis for CORSOR were acquired at pressures of less than 2 atmospheres whereas reactor accidents can involve pressures in excess of 100 atmospheres. Unappreciable errors may arise then when CORSOR is applied to pressurized accident sequences.

Because CORSOR is the state-of-the-art model for analysis of release during core degradation including melting, it has been examined closely in the past. A variety of criticisms have been formulated.

One of the most frequently raised criticisms is the unusual temperature dependence of the CORSOR release rate coefficients. Most would prefer to see an Arrhenius temperature dependence:

$$K_i(T) = K_o(i) \exp(-E_i/RT)$$

where $K_o(i)$ and E_i are release rate parameters for the i^{th} species and T is the absolute temperature rather the temperature in Celsius used in CORSOR. First, it must be noted that the Arrhenius form of the temperature dependence is no more "fundamental" nor theoretically sound that the temperature dependence used now in CORSOR. Especially when applied to reactions involving solids or liquids, the Arrhenius temperature dependence is just an empirical correlation of experimental observations. To be sure this base of experimental observations is quite large.

Second, it should be noted that the CORSOR temperature-dependence can be readily converted to have the Arrhenius form. This can be done retaining the temperature regimes defined by the model (which may indeed have some physical significance) of by fitting to a single Arrhenius expression for the entire temperature range of interest. Results of such a conversion are shown in Figure 3.7. Parametric values derived by the conversion are shown in Table 3.9.

The activation energies, E_i, available from the Arrhenius expression are sometimes interpreted as physically significant. For instance, Andriesse and Tanke [95] have noted the similarity of the activation energies for Cs, I, Xe, and Kr release to the activation energy for oxygen diffusion in the UO_{2+x} lattice. Such interpretations may be useful for some insights about further experiments. They ought not be the basis for extrapolation of the CORSOR model. The parameters [$K_o(i)$ and E_i] are simply too highly correlated and the data base too sparse to attach much credence to the interpretation of the E_i values.

In application, CORSOR is used on a node-by-node basis in accident analyses. However, the release from a given node in the reactor core is treated as independent of releases from

Table 3.9

Coefficients for the CORSOR Model

Element	1173-1673 K CORSOR		1173-1673 K Arrhenius		1673-2473 K CORSOR		1673-2473 K Arrhenius		2473 K CORSOR		2473 K Arrhenius		Single Arrhenius Coefficient	
	A_i	B_i	K_i	E_i	A_i	B_i	K_i	E_i	A_i	E_i	K_i	E_i	$K_i^o(min^{-1})$	E_i (cal/mo
Cs	$7.53x10^{-12}$	0.0142	$3.9356x10^{4}$	55573	$2.02x10^{-7}$	0.00607	$2.5248x10^{4}$	55091	$1.74x10^{-5}$	0.0046	$4.608x10^{5}$	68640	$3.504x10^{4}$	55591
I	$7.02x10^{-9}$	0.00886	45.042	34674	$2.02x10^{-7}$	0.00667	$2.5248x10^{4}$	55091	$1.74x10^{-5}$	0.0046	$4.608x10^{5}$	68640	$1.108x10^{4}$	50371
Xe	$7.02x10^{-9}$	0.00886	45.042	34674	$2.02x10^{-7}$	0.00667	$2.5248x10^{4}$	55091	$1.74x10^{-5}$	0.0046	$4.608x10^{5}$	68640	$1.108x10^{4}$	50371
Kr	$7.02x10^{-9}$	0.00886	45.042	34674	$2.02x10^{-7}$	0.00667	$2.5248x10^{4}$	55091	$1.74x10^{-5}$	0.0046	$4.608x10^{5}$	68640	$1.108x10^{4}$	50371
Te	$3.88x10^{-12}$	0.01350	3405.7	52833	$9.39x10^{-8}$	0.00630	2844.2	52035	$1.18x10^{-5}$	0.00411	$2.424x10^{4}$	61328	$6.085x10^{3}$	54590
Sr	$2.74x10^{-8}$	0.0036	$2.6464x10^{-4}$	14089	$2.78x10^{-11}$	0.00853	4319.1	70453	$9x10^{-7}$	0.0037	217.72	55210	23.786	46717
Ba	$7.50x10^{-14}$	0.0144	652.626	56356	$8.26x10^{-9}$	0.00631	259.966	52117	$1.38x10^{-5}$	0.0029	51.387	43273	524.4	55476
Sb	$1.9\ x10^{-12}$	0.0128	280.085	50094	$5.88x10^{-9}$	0.00708	3534.8	58477	$2.56x10^{-6}$	0.00426	$1.1502x10^{4}$	63566	2602.2	56512
Ag	$3.88x10^{-10}$	0.0135	3405.7	52833	$9.39x10^{-8}$	0.00630	2844.2	52035	$1.18x10^{-5}$	0.00411	$2.424x10^{4}$	61328	$6.085x10^{3}$	54590
Mo	$5.01x10^{-12}$	0.0115	26.877	45006	$5.93x10^{-8}$	0.00523	29.80	43197	$3.7x10^{-5}$	0.0020	1.2587	29843	24.381	44057
Ru	$1.36x10^{-11}$	0.00768	0.004312	30056	$1.36x10^{-11}$	0.00768	81.422	63433	$1.4x10^{-6}$	0.00248	0.5827	37006	3.776	49402
Zr	$6.64x10^{-12}$	0.00631	$6.409x10^{-5}$	24695	$6.64x10^{-12}$	0.00631	0.209	52117	$1.48x10^{-7}$	0.00177	$1.5164x10^{-3}$	26411	0.01374	39977
UO_2	$5x10^{13}$	0.00768	$1.585x10^{-4}$	30056	$5x10^{-13}$	0.00768	2.9935	63433	$5x10^{-13}$	0.00768	$1.261x10^{+5}$	114599	1.090	55811
Clad Zr	$6.64x10^{-12}$	0.00631	$6.409x10^{-5}$	24695	$6.64x10^{-12}$	0.00631	0.209	52117	$1.48x10^{-7}$	0.00177	$1.5164x10^{-3}$	26411	0.01374	39977
Clad Sn	$1.9x10^{-12}$	0.0128	280.085	50094	$5.88x10^{-9}$	0.00708	3534.8	58477	$2.56x10^{-6}$	0.00426	$1.1502x10^{-4}$	63566	2602.2	56512
Struct Fe.	$6.64x10^{-12}$	0.00631	$6.409x10^{-7}$	24695	$6.646x10^{-12}$	0.00631	0.00209	52117	$1.48x10^{-11}$	0.00177	$1.516x10^{-5}$	26411	0.0001374	39977

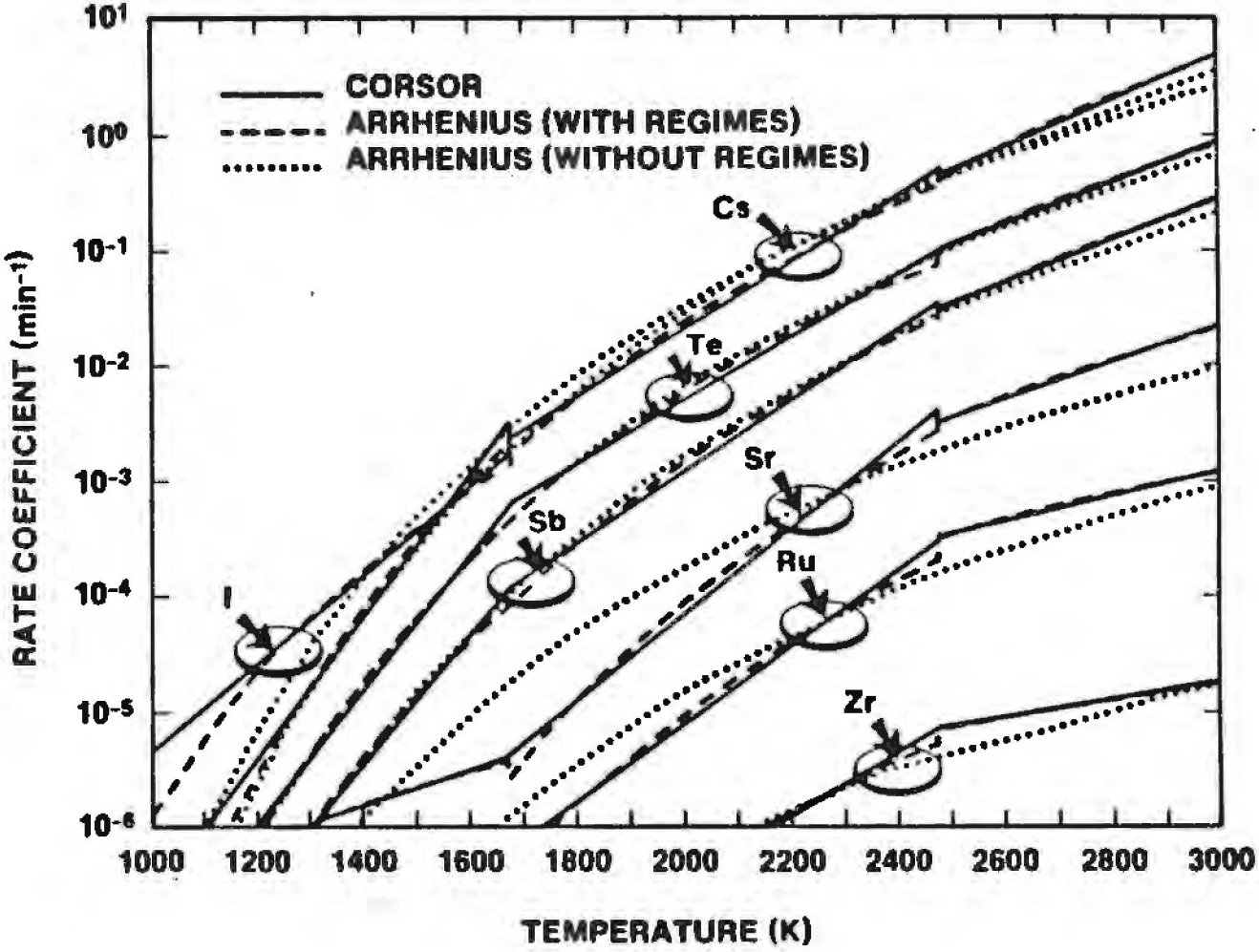

Figure 3.7. Comparison of the Temperature Dependencies of Release Rate Coefficients Calculated with the Original CORSOR Model and with Parameters For the Model Modified to Have an Arrhenius Temperature Dependence

adjacent nodes. This violates the thermodynamic principle described in Subsection III that release rates ought to be proportional to the difference between vapor concentrations at equilibrium and vapor concentrations in the ambient gas. Releases from a given node ought not be independent of releases from adjacent nodes.

CORSOR contains no explicit representation of surface area. Minimal changes in the surface areas for release--such as those caused by grain growth, microcracking of the fuel, etc.--may be hidden within the empirical coefficients of the model. More substantive changes in surface area such as those that accompany fuel melting or liquefaction cannot be treated easily by altering the release coefficients. No formalism is included in the model to describe dilution of the condensed phase as clad and fuel mix and melt. In many applications to date [7], CORSOR predictions of release have been stopped when core slumping is assumed to begin. Continued application of CORSOR as molten core material begins to slump and the surface-to-volume ration of the material changes dramatically is clearly in error.

The CORSOR model relies on a lot of physical and chemical processes being adequately represented by the assumed rate expression and empirical parameters. Unfortunately, the first-order rate expression assumed in the model is not a very flexible format for the representation of these processes. Of all the empirical descriptions of heterogeneous processes, some of which are listed in Table 3.10, the hardest to rationalize is the first-order rate description [96]. Data available to date for evaluating the CORSOR model have been integral releases measured, typically, posttest. These data do not test the validity of the first order assumption. Some examination of the first order assumption is made below.

3.6 Discussion of the First Order Assumption

The assumption that the kinetics of radionuclide release from the fuel is dependent to first order on the radionuclide concentration in the fuel is widely accepted. This acceptance arrives despite the fact first order dependence has not been demonstrated experimentally. Sophisticated fuel behavior models do not predict a first order dependence. The assumption of first order behavior is apparently an approximation made to simplify the modeling. Models involving first order composition dependence and Arrhenius-type temperature dependence are notorious for being sufficiently flexible to "fit" data involving radically different mechanisms. It is of interest then to ascertain if the assumption of first order kinetics is likely to have any appreciable effect on predictions of radionuclide release.

Table 3.10

Some Kinetic Expressions for Solid Decomposition Reactions

	Mechanism	F(f)	G(f)
1.	Prout Tompkins	$f(1-f)$	$\ln(f/(1-f))$
2.	Topotactic	$f^{2/3}(1-f)^{2/3}$	
3.	1D Diffusion	$1/2f$	f^2
4.	2D Diffusion	$-1/\ln(1-f)$	$(1-f)\ln(1-f) + f$
5.	3D Diffusion	$3/2((1-f)^{-1/3}-1)$	$(1-2f/3) - (1-f)^{2/3}$
6.	D3	$1.5/((1-(1-f)^{1/3})/(1-f)^{5/3})$	$((1+f)f^{1/2}-1)^2$
7.	D5		$(1/(1-f)^{1/3}-1)^2$
8.	P4	$4(1-f)(-\ln(1-f))^{3/4}$	$(-\ln(1-f))^{1/4}$
9.	P2	$2(1-f)(-\ln(1-f))^{1/2}$	$(-\ln(1-f))^{1/2}$
10.	P3	$3(1-f)(-\ln(1-f))^{2/3}$	$(-\ln(1-f))^{1/3}$
11.	P4/3	$(4/3)(1-f)(-\ln(1-f))^{1/4}$	$(-\ln(1-f))^{3/4}$
12.	P2/3	$1.5(1-f)(-\ln(1-f))^{1/3}$	$(-\ln(1-f))^{2/3}$
13.	First Order	$1-f$	$-\ln(1-f)$
14.	Second Order	$(1-f)^2$	$f/(1-f)$
15.	2D Phase Bound	$2(1-f)^{1/2}$	$1-(1-f)^{1/2}$
16.	3D Phase Bound	$3(1-f)^{2/3}$	$1-(1-f)^{1/3}$
17.	Jander Approx.	$3(1-f)^{2/3}/2(1-(1-f)^{1/3}$	$(1-(1-f)^{1/3})^2$

Data for the release of cesium from irradiated fuel obtained in tests at Oak Ridge National Laboratory are shown in Table 3.11. These data were obtained by heating fuel in flowing steam to an arrest temperature. The sample was held at the arrest temperature for a prescribed length of time and then cooled. At least early in the cooling, temperatures fell at a near constant rate. Heating rates, arrest temperatures, and hold times for the ORNL experiments are shown in Table 3.11.

The heating and cooling ramps of the tests pose an added complexity to analysis of the release data. For some of the tests, the durations of the heating and cooling stages constitute a major portion of the time the irradiated fuel specimen was at elevated temperatures. To properly analyze these test results the release that must have occurred during heating and cooling should be recognized.

Assume the rate of radionuclide release is described by the expression:

$$\frac{df}{dt} = K_o \, F(f) \, \exp\,[-E/RT_a]$$

where f = fraction of the radionuclide that has escaped the fuel

$F(f)$ = function that describes the compositional dependence of the release rate

R = gas constant

t = time

T_a = arrest temperature (K)

K_o and E = parameters to be determined from release data.

If the temperature is fixed, the release rate is easily integrated to yield

$$\int_{F_1}^{F_2} \frac{df}{F(f)} = K_o \exp\,[-E/RT_a]\,(t_2 - t_1)$$

where F_1 = release that occurred before the arrest temperature, Ta, was reached

Table 3.11

Some Data From Out-of-Pile Tests of Radionuclide Release from Irradiated Fuel Rods [97]

Test	T_a (K)	Δt (min)	β (K/s)	β' (K/s)	Fraction of Cs Released
HI-1	1673	30	0.97	0.6	0.0204
HI-3	2273	20	2.78	1.67	0.577
HI-4	2123	20	1.93	1.58	0.319
HT-1	1598	10	9.9	12.2	0.00224
HT-2	1718	7	11.1	11.1	0.0964
HT-4	1673	0.33	18.5	11.0	0.06108

T_a = Arrest temperature.

Δt = Time the fuel was held at the arrest temperature.

β = Rate of temperature rise during heatup of the fuel to the arrest temperature.

β' = Rate of temperature fall during cooling at the fuel from the arrest temperature.

F_2 = release that occurred by the end of the time the sample was held at the arrest temperatures

t_1 = time the arrest temperature, T_a, was reached

t_2 = time when cooling the sample from the arrest temperature began.

To treat the case when the sample is being heated, it is convenient to transform the release kinetics expression. Assume temperature increases at the constant rate ß to the arrest temperature T_a. Then,

$$\frac{df}{dT} = \frac{K_o}{ß} F(f) \exp(-E/RT_a) .$$

Integration of this expression yields

$$\int_{F_0}^{F_1} \frac{df}{F(f)} = \frac{K_o}{ß} \int_{T_o}^{T_a} \exp(-E/RT)dT$$

where F_0 = release that had occurred prior to the start of the experiment which is typically assumed to be zero

T_o = temperature of the fuel at the start of the experiment.

The integral on the right-hand side of the above equation cannot be reduced to elementary functions. A variety of approximations for this integral have been found. Coats and Redfern [98] described the most popular approximation:

$$\int_{o}^{T} \exp(-E/RT)dT = \frac{RT^2}{E} (1 - 2RT/E) \exp(-E/RT)$$

Gorbaschev [99] has suggested a somewhat more accurate approximation:

$$\int_0^T \exp(-E/RT)dT = \frac{RT^2}{(E + 2RT)} \exp(-E/RT)$$

Van Tets [100] has derived an expansion that allows the integral to be evaluated to any desired level of accuracy.

With expressions for the integral of the temperature dependence during isothermal periods and during periods of heating at a constant rate, it is possible to fit a model to the Oak Ridge data. Here three models of the composition data are considered:

1. First order dependence:
   $F(f) = 1 - f$

2. Three-dimensional phase boundary model:
   $F(f) = 3(1 - f)^{2/3}$

3. Three-dimensional diffusion model:
   $F(f) = 1.5[(1 - f)^{-1/3} - 1]^{-1}$

The first of these models is, of course, the conventional assumption. The motivation for the second model, three-dimensional phase boundary motion, is the suggestion by Cubicciotti that release is controlled by sintering. It must be emphasized, though, that this second model is not either identical to or a reformulation of Cubicciotti's model. The motivation for the third model, three-dimensional diffusion, is the formulation of release processes in the GRASS-SST code where diffusion of radionuclides is heavily emphasized. Again, this third model is not intended to be an approximation or a simplification of the GRASS-SST code.

The parameters K_o and E were adjusted for each of the three models to get a best fit in the least squares sense to the cesium release data in Table 3.11. The quality of the fit was judged from the chi-squared statistic

$$x^2 = \sum_{i=1}^{N} (f_{obs} - f_{calc})^2$$

where: N = number of data points

f_{obs} = observed release fraction

f_{calc} = calculated release fraction.

Parametric values derived in this way and the values of the chi-squared statistic are shown in Table 3.12.

Table 3.12

Kinetic Parameters and the Chi-Squared Statistic for the Quality of Fit of Three Models to the Cesium Release Data

Model	$K_o(S^{-1})$	E(cal/mole)	x^2
First order	0.855	34,617	0.073
3d phase boundary	1.732	41,513	0.0527
3d diffusion	7869	86280.7	0.04297

The first thing to note about results in Table 3.12 is that both the three-dimensional phase boundary model and the three-dimensional diffusion model actually fit the data better than does the first order model. If linear statistics are actually applicable to this least-squares fitting problem, then the quality of the fits are not significantly different. To a relatively high level of confidence it can be said all three models fit the data equally well.

The next feature of the results to note is the value of the parameter E. Values of E, the activation energy, differ by only about 15 percent for the first order and the three-dimensional

phase boundary models. But, the three-dimensional diffusion model yields an activation energy nearly twice that obtained with the first order model. This illustrates a very important point. The activation energy for the release of radionuclides cannot be derived from integral release data if the compositional dependence of the release rate is not known. Physical interpretation of activation energies derived from data, assuming a particular compositional dependence of the release rate, is an idle exercise. Activation energies derived in this way are simply empirical parameters and ought not to be used as a basis for extrapolating away from the underlying data base.

So far, it has been shown that alternative models will describe the release data as well as does the assumed first order model. What remains to be done is to show whether the precise form of the model will make any significant difference to release predictions. To do this, a single node of fuel in a degrading core is considered. Release from this node is treated as it is in the CORSOR model. That is, release is strictly a function of time and temperature. It is independent of flow, gas composition, pressure, or release from adjacent nodes. Two situations are considered then:

a. The node heats so that the temperature rises at a constant rate of 4 K/s to 2500 K. The temperature is then fixed at 2500 K.

b. The node temperature rises at 4 K/s to 2000 K and thereafter rises at 0.3 K/s until it reaches 2800 K.

The first of these scenarios is reminiscent of the core heatup predicted with the MARCH code [78]. The alternative scenario reflects somewhat the effects that natural circulation and the like are thought to have on core heatup [101]. Cesium releases predicted with the first order and the three-dimensional diffusion models for the two heating scenarios are shown in Figures 3.8 and 3.9. In general, the diffusion model yields higher release rates early in time and lower releases late in time than does the first order model. The maximum release rate during the MARCH-like heating scenario is nearly 10 times the maximum release rate in the heating scenario based on calculations that include natural circulation. In the natural circulation case, cesium release ontinues for nearly twice as long by first order kinetics than by diffusion kinetics.

3.7. Modifications of the CORSOR Model for use in the MELCOR Code

None of the models described in the preceding section are entirely satisfactory. Clearly, the GRASS-SST and FASTGRASS

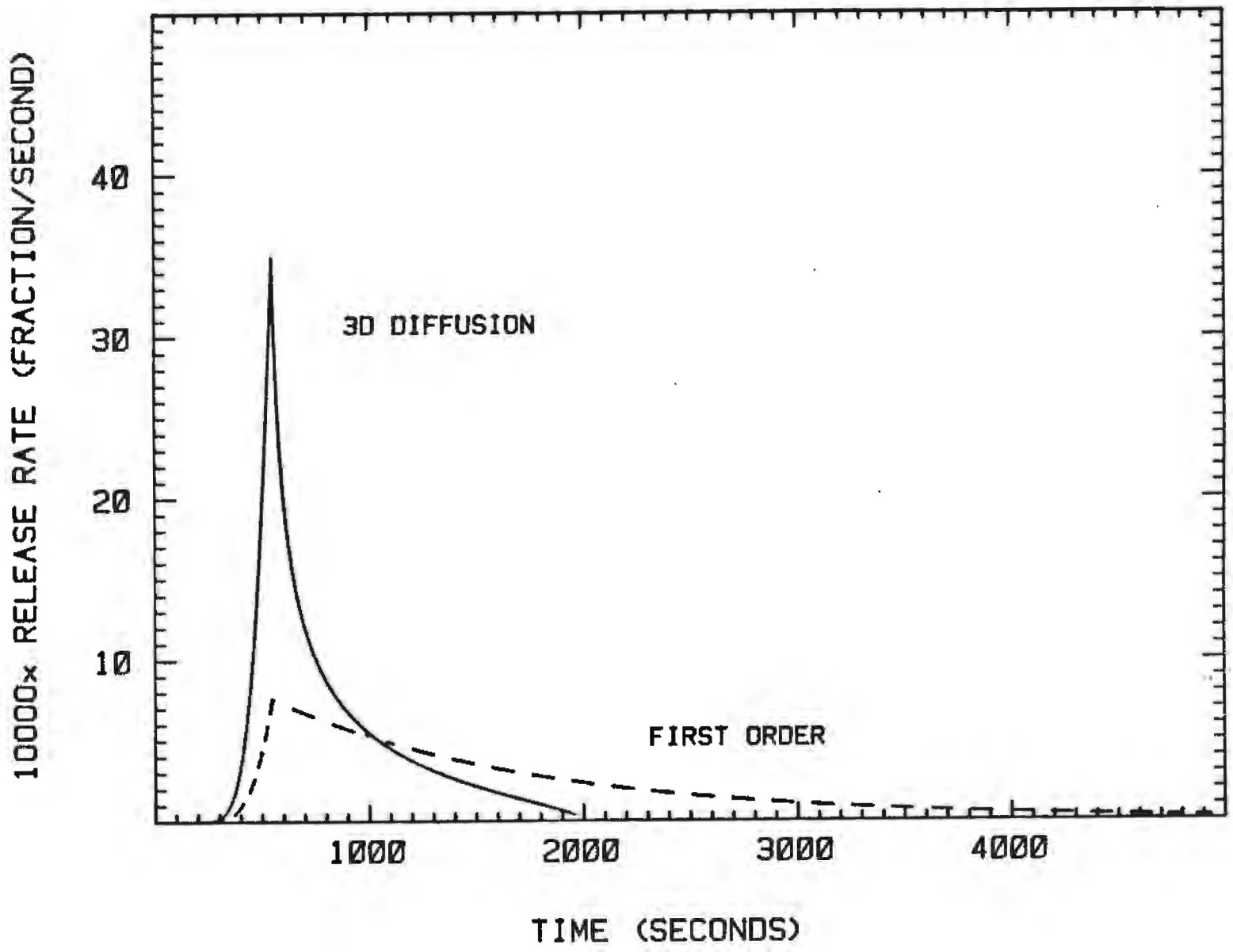

Figure 3.8. Comparison of the Predictions of Cesium Release by Two Models of the Release Kinetics Assuming the Core Heats at 4 K/s to 2500 K

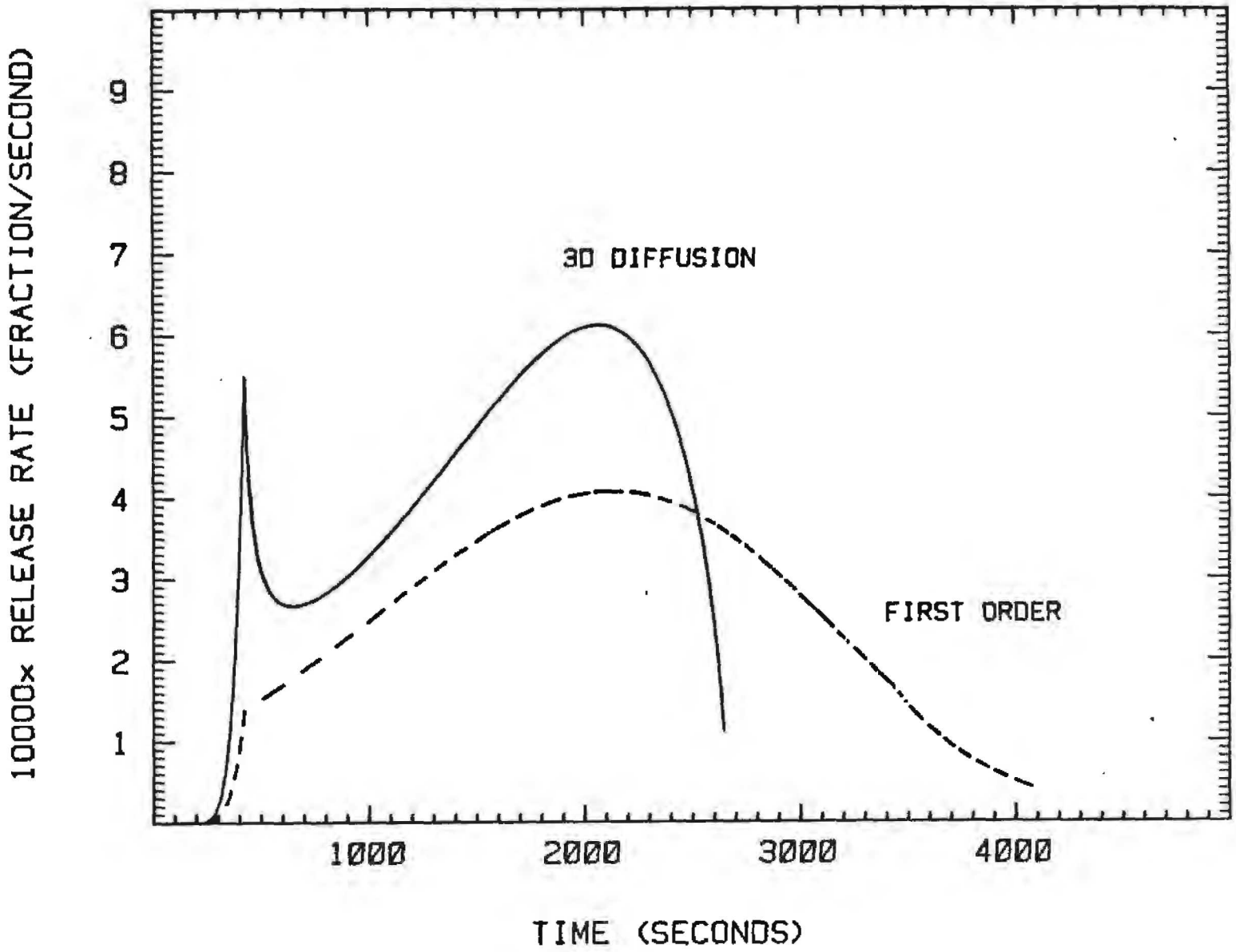

Figure 3.9. Comparison of the Predictions of Cesium Release From Two Models of the Release Kinetics Assuming the Core Heats to 2000 K at 4K/s and to 2800 K at 0.3 K/s

models are the most sophisticated. But, they do not treat all the radionuclides of interest and their complexity precludes them from inclusion in a systems code such as MELCOR. The CORSOR model has many attractive features, and it has already been used in reactor analyses [7]. The deficiencies and the virtues of the CORSOR model all stem from its close association with experimental data. The CORSOR model is, essentially, a correlation of experimental data. As such, the effects of many phenomena and processes have been encompassed by the empirical parameters of the model. But, the data base from which these empirical parameters are derived is quite limited. Use of the model for circumstances well removed from those that arise in the experimental data base is a concern. Unfortunately, reactor accident analyses frequently require release estimates for situations in which the CORSOR model extrapolates the data base. For instance, many of the most important reactor accidents involve core degradation within a reactor vessel pressurized to over 150 atmospheres. The CORSOR data base involves tests at pressures no greater than about 2 atmospheres. Gas flows through the core of a reactor can be quite slow--sometimes velocities as low as 1-2 cm/s are estimated. Yet, the CORSOR data base involves tests with gas flows on the order of 30 cm/s. Core degradation eventually leads to melting and slumping of the core materials. In analyses to date, the CORSOR model has been used only up to the time the core slumps.

The CORSOR model can be modified to broaden its range of applicability. In the sections below this is done to take into account the effects:

1. Changes in the surface area and geometry of the core materials,

2. Dilution of the fuel by interaction with the fuel cladding, and

3. The effects of ambient pressure and flow velocities through the core.

In making these modifications, some of the conceptual difficulties with the model are corrected:

4. Release does not exceed the limit prescribed by the thermochemistry of the volatile material,

5. Release becomes reversible,

6. Release at a given location becomes dependent on releases from preceding locations along the flow pathway, and

7. The effects of fuel burn up and initial grain size are explicitly depicted in the model.

The modifications made to the CORSOR model do not include all the phenomena known or suspected to affect radionuclide release. A barrier to broader modification of the model is the limitations on size posed by the systems code. Another barrier is that it is not always clear if processes and phenomena were operative in release experiments and consequently are reflected by the CORSOR release rate expressions.

A. Modifications To Account For Surface Area Changes and Dilution During Core Degradation

The CORSOR release rate expression for the volatile element i, altered to have an Arrhenius temperature dependence but retaining the assumption of first order kinetics, is:

$$\frac{dF_i}{dt} = K_o(i)\ (1 - F_i)\ \exp\ [-E(i)/RT]$$

where F_i is the fraction of the element i that has been released by time t. Suppose attention is focused on a single node of the core which contains a volume V_o of fuel. Let the initial amount of element i present in this fuel be $N_i(0)$ moles. Then, the release rate expression can be rewritten as:

$$-\frac{1}{N_i(0)}\frac{dN_i(t)}{dt} = K'_o(i)\ \exp\ [-E(i)/RT]\ \frac{1}{N_i(0)}\frac{N_i(t)}{V}$$

where $K'_o(i) = V_o K_o(i)$, $N_i(t)$ is the number of moles of the element i still present in the fuel, and V is the volume of core material containing element i.

Suppose now that the free surface through which release takes place has an area βA where A is the geometric surface area of the fuel and β is a coefficient that relates the geometric surface area to the actual surface area. Then, the rate expression can be further modified to be:

$$-\frac{dN_i(t)}{dt} = K''_o(i)\ \exp\ [-E(i)/RT]\ \beta A\ \frac{N_i(t)}{V}$$

where $K''_o(i) = \dfrac{V_o K_o(i)}{\beta A_o}$, and $\dfrac{A_o}{V_o}$ is the geometric surface area to

volume ratio of fuel used in the tests to define the CORSOR release rate coefficients.

The term $N_i(t)/V$ is the concentration of element i in the condensed phase at time t. Initially, element i is dissolved in just a volume V_o of fuel. But, as core degradation progresses, oxidized cladding can be incorporated into the fuel and this will reduce the concentration of the element i and consequently its rate of release. For typical pressurized water reactor fuel, there are 0.56 moles of zirconium clad for each mole of urania fuel. Were all of this clad to be oxidized and incorporated into the fuel, the concentrations of the volatile elements would be reduced by about 30 percent.

Incorporation of clad into the fuel will assuredly occur when the clad and fuel melt. If clad incorporation is complete then the release rate expression would have to be modified to be:

$$- \frac{dN_i(t)}{dt} = K''_o(i) \exp [-E(i)/RT] \beta A \frac{N_i(t)}{1.44\ V_o}$$

ignoring thermal expansion, the volume change of melting, and any excess volume of mixing fuel and clad.

Dilution of the fuel can also occur prior to melting. In pressurized accident sequences clad collapses onto the fuel and can chemically attack the fuel. This attack has been extensively studied recently [102]. If it is assumed that the volatile element instantaneously redistribute into the zone of fuel/clad interactions then the release rate expression becomes:

$$- \frac{dN_i(t)}{dt} = K''_o(i) \exp [-E(i)/RT] \beta A \frac{N_i(t)}{[V_o + v(t)]}$$

where $\frac{dv(t)}{dt} = 0.814 \exp [-20{,}785/T]\ cm^3/s$ and $v(0) = 0$.

The coefficient β also presents some difficulties. Once melting has occurred, the geometric surface area and the actual surface area are the same, so $\beta = 1$.

Prior to melting, β is more complex because the fuel is not fully dense.

In the Booth-type diffusion models, the solid fuel was hypothesized to consist of spherical grains of diameter "a."

Then

$$\beta = \frac{6}{a}\left[\frac{V_o}{A_o}\right]$$

where V_o/A_o is the fuel volume divided by the geometrical surface area. The hypothesis in the Booth models is that all surfaces of the grains contribute to the release process and that the grains are fixed in size. It is now recognized that neither of these hypotheses are correct. Only the surfaces of grains adjacent to interconnected porosity of the fuel can contribute to the release. The nature of the pore network is affected both by the past irradiation history of the fuel and the behavior of volatile species in the fuel. The FASTGRASS model involves elaborate descriptions of how porosity is affected during normal fuel operation and during the core degradation process. Here, a simpler description is developed.

Assume only a fraction E of the grain surface contributes to the release process. Assume E is a function only of fuel burnup. In examining the effects of fuel burnup on release, authors of the ANS 5.4 model concluded the release rate increased with burnup as

$$E(Bu) = E_o \exp [1.6\ Bu/10{,}000]$$

where Bu is the burnup in units of megawatt days per metric ton of uranium.

It is also understood now that the fuel grains will grow in an accident transient. A model by Malen used in Cubicciotti's model is

$$a(t,T) = a_o[1 + (2.92 \times 10^4 t/a_o^2) \exp (-32100/T)]$$

where a_o is in units of micrometers.

Time scales for core degradation in a severe reactor accident are estimated typically to be on the order of 1-2 hours [7]. The Malen growth model indicates that temperatures must exceed about 2200 K for grain growth to be significant for such short times. Experiments with solid, irradiated fuel such as those listed in Table 3.11 probably did not involve significant grain growth with the possible exception of test HI-3 [86]. The rate coefficients derived from these tests for the CORSOR model do not reflect, then, any significant grain growth.

Grain growth is treated here simply as a mechanism for reducing the actual surface area available for release. Grain growth can have another effect which enhances the rate of release. As grain boundaries migrate they can sweep impurities to the void structure between the grains. In the case of reactor fuel the impurities can be, of course, volatile radionuclides. When these radionuclides reach to void network they can escape the fuel. No modifications of the CORSOR model is made here to reflect this effect.

The Malen model of grain growth is strictly applicable for urania in inert or slightly reducing circumstances. As noted in the description of Cubicciotti's model grain growth in oxidizing and especially in steam can be very rapid. Following the suggestion made by Cubicciotti, an alternative to Malen's model for grain growth in steam might be constructed assuming growth is proportional to the rate of steam oxidation of urania. Circumstances of fuel degradation in strongly oxidizing environments are rare. Consequently, no such model of the so-called "steam sintering" of UO_2 is developed here.

Incorporating grain growth and burnup effects into the CORSOR model yields the rate expression:

$$-\frac{dN_i(t)}{dt} = 2.75\times10^{-3}\, K_o(i)\, \exp\left[-\left[\frac{E(i)}{RT} + \frac{1.6\ Bu}{10{,}000}\right]\left[\frac{10}{d_o}\right]\right]\frac{AN_i(t)}{V(t)\xi(t)}$$

where d_o = initial grain size of the fuel and $\xi(t)$ is defined by:

$$\frac{d\xi(t)}{dt} = \frac{2.92\times10^{4}}{d_o^2}\exp\,[-32{,}100/T]$$

with the initial condition that $\xi(0) = 1$. For this incorporation it was assumed that the rate coefficients for the CORSOR model were derived from fuel with a burnup of 28,000 MWd/t and initial grain sizes of 10 μm. In fact, fuel used in tests at lower temperatures had burnups varying between 15,000 and 39,000 MWd/t. Initial grain sizes of the fuel are seldom reported.

When the fuel is liquefied the modified model becomes simpler:

$$-\frac{dN_i(t)}{dt} = \frac{K_o(i)}{4.225}\exp\left[-\frac{E(i)}{RT}\right]\frac{AN_i(t)}{V}$$

Note that the modified CORSOR model developed here has retained the original assumption of first order kinetics. This was not necessary. In fact, an entirely similar development could have been conducted for any one of the other kinetic models mentioned above such as the three-dimensional diffusion or the three-dimensional phase boundary models.

The modified model that has been derived here is still quite crude. In some cases processes and phenomena have been omitted simply because it is unclear whether these processes or phenomena are already reflected in the rate coefficients of the original CORSOR model. There are also cases where significant phenomena known not to be reflected in the coefficients have been omitted. Sweeping of radionuclides by grain boundary migration and the effects of fuel/clad interactions are areas where the model could be refined further.

Though the modified CORSOR model derived here is still crude, it can be used to demonstrate the effects on radionuclide release of fuel and accident features other than just time and temperature. The modifications to CORSOR are arrested here to demonstrate some of these effects.

In Figure 3.10 the extents of cesium release from fuel heated from 700 K at rates of 0.1, 1, and 10 K/s are shown as functions of temperature. Liquefaction and fuel/clad interactions were neglected in preparing this figure. The burnup and initial grain size were assumed to be 28,000 MWd/t and 10 μm, respectively. The effect of heating rate on release is as would be expected. As the heating rate decreases there is an opportunity for more extensive release at any given temperature.

The sensitivity of the extent of release to heating rate shown in Figure 3.10 can be used to evaluate the sensitivity of cesium release to burnup and initial grain size shown in Figures 3.11 and 3.12, respectively. For these plots heating rates were taken to be 1 K/s. From these figures, it is apparent that burnup and initial fuel grain size can have effects on release comparable to the effects of heating rate.

In Figure 3.13 cesium release from fuel during a stylized meltdown sequence is shown. Again, it is assumed the fuel is heated at 1 K/s from 700 K. However, it was assumed that once a temperature of 2200 K was reached clad began to be incorporated into the fuel. After 100 seconds at 2200 to 2300 K all the clad was assumed to have been incorporated in the fuel. Then, it was assumed that the fuel began to slump into a spherical mass. After 400 s it was assumed the fuel was part of an 80 ton spherical mass of fuel and clad. The releases predicted neglecting the fuel/clad interactions, melting, and slumping are shown in the figure for comparison. The comparison shows that fuel/clad interaction of the type hypothesized here has a small but detectable effect. Slumping of the molten fuel has a more dramatic

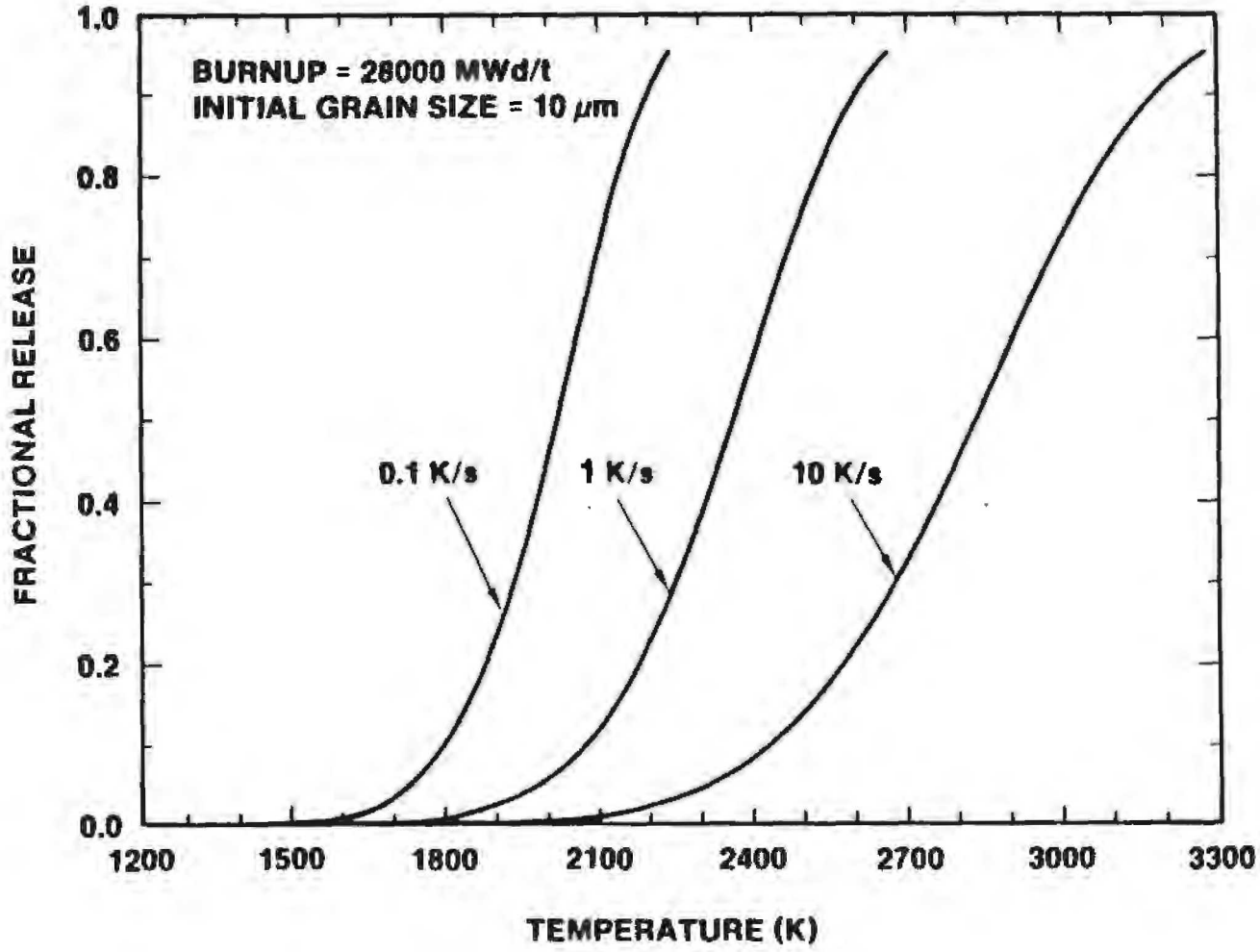

Figure 3.10. Effects of Heating Rate on the Release of Cesium

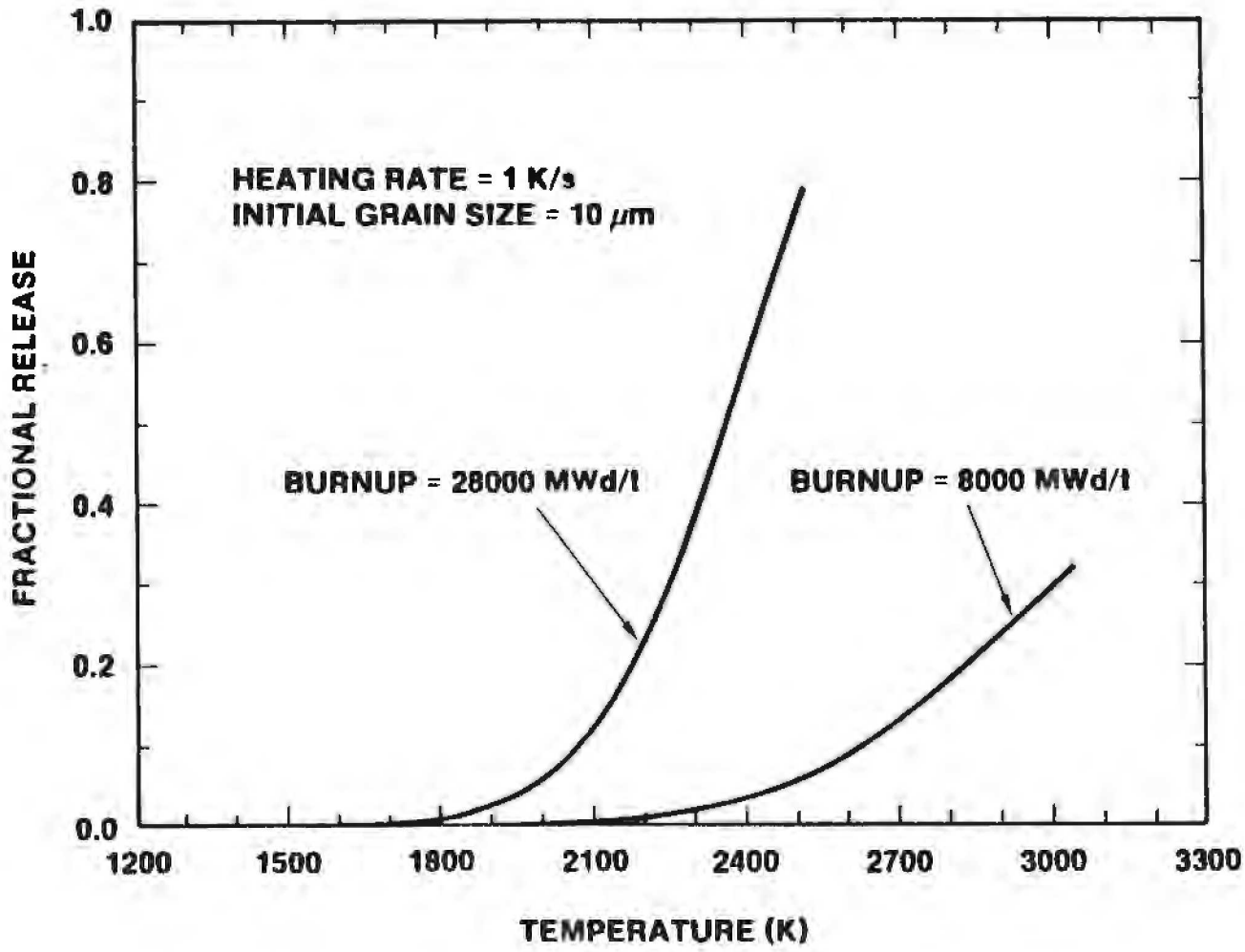

Figure 3.11. Effects of Burnup on Release of Cesium From Fuel Heated From 700 K at 1K/s

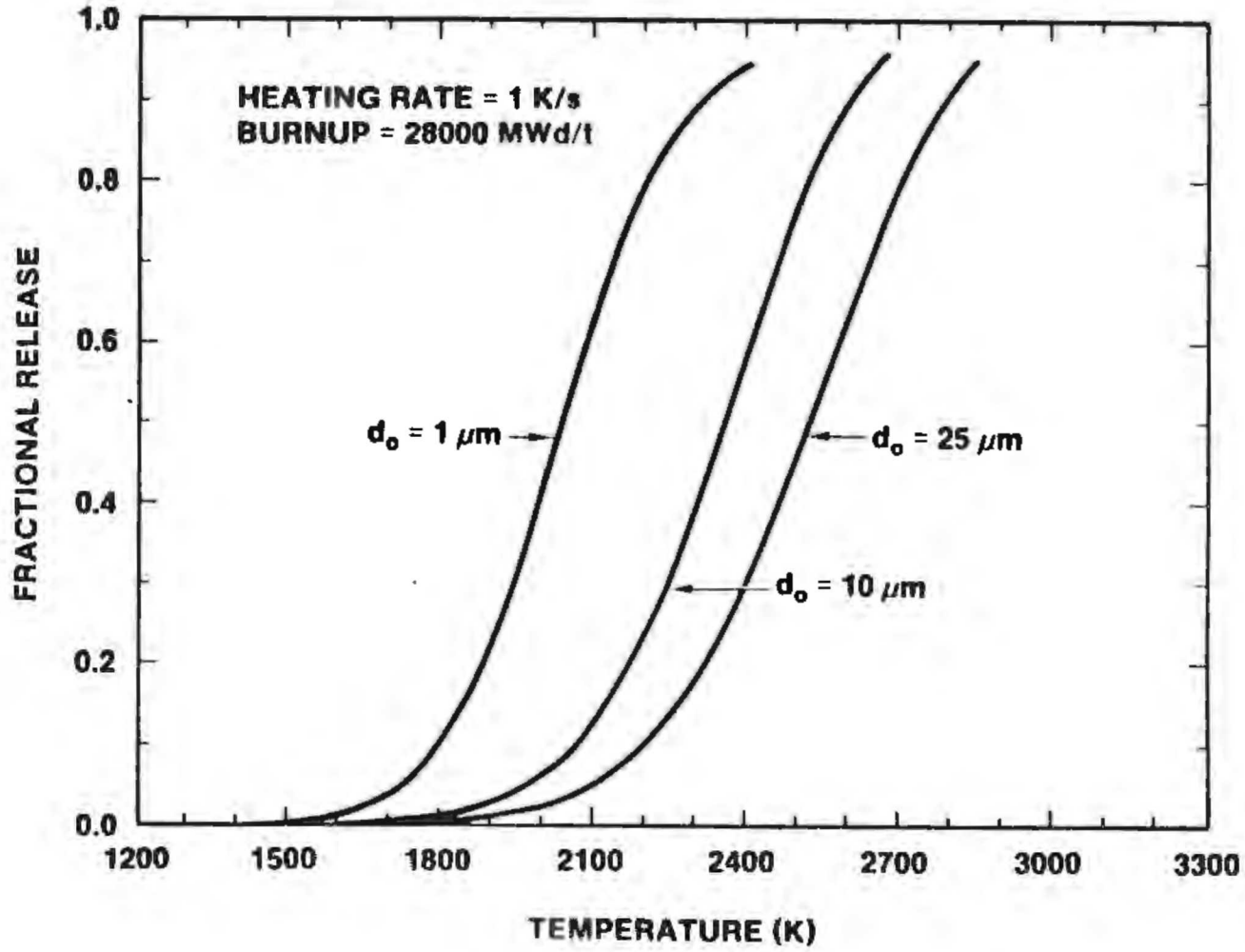

Figure 3.12. Effects of Initial Grain Size on Release of Cesium From Fuel Heated From 700 K at 1K/s

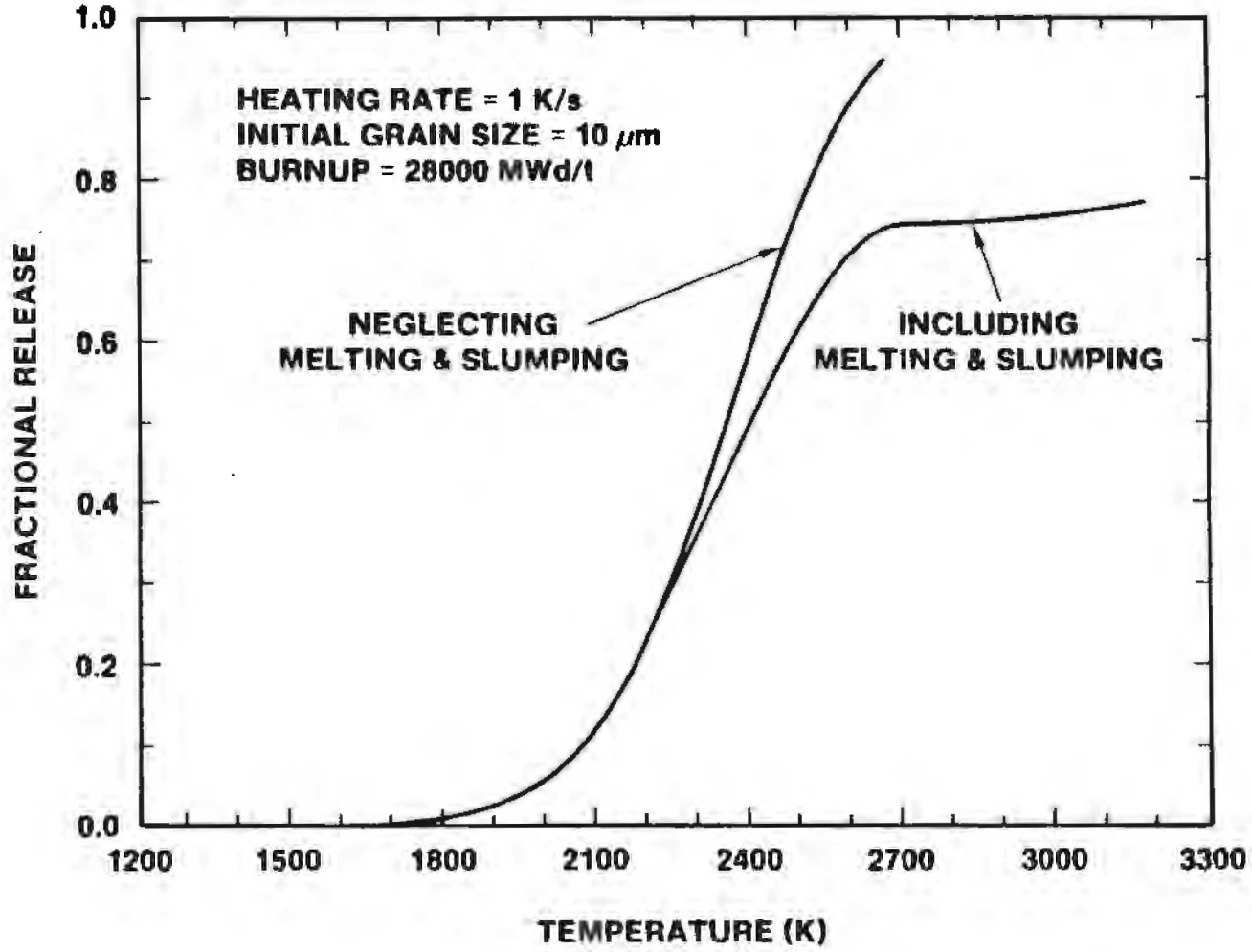

Figure 3.13. Effects of Melting and Slumping of the Fuel on Release of Cesium

effect. The very small surface to volume ratio that develops as the molten sphere grows leads to very much reduced release rates.

B. Modifications To Account For Gas Phase Mass Transport

The description of radionuclide release from fuel has focused in the past nearly exclusively on the limitations in the condensed phase. Assuredly, this rate limitation is quite important at low temperatures and for the more volatile species such as Cs, I, and the noble gases. The exception to this concentrated attention on condensed phase mass transport is Miller's so-called "light-bulb" model in which condensed phase mass transport is assumed a negligible resistance to release and gas phase mass transport is considered a dominant resistance. The many diverse circumstances that can be hypothesized for severe reactor accidents make it apparent that neither gas phase nor condensed phase mass transport can be exclusively the source of release rate limitations. In this section, the CORSOR model is modified to account for the possibility of gas phase mass transport resistance to release.

Before delving into the modifications of the model, it is important to understand qualitatively how radionuclides will behave once they escape the fuel. Early in an accident radionuclides that emerge from the urania lattice will enter a network of interconnected porosity that provides a pathway to any gap between the fuel and the clad. The radionuclide vapor will have to traverse this pathway in order to reach a breach in the clad from which it can escape into the bulk flow of gas through the reactor core. If the clad has "ballooned" due to internal pressurization during an accident, a substantive gap will exist between the fuel and the clad. In this case, the primary resistances to release of the radionuclide once it has escaped the urania lattice are:

1. Transport through the pore network to the fuel/clad gap, and

2. Possible chromatographic resistance brought on by reaction with the clad and revaporization within the fuel/clad gap.

The low temperature experiments with clad, irradiated fuel that provided the CORSOR release rate coefficients examined this circumstance. That is, there were relative large gaps between the fuel and the clad in these tests. Thus, the CORSOR release rate coefficients fully reflect resistances to radionuclide release in these circumstances.

In a pressurized reactor accident sequence, the clad need not "balloon." Rather, as high temperatures are reached the high, external, pressures could cause the clad to collapse onto the fuel. A very narrow fuel/clad gap would then exist. The gap would be further complicated as chemical interactions between the clad and fuel progress. The nature of resistances to radionuclide release in this circumstance would be qualitatively similar to those arising when the clad balloons. However, the distance a vapor must travel through narrow pore structures to reach a breach in the cladding might be longer. On the other hand, because the clad and the fuel are in intimate contact, and the clad and fuel chemically interact, there may be more frequent breaches in the clad through which radionuclides can escape.

As temperatures rise further, the interaction of the fuel and the clad lead to liquid formation. At this point the clad no longer constitutes a major barrier to release. Experimental studies of fuel rod melting have been conducted extensively by Hagan et al. [105]. If oxidation of the clad by steam has been extensive, there is a tendency for liquid to flow downward in the annular space between the solid fuel and a ZrO_2 shell. Even so, there are frequent breaks in the shell through which radionuclides could escape. If clad oxidation is not extensive, then what little ZrO_2 has been formed dissolves in the liquefied fuel/clad mixture and the melting clad provides little resistance to release.

Once a radionuclide migrates to a free surface adjacent to bulk flow through the core, there is still a resistance to escape that must be negotiated. The radionuclide vapor must traverse a boundary layer between the free surface and the bulk flow.

The gas phase mass transport resistance posed to vaporized radionuclides while the clad is present is complex. Some sort of a model of this process could be formulated assuming, say, that transport through the flow passages was by Knudsen diffusion. Mean pore diameters and transport distances could be hypothesized and an additional release resistance incorporated into the model. These effects will be most important only for the more volatile radionuclides. Vaporization of species such as Sr, La, and the like will not be extensive until liquefaction begins and the resistance to release posed by the clad and the clad/fuel gap has disappeared.

The resistance to release posed by the boundary layer between the condensed phase and the bulk flow through the reactor core is pandemic. It is operative throughout the accident and affects the release of all radionuclides.

Here the complex resistance to release that arises because of the clad is neglected. It is assumed that limitations on the release that arise from such resistances are adequately reflected

by the CORSOR release rate coefficients. This assumption is open to doubt simply because the data base used to develop the release rate coefficients does not include the diversity of circumstances that can be hypothesized to arise in reactor accidents. Relief from this assumption is yet another area where the model developed here could be refined further.

The modification of CORSOR to account for gas phase mass transport will be confined here to the examination of the effects of the boundary layer between bulk flow and the condensed phase.

The rate expression for release from the condensed phase derived in the previous section can be written in the form

$$-\frac{dN_i(t)}{dt} = AK(i)\ \exp\ [-E(i)/RT]\ \frac{dC_i(t)}{dx}$$

where K(i) is a complex function of burnup, grain size, and physical state of the condensed phase and $dC_i(t)/dx$ is the gradient in volatile element concentration in the condensed phase. This gradient can be expressed as:

$$\frac{dC_i(t)}{dx} = \frac{C_i(t) - C_i(surface)}{\delta}$$

where $C_i(t)$ = bulk concentration of the volatile element

$C_i(surface)$ = concentration of the volatile element at the condensed phase surface

δ = length scale.

When resistances other than condensed phase mass transport are neglected, $C_i(surface)$ is assumed to be zero. When these other resistances are to be considered, allowance for a finite surface concentration must be made and the release rate expression becomes:

$$-\frac{dN_i(t)}{dt} = AK'(i)\ \exp\ [-E(i)/RT]\ [C_i(t) - C_i(surface)]$$

Examination of the other resistances to release must provide an estimate of the unknown surface concentration.

Suppose now that a surface of area A' in a node is exposed to the bulk flow of gases through the core. A general expression for the rate at which a volatile element passes through the exposed surface into the bulk flow is given by:

$$-\frac{dN_i(t)}{dt} = \frac{A'k_g}{RT}\,[P_i(\text{surface}) - P_i(\text{bulk})]$$

where P_i(surface) = vapor pressure at the surface

P_i(bulk) = partial pressure in the bulk gas phase

k_g = gas phase mass transport coefficient.

If a quasi-steady state has been reached then the rate at which element i is released from the condensed phase must equal the rate at which it passes through the area exposed to the flow. Thus,

$$-\frac{dN_i(t)}{dt} = AK'(i)\exp[-E(i)/RT][C_i(t) - C_i(\text{surface})]$$

$$= \frac{A'k_g}{RT}\,[P_i(\text{surface}) - P_i(\text{bulk})]$$

To progress in the analysis it is necessary to relate the surface concentration of element i to the partial pressure P_i(surface). It was unnecessary in the development of the condensed phase mass transport equation to specify the chemical form of the migrating species. Specification of the chemical form of the vapor species can be deferred, but not avoided entirely, by recognizing that regardless of the complexity of the chemistry the surface partial pressure can be specified as:

$$P_i(\text{surface}) = \frac{C_i(\text{surface})}{\rho_{\text{molar}}}\,P_i^{\circ}(\text{eq})$$

where ρ_{molar} = moles of condensed species per cubic centimeter of condensed phase

P_i°(eq) = equilibrium partial pressure that would develop over the pure migrating species i under the ambient conditions.

Similarly, an equilibrium partial pressure can be associated with the concentration of element i in the condensed phase:

$$P_i(t) = \frac{C_i(t)}{\rho_{molar}} P_i^o(eq)$$

Then,

$$-\frac{dN_i(t)}{dt} = \frac{AK(i)\ \exp\ [-E(i)/RT]}{P_i^o(eq)} \rho_{molar}\ [P_i(t) - P_i(surface)]$$

$$= \frac{A'k_g}{RT}\ [P_i(surface) - P_i(bulk)]$$

Eliminating the unknown partial pressure $P_i(surface)$ yields:

$$-\frac{dN_i(t)}{dt}\left[\frac{1}{AK'(i)\ \exp\ [-E(i)/RT]\ \rho_{molar}} + \frac{RT}{A'k_g P_i^o(eq)}\right]$$

$$= \left[\frac{P_i(t) - P_i(bulk)}{P_i^o(eq)}\right]$$

or,

$$-\frac{dN_i(t)}{dt} = K_{Total}\left[\frac{N_i(t)}{V\rho_{molar}} - \frac{P_i(bulk)}{P_i^o(eq)}\right]$$

where $$\frac{1}{K_{Total}} = \frac{1}{AK'(i)\ \exp\ [-E(i)/RT]\ \rho_{molar}} + \frac{RT}{A'k_g P_i^o(eq)}$$

or,

$$\frac{dF_i(t)}{dt} = \frac{K_{Total}}{V\rho_{molar}}\left[1 - F_i(t) - \frac{P_i(bulk)}{P_i(o)}\right]$$

where $P_i(o)$ is the partial pressure that would develop over the condensed phase had no release occurred.

Inspection of this revised release model shows that several important effects not available in the original CORSOR model have been introduced. First, the release of volatiles is now reversible. That is, if the vapor concentration in the bulk gas phase is sufficiently high, the flux of element i is back into the condensed phase. The release of element i from a particular node in the core is dependent now on the extent of release from nodes that precede it along the flow path. Chemistry of the element i has been introduced albeit formally at this point. This chemistry will have to be made explicit before the rate expression can be applied. Once the chemistry is explicit, it will be possible to recognize changes that occur in the chemical conditions along the flow pathway. Because the chemistry is included, the revised release model assures that vapor phase concentrations do not exceed the thermochemical limit appropriate for the ambient temperature and chemical conditions.

To apply the model for release developed here, it is necessary to have values of the mass transport coefficient, k_g. It is possible, in principle, to determine k_g in a totally theoretical manner. But, the exercise can be enormously complex. Solution of the equations can be done usually in only a very approximate manner. Consequently, correlations of experimental data are an attractive source of information on the mass transport coefficient. Such correlations are not universal in nature. Separate correlations have been developed for various flow and geometry configuration.

The patterns of gas flow through a degrading reactor core are poorly known. It is likely that the geometry of the core as it degrades evolves in a very complicated fashion. Details of this evolution may not be, however, exceptionally important for the analysis of radionuclide release. Here a stylized description of the degradation process is outlined. This description emphasizes "limiting" core geometries that have at least a transient existence during the degradation process. Though these "limiting" geometries and gas flows may be complicated in detail, they can be idealized to be simple forms for which correlations of experimental data are available.

When the core degradation process begins, the fuel consists of vertical arrays of rods. These rods may be distorted somewhat as a result of clad ballooning and rupture. The simplest description of gas flow through the core during this early stage of an accident is flow parallel to the rod axes. This type of flow has been enforced in out-of-pile release experiments with irradiated fuel rods.[86,88-93] This is also the flow pattern sought in recent in-pile, core degradation experiments.[87] It

is the flow pattern allowed by the MARCH model [7] of core degradation. It is probably a particularly accurate description of flow during boil-off of coolant from the core.

Once most of the coolant has boiled from the core, the flux of steam into the core drops sharply [103]. Heatup of the fuel means that a significant temperature difference exists between the core and structures above the core. This temperature difference will induce natural circulation of gases through the core [104]. In pressurized water reactors, the open lattice of fuel will be exposed in some regions to a flow perpendicular to the rod axes. Fuel in boiling water reactors is unlikely to be exposed to such perpendicular flows since fuel bundles are shielded in channel boxes.

As the degradation process proceeds, cladding will interact chemically with the fuel and liquid will be formed. Here, it is supposed that liquefied clad and fuel drains down the rod. This draining has been observed in out-of-pile experiments [105] and is described in greater detail elsewhere [103,106]. The flow is not necessarily continuous. Rather, liquid forms first in an especially warm region, flows downward until it freezes temporarily. It then remelts, as does some of the underlying material of the rod. This combined mass then flows down along the rod until it is again frozen.

Not all the fuel in a particular location need be liquefied as a result of interaction with the clad. That which is not may remain in place until much higher temperatures are reached. It is more likely though that once the cladding is lost, the fuel that is not liquefied will collapse into a debris bed composed of coarse particles. Temperatures in this debris bed may become high enough that the bed material melts and flows down through the core.

As more liquefied material forms, the individual streams of melt flowing down the rods coalesce into a single mass of liquid. This mass is characterized here as a sphere though it is undoubtedly a far more complex shape. Initially, the flow pattern around a sphere can be used to determine the mass transport coefficient. As the mass becomes a significant fraction of the core mass the geometry might better be characterized as one consisting of a downward facing surface and an upward facing surface. At low flows, the mass transport in the gas phase from these surfaces is determined by natural convection.

In summary, the stylized description of core degradation presented above requires that mass transport coefficients be known for the following geometries and flow patterns:

1. Longitudinal flow parallel to the axes of the rods with and without discontinuities created by clad ballooning or fuel liquefaction.

2. Transverse flow perpendicular to the axes of the rods.

3. Flow around a spherical mass.

4. Flow through a debris bed.

5. Natural convection flow from a downward facing surface and from an upward facing surface.

Experimental data are available in greater abundance for convective heat transport than for convective mass transport. A conventional approach is to draw an analogy between heat and mass transport. Then correlations of data for heat transfer can be used to estimate the mass transfer coefficients.

The mass transfer coefficients for the geometries and flows that arise in the simplified description of core degradation presented above are summarized in Table 3.13. The bases for these values are discussed below.

Flow Around a Sphere. Heat and mass transport around a sphere has been studied much. The correlations shown in Table 13 provide values averaged over the surface of a sphere. As such, the correlations are most useful when the sphere is small. As the sphere diameter increases, local variations in the mass transport become important. Schutz [109] has studied the local mass transport under natural convection conditions. He finds the minimum mass transport occurs at an angle of about 135° to the direction of the flow. Mass transport at angles less than 90° and larger than 140° is relatively insensitive to the angle. Mass transport coefficients from surfaces bounded by angles greater than 140° can be as much as two times the mass transport from surfaces bounded by an angle of 90°.

The natural convection regime of flow can be characterized in greater detail than shown in the table:

$$N_{Sh}(\text{natural convection}) = 2 + K(N_{Gr}N_{Sc})^{1/4}$$

$K = 0.3$	for	$0 < N_{Gr}N_{Sc} < 50$
$K = 0.4$	for	$50 < N_{Gr}N_{Sc} < 200$
$K = 0.5$	for	$200 < N_{Gr}N_{Sc} < 10^6$
$K = 0.6$	for	$10^6 < N_{Gr}N_{Sc} < 10^8$

Table 3.13

Mass Transfer Coefficients for Configurations
That Develop During Core Degradation

Geometry, Flow, and References	Sherwood Number	Limitations
Flow around a sphere [107,108]	$Sh = 2 + K(N_{Gr}N_{Sc})^{b} + 0.347(N_{Re}N_{Sc}^{1/2})^{0.62}$	$N_{Gr}N_{Sc}<10^{8}$, K=0.569, b=0.25
	$Sh = k_g d/D$	$N_{Gr}N_{Sc}>10^{8}$, $K=0.0254\ N_{Sc}^{0.244}$, b=0.5
	d = diameter of sphere	
	$N_{Sc} = \mu/\rho D_{AB}$	
	μ = gas viscosity	
	ρ = gas density	
	$N_{Re} = dv\rho/\mu$	
	v = gas velocity	
	$N_{Gr} = \frac{g\rho^2 d^3}{\mu^2}\frac{\Delta T}{T}$	
Natural convection from a downward facing surface	$Sh = 0.27(N_{Gr}N_{Sc})^{1/4}$	$3x10^{5}<N_{Gr}<3x10^{10}$
	$N_{Gr} = \frac{g\rho^2 L^3}{2_\mu}\frac{\Delta T}{T}$	
	L = characteristic length of surface	

Table 3.13 (Continued)

Geometry, Flow, and References	Sherwood Number	Limitations
Natural convection from an upward facing surface	$Sh = 0.54(N_{Sc}N_{Gr})^{1/4}$	$10^5 < N_{Gr} < 7 \times 10^7$
	$Sh = 0.12(N_{Sc}N_{Gr})^{1/3}$	$N_{Gr} > 7 \times 10^7$
	$N_{Gr} = \frac{g\rho^2 L^3}{\mu^2} \frac{\Delta T}{T}$	
	L = characteristic length of surface	
Flow parallel to rod axis [114,115,118,119]	$Sh = Nu(laminar) + A\, N_{Re}^{0.8}\, N_{Sc}^{1/3}$	
	$Nu(laminar) = [7.55x - 6.3x^{-b}]\,[1 - 3.6x/(3.2+x^{20})]$	
	$b = 17x(x - 0.81)$	
	$x = S/D$	
	$A = [0.042x - 0.024][1.103x^2 - 1]^{-0.2}$	triangular arrays
	$A = [0.026x - 0.006][1.273x^2 - 1]^{-0.2}$	square arrays
	The length dimension in Sh and N_{Re} is the rod diameter	

Table 3.13 (Continued)

Geometry, Flow, and References	Sherwood Number	Limitations
Effects of a discontinuity in flow [121]	$\frac{Sh}{Sh(*)} = \min\left\{ N_{max},\ K\left[\frac{y}{D_h}\frac{1}{N_{Re}N_{Pr}}\right]^m \right\}$	N_{max} defined in text
	$K = 4.42 - 1.05 \log_{10}(N_{Re}) - 2.25\epsilon$ $m = -0.001855\ N_{Re}\ \epsilon^2$	$N_{Re}<3000$
	$K = 0.426 + 0.113 \log_{10}(N_{Re}) - 2.25\epsilon$ $K > 0.895 - 2.25\epsilon$ $m = -30.34\ N_{Re}^{-0.253}\ \epsilon^2$ $m > -4\epsilon^2$	$N_{Re}>3000$ and smooth tubes
	$K = \min\left\{ \begin{array}{c} -0.344 + 0.35 \log_{10}(N_{Re}) - 2.25\epsilon \\ \text{and} \\ -1.8478 + 1.2466 \log_{10}(N_{Re}) \\ -0.1298\ [\log_{10}(N_{Re}0)]^2 - 2.25\epsilon \end{array} \right.$ $K \geq 0.885 - 2.25\epsilon$ $m = -(1 + 4.9\times10^4\ N_{Re}^{-1.2})\epsilon^2$ $m \geq -4\epsilon^2$	$N_{Re}>3000$ and rough tubes

Table 3.13 (Continued)

Geometry, Flow, and References	Sherwood Number	Limitations
	where $Sh(*)$ = Sherwood number for undisturbed flow ϵ = blockage factor which is the fraction of the flow occluded by rods and the obstacle y = distance from the front edge of the flow discontinuity along the rod	
Flow through a debris bed [122]	$Sh = \frac{k_g d_p}{D_{AB}} = \frac{2}{1-(1-\epsilon)^{1/3}} + \frac{2}{3\epsilon} N_{Re}^{n} N_{Sc}^{1/3}$ d_p = particle diameter ϵ = porosity of the bed $\frac{2-n}{3n-1} = 4.65\, N_{Re}^{-0.28}$	$N_{Re} > 80$ and isothermal debris beds
Flow perpendicular to the axes of the rods	$Sh = a + (0.5\, N_{Re}^{1/2} + 0.2\, N_{Re}^{2/3})\, N_{Sc}^{1/3}$ $a = 2/[\ln\{1 + 2/[0.468(N_{Gr}N_{Sc})^{1/4}]\}]$ $N_{Gr} = \frac{g\rho^2 D^3 \Delta T}{\mu^2 T}$ D = diameter of a rod $N_{Re} = \frac{Dv\rho}{\mu}$	

Natural Convection from Upward and Downward Facing Surfaces. The correlations shown in Table 3.13 are actually for natural convection from upward and downward facing squares. The correlations were developed from correlations of natural convection heat transfer by replacing the dimensionless Prandtl number ($C_p\mu/k$) with the dimensionless Schmidt number ($\mu/\rho D_{AB}$). Density differences that drive natural convection are assumed the result of temperature differences between the bulk gas and the condensed phase surface temperature with no contribution from the vaporizing material.

Based on Schutz's data for natural convection from a sphere the length scales in the correlations can be taken to be:

$$L(\text{upward}) = 0.7\ D(\text{equivalent})$$

$$L(\text{downward}) = 1.6\ D(\text{equivalent})$$

where D(equivalent) is the diameter of the sphere containing an equivalent amount of mass as the body in question.

Flow Perpendicular to the Rod Axes. The correlation in Table 13 for mass transfer during flow perpendicular to the axes of the rods was developed from a correlation proposed by Whitaker for heat transfer from staggered tube arrays [110]. The transformation to mass transfer was accomplished by replacing the Prandtl number and Nusselt numbers in Whitaker's correlation with the Schmidt and Sherwood numbers, respectively. A natural convection correlation appropriate for a single cylinder was then added to the expression. Again, density differences that drive natural convection were assumed to be the result of temperature differences between the bulk gas phase and the condensed phase surface with no contribution from the changing composition of the gas.

Whitaker's correlation was developed to comply with the theoretical condition that in the absence of natural convection the convective heat transfer from a single cylinder should go to zero as velocity goes to zero. Correlations of experimental data at low flow rates such as that obtained by Collis and Williams [111]:

$$Nu = 0.24 + 0.56\ N_{Re}^{0.45}$$

for air and $0.02 < N_{Re} < 44$ support this condition.

An alternate correlation found from actual mass transport studies of flow perpendicular to the axes of tubes is [112]:

$$Sh = 0.169\ [1-0.5\ \exp(-0.69\ N)]\ N_{Re}^{0.68}\ N_{Sc}^{0.33}$$

where N is the number of rows of tubes.

Whitaker's correlation does not describe data for in-line tube arrays as well as data for staggered tube arrays.

Flow Parallel to the Rod Axes. Investigations of flow parallel to the axes of the rods have concentrated on situations in which the Reynolds number is high. Weisman [113] derived the following correlations for water flow through bundles:

$$Nu = C\ N_{Re}^{0.8}\ Pr^{1/3}$$

where $C = 0.042\ S/D - 0.024$ for square arrays with $1.1 < S/D < 1.3$

$C = 0.026\ S/D - 0.006$ for triangular arrays with $1.1 < S/D < 1.5$

S = center-to-center rod separation

D = rod diameter.

Dingee and Chastain [114] found adequate correlation of data for water flow through various types of arrays with a Dittus-Boelter type equation:

$$Nu = 0.023\ N_{Re}^{0.8}\ N_{Pr}^{1/3}$$

in which the dimension for the Nusselt and Reynolds numbers is the equivalent hydraulic diameter.

Sparrow et al. [115] have analyzed the problem for triangular arrays and laminar flows. They present a nomograph for the

average Nusselt number which can be approximated by the expressions:

$$Nu = 3.6 + 16.25(S/D) \text{ for } 1 < S/D \leq 1.4$$

$$Nu = 10 + 9.23(S/D) \quad \text{for} \quad S/D > 1.4$$

The dimension for the Nusselt number is the rod diameter in this case.

Gimble et al. [120] have examined parallel flow in a configuration proposed for early nuclear power plant fuel. Their experimental data were obtained with air and for Reynolds numbers between 8000 and 30,000. Heat transfer data were correlated by the expression

$$Nu = (0.040 + 5.96x^{-1/2} N_{Re}^{1-\beta} N_{Pr}$$

where $$\beta = \frac{0.00104 + 0.347/x}{0.00434 + x}$$

$$x = S/D$$

The length scale for the dimensionless parameters is the rod diameter.

There have been several studies of parallel flow for liquid metals. Dwyer [116] presents the correlations:

$$Nu = 6.66 + 3.126x + 1.184x^2 + 0.0155 (\bar{\psi}RePr)^{0.86}$$

for $100 < RePr < 10^4$

$$Nu = 7 + 3.8x^{1.52} + 0.027 (\bar{\psi}RePr)^{0.8} x^{0.27}$$

for $0 < RePr < 10^5$ and where

$$x = S/D$$

$$\bar{\psi} = 1 - \frac{1.82}{Pr\ (\epsilon_M/V)_{max}^{1.4}}$$

and $(\epsilon_M/V)_{max}$ values are presented in a graph. Dwyer recommends for the low turbulence regime the correlation for molecular conduction:

$$Nu = -2.79 + 3.97x + 1.025x^2 + 3.12 \log_{10}N_{Re} - 0.265 (\log_{10}N_{Re})^2$$

Ushakov et al. [118] cite the following correlations:

$$Nu = Nu(laminar) + \frac{3.67}{90x^2} (N_{Re}N_{Pr})^a$$

where $a = 0.56 + 0.19x$

$Nu(laminar) = 7.55x - 6.3x^{-b}$

$b = 17x\ (x - 0.81)$

$x > 1.3$

and

$$Nu = Nu_o + \beta N_{Re}^{0.87} N_{Pr}^m$$

where $m = 0.4 + (2 + 4N_{Pr})^{-1}$

$\beta = 0.0083\{1-\exp[-10.4(x-1)-0.1\ \alpha]\} + 0.008(x - 1)$

$\alpha = 1 + 4/(1 + 10N_{Pr})$

for $0 \leq Pr < 10$ and $10^4 < N_{Re} < 10^5$. Values of Nu_o are reported to be tabulated, but this author could not retrieve the document. Some values Nu_o from Reference 118 are:

x	Nu_o
1.5	14
1.4	13
1.32	12

1.15	8.2
1.113	8
1.01	1.7

The recommended correlation for the Sherwood number is derived from the correlation by Ushakov et al. of Nu(laminar) and Weisman's description of turbulent flow. Values of the Nusselt number for laminar conditions match well tabulated values in Reference 119.

Effects of Discontinuities. In the stylized description of core degradation outlined above, melt flowing down a rod would freeze temporarily on the rod. This introduces a discontinuity in an otherwise smooth rod. Discontinuities could also be created by clad ballooning and rupture. The mass transport and heat transport consequences of melt formation and freezing have apparently not been investigated. It is readily apparent that the efficiency of mass and heat transport should go up when flow encounters a discontinuity such as melt frozen on a rod.

Hassan and Rehme [121] have investigated the effects on heat transfer caused by a grid spacer. They found that the increase in the local Nusselt number could be correlated in terms of the Reynolds number and some geometric factors. The "blockage factor" created by an obstacle is an important geometrical quantity in the correlation. This blockage factor is just the fraction of the flow area occluded by the rods and the obstacle.

The Hassan and Rehme model asserts that about one hydraulic diameter ahead of a blockage the local Nusselt number begins to rise to a maximum. The rise rate is given by

$$\frac{Nu(y)}{Nu(undisturbed)} = 1 + \frac{\left[\frac{Nu(max)}{Nu(undisturbed)}\right]\left[\frac{y}{D_h} + 1\right]}{A + 1}$$

where D_h = hydraulic diameter

y = distance from the leading edge of the obstacle

$A = L_A/2D_h$ for $N_{Re} < 3000$ or for rough surfaces

$A = L_A/D_h$ for smooth surfaces and $N_{Re} > 3000$

L_A = obstacle length

After passing the obstacle the disturbance caused by the obstacle begins to decay. The relative Nusselt number is then given by

$$\frac{Nu(y)}{Nu(undisturbed)} = \min \left[Nu(max), K \frac{y}{D_h} \frac{1}{N_{Re} N_{Pr}} \right]^m$$

where values of K and m are given in Table 3.13 and Nu(max) is given by

$$Nu(max) = \min \begin{cases} 1 + 0.174\ \epsilon^2 N_{Re}^{1/2} \\ \quad \text{and} \\ 1 + \left[3.3 + 72{,}700\ N_{Re}^{-1.2} \right] \epsilon^2 \end{cases} \quad \text{for rough surfaces}$$

$$Nu(max) = \min \begin{cases} 1 + 0.174\ \epsilon^2 N_{Re}^{1/2} \\ \quad \text{and} \\ 1 + 6.38 + 4550\ N_{Re}^{-0.8}\ \epsilon^{2.4} \end{cases} \quad \text{for smooth surfaces}$$

Of course, Nu(y)/Nu(undisturbed) is never allowed to be less than one.

The correlation for the increase in the Sherwood number caused by a flow discontinuity was created from the Hassan and Rehme correlation by assuming the relative effects on mass transport and heat transport were the same. Based on the simplified description of core meltdown outlined above, slumping melt or local clad ballooning creates a local increase in the rod diameter. Blockage factors are then, for triangular arrays:

$$\epsilon = \frac{0.907\ D_{max}^2}{S^2}$$

and for square arrays

$$\epsilon = \frac{0.785\ D_{max}^2}{S^2}$$

where D_{max} is the maximum rod diameter at the discontinuity. The correlations also account for surface roughness of the rods. Surface roughness has an effect only at Reynolds numbers greater than 3000. For the purposes here, it is recommended that the correlation for rough surfaces be used when the flow discontinuity is created by melting. Otherwise, the smooth rod correlation should be adequate.

Plots of the effects of discontinuities on local Sherwood numbers as functions of distance and Reynolds numbers are shown in Figure 3.14.

A somewhat simpler expression for the effects of discontinuities can be derived from correlations of heat transfer data by Gimble et al. [121]. These investigators examined the effects of a transverse grid spacer and correlated their data in the turbulent regime ($8000 \leq N_{Re} < 30{,}000$) with the expression:

$$\frac{Nu}{N_{Re}N_{Pr}} = (0.0850 + 0.612/x^{1/2})N_{Re}^{-\alpha}$$

$$\alpha = \frac{0.00780 + 0.350/x}{0.00257 + x}$$

Then, in the turbulent regime

$$Sh \cong A\, N_{Re}^{1-\alpha}\, N_{Pr}^{2/3} Sc^{1/3}$$

where $A = (0.0850 + 0.612x^{-1/2})$

$$\alpha = \frac{0.00780 + 0.350/x}{0.00257 + x}$$

This correlation yields an overall effect rather than a local effect. Because of the way data were obtained by Gimble et al. the correlation applies only to regions beyond the location of the obstacle in the flow path.

Flow Through a Debris Bed. The recommended correlation in Table 3.13 is one provided by Rowe and Claxton [122]. It is for fixed, isothermal beds with $N_{Re} > 80$. For low Reynolds numbers, correlations appropriate for flow over single sphere should be used.

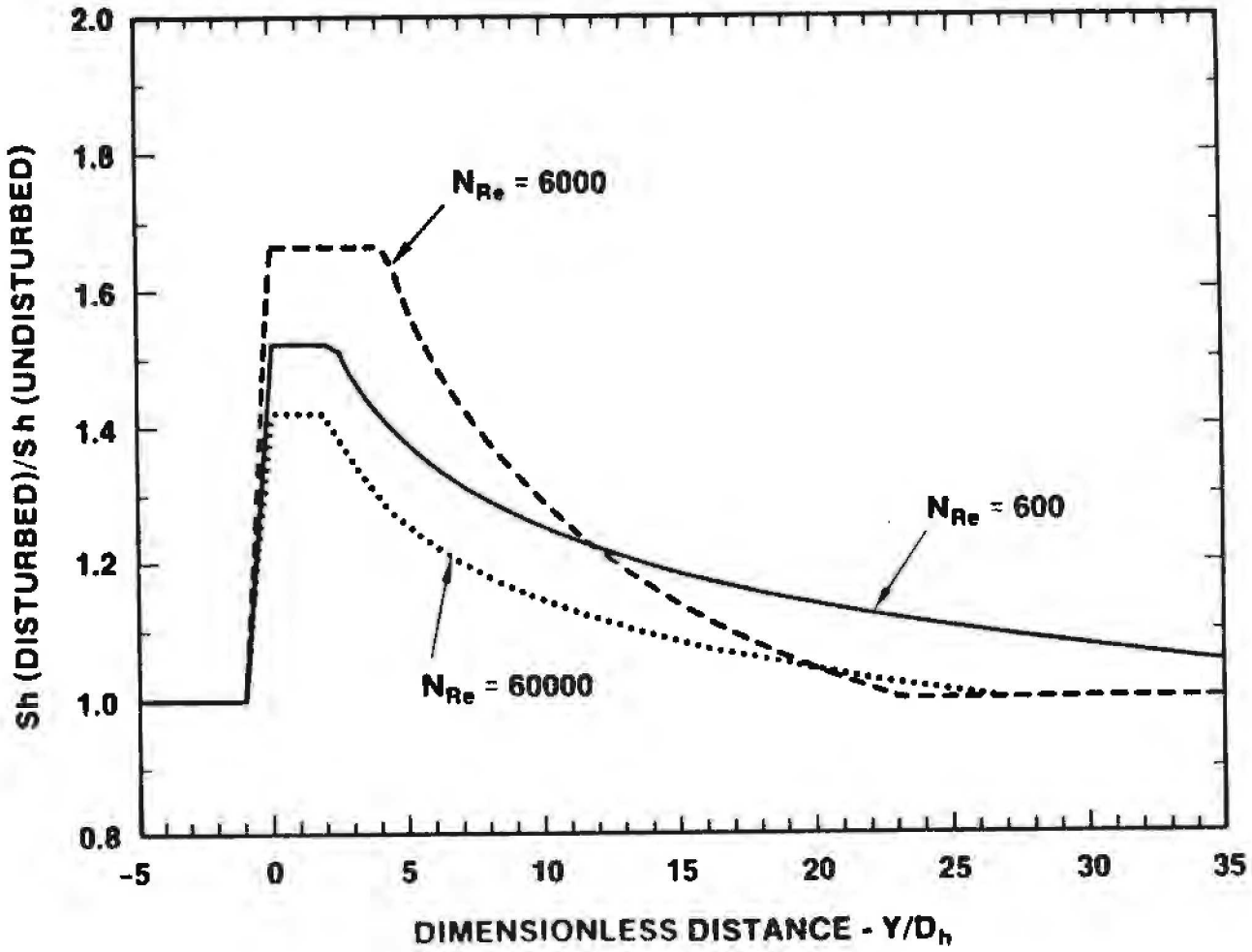

Figure 3.14. Effects of an Obstacle 1 Hydraulic Diameter Wide on the Relative Sherwood Number. Flow blockage was taken to be 0.35 and formulae for rough tubes were used to prepare this figure.

Whitaker [110] has offered an alternate correlation of heat transfer data that appears adequate to Reynolds numbers of 10:

$$Nu = (0.5\ N_{Re}^{1/2} + 0.2\ N_{Re}^{2/3})\ N_{Pr}^{1/3}$$

Should gas velocities become high enough to fluidize the debris bed, then the following correlation [123] may be used to obtain gas phase mass transport coefficients:

$$Sh = 0.374\ N_{Re}^{1.2}\ N_{Sc}^{1/3} \qquad \text{for} \quad 0.1 < N_{Re} < 15$$

$$Sh = 2.01\ N_{Re}^{1.5}\ N_{Sc}^{1/3} \qquad \text{for} \quad 15 < N_{Re} < 250$$

where $N_{Re} = d_p v\rho/\mu$.

Correlations for Steel Structures. Vaporization of constituents of steel can be important for some accidents. A major fraction of the steel in a reactor core is configured as long vertical surfaces. The Sherwood number and consequently the gas phase mass transport coefficient for this type of surface subjected to forced convection can be found from correlations for flow along a flat plate:

1. Laminar flow: $Sh = 0.646\ N_{Re}^{1/2}\ N_{Sc}^{1/3}$

2. Turbulent flow: $Sh = 0.0365\ N_{Re}^{08}$

The length dimension used for both the Sherwood and Reynolds numbers is the length of the structure.

Evaluating k_g. To evaluate the gas phase mass transport coefficient, it is necessary to have the diffusion coefficient of the volatile species in the ambient gas. The ambient gas is, to a first approximation, a mixture of steam and hydrogen. Especially at higher temperatures, the ambient gas becomes more complex since species such as H(gas), OH(gas), and O(gas) become more prevalent. If this complexity is neglected, then the diffusion coefficient of a volatile species in the ambient gas mixture, D_{Am}, is given by

$$D_{Am} = (P_{H_2}/D_{A,H_2} P_T + P_{H_2O}/D_{A,H_2O} P_T)^{-1}$$

where D_{A,H_2} = diffusion coefficient of A in hydrogen

D_{A,H_2O} = diffusion coefficient of A in steam

$$P_T = P_{H_2} + P_{H_2O}$$

The binary diffusion coefficients, D_{A,H_2} and D_{A,H_2O}, can be found from:

$$D_{A,H_2} = \frac{3.2\text{x}10^{-4}\ T^{1.622}}{P_T}$$

$$D_{A,H_2O} = \frac{1.2\text{x}10^{-4}\ T^{1.622}}{P}$$

where P is in atmospheres.

The viscosity of the ambient gas can be found from the Herning-Zipperer equation [124]:

$$\mu_{mix} = \frac{4.24\ P_{H_2O}\ \mu_{H_2O} + 1.41\ P_{H_2}\mu_{H_2}}{4.24\ P_{H_2O} + 1.41\ P_{H_2}}$$

where $\mu_{H_2} = 1.9\text{x}10^{-6}\ T^{0.674}$

$$\mu_{H_2O} = 0.179\text{x}10^{-6}\ T^{1.106}.$$

C. Radionuclide Release From Fragmented Core Debris

The preceding discussions have addressed release as the core degrades from intact fuel rods to a slumped molten pool. Once the molten pool has been formed, some hypothesized accident scenarios assert that the pool cascades from the core region into a water pool in the lower plenum of the reactor vessel. Sudden quenching of the core debris causes it to fragment into particles. Formation of a particle bed could also occur if water were sprayed onto overheated core materials during the core degradation process.

Once a particle bed is formed, it may not be coolable. The supply of coolant might be insufficient to keep the debris quenched. Or, the particle size and the bed structure may be such that coolant cannot flood the bed and keep the core debris particles quenched. If the bed is not coolable, it will heat to sufficient temperatures that the release of radionuclides and other volatiles can resume. The CORSOR model can be modified to predict this release from a debris bed.

Assume the debris has been fragmented into particles which if deformed into spheres would have diameters d_p. Assume the particles are packed so that the porosity of the debris bed is E. The rate of release of the volatile element i from the bed is given then by:

$$\frac{dF_i}{dt} = \frac{6K_{bed}}{d_p \rho_{molar}} \left[1 - F_i(t) - \frac{P_i(bulk)}{P_i(o)} \right]$$

where

$$\frac{1}{K_{bed}} = \frac{1}{K_b(i)\ \exp[-E(i)/RT]\ \rho_{molar}} + \frac{RT}{k_g P_i^o(eq)}$$

$$K_b(i) = 2.75 \times 10^{-3}\ K_o(i)\ \exp\ [1.6\ Bu/1000)\ \left[\frac{10}{d_o}\right]^{\frac{1}{\xi}}$$

if burnup and porosity have not been annealed from the fuel or

$$K_b(i) = K_o(i)/4.225$$

if fuel melted prior to quenching.

If the bed is assumed isothermal and that the gas flow through the bed is not sufficient to levitate the particles, then the gas phase mass transport coefficient is given by [122]:

$$K_g = \frac{D_{AB}}{d_p}\left\{\frac{2}{1-(1-\varepsilon)^{1/3}} + \frac{2}{3\varepsilon}\left[\frac{d_p U_o \rho_g}{\mu}\right]^n \left[\frac{\mu}{\rho_g D_{AB}}\right]^{1/3}\right\}$$

where U_o = superficial velocity of gas through the bed

ρ_g = gas density in g/cm^3

μ = gas viscosity

and n is defined by the equation

$$\frac{2-n}{3n-1} = 4.65\left[\frac{d_p U_o \rho_g}{\mu}\right]^{-0.28}$$

Inspection of the release rate expression shows that for any severe comminution of the debris and if volatile concentrations are not too small, release is controlled almost exclusively by mass transport in the gas phase. When this is the case, greater attention to the mass transport coefficient may be needed. In particular, the assumption that the bed is isothermal may be removed. Heat and mass transport in the bed are then coupled and a substantially more complicated release expression is derived [123].

3.7 Recommendations for MELCOR

1. The MELCOR model should include models of gap release, release during heating, melting, and slumping of the core, and release from fragmented debris.

2. The ORNL gap release is recommended to MELCOR. Inventories of the fuel/clad gap that participate in the gap release are not certain. The inventories used in Reference 7 are recommended to MELCOR. Some care in selecting the gap inventories may be merited since conclusions drawn in severe accident analyses have a tendency to "creep" into design basis considerations where they may not be applicable.

3. The modified CORSOR model derived in this chapter is recommended to MELCOR. Unlike the original form of CORSOR, this modified version can be applied during

melting and slumping. The modified model also allows the effects of fuel burnup, initial grain size of the fuel, ambient pressure, gas flow velocities, and gas composition to be recognized in the analyses. Recommended default values for burnup and initial grain size are 28,000 MWd/t and 10 μm, respectively.

4. If MELCOR will permit core debris to quench and fragment then a model of release from the fragmented debris is needed. The model outlined here is recommended. If release from the debris in this state is significant, an improved model may be needed.

REFERENCES

1. USNRC, Reactor Safety Study: An Assessment of Accident Risks in US Commercial Nuclear Power Plants, WASH-1400, October 1975 and especially R. L. Ritzman et al. "Release of Radioactivity in Reactor Accidents," Appendix VII to the report.

2. Report of the President's Commission on the Accident at Three Mile Island, J. G. Kemeny, Chairman, August 1979 and also the Reports of the Te. Library of Congress Card Number 79-25694 ISBN 0-935758-00-3

3. D. O. Campbell, A. P. Malinauskus, and W. R. Stratton, Nucl. Tech. 53, p. 111 (1981).

4. USNRC, Office of Nuclear Regulatory Research, NUREG 1053, to be published.

5. USNRC, Technical Bases for Estimating Fission Product Behavior During LWR Accidents, NUREG-0772, June 1981.

6. S. J. Niemczyk and L. M. McDowell-Boyer, Interim Source Term Assumptions for Emergency Planning and Equipment Qualification, NUREG/CR-2629, ORNL/TM-8274, and Technical Considerations Related to Interim Source Term Assumptions for Emergency Planning and Equipment Qualification, ORNL/TM-8275, September 1982 Oak Ridge National Laboratory, Oak Ridge, TN.

7. J. A. Gieske et al. Radionuclide Release Under Specific LWR Accident Conditions-Volumes 1-6, BMI-2104, Batelle Columbus Laboratory, Columbus, OH.

8. IDCOR, Industry Degraded Core Rule Making Program, Subtasks 11.1, 11.3, 11.4, and 11.5.

9. See for example G. J. Kolb et al., Reactor Safety Study Methodology Applications Program: Oconee #3 PWR Power Plant, NUREG/CR-1659, SAND80-1897, Rev; Sandia National Laboratory, Albuquerque, NM, May 1981.

10. Commonwealth Edison, Inc., Zion Probabilistic Safety Study, 1981.

11. P. Baybutt, "Radionuclide Release and Transport," Chapter 8, PRA Procedures Guide, Volume 1, NUREG/CR-2300, January 1983.

12. C. Politus, KfK-2167, 1975.

13. D. A. Powers, Transactions American Nuclear Society, 34, p. 563 (1980).

14. Y. B. Katayama, "Leaching of Irradiated LWR Fuel Pellets in Deionized and Typical Ground Water," BNWL-2057, Pacific Northwest Laboratory, July 1976.

15. T. T. Vandergraaf, L. H. Johnson, and D. W. P. Lau, Leaching of Irradiated CANDU UO_2 Fuel," Scientific Basis for Nuclear Waste Management, p. 335.

16. U. B. Ekland and R. Forsyth, Leaching of Irradiated UO_2 Fuel, KBS Report 70, February 1978.

17. R. A. Lorenz, J. L. Collins, and A. P. Malinauskus, Nuclear Technology, 46, p. 404 (1979).

18. J. Brockmann and T. Stalker, Sandia National Laboratories, Albuquerque, NM, unpublished results.

19. G. Parker, G. E. Creek, and A. L. Sutton, Jr., "Influence of Variable Physical Process Assumptions on Core Melt Aerosol Release," Proc. Int'l Mtg. on Thermal Reactor Safety, Chicago, IL, NUREG/CP-0027, Volume 2, p. 1078, 1983.

20. J. P. Mitchell, A. L. Nichols, and J. A. H. Simpson, "The Characterization of Ag-In-Cd Control Rod Aerosols Generated at Temperatures Below 1900 K," CSNI Specialists Meeting on Nuclear Aerosols in Reactor Safety, Karlsruhe, West Germany, September 1984.

21. Major sources of data necessary to calculate $\Delta G_i(T)$ are:

    a. D. R. Stull and H. Prophet, JANAF Thermochemical Tables, 2nd edition, NSRDS-NBS37, June 1971.

    b. M. W. Chase et al. "JANAF Thermochemical Tables 1974 Supplement," J. Phys. Chem. Ref. Data 3, pp. 311-480 (1974).

    b. M. W. Chase et al. "JANAF Thermochemical Tables 1975 Supplement," J. Phys. Chem. Ref. Data 4, pp. 1-175 (1975).

    c. M. W. Chase, Jr. et al. "JANAF Thermochemical Tables 1978 Supplement," J. Phys. Chem. Ref. Data 7, pp. 793-940 (1978).

d. M. W. Chase, Jr. et al. "JANAF Thermochemical Tables 1982 Supplement," J. Phys. Chem. Ref. Data 11, pp. 695-940 (1982).

e. I. Barin and O. Knacke, Thermochemical Properties of Inorganic Substances, Springer-Verlag, 1973.

f. I. Barin, O. Knacke, and O. Kubachewski, Thermochemical Properties of Inorganic Substances, Supplement, Springer-Verlag, 1977.

g. K. C. Mills, Thermodynamic Data for Inorganic Sulphides, Selenides and Tellurides, Butterworths, London, 1974.

h. R. A. Robie et al. Thermodynamic Properties of Minerals and Related Substances at 298.15 K and 1 Bar (10^5 Pascals) Pressure and at Higher Temperatures, Geological Survey Bulletin 1452.

i. D. D. Jackson, Thermodynamics of Gases Hydroxides, UCRL-51137, 1971.

j. P. E. Blackburn and C. E. Johnson, ANL-82-42, Argonne National Labs, 1982.

k. F. Garisto, Thermodynamics of Iodine, Cesium, and Tellurium in the Primary Heat Transport System Under Accident Conditions, Atomic Energy of Canada, Ltd., AECL-7782.

l. D. D. Wagman et al. "The NBS Tables of Thermodynamic Properties," J. Phys. Chem. Ref. Data 11 (1982) Supplement 2.

m. R. Hultgren, R. L. Orr, P. D. Anderson, and K. K. Kelley, Selected Values of Thermodynamic Properties of Metals and Alloys, J. Wiley and Sons.

22. D. A. Powers, Control Rod Behavior During Core Degradation I: Pressurization of Ag-In-Cd Control Rods, NUREG/CR-4401, SAND85-0469, Sandia National Laboratories, Albuquerque, NM. Sept., 1985.

23. D. A. Powers and J. E. Brockmann, VANESA: A Mechanistic Model of Radionuclide Release and Aerosol Generation During Core Debris/Concrete Interactions, NUREG/CR-4308, Sandia National Laboratories, Albuquerque, NM, July, 1986.

24. J. F. Muir et al., CORCON-MOD1: An Improved Model for Molten-Core/Concrete Interactions. NUREG/CR-2142, SAND80-2415 Sandia National Laboratories, Albuquerque, NM, 1981.

25. W. R. Smith, Industrial and Engineering Chemistry, Fundamentals 19, p. 1 (1980).

26. W. B. White, S. M. Johnson, and G. B. Dantzig, J. Chem. Phys. 28, p. 751 (1958).

27. T. Gerlach, FLUEQU, unpublished code used in the calculations for Reference 5.

28. G. Eriksson and E. Rosen, Chem. Scripta 4, p. 193 (1973).

29. G. Eriksson, Acta Chem. Scand. 25, p. 2651 (1971).

30. S. R. Brinkley, Jr., J. Chem. Phys. 15, p. 107 (1947).

31. D. A. Powers in Advanced Reactor Safety Research Quarterly Report April-June, 1979, NUREG/CR-0984 SAND79-1597, Sandia National Laboratories, Albuquerque, NM, November 1979.

32. Electric Power Research Institute, Technical Reports 11.1, 11.4 and 11.5 Estimation of Fission Product and Core Material Characteristics, Atomic Industrial Forum, October 1983.

33. K. Konashi, T. Yato, and H. Kaneko, J. Nucl. Mat'ls 116, p. 86 (1983).

34. G. A. Somorjai, "High Temperature Vaporization Mechanisms," p. 73 in High Temperature Technology Proceedings of the 3rd International Symposium, Asilomar, CA, 1967.

35. J. P. Hirth and G. M. Pound, Condensation and Evaporation, Pergamon Press, New York, 1963.

36. S. E. Ziemniak, "A Study of Interfacial Resistance to Mass Transfer at High Evaporation Rates," Thesis, Rensselaer Polytechnic Institute, August 1968.

37. R. G. Ward, J. Iron and Steel Institute, 201, p. 11 (1963).

38. R. A. Lorenz, "The Vaporization of Structural Materials in Severe Accidents," Proc. Int'l Mtg. on Thermal Nuclear Reactor Safety, Chicago, IL, NUREG/CP-0027, 1983.

39. E. A. Mason, A. P. Malinauskus, and R. B. Evans, J. Chem. Phys. 46, p. 3199 (1967).

40. S. Chapman and T. G. Cowling, Mathematical Theory of Non-uniform Gases, 2nd edition, Cambridge Press, 1961.

41. E. R. Gilliland, Ind. Eng. Chem. 26, p. 681 (1934).

42. P. C. Singh and S. Singh, Int. Comm. Heat Mass Transfer 10, p. 123 (1983).

43. E. T. Turkdogan, P. Grieveson, and L. S. Darken J. Metals 5, p. 21 (1962).

44. A. W. D. Hills and J. Szekeley, Int'l J. Heat and Mass Transport 12, p. 111 (1969).

45. E. T. Turkdogan and K. C. Mills, Trans. AIME 230, p. 750 (1964).

46. F. F. Abraham, Homogeneous Nucleation Theory, Academic Press, 1974.

47. R. Becker and W. Dîring, Ann. Phys. (Leipzig) 24, p. 719 (1935).

48. J. Lothe and G. M. Pound, J. Chem. Phys. 36, p. 208c (1962).

49. W. Camp, Sandia National Laboratories, unpublished results.

50. B. M. Jeffery, J. Nucl. Mat'l. 22, p. 33 (1967).

51. J. I. Bramman et al., J. Nucl. Mat'l 25, p. 201 (1968).

52. F. Schmitz et al, Int'l Mtg. on Fast Reactor Fuel and Fuel Elements, p. 336 (1970).

53. K. C. Russel, J. Chem. Phys. 50, p. 1809 (1969).

54. M. W. Mallett, A. F. Gerds, A. W. Lemmon, Jr., and D. L. Chase, BMI-1028 (1956).

55. P. Hofmann, D. Kerwin-Peck, and P. Nikolopoulos, Physical and Chemical Phenomena Associated with the Dissolution of Solid UO_2 by Molten Zircaloy-4, PNS-Nr 675812, Kernforschungszentrum Karlsruhe, 1982.

56. C. Politus, KfK 2167 (1975).

57. D. A. Powers, "Chemical and Physical Processes of Reactor Core Meltdown, Chapter 4 in Core Meltdown Experimental Review, SAND74-0382 (Revision) NUREG-0205, Sandia National Laboratories, Albuquerque, NM, March 1979.

58. J. Fischer, J. D. Schilb, and M. G. Chasanov, J. Nucl. Mat. 48, p. 233 (1973).

59. R. A. Lorenz, J. L. Collins, and A. P. Malinauskus, Nuclear Technology, 46, p. 404 (1979).

60. R. A. Lorenz, "Status of Validation of the CORSOR Computer Code Used for the Accident Source Term Reassessment Study," in Review of the Status of Validation of the Computer Codes Used in the NRC Accident Source Term Reassessment Study (BMI-2104), ORNL/TM-8842, Oak Ridge National Laboratory.

61. A. H. Booth, AECL CRDC-721, Atomic Energy of Canada, Ltd. 1954.

62. D. R. Olander, Fundamental Aspects of Nuclear Reactor Fuel Elements, UC 736 TID 26711, 1975.

63. J. Rest, GRASS-SST: A Comprehensive, Mechanistic Model for the Prediction of Fission-gas Release in UO_2-Base Fuels During Steady-State and Transient Conditions, NUREG/CR-0202, ANL78-53, Argonne National Laboratory, June 1978.

64. S. E. Turner et al., Background and Derivation of ANS5.4 Standard Fission Product Release Model, NUREG/CR-2507, January 1982.

65. D. M. Haaland, "Release of Radioactivity from the Core," Chapter 7 in Core Meltdown Experimental Review, SAND74-0382 (Revision), NUREG-0205, Sandia National Laboratories, Albuquerque, NM, 1977.

66a. W. Herning, J. Nucl. Mat'ls. 114, p. 41 (1983).

66b. I. R. Brearly and D. A. MacInes, SINGAR-A Model to Examine Fission Product Release in Accident Studies, SRD R-258, Safety and Reliability Directorate, UK Atomic Energy Authority, June 1983.

66c. K. Malen, AFISS-A Computer Code for Calculation of Accident Fission Product Release from Fuel Rods, Studsvik/NF(p)-81/62, 1981.

67. P. E. Blackburn, J. Nucl. Mat'ls. 46, p. 244 (1973).

68. S. W. Tam, P. E. Blackburn, and C. E. Johnson, "Effect of Core Chemistry on Fission Product Release," Proc. Int'l Mtg. on Thermal Nuclear Reactor Safety, Chicago, IL, NUREG/CP-0027, Vol. 1, pp. 101-110, February 1983.

69. H. Kleykamp, J. Nucl. Mat'ls. 84, p. 109 (1979).

70. O. Gotzmann, J. Nucl. Mat'ls. 107, p. 185 (1982).

71. D. Cubicciotti and J. H. Davies, Nucl. Sci and Eng. 60, p. 314 (1976).

72. C. E. Miller, Jr., Nuclear Applications 5, p. 1 (1968).

73. D. Cubicciotti, Nuclear Technology 53, p. 5 (1981).

74. W. I. Stuart and R. B. Adams, J. Nucl. Mat'ls. 58, p. 201 (1975).

75. M. J. Bannister and W. J. Buykx, J. Nucl. Mat'ls. 64, p. 57 (1977).

76. J. T. Bittel, L. H. Sjodakl, and J. F. White, J. Am. Ceram. Soc. 52, p. 446 (1969).

77. S. C. Jain, Proc. Roy. Soc. (London) A 243, p. 359 (1957).

78. R. O. Wooton and H. I. Avci, MARCH 1.1 (Meltdown Accident Response Characteristics) Code Description and User's Manual, NUREG/CR-1711, October 1980.

79. H. Albrecht, V. Matschoss, and H. Wild, "Experimental Investigation of Fission and Activation Product Release from LWR Fuel Rods at Temperatures Ranging from 1500-2800°C," Proc. Specialists Mtg. on the Behavior of Defected Zr Alloy Clad Ceramic Fuel in Water Cooled Reactors, CONF-790935-3 (1979).

80. H. Albrecht and H. Wild, "Investigation of Fission Product Release by Annealing and Melting LWR Fuel Pins in Air and Steam," Proc. Topical Mtg. on Reactor Safety Aspects of Fuel Behavior, Sun Valley, ID, August 1981.

81. H. Albrecht, "Out-of-Pile Release Tests Under Core Melting Conditions," OECD-NEA-CSNI/IAEA Specialists Mtg. on Water Reactor Safety and Fission Product Release in Off-Normal and Accident Conditions, 1983.

82. H. Albrecht and H. Wild, "Behavior of I, Cs, Te, Ba, Ag, In, and Cd During Release from Overheated PWR Cores," Proc. Int'l Mtg. on LWR Severe Accident Evaluation, August 1983 Cambridge, MA, paper TS4.2.

83. H. Albrecht, K. Nolte, and H. Wild, KfK 2950, Kernforschungszentrum Karlsruhe, West Germany, 1980.

84. H. Albrecht, K. Nolte, V. Prech, K. H. Simon, and H. Wild, KfK-3250, Kernforschungszentrum Karlsruhe, West Germany, 1981.

85. H. Albrecht, V. Matschoss, K. Nolte, and H. Wild, KfK-2750, Kernforschungszentrum Karlsruhe, West Germany, 1978.

86. M. F. Osborne, R. A. Lorenz, K. S. Norwood, J. R. Travis, and C. S. Webster, Data Summary Report for the Fission Product Release Test HI-3, NUREG/CR-3335 ORNL/TM-8783, Oak Ridge National Laboratory, Oak Ridge, TN.

87. D. J. Osetek, K. Vinjamuri, D. E. Kuders, and R. R. Hobbins, "Iodine and Cesium Behavior During the First PBF Severe Fuel Damage Test," Proc. Int'l Mtg. on LWR Severe Accident Evaluation paper TS 4.3, Cambridge, MA, 1983.

88. R. A. Lorenz et al., Fission Product Release from Highly Irradiated Fuel Heated to 1300-1600°C in Steam, NUREG/CR-1386, ORNL/NUREG/TM-346, Oak Ridge National Laboratories, Oak Ridge, TN, December 1980.

89. R. A. Lorenz et al., Fission Product Release from BWR Fuel Under LOCA Conditions, ORNL/NUREG/TM-388, Oak Ridge National Laboratories, Oak Ridge, TN, July 1981.

90. R. A. Lorenz, J. L. Collins, and A. P. Malinauskus, Fission Product Source Terms for the LWR Loss-of-Coolant Accident, NUREG/CR-1288, ORNL/NUREG/TM-321, July 1980.

91. M. F. Osborne, R. A. Lorenz, J. R. Travis, and C. S. Webster, Data Summary Report for the Fission Product Release Test HI-1, NUREG/CR-2928, ORNL/TM-8500, Oak Ridge National Laboratories, Oak Ridge, TN, December 1982.

92. M. F. Osborne, R. A. Lorenz, J. R. Travis, C. S. Webster and K. S. Norwood, Data Summary Report for the Fission Product Release Test HI-2, NUREG/CR-3171, ORNL/TM-8667, Oak Ridge National Laboratory, Oak Ridge, TN.

93. M. F. Osborne, R. A. Lorenz, K. S. Norwood, and R. P. Wichner, "Fisson Product Release Under LWR Accident Conditions," Proc. Int'l Mtg. on LWR Severe Accident Evaluation paper TS 4.1, Cambridge, MA, 1983.

94. R. A. Lorenz, E. C. Beahm, and R. P. Wichner, "Review of Tellurium Release Rates from LWR Fuel Elements Under Accident Conditions," Proc. Int'l Mtg. on LWR Severe Accident Evaluation, paper TS 4.4, Cambridge, MA, 1983.

95. C. D. Andriesse and R. H. J. Tanke, Nuclear Technology 65, p. 415 (1984).

96. D. A. Young, Decomposition of Solids, Pergamon Press, 1966.

97. R. A. Lorenz, "Status of Validation of the CORSOR Computer Code Used for the Accident Source Term Reassessment Study," in Review of the Status of Validation of the Computer Codes Used in the NRC Accident Source Term Reassessment Study (BMI-2104), T. S. Kress, editor, ORNL/TM-8842, Oak Ridge National Laboratory, Oak Ridge, TN.

98. A. W. Coats and J. P. Redfern, Nature 201, p. 68 (1964).

99. V. M. Gorbaschev, J. Thermal Analysis 8, p. 349 (1975).

100. A. Van Tets, Thermochemical Acta 17, p. 372 (1976).

101. V. Denny and B. Raj Schgal, "Analytical Predictions of Core Heatup/Liquefaction/Slumping" paper TS-5.4 in Proc. Int'l Mtg. LWR Severe Accident Evaluation Vol. 1, August 28-September 1, 1983, Cambridge, MA.

102. B. D. Johnston, The Zircaloy-Uranium Dioxide Reaction, SRD R294, Safety and Reliability Directorate, United Kingdom Atomic Energy Authority, Culcheth Warrington, Great Britian, September 1984.

103. J. Rivard, Review of In-vessel Meltdown Models, NUREG/CR-1493, SAND80-0455, Sandia National Laboratories, Albuquerque, NM, July 1980.

104. D. Williams and J. B. Rivard, "Range of Possible Net Release from the RCS," Appendix B in R. J. Lipinski, et al. Uncertainty in Radionuclide Release Under Specific LWR Accident Conditions, Volume 2, SAND84-0410/2, Sandia National Laboratories, Albuquerque, NM, February 1985.

105. S. Hagan et al. Projekt Nuklease Sicherheit, KfK-2750 4300-62, Kernforschungszentrum Karlsruhe, West Germany, November 1978.

106. J. Rivard, "RCS Assessment for MELCOR," Chapter 2 in Thermal-Hydraulic Process Modeling in Risk Analysis: An Assessment of The Relevant Systems, Structures, and Phenomena, NUREG/CR-3986, SAND84-1219, Sandia National Laboratories, Albuquerque, NM, August 1984.

107. R. L. Steinberger and R. E. Treybal, AICHE J. 6, p. 227 (1960).

108. D. C. T. Pei, C. Narasimham, and W. H. Gauvin, Proc. Symp. on Interactions between Fluids and Particles, Institute of Chemical Engineering, London, June 1962.

109. G. Schlitz, Intern J. Heat and Mass Transfer 6, p. 873 (1963).

110. S. Whitaker AIChE J. 18, p. 361 (1972).

111. D. C. Collins and M. J. Williams, J. Fluid Mechanics 6, p. 357 (1959).

112. H. Smyczek and J. Zablocki, Pr. Nauk Inst. Inz. Chem. Urzadzen Cielplnych Politech. Wroslaw 24, pp. 261-266 (1974); CA:82:142094a.

113. J. Weisman, Nucl. Sci. and Eng. 6, p. 78 (1959).

114. D. A. Dingee and J. W. Chastain, "Heat Transfer from Parallel Rods in Axial Flow," Reactor Heat Transfer Conference of 1956, J.E. Viscardi, editor, TID-7529 pt. 1, p. 462, 1957.

115. E. M. Sparrow, A. L. Loeffler, Jr., and H. A. Hubbard, Trans. ASME J. of Heat Transfer, pp. 415-422, November 1961.

116. O. E. Dwyer, Nucl. Eng. Design 10, p. 3 (1969).

117. O. E. Dwyer, AIChE J. 9, p. 261 (1963).

118. P. A. Ushakov, A. V. Zhukov and N. M. Matyukhin, Teplofizika Vysokikh Temperatur 15, p. 1027 (1977).

119. R. K. Shah and A. L. London, "Laminar Flow Forced Convection in Ducts," Advances in Heat Transfer Supplement 1, Academic Press, 1978.

120. R. E. Gimble, W. H. Bell, and S. L. Fawcett, Heat Transfer and Friction-Flow Characteristics of Cylindrical Parallel Rods with Transverse Cylindrical Spacers, AECD-3975, Batelle Memorial Institute, Columbus, OH, 1954.

121. M. A. Hassan and K. Rehme, Nucl. Technology 52, p. 401 (1981).

122. P. N. Rowe and K. T. Claxton, Trans. Inst. Chem. Eng. 43, p 10 T321 (1965).

123. O. Mathews, Trans. Can. Inst. Min. Met. 52, p. 97 (1939).

124. F. Herning and L. Zipperer, Gas Wasserfach. 73, p. 49 (1936).

125. C. F. Clement, Aerosol Growth in Vapour-Gas Mixtures Cooled Through Surfaces, TP. 897, AERE Harwell, May, 1982.

126. A. D. Emery, D. B. Scott, and J. R. Stewart, Nucl. Technology 11 (1971) 474.

CHAPTER 4

FISSION PRODUCT RELEASE AND AEROSOL GENERATION WITHIN THE REACTOR CONTAINMENT

D. A. Powers

4.1 Introduction and Definitions

An accident severe enough to melt the reactor fuel in a light water reactor will lead to release of radioactive material from the fuel. This released material, primarily in the form of aerosols, may escape into the reactor containment and, perhaps, from there into the environment. The nature of radioactive material released from the fuel -- its composition, form, release rate, and integral release fraction -- is called the "source term".

Radioactive material released from fuel that has penetrated the reactor pressure vessel is the "ex-vessel source term". Ex-vessel release of radioactive material is one of the four release processes considered in the Reactor Safety Study [1]. At the time of the Reactor Safety Study, little was known about any of the release processes. Approximate calculations, possible then, placed the greatest emphasis on release from fuel within the reactor primary system. The relatively volatile species emitted from the fuel during the early stages of a severe reactor accident were assumed to pose the greatest radiological threat. In an effort to provide bounding estimates of released radio activity that would be applicable to the severest accident at a wide variety of nuclear plants, the analyses in the Reactor Safety Study [2] neglected many processes that mitigate the source term. One consequence of the conservative approach was to make the ex-vessel source term appear less significant than the source terms from in-vessel processes.

The more sophisticated understanding of severe accident source terms that has developed since the Reactor Safety Study has kindled a greater interest in ex-vessel release processes. Modern treatments of source terms distinguish between radioactive material released from the fuel - the "phenomenological source term" - and the radioactive material that escapes from a reactor plant - the "radiological source term". Much of the new interest in the ex-vessel source term arises because of the mechanistic relationship between the phenomenological and the radiological source terms as well as the inherent nature of ex-vessel release of radioactive material. Some specific reasons for this interest are:

(1) Ongoing studies of fission product behavior under reactor-accident conditions have shown that much of the radioactive material released in-vessel may not escape

the reactor primary system and contribute to the inventory of material in the containment available for the radiological source term. · Proportionately, the contribution of material released ex-vessel to this inventory may be greater than heretofore supposed because ex-vessel releases are less susceptible to mitigation during transport from the point of release to the reactor containment.

(2) Radioactive material released ex-vessel includes more refractory isotopes than does the in-vessel release. The qualitative nature of the radiological source term may be changed if the ex-vessel release contributions are greater than expected.

(3) Aerosol processes naturally mitigate the phenomenological source term. Significant delays between in-vessel emissions of radioactivity from the fuel and gross containment failure are possible and provide an opportunity for great reduction in the amount of material released in-vessel that will escape into the environment. The ex-vessel sources are likely to be operative even after gross containment failure has occurred. Then the ex-vessel sources are less susceptible to mitigation by aerosol processes.

(4) The aerosol processes that can cause such mitigation of the in-vessel source proceed among particles whether they are radioactive or not. The copious emission of non-radioactive materials typically associated with the ex-vessel sources provide a means to greatly enhance mitigation of the phenomenological source term particularly that portion of the source term created of the ex-vessel source term could lead to both quantitative and qualitative changes in the perceived radiological consequences of severe reactor accidents.

The second of the above points deserves some elaboration. Fission product releases during the ex-vessel debris interactions do involve the more refractory elements since volatile species would escape the fuel before the onset of ex-vessel phenomena. The radiological effects of refractory fission products have not received a great deal of attention in the past: first, because the releases of these elements were deemed small, and second, the effects would be swamped by the releases of large amounts of cesium and iodine from fuel in the vessel. If the volatile species such as iodine do not escape the reactor coolant system, then the radiological consequences of releasing refractory fission product species need further examination. Results of a first attempt to do so are assembled in Table 4.1. To prepare this table, the radiological consequences of the release of 10%

TABLE 4.1

Radiological Effects of Refractory Fission Products in Comparison to Cesium and Iodine [6]

Element	Relative Early Bone-Marrow Dose
I	1.0
Cs	0.1
Te	0.6
La	0.8
Ce	0.2
Pr	0.0001
Nd	0.3
Np	1.2
Pu	1×10^{-6}
Mo	0.1

Element	Relative Long Term Dose
Cs	1.0
Ce	0.21
Nb	0.7
Zr	1.4
Ru	0.7

of the cesium inventory and 10% of the iodine inventory were normalized to unity. The consequences of the release of 10% of the inventory of other, selected, isotopes were then determined on this relative scale. It is apparent from these results that the refractory isotopes can be every bit as consequential as the volatile isotopes that have received so much attention in the past.

In the sections that follow, the current state-of-the-art in predicting the ex-vessel phenomenological source term is described. To present this discussion, it is convenient to divide the topic into two categories - primary ex-vessel source processes and secondary source process. The primary source processes give rise to release as a direct consequence of the ex-vessel behavior of the fuel. Release of radioactivity during (1) ejection of fuel from the primary system into the reactor containment, (2) interaction of fuel and core debris with concrete, and (3) ex-vessel interaction of molten material with water are all primary source processes. Leaching of radioactive materials from core debris by groundwater should the reactor basemat be penetrated is considered also to be a primary process.

Secondary source processes are those that arise because of the behavior of materials previously released from the fuel whether this release occurred during the in-vessel or ex-vessel stages of an accident. Resuspension of deposited aerosols and radiolytic release of iodine in sump waters are examples of secondary processes.

The focus of the discussions below is on the release of radioactivity from the fuel ex-vessel. Mitigation of this phenomenological source term by the presence of non-radioactive aerosols and enhancement of the source by secondary processes have become quite important aspects of severe reactor accident analyses (3). To meet the needs of these analyses, release of non-radioactive materials from concrete and structural materials in a reactor containment are also discussed. The processes by which the phenomenological ex-vessel source term is converted into a radiological source term are reserved for treatment elsewhere [4].

4.2 Primary Fissions Product Release

A. Release Associated with Melt Ejection

The ex-vessel phase of a severe reactor accident begins with the expulsion of core debris from the reactor coolant system. Most previous analyses of severe reactor accidents have devoted little attention to the details of the expulsion process. Reactor accident phenomena have been described in these previous studies as though the coolant system were depressurized - a

situation appropriate for accidents initiated by large breaks in the coolant system. Consequently, expulsion of the molten core material from the primary system was considered to be driven by gravity. Some small amount of fission product and aerosol release could come from the core debris as it fell from the primary system into the reactor cavity. But, any error caused by neglecting this release has been judged small in comparison to uncertainties concerning aerosol generation and fission product release associated with the behavior of the core debris once it has been expelled. This judgement is supported by the results of recent tests with large-scale UO_2 melts expelled under the force of gravity from a furnace [5a].

The past systematic analyses of severe reactor accidents have concluded unanimously that accidents initiated by large breaks in the primary coolant system do not dominate the risk associated with the commercial use of nuclear power (for examples, see references 1 and 7). Accidents initiated by small breaks in the coolant system or transient events are more frequent. Descriptions of the phenomena during accidents initiated by small breaks or transients assuming a depressured primary system have been criticized [5]. It is expected that prior to melt expulsion in these more frequent accidents, the primary system would be at or near operating pressure. Even in boiling water reactors where operation procedures dictate primary system depressurization during off-normal events, the system would be at an elevated pressure (> 200 psig) throughout the process of core melt formation and up to the time of melt expulsion.

Henry has attempted to determine how the process of melt expulsion might be affected if the reactor coolant system were pressurized [7]. His analysis concluded that hydrodynamic phenomena exist which could disperse the core debris broadly if it were expelled from a pressurized system. The fraction of the core so broadly distributed (nominally 50%) could easily be quenched and kept cool so it would not further interact with materials outside the coolant system. Consequently, this debris would not be a continuing source of fission product release or aerosol generation.

These first attempts to ascertain how expulsion of the core debris from a pressurized primary system might affect the course of ex-vessel phases of a severe reactor accidents have not considered fission product release and aerosol production during melt expulsion. Early attempts to study melt ejection from pressurized systems have demonstrated that the ejection process process can be a formidable source of aerosols [8]. Figure 4.1 is a series of photographs taken of an experiment in which a thermitically generated melt weighing 2.5 kg was ejected from a vessel pressurized to 40 atmospheres. Aerosol production begins

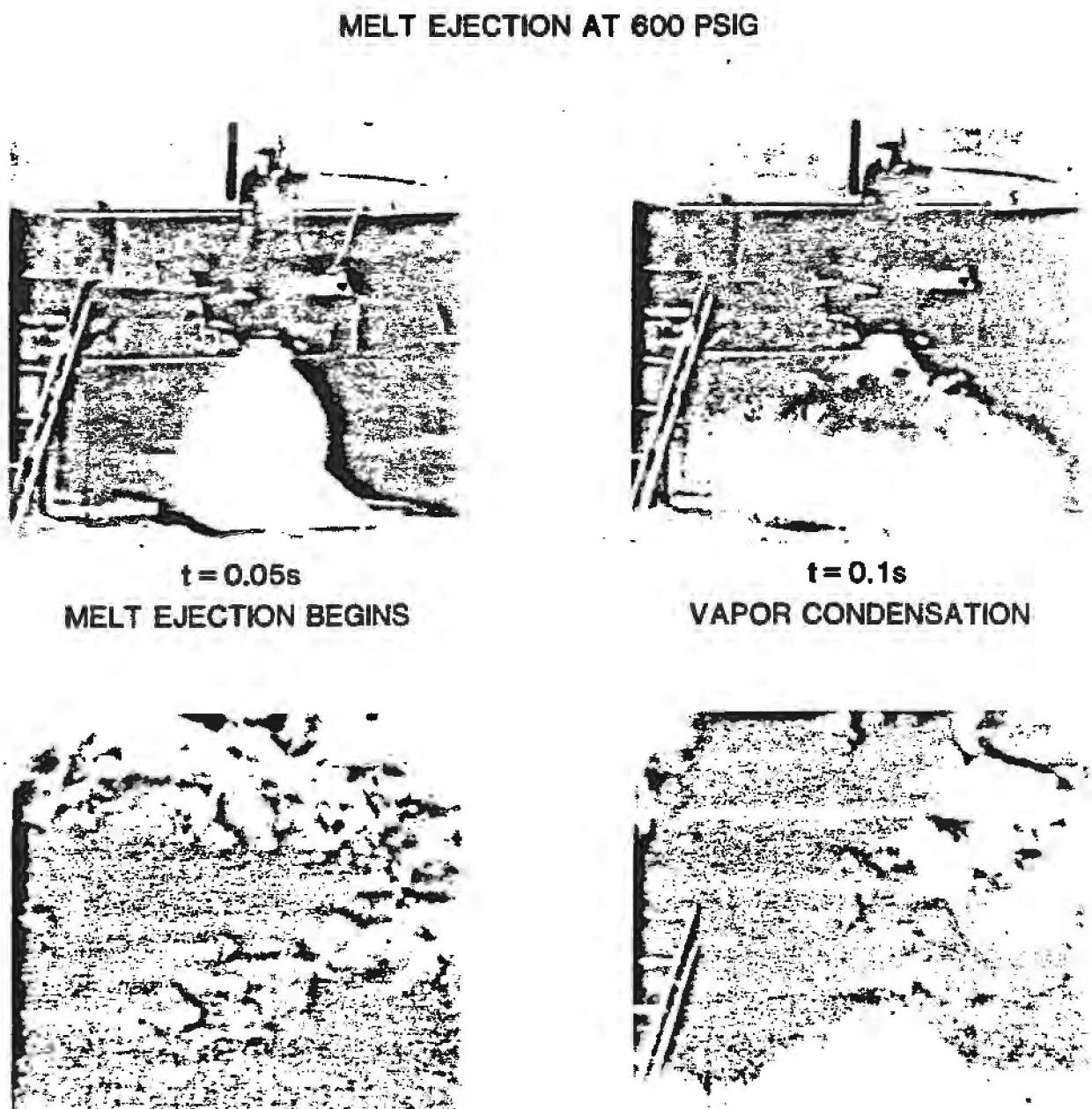

Figure 4.1 Sequence of Photographs Taken During Expulsion of 2.5 Kg of Melt from a Vessel Pressurized to 40 Atmospheres.

in this experiment with the initial emergence of melt and continues throughout the expulsion process. The aerosol production becomes so intense, the experimental apparatus is completely obscured about one second after the start of the test.

Samples taken during this and similar tests show a size distribution that may be trimodal (See Figure 4.2). Modes appear at 0.5 μm, 5 μm and at a larger size - nominally 65 μm [8]. The finest particles seem to be composed of compact agglomerates of 0.1 μm particles. The material of size near 5 μm is composed of nearly spherical particles that have the appearance of frozen liquid. The coarse mode material consists of both spherical and granular shapes. These particles, too, may have been liquid droplets once. The irregular shapes of some of the particles may have been caused by shrinkage during solidification or because the particles were broken during sampling. These coarse particles may not represent a mode in the aerosol size distribution. They may, in fact, be the "tail" of the distribution of very coarse particulate debris produced by the pressurized melt ejection. The large particle size sampling efficiency cutoff causes the aerosol sampling equipment to produce an inaccurate characterization of the coarse material.

Pressurized melts have also been expelled into scaled models of reactor cavities. Aerosols collected during these tests have size distributions with only two modes. The fine material (<1 μm) is similar to that described above. There is no indication of aerosol material concentrations in the 3-8 μm size range. There is a significant amount of coarse material. Again, this coarse material collected with the aerosol sampling equipment is probably the "tail" of the size distributed debris particulate produced during expulsion from the reactor cavity model. This debris has been characterized by flash x-rays as it emerged from the cavity and by post-test sieve analyses. The material has been found to be log-normally distributed in size with mean particle sizes of 0.4 to 0.8 μm and a geometric standard deviation of about 3.4 (See Figure 4.3). This size distribution implies that less than 4% of the mass expelled from the cavity would have particle sizes of less than 50 μm.

Few measurements of the mass of expelled melt converted into aerosols have been reported. In tests involving melt expulsion into a reactor cavity, 0.5-1% of the melt mass aerosolized. About half of this material was smaller than 10 μm and about 35% was smaller than 1 μm. In tests involving melt expulsion into a gravel bed, 0.3 to 6% of the melt mass was estimated to be in the form of aerosols.

Several mechanisms of aerosol generation may be operative in the pressurized melt ejection tests:

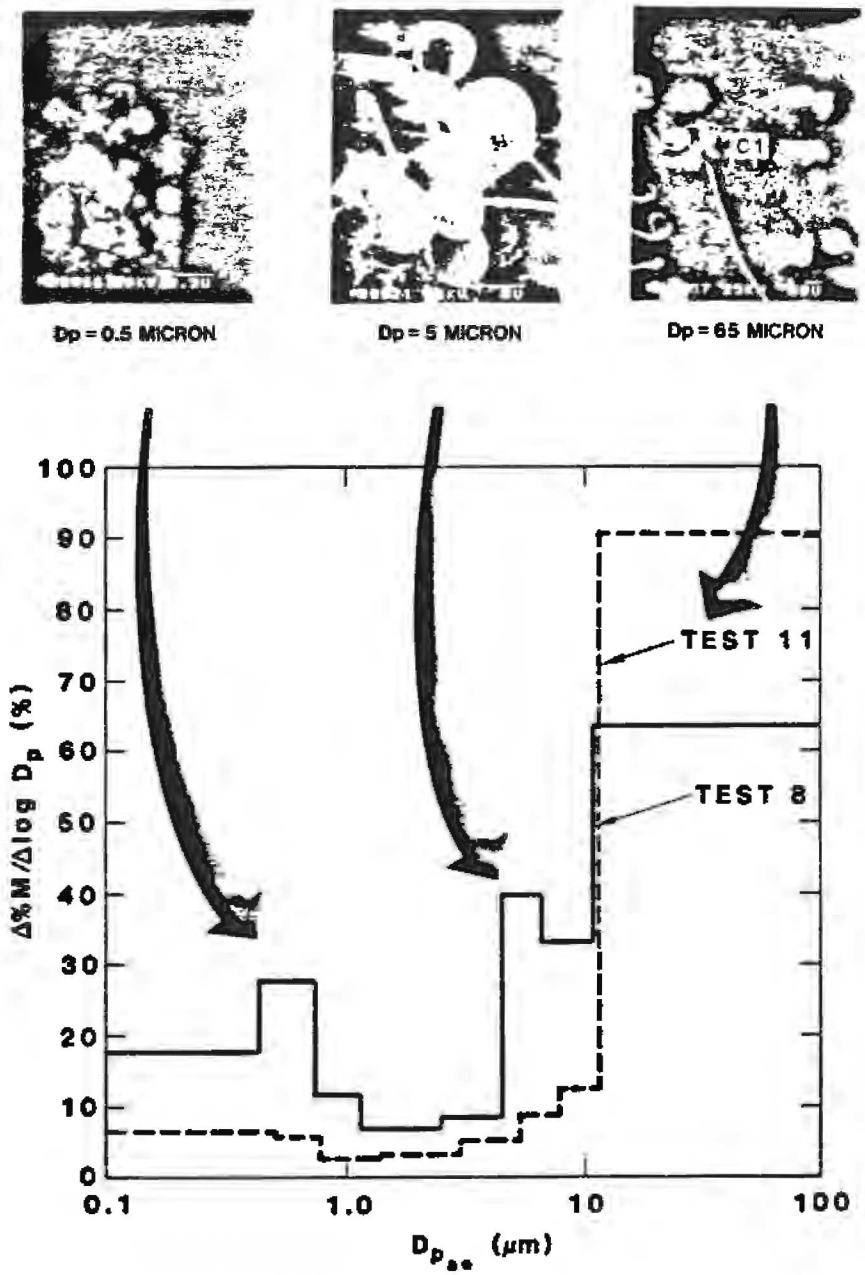

Figure 4.2 Size Distribution of Aerosols Produced During Pressurized Ejection of Melts.

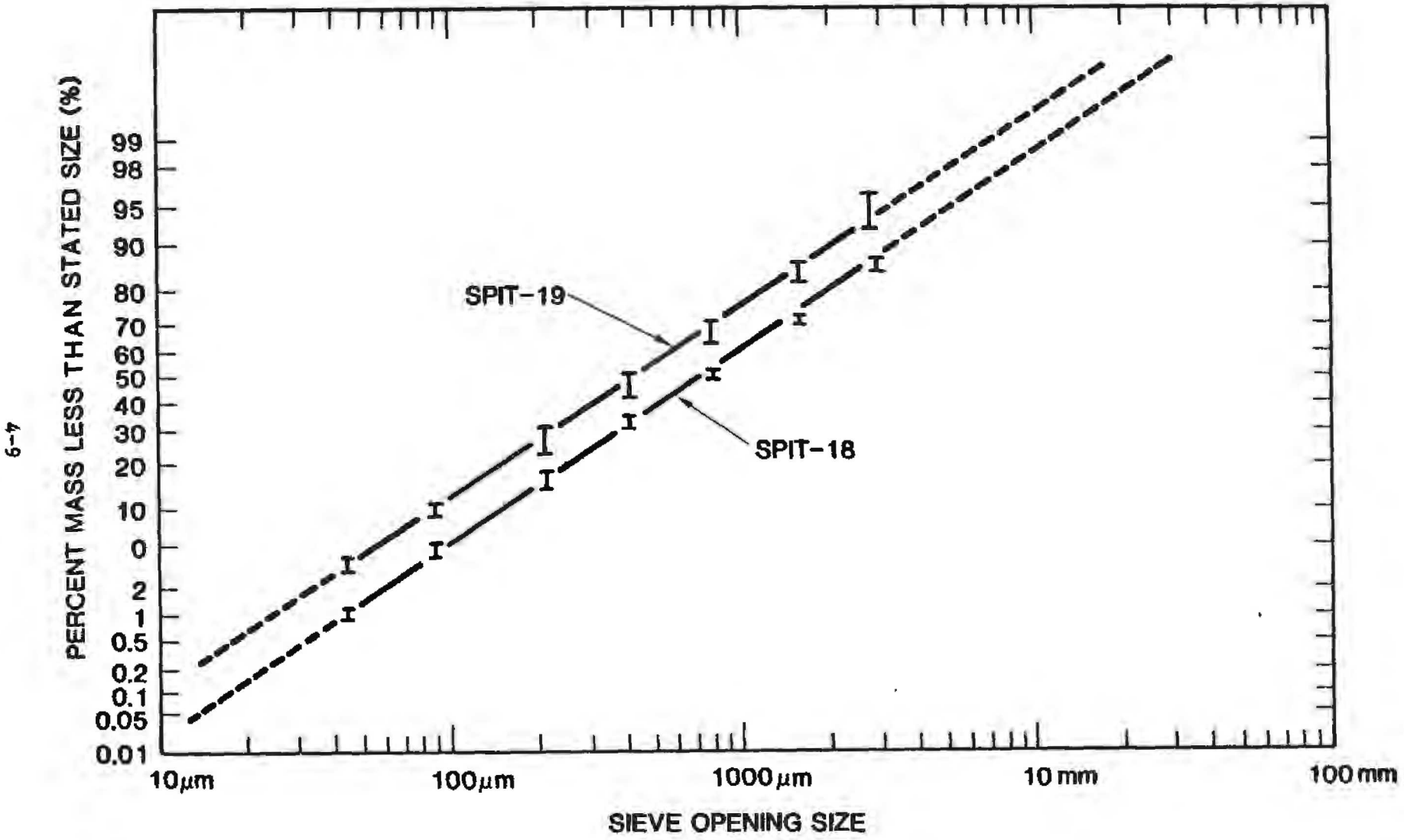

Figure 4.3 Size Distribution of Debris Produced When Melt is Ejected from a Pressurized Vessel into Scaled Models of a Reactor Cavity (SPIT Test Series).

(a) simple vaporization of volatile species from the melt,

(b) disruption of the jet of melt by hydrodynamic processes or by effervescence of gases dissolved in the melt,

(c) pneumatic atomization of the melt at the point of discharge from the pressure vessel, and

(d) chemical reaction of coarse debris lofted into the atmosphere by the expulsion process.

Vaporization of melt constituents followed by condensation of these vapors is the most obvious means of aerosol production. Photographic records of pressurized melt ejection suggest this mecnanism is operative in the tests (see Figure 4.1). The finest particles observed in the pressurized melt ejection tests have been attributed to this vaporization process. Microscopic examination of the 0.5 mm particles shows that these particles are probably agglomerates of yet finer particles. The sizes of these finer particles, 0.05 - 0.1 mm, are consistent with a nucleate condensation mechanism of formation.

The vaporization process should yield particles whose compositions reflect the relative volatility of melt constituents rather than the bulk melt composition. In reactor accident situations, this aerosol could be enriched in fission products relative to the bulk melt. The vaporization aerosol could be enriched in steel constituents because of the high vapor pressures of these constituents relative to reactor fuel oxides.

The rate of aerosol formation by vaporization depends on the melt surface area. If the melt stream is compact as depicted in the analyses to date, the fractional aerosolization of the melt will vary with the reciprocal of the diameter of the melt stream. If, on the other hand, the melt stream disintegrates because of aerodynamic forces or other processes to create more surface area, the aerosolization by vapor formation will become invariant with respect to scale. X-ray photographs of melt jets emerging from pressurized vessels show the melt badly disrupted and not compact [8].

Disintegration of the melt jet can lead to aerosol formation because melt droplets streaming at high velocities through the nearly stagnant atmosphere are unstable. These droplets will disintegrate until surface tension forces can balance the inertial forces on the droplets. Pilch [9] has investigated this process and has found that the criterion for droplet stability is:

$$We = \rho_g \frac{V^2 D}{\sigma} > 12$$

where ρ_g = density of the atmosphere gas

V = droplet velocity

D = diameter of the melt droplet, and

σ = surface tension

Pilch's analysis suggests that disintegration of melt droplets will yield an aerosol with a mass mean diameter of 60-70 μm. This aerosol is consistent with the coarsest aerosol observed in the pressurized melt ejection tests. Unfortunately, sampling such coarse aerosols is difficult, so it has not been possible to verify all of Pilch's predictions with the test data.

Aerosols produced by the aerodynamic mechanism will have compositions similar to those of the bulk melt. The fraction of melt aerosolized by this process depends on how disrupted is the melt jet. If melt jets are as badly disrupted as observed in tests of pressurized melt ejection, then the fraction of melt aerosolized will be scale independent. If the jet remains compact, then droplets of melt that disintegrate to form the aerosol are produced by Helmholtz instabilities at the melt stream surface. In this case, the fraction of the melt converted to aerosols will vary with the reciprocal of the stream diameter.

The stability of the melt jet is obviously a critical feature of pressurized melt ejection. Powers [10] has suggested that melt jets under accident conditions will not be stable because of gas effervescence. Gases in the primary system of a nuclear reactor during a severe accident are predominantly steam and hydrogen. Steam and hydrogen will dissolve in molten core debris. Some estimates of the solubilities of these gases in the oxidic and metallic phases of core debris under severe accident conditions are listed in Table 4.2. The solubility of the H_2 in iron was obtained from the correlation [11]:

$$\log_{10} (\xi 10^4) = -1637/T + 2.1326 + 0.5 \log_{10} P_{H_2}$$

where ξ = atomic hydrogen in solution

T = absolute melt temperature (K)

P_{H_2} = partial pressure of hydrogen

Solubilities for hydrogen and steam in UO@ were obtained with Blander's correlation for gas solubility in molten salts (12):

Table 4.2

Solubilities of Steam and Hydrogen in Core Debris

Temperature (°K)	Partial Pressure (atm)		Solubility (liter gas-STP/liter melt)			
			Oxide		Metal	
	H_2	H_2O	H_2	H_2O	H_2	H_2O
2800	75	75	0.43	0.62	39.55	-
	15	135	0.086	1.10	17.71	-
	1.5	-	0.009	-	5.6	-
1800	75	75	0.132	0.24	18.97	-
	15	135	0.026	0.42	8.47	-
	1.5	-	0.003	-	2.66	-

$$\ln (RTC/P) = - 9.104 \times 10^{16} r^2 \sigma / T$$

where σ = surface tension of the melt (dyne/cm)
C = concentration of the gas in solution (moles/cm^3)
R = gas constant (cm^3-atmospheres/K)
r = radius of the dissolved gas molecule (cm)
P = partial pressure of the dissolving gas in the atmosphere surrounding the melt prior to ejection (atms)

Blander's correlation probably produces a lower bound on the true solubility of steam in UO_2 since it ignores chemical effects known to greatly increase the solubility of steam in high temperature melts [13].

Inspection of the variation in gas solubility with ambient pressure shows that there will be a tremendous driving force to

desorb gas when molten material emerges from a pressurized vessel into an environment of near normal atmospheric pressure. This is especially true for the metallic phase in which the volume of gas that must desorb is many times the volume of melt. The desorption process should radically disrupt the melt stream.

Tarbell [14] has verified the disruptive effect of effervescing gases in tests that compare melt ejection from vessels pressurized with nitrogen or with carbon dioxide. In tests with nitrogen, which is quite soluble in high temperature melts, the emerging jets disintegrated into fine droplets. In tests with the vessel pressurized with CO_2, which is much less soluble than nitrogen, the melt stream remained compact as it emerged though some surface disruption due to Helmholtz instability was evident.

Effervescence of gas can also be a source of aerosols. Bursting gas bubbles will throw off aerosol particles 1 to 10 μm in diameter [15]. These aerosols will have the bulk melt composition. The fraction of melt aerosolized in this way should be approximately scale-independent.

Another mechanism of aerosol formation during melt ejection arises if both gas and melt can emerge from the breach in the vessel simultaneously. This pneumatic atomization is likely to develop during later stages of melt ejection of a reactor accident but may not have been operative in tests to date. Analysis of this process by Pilch [9] showed that it can yield UO_2 aerosols 1-10 μm in size and steel aerosols 2-60 μm in size. The fraction of melt aerosolized by this process will depend critically on the details of the breach in the vessel and the melt ejection process. Simple, scoping calculations indicate up to 10% of a core melt could be converted into aerosols this way.

Most of the aerosols produced by melt ejection processes are quite unlike aerosols produced by other severe reactor accident phenomena. With the exception of those aerosols generated as a result of vaporization, the aerosols produced during melt ejection have the bulk melt composition.

Both the oxide and the metallic phases of a core melt are quite reactive in the steam and air atmospheres likely to be present in reactor containments. If aerosol emissions are as intense under accident conditions as in the tests, cloud effects will prevent the aerosols from cooling rapidly. The hot, perhaps molten, aerosols produced by melt ejection would be expected to react rapidly once they emerge from the reactor cavity into the reactor containment.

The air oxidation of UO_2 has been studied extensively (see for example references 17 and 18). Bittel [15] has examined

steam oxidation of solid UO_2. Oxidation of UO_2 appears to be a two step process in which first U_4O_9 or U_3O_7 is formed which subsequently reacts to form U_3O_8. Both reaction steps are mildly exothermic. Substantial structural change brought on by the oxidation causes the condensed material to fragment.

Cubaciotti [20] has argued that sintering and oxidation of UO_2 will allow fission products to escape the UO_2 matrix and, presumably, form new aerosols. Cubaciotti has formulated a rate expression for this type of release based on Bittel's rate of steam oxidation of UO_2.

The high, potential reactivity of metallic melt ejection aerosols is worrisome not only from concerns over the release of radioactivity but also concerns of containment integrity. Recent reactor accident analyses have indicated that much of the zirconium clad from the reactor core will not have been oxidized at the time melt penetrates the primary vessel [7]. The rapid, exothermic, oxidation of fine particles of metal containing zirconium could be a dramatic event in the containment. It could influence hydrogen generation and deflagration. The ability of equipment to survive the rapid oxidation reaction is an interesting question.

Nelson [21] has studied the nature of metal particle oxidation in air. Particles of zirconium 250 μm in diameter ignite spontaneously when dropped into an air column. After these particles have burned for about 0.23 s, they disintegrate in a brilliant flash to yield finer rapidly burning particles. Such behavior is also observed in pure nitrogen, except the reaction is nitriding instead of oxidation.

Nelson's experiments did not address the behavior of zirconium diluted in either steel or UO_2. Nelson does suggest iron, chromium and manganese will combust in air and emit finer aerosol particles.

Experimental studies of other metals burning in oxygen suggest that the deflagration process may also generate aerosols and release fission products [22].

Recommendations For MELCOR Development Concerning the Source Term from Pressurized Melt Ejection. The information available concerning aerosol formation during pressurized melt ejection is not adequate for defining a highly mechanistic model of the process. The duration of the process is quite short, amounting to only a few seconds. Consequently, a detailed model of the process may not be important for a comprehensive code such as MELCOR. Until further evidence from experimental studies becomes

available, an approximate description of the high pressure melt ejection source term developed for a study of source term uncertainties [23] may be adequate:

(1) 1% of the mass expelled from the reactor coolant system is assumed to be instantly converted into aerosol.

(2) The size distribution of the aerosol is described by two log-normal distributions. Mean sizes are 0.7 and 30 μm. The geometric standard deviations are 1.6 and 2, respectively. Half the mass of aerosol is apportioned to each of the distributions.

(3) The composition of the coarser mode material is taken to be the bulk melt composition.

(4) The composition of the finer mode in the size distribution is taken to be:

(a) alkali metals as Cs	0.8 w/o
(b) alkaline earths as BaO	3.6 w/o
(c) halogens as I	0.2 w/o
(d) Chalcogens as Te	0.3 w/o
(e) platinoids as Ru	3×10^{-5} w/o
(f) early transition as FeO	17 w/o
(g) tetravalents as CeO_2	4 w/o
(h) trivalents as La_2O_3	2.7 w/o
(i) uranium as UO_2	balance
(j) volatile main group as Cd	20 w/o
(k) main group as Sn	18 w/o

A check must be made in the code to assure that the emissions of an element do not exceed the inventory. If the inventory is exceeded, the composition numbers above would have to be re-normalized.

The energetic effects on the containment atmosphere produced by high pressure melt ejection constitute a serious threat to the containment integrity. Though not considered in detail in this chapter, these effects should be considered in the MELCOR code. Approximate models for these effects have been formulated by Pilch [24].

B. Release Associated with Core Debris Interactions with Coolant.

For many types of accidents, in most reactors, the cavity below the reactor pressure vessel may contain water at the time melt penetrates the vessel. Even if water is not present in the cavity initially, it could possibly be poured onto the melt later, either as a natural consequence of the accident

progression or as result of some accident mitigation strategy. In any case, it is very likely that ex-vessel core debris interactions with water will occur.

The subject of core debris interactions with water has occupied a great deal of attention in the past. The concerns over these interactions have focused on the possibility of steam explosions that rupture the primary vessel or the reactor containment building. To a lesser extent, there has been concern that the quasi-static pressurization of containment brought on by steam generation during the interactions might exceed the capabilities of reactor containments.

The structural consequences of violent core debris interactions with water are not at issue here. The question addressed in this section is the fission product release that should accompany core debris interactions with water particularly when those interactions take the form of a steam explosion. The Reactor Safety Study did associate a release with steam explosions and this release is listed in Table 4.3. Rather large release fractions are associated with the volatile halogens and noble gases in this release estimate. The estimate is, however, based on the inventory of the element present in the melt participating in the explosion. Whether the explosion took place in-vessel or ex-vessel, most of the noble gases and the halogens would have already escaped the fuel. The steam explosion release fractions for these elements estimated in the Reactor Safety Study are not especially significant.

A high release fraction is associated also with tellurium. Again, this release estimate is not especially significant. Were the steam explosion not to occur, tellurium release from the melt would still be nearly complete because of releases associated with other in-vessel and ex-vessel processes.

Omissions in the Reactor Safety Study estimate of steam explosion release might be significant. No releases of the alkali metal group elements (Cs, Rb), alkaline earth group elements (Sr, Ba), and the lanthanide group elements (La , Ce, U, Zr, Nb, Pm) are considered.

The Reactor Safety Study estimate of nearly complete ruthenium release, and by implication nearly complete release of the analogous metals Mo, Pd, Tc, and Rh, is significant. The combination of all other events in a severe reactor accident would release 8% of the ruthenium inventory according to the Reactor Safety Study. Participation of only 10% of the reactor core in a steam explosion would yield an equivalent release of ruthenium.

The Reactor Safety Study estimate of steam explosion release was prepared under the handicap of a total lack of pertinent,

Table 4.3

Radionuclide Release Associated with Steam Explosions in the Reactor Safety Study (1).

Element	Release* (%)
Xe, Kr	80-100
I, Br	80-100
Te, Se, Sb	40-80
Ru**	80-100

* Percent released of the inventory of the indicated element remaining in the melt involved in the explosion.

** Also stands for Mo, Tc, Pd and Rh

nuclear-reactor-related data. The rather dire structural consequences of steam explosions predicted in the Reactor Safety Study have prompted considerable research into the fundamentals of the steam explosion process. Unfortunately, none of these research efforts directed their attentions to the fission produce release caused by steam explosions. The research has provided a good physical portrait of steam explosions and enough information to permit a limited re-evaluation of the Reactor Safety Study Release estimate.

There appear to be two steps essential to the steam explosion process:

(1) When molten core debris enters water, the melt coarsely fragments into droplets about 1 cm in diameter, intermixed and surrounded by coolant in film boiling.

(2) The steam film surrounding the coarse fragments collapses permitting efficient transfer of heat from the melt into the coolant and consequently, rapid steam formation.

Thermal shock, quench fragmentation, or mechanical shock by the rapid steam generation reduces the debris to fine particulate material which is ejected into the atmosphere. Within the primary system, this atmosphere is a mixture of steam and hydrogen. Within the containment, air may also be present.

The considerations that led to the Reactor Safety Study estimate of steam explosion release were directed toward the behavior of the fine particulate debris thrown into the atmosphere. Experiments by Parker [25] have shown remarkable ruthenium release when irradiated fuel pellets are heated in air. The speciation of ruthenium vapors in air as a function of temperature shown in Figure 4.4 suggests the high release rates are probably due to formation of $RuO_4(g)$ or $RuO_3(g)$. The rate of ruthenium release observed in Parker's experiments followed different kinetic paths above and below 800°C which parallels the kinetics of UO_2 oxidation in air [13,14]. In this, Parker's results are consistent with Cubaciotti's argument that oxidation of the UO_2 is a key first step in the release of fission products [20].

In the current position of superior, but still far from adequate, information, it is possible to critique the Reactor Safety Study analysis of the steam explosion release on several grounds:

(1) Whereas in irradiated fuel rods ruthenium may be present as isolated alloy nodules containing 20-25% Ru [26], by the time a steam explosion can occur, the ruthenium will

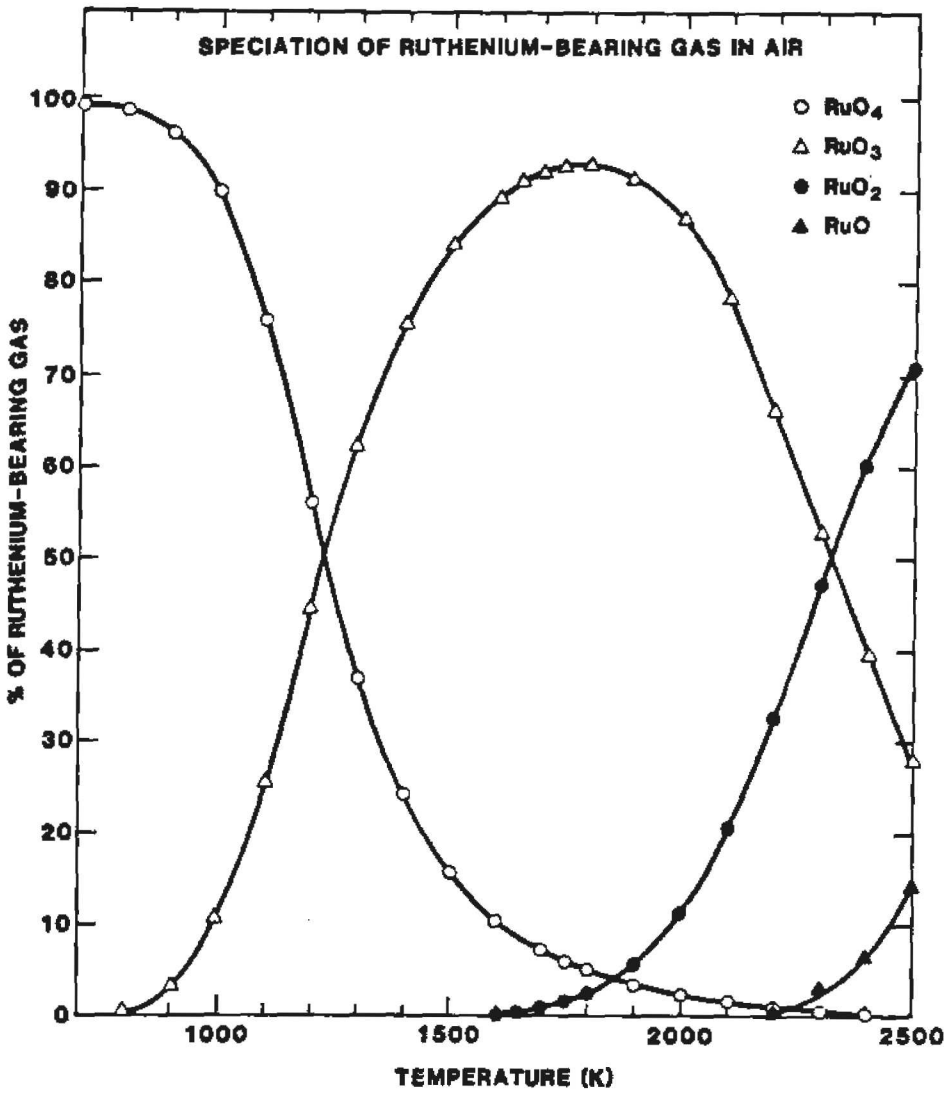

Figure 4.4 Speciation of Ruthenium Vapors in Air as a Function of Temperature.

probably have been incorporated as a very dilute constituent of the metallic phase of the core melt. In this dilute alloy, reaction of ruthenium to form a volatile oxide should be greatly slowed relative to the rates observed in Parker's experiments since the mechanism hypothesized by Cubaciotti is unavailable.

(2) Even if the ruthenium is isolated in a urania matrix as in Parker's experiments, the time the urania particles remain suspended in the containment atmosphere may be too short to achieve the very high release rates implied by the release estimated in the Reactor Safety Study. Chemical conditions to which fragmented debris is exposed may not be conducive to high releases.

(3) If release of ruthenium does occur as expected in the Reactor Safety Study, the other fission products notably the alkali metals, alkaline earths and the lanthanides - should also be released.

The second of these points is most critical to the re-assessment of the steam explosion source term.

In the first step of the steam explosion process, the coarse, very hot, fragments are immersed in a strong oxidant water. As shown by Corradini [27] this strong oxidant also attacks the bulk debris to form significant amounts of hydrogen. The vapor film surrounding the coarse fragments at this state is not steam, but rather a mixture of steam and hydrogen.

The total partial pressure of ruthenium-bearing gases in equilibrium with pure ruthenium or ruthenium dioxide is shown in Figure 4.5 as a function of temperature for several values of the ratio of hydrogen partial pressure to steam partial pressure. Also shown is the partial pressure of ruthenium-bearing gases when the atmosphere is air. Clearly, when even small hydrogen partial pressures exist, the partial pressure of ruthenium-bearing gases is significantly depressed relative to the partial pressure in the air. Because hydrogen is formed, the volatility of ruthenium must be quite low during the first stage of the steam explosion process. Total release of ruthenium during this stage must also be low since the volatility is low and the duration of the coarse fragmentation and intermixing process is short (~0.2 s).

The steam explosion comminutes the debris into fine particles. These particles have been characterized in some of the steam explosion research programs. In general, the characterization has been by sieve analysis over the size range of 10^4 - 45 μm. Some typical size distribution data are shown in Figure 4.6. No characterizations of the debris in the size

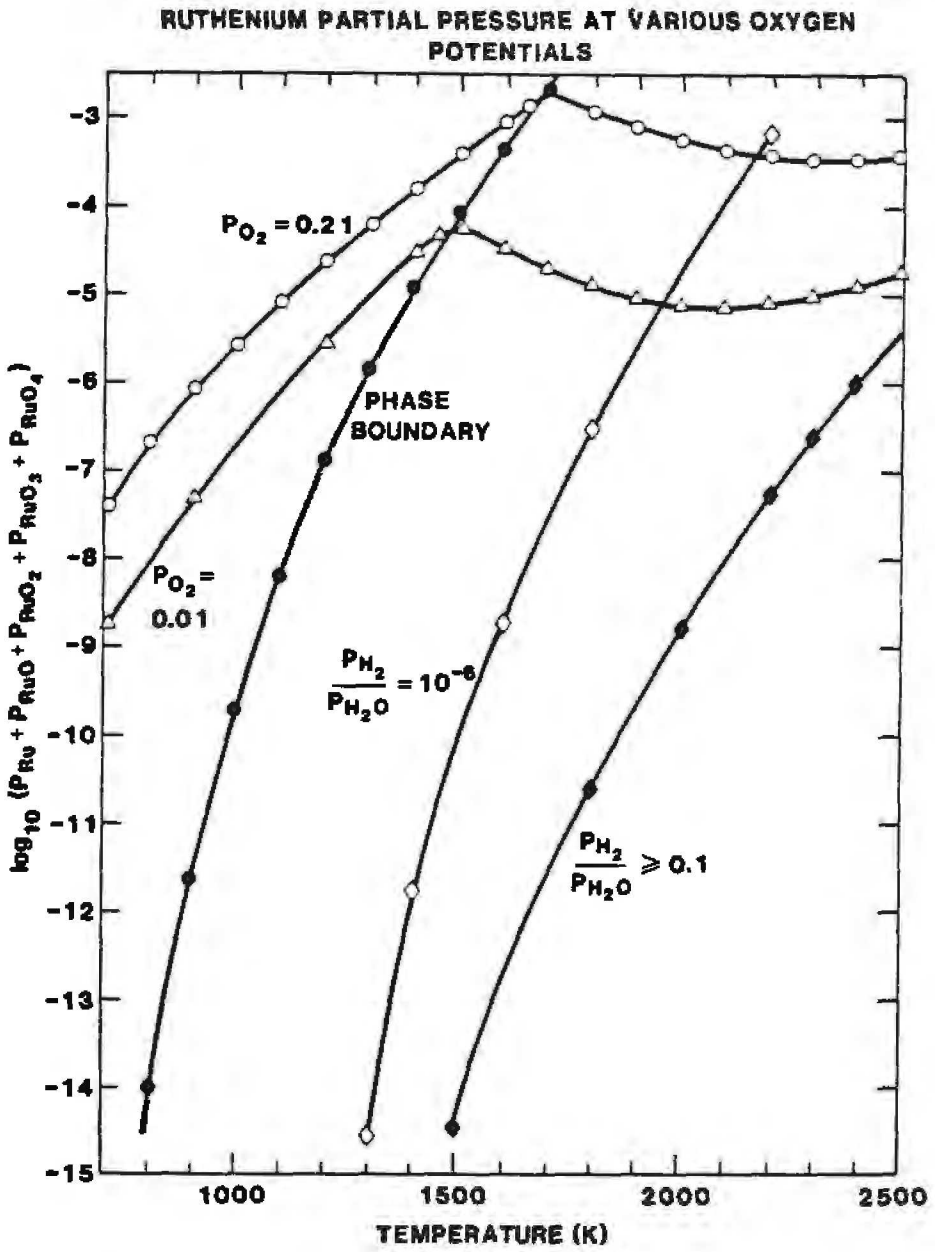

Figure 4.5 Total Partial Pressure of Ruthenium-Bearing Vapors in Various Atmospheres as a Function of Temperature.

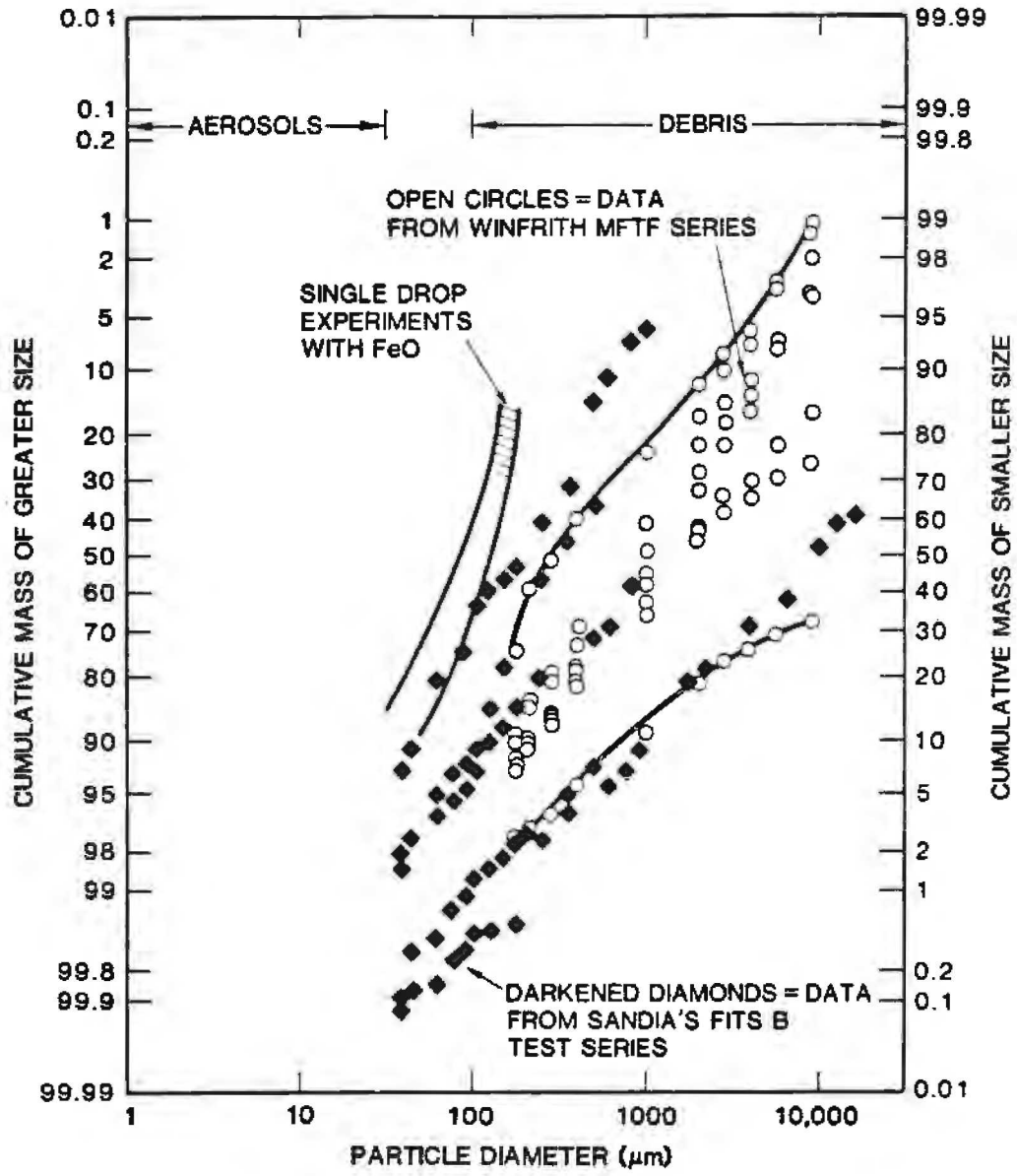

Figure 4.6 Size Distribution of Debris Formed by Melts Involved in Steam Explosions.

interval typical of aerosols that will remain suspended for long periods of time have been reported. If the characterization of the debris size distribution as log-normal is accepted, then it is possible to estimate the amount of material in the aerosol size range (<38 μm). It is apparent from such estimates that aerosol formation by steam explosions is an insignificant contributor to fission product release.

The route to significant ruthenium release from debris formed by steam explosions lies through chemical reaction of the debris to form volatile ruthenium oxides. If the steam explosion takes place within the reactor pressure vessel and the vessel does not rupture, the atmosphere encountered by the ejected debris is a mixture of steam and hydrogen. The suppression of release described above for the first stage of the steam explosion process will also be operative for debris in the vessel atmosphere. The suppressive effect of the atmosphere is likely to be stronger since the debris will, of necessity, be cooler than the coarse fragments formed in the first stage of a steam explosion.

When the steam explosion takes place ex-vessel, the chemical constraint on ruthenium release is not present. To estimate the release possible when debris is injected into an air atmosphere, it is necessary to consider the kinetics of release. The kinetics will depend on the temperature of the debris and the surface area of the debris. Total release will depend on these factors and the time the particles are suspended in the containment atmosphere.

Recent analyses of the steam explosion process show that the time particles suspended in the containment atmosphere is a critical factor that controls the release of ruthenium [28]. The mass weighted mean residence time of the particles of fuel is only a few seconds. Unless a strongly exothermic reaction can be triggered when these particles are injected into the containment atmosphere, there is insufficient time to achieve releases exceeding a few percent.

The likelihood of causing the particulate material ejected during a steam explosion to burn is much less than the likelihood of igniting aerosol particles produced by pressurized ejection. The steam explosion particles are much coarser than the pressurized ejection aerosol, they have been cooled to lower temperatures because of their interaction with water, and they have already been extensively oxidized during early stages of the steam explosion process [27].

Though these arguments cannot be considered definitive in the absence of supporting experimental data, they are cause for questioning the rather high ruthenium release fractions cited in the Reactor Safety Study.

Recommendations for MELCOR Development of a Source Term Associated with Steam Explosions. The following recommendations are made concerning the treatment of the steam explosion source term in the MELCOR code:

(1) The generation of aerosols during a steam explosion takes place over such a small period of time that the MELCOR model need not include a highly mechanistic description of the process.

(2) Aerosols produced by the steam explosion can be assumed to amount to a constant fraction of the melt mass participating in the explosion. This fraction should be user adjustable. A default value of 0.2% would be appropriate.

(3) The size of the aerosol should be user selected with a default value of 10 μm. The composition of the aerosol may be assumed to be the bulk melt composition.

(4) There is no need to consider the aerosol produced by steam explosions to be enriched in volatiles. In latter versions of MELCOR, a more sophisticated treatment of aerosol composition may be adopted if on-going research indicates a need.

C. Release During Core Debris/Concrete Interactions

The most frequently mentioned source of aerosols and fission products outside the reactor coolant system is that associated with core debris/concrete interactions. This source was recognized in the Reactor Safety Study. Experimental studies have verified the existence of the core debris/concrete interactions source term and established some important features of the source.

The Reactor Safety Study analysis of the core debris/concrete interaction source term considered only the release of radioactive constituents that were present in the debris when it penetrated the reactor vessel. Qualitative thermochemical arguments were used to define ultimate release fractions for various categories of fission products. These release fractions are listed in Table 4.4. The time-dependencies of fission product release were assumed to be the same for all fission products and to be of the form

$$VRF_i(t) = \begin{cases} VRF_i(\infty)\,[1 - \exp(-0.0231t)] & \text{for } 0 \text{ min} \leq t \leq 90 \text{ min} \\ VRF_i(\infty)\,[0.87 + \frac{0.13}{30}(t-90)] & \text{for } 90 \text{ min} < t \leq 120 \text{ min} \end{cases}$$

Table 4.4

Release During Core Debris Interactions with Concrete as Estimated in the Reactor Safety Study

Fission Product	Release
Xe, Kr	100
I, Br	100
Cs, Rb	100
Te, Se, Sb	100
Ru, Rh, Pd, Mo, Te	5
Ba, Sr	5
La, Nb, Eu, Y, Ce, Pr Pm, Sm, Np, Pu, Zr, Nb	1

* % of the amount remaining in the core debris at the start of interactions with concrete

where $VRF_i(t)$ = release fraction of the i^{th} element at time t(min.).

$VRF_i(\infty)$ = release fraction of the i^{th} element listed in Table 4.4.

Authors of the Reactor Safety Study were aware that materials other than fission products would vaporize to form aerosols during core debris interactions with concrete. Experimental investigations of these interactions have yielded some information both on fission product release and the formation of aerosols by constituents of concrete, steel and UO_2 [29]. The total aerosol production rate has been found to vary from about 5-10 g/m^3 of gas evolved from the interaction of concrete with melts at 1500-1700°C (see Figure 4.7) to over 150 g/m^3 when melts in contact with concrete are at about 2400°C. Aerosol generation has been found to correlate with the superficial velocity of gas sparging through the melt. The contribution of non-fuel species to the aerosol has been observed to be 60-90% of the total aerosol in experiments with compositionally prototypic melts.

Murfin and Powers [30] developed an empirical correlation of the experimental data for total aerosol production during melt/concrete interactions:

$$[A] = 10^4 \, (24V_g + 3.3) \exp [-19000/T(K)]$$

where [A] = mass concentration (g/m^3 STP) of aerosol in gas evolved during core debris/concrete interactions

T = absolute temperature (K)

V_g = superficial velocity of gas sparging through the melt (m/s)

When this correlation and an experimentally determined aerosol composition are applied to a reactor accident, 1-10 tons of aerosol are predicted to form. Release fractions for some fission product isotopes (La, Ce, Ba, Sr, and Mo) are predicted to be much higher than estimated in Reactor Safety Study.

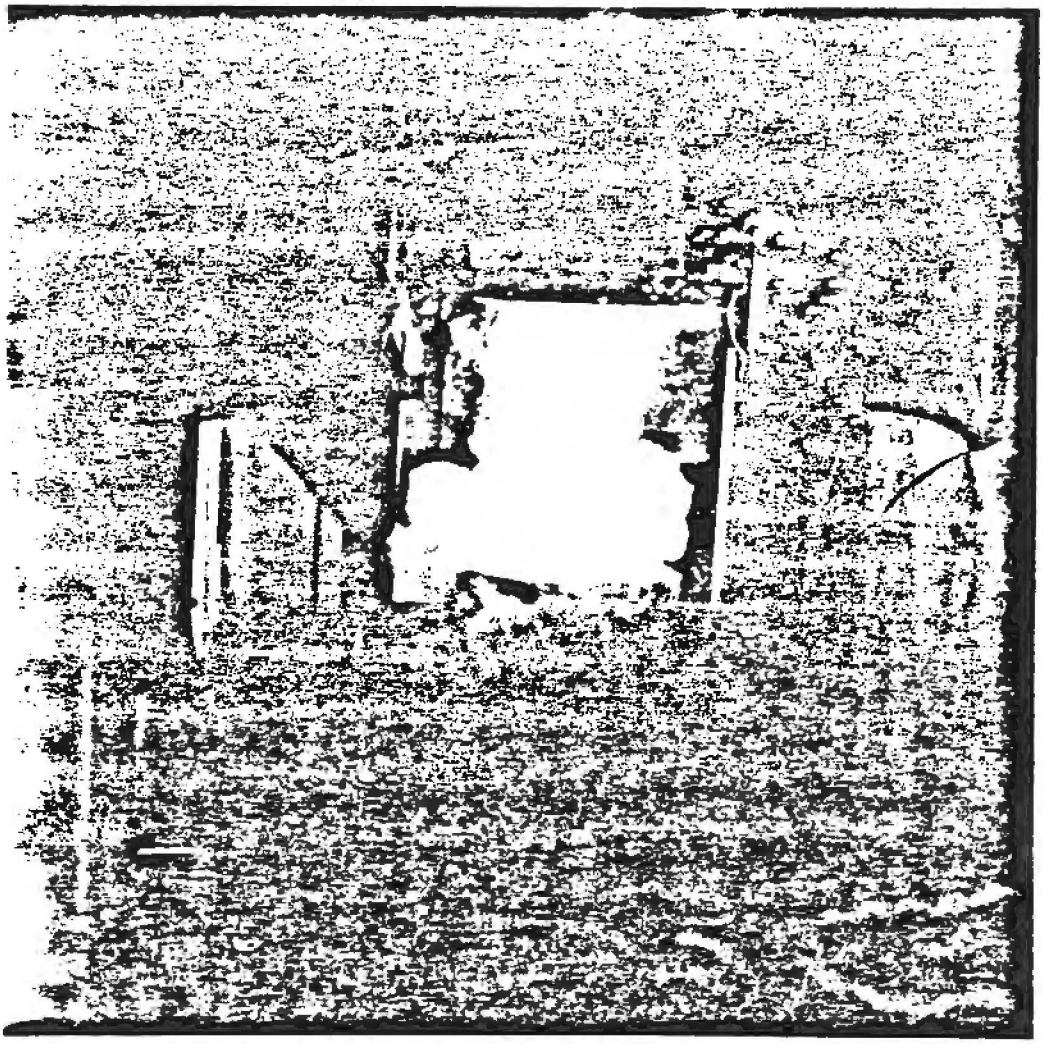

Figure 4.7 Aerosol Production During Interaction of 200 Kg Molten Steel at 1700°C with Concrete.

Application of the empirical correlation to accident situations involves such strenuous extrapolation that it is difficult to attach much confidence to the resulting predictions. The predictions do form a basis for questioning the Reactor Safety Study estimates of the release to associate with core debris/concrete interactions.

Powers and Brockmann [31] have attempted to formulate a mechanistic model of aerosol formation during core debris interactions with concrete. The operative physics embodied in their model includes:

(1) release is assumed to occur both by vapor formation processes and by the mechanics of bubbles breaking at the surface of a melt.

(2) the rate of vapor formation depends on the amount of free surface available, mass transfer in the liquid phase, surface vaporization, and gas phase mass transport.

(3) the amount of surface available for vaporization is dominated by that created by gases sparging through the melt.

(4) vapor formation processes are considered for species in ternary M-O-H systems where M is the fission product of interest.

(5) gases and liquid mixtures are assumed to be ideal.

(6) the model recognizes 250 chemical species made from 27 elements. The elements recognized in the model are shown in Table 4.5.

Examples of the predictions from the mechanistic model, called "VANESA", are shown in Figure 4.8 which is a plot of the estimated rate of aerosol production against the time from the start of core debris interactions with concrete. The calculations were done for the Surry Nuclear Power Plant. The reactor cavity concrete was assumed to be siliceous in nature. The molten core debris was assumed to have spread over an area of 55.7 m^2 at the start of the core debris/concrete interactions. The nature of the core debris interactions in the cavity were estimated with the CORCON code [32]. For the aerosol production rate designated "ANS-Surry-NoZr", it was assumed that all the zircaloy clad in the reactor core had been oxidized to ZrO_2 prior to the onset of core debris interactions with concrete. For the estimate designated "ANS-Surry-1/2Zr", it was assumed that only half the zircaloy was oxidized. Also shown in the figure are aerosol generation rates predicted for the Surry plant with the

Table 4.5

Elements and Vapor Species Considered in the VANESA Code

Element	Vapor Species
Hydrogen	H, H_2, OH, H_2O
Oxygen	O, O_2, OH, H_2O, CO, CO_2
Carbon	CO, CO_2
Iron	Fe, FeO, FeOH, $Fe(OH)_2$
Chromium	Cr, CrO, CrO_2, CrO_3, H_2CrO_4
Nickel	Ni, NiO, NiOH, $Ni(OH)_2$
Molybdenum	Mo, MoO, MoO_2, MoO_3, H_2MoO_4, $(MoO_3)_2$, $(MoO_3)_3$
Ruthenium	Ru, RuO, RuO_2, RuO_3, RuO_4
Tin	Sn, SnO, SnOH, $Sn(OH)_2$, SnTe
Antimony	Sb, SbOH, $Sb(OH)_2$, Sb_2, Sb_4, SbTe
Tellurium	Te, TeO, TeO_2, Te_2O_2, H_2TeO_4, Te_2, H_2Te, SnTe, SbTe, AgTe
Silver	Ag, AgOH, $Ag(OH)_2$, AgTe
Manganese	Mn, MnOH, $Mn(OH)_2$
Calcium	Ca, CaO, CaOH, $Ca(OH)_2$
Aluminum	Al, AlO, AlOH, Al_2O, AlO_2, Al_2O_2, $Al(OH)_2$, AlO(OH)
Sodium	Na, Na_2, NaOH, $(NaOH)_2$, NaO, NaH
Potassium	K, K_2, KOH, $(KOH)_2$, KO, KH
Silicon	Si, SiO, SiO_2, SiOH, $Si(OH)_2$, $Si(OH)_4$
Uranium	U, UO, UO_2, UO_3, H_2UO_4
Zirconium	Zr, ZrO, ZrO_2, ZrOH, $Zr(OH)_2$
Barium	Ba, BaO, BaOH, $Ba(OH)_2$
Strontium	Sr, SrO, SrOH, $Sr(OH)_2$
Cesium	Cs, Cs_2, CsOH, $Cs_2(OH)_2$, Cs_2O, CsO, CsI
Lanthanum	La, LaO, LaOH, $La(OH)_2$
Cerium	Ce, CeO, CeOH, $Ce(OH)_2$
Niobium	Nb, NbO, NbO_2, NbOH, $Nb(OH)_2$
Iodine	CsI, HI, I_2, I

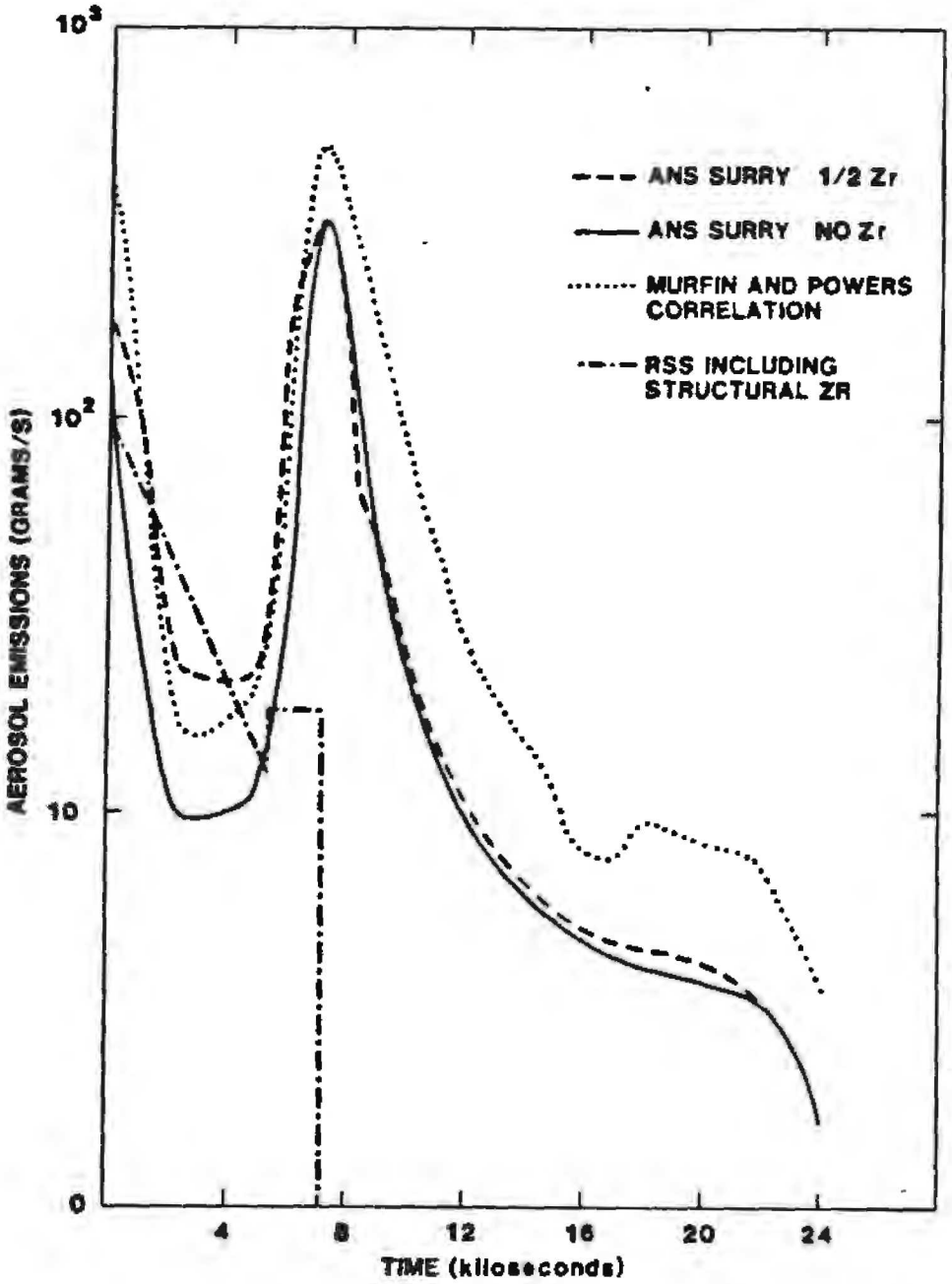

Figure 4.8 Aerosol Production Rates Estimated for Core Debris/Concrete Interactions at the Surry Plant.

empirical correlation mentioned above and with the release model used in the Reactor Safety Study. Zirconium from the fuel cladding as well as fission product zirconium were considered in making the release rate estimate with the Reactor Safety Study model. Otherwise, structural or concrete materials were neglected in estimates with this model.

The mechanistic model predicts that initially high aerosol generation rates arise. These rates fall because the melt is quenched somewhat after entering the reactor cavity. Fission product decay heating and, especially in the "ANS-Surry-1/2Zr" case, heat generated as the metallic phases of the melt are oxidized by gases from the decomposing concrete, cause the melt temperature to rise. Aerosol generation increases with melt temperature. Eventually, a maximum melt temperature and maximum aerosol generation rate are reached. Following this maximum, the temperature of the melt slowly decreases. Aerosol generation also decreases but much more dramatically because of the inherently exponential dependence of vaporization on temperature.

The mechanistic model predicts that core debris containing metallic zirconium will produce aerosols at greater rates than does core debris in which all zirconium has been oxidized. The effect arises both because the oxidation of zirconium keeps the melt hotter and because metallic zirconium chemically reduces some melt species to more volatile oxidation states. Oxidation of residual zirconium by steam from the concrete is complete at about the time of maximum aerosol generation rate. Once the zirconium by steam from the concrete is complete at about the time of maximum aerosol generation rate. Once the zirconium has been completely oxidized, predictions for the "ANS-Surry-NoZr" and "ANS-Surry-1/2Zr" cases are quite similar.

The mechanistic model of aerosol generation and fission product release during core debris/concrete interactions is of too recent a vintage to have been subjected to extensive validation by comparison with experimental results. It is encouraging that there is generally good agreement between the estimates of aerosol generation for the Surry case obtained with the Murfin and Powers correlation and the mechanistic model predictions. Nowhere do estimates obtained with this correlation differ by more than about a factor of two from the model predictions. At early times, estimates obtained with the empirical correlation are bracketed by the two mechanistic predictions. At late times, when aerosol generation rates are low, the empirical correlation yields higher estimates than does the mechanistic model.

Estimates of aerosol generation obtained with the mechanistic model or the empirical correlation are unlike predictions obtained with the Reactor Safety Study model. The most important difference is that these more recent descriptions of the process

show aerosol generation to continue far longer than is predicted by the Reactor Safety Study model. In fact, aerosol generation predicted by the Reactor Safety Study model has stopped when mechanistic predictions indicate the aerosol generation rate has reached a maximum. Predictions of the amount of aerosol suspended in the reactor containment atmosphere and the amount of aerosol that escapes should the containment rupture will differ dramatically depending on which of these models is used to estimate the aerosol source term from core debris interactions with concrete.

Other differences arise between the mechanistic model and the Reactor Safety Study model with regard to the releases of individual elements. The fraction of tellurium remaining in the core debris as predicted by the two models is shown as a function of time in Figure 4.9. The Reactor Safety Study model predicts the release of this relatively volatile element to be more extensive and more rapid than does the mechanistic model. The extents of Sr and Ra predicted by the mechanistic and Reactor Safety Study models are shown as functions of time in Figure 4.10. For these elements, assumed to be present in the core debris as relatively non-volatile oxides, the mechanistic model predicts more rapid and more extensive release than does the Reactor Safety Study model.

Experimental studies necessary to validate and to improve these and other predictions of the mechanistic model are underway.

The mechanistic model includes a description of the effect an overlying pool of water would have on the source term of aerosols to the containment caused by core debris interactions. Such an effect was neglected in the Reactor Safety Study. The model, essentially la modification of the description of aerosol entrapment from bubbles passing through water formulated by Fuchs [33], is based on the following assumptions:

(1) The overlying water pool is in film boiling over the core debris/concrete mixture. The water affects in no way the generation of aerosols from the melt. The aerosols evolve from the melt into the gas film between the melt and the water pool.

(2) Aerosol-laden gas thermally equilibrates with the water pool in vapor film between the pool and the melt. The gases are assumed to be non-condensible.

(3) The bubbles enter the pool at an initial size of 1 cm. There are no bubble-bubble interactions.

(4) Entrapment of aerosols is by inertial deposition from internally circulating flows, diffusion of aerosols to the bubble walls and by sedimentation.

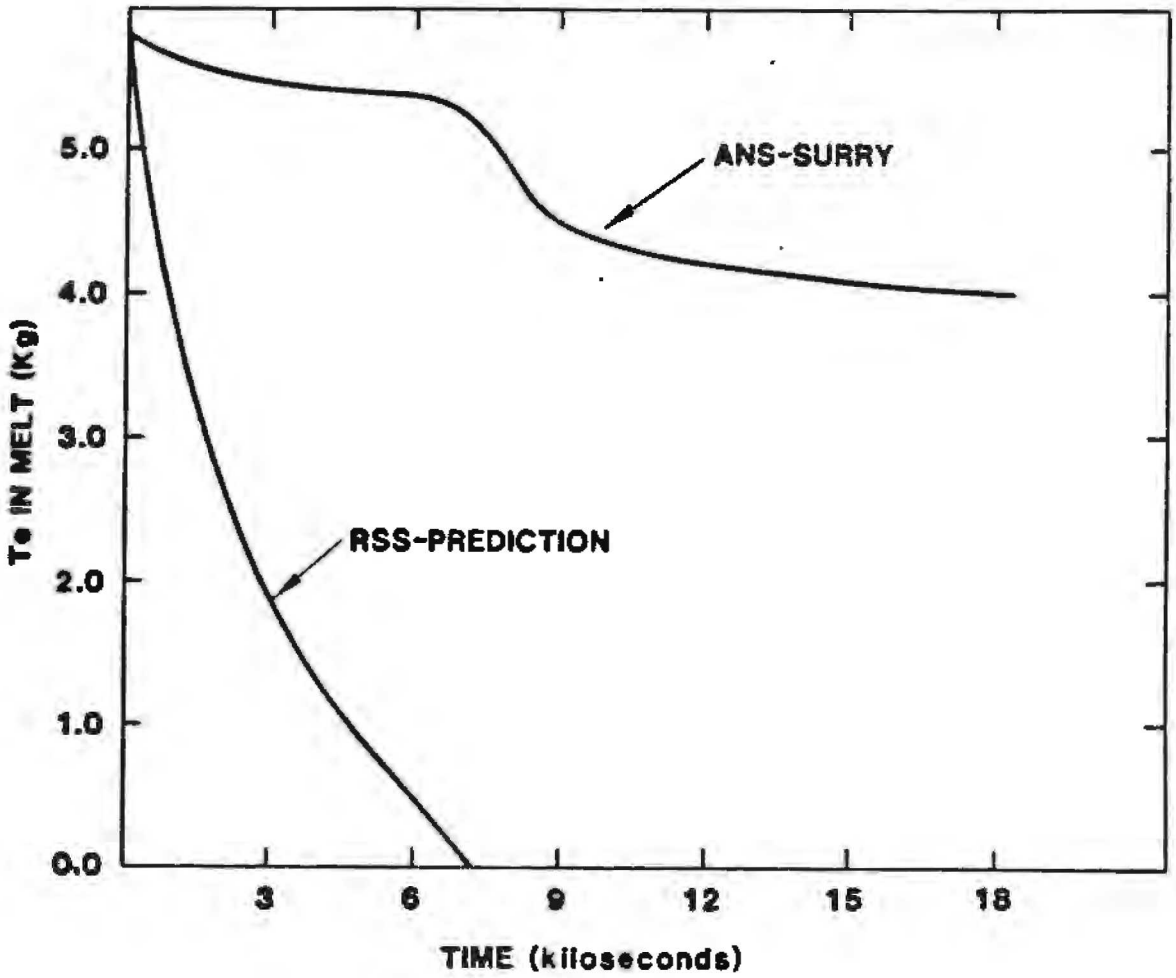

Figure 4.9 Estimates of the Amount of Tellurium Remaining in the Core Debris During Interactions with Concrete.

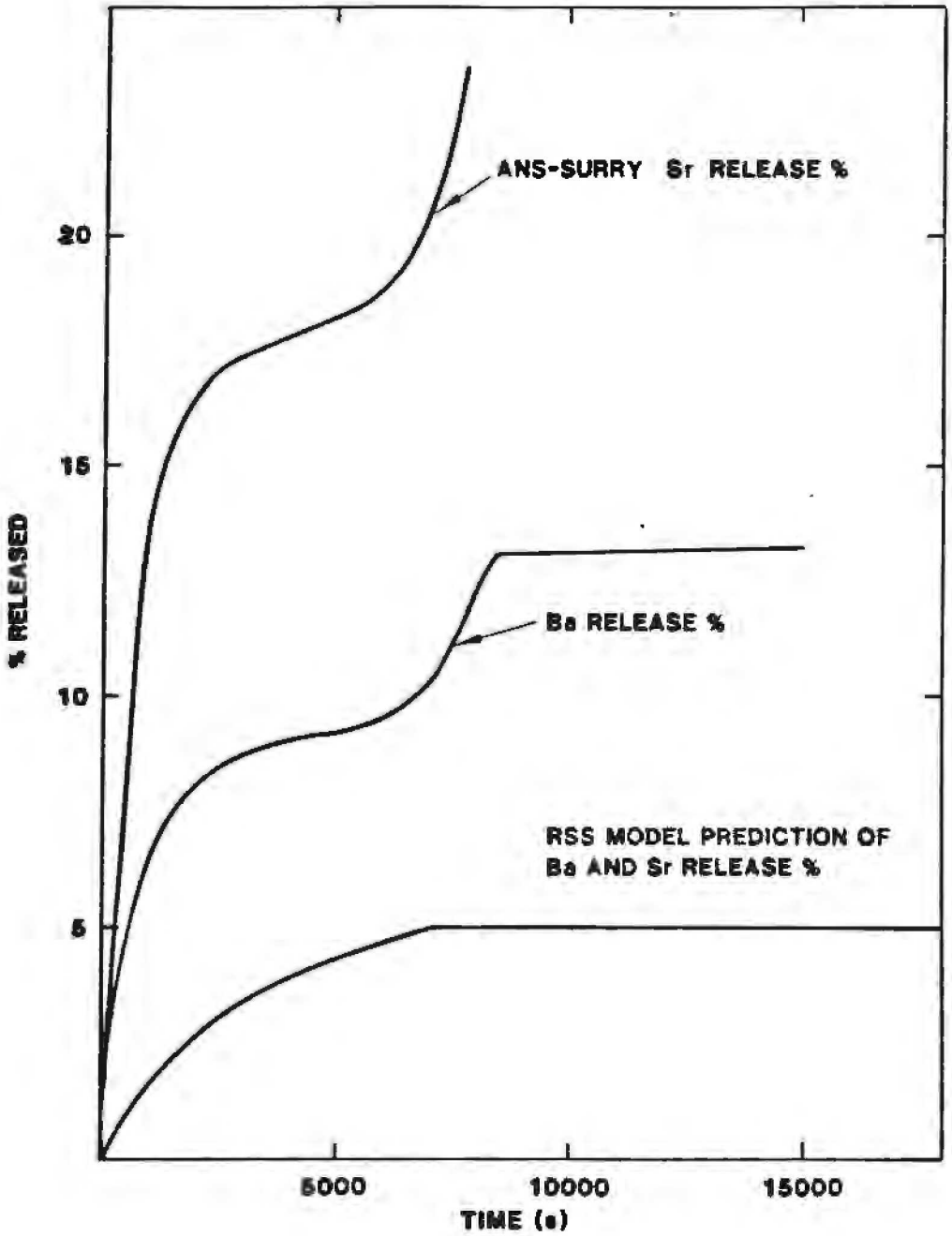

Figure 4.10 Estimates of the Release of Ba and Sr During Core Debris/Concrete Interactions.

The expansion of the bubble caused by the loss of hydrostatic head as the bubble rises is taken into account:

$$\frac{V(x)}{V_o} = P_{atms} + \frac{x}{1033.6}$$

where

$$V_o = \frac{4}{3} \pi R_o^3$$

$$R_o = 0.5 \text{ cm}$$

P_{atms} = absolute pressure of the containment atmosphere (atms)

x = distance from the top of the water pool (cm)

$V(x)$ = volume of the bubble at $x = \frac{4}{3} \pi R(x)^3$

Then, if n is the number of aerosol particles within the bubble,

$$\frac{dn}{dt} = -(\alpha_i + \alpha_s + \alpha_d)n$$

where t = time

α_i = impaction coefficient = $\frac{9V\tau}{2R^2}$

α_s = sedimentation coefficient = $\frac{3g\tau}{4RV}$

α_d = diffusion coefficient = $1.8\ (D/VR^3)$

V = bubble rise velocity

g = gravitational constant

τ = relaxation time = $\pi\ Dp^3 \rho_p B/6$

ρ_p = particle material density

D = kTB

k = Boltzmann's constant

T = absolute temperature

B = $C(D_p)/3\pi\mu_g D_p$

D_p = particle diameter

μ_g = gas viscosity

$$C(D_p) = 1 + \frac{2\lambda}{Dp}\ [1.257 + 0.4\ \exp\ (-0.55\ Dp/\lambda)]$$

λ = molecular mean free path in gas

Examples of the decontamination of the aerosol-laden gas by an overlying pool as a function of particle size and as a function of pool depth are shown in Figures 4.11 and 4.12. Log-normally distributed particle sizes were assumed to make the decontamination calculations shown in these figures. Decontamination factors used in these figures are defined as the ratio of mass input to mass that passes through the pool. Note that a minimum occurs in the decontamination factor when plotted against particle size. The particle size range where little decontamination occurs broadens as the geometric standard deviation of the log-normal size distribution increases.

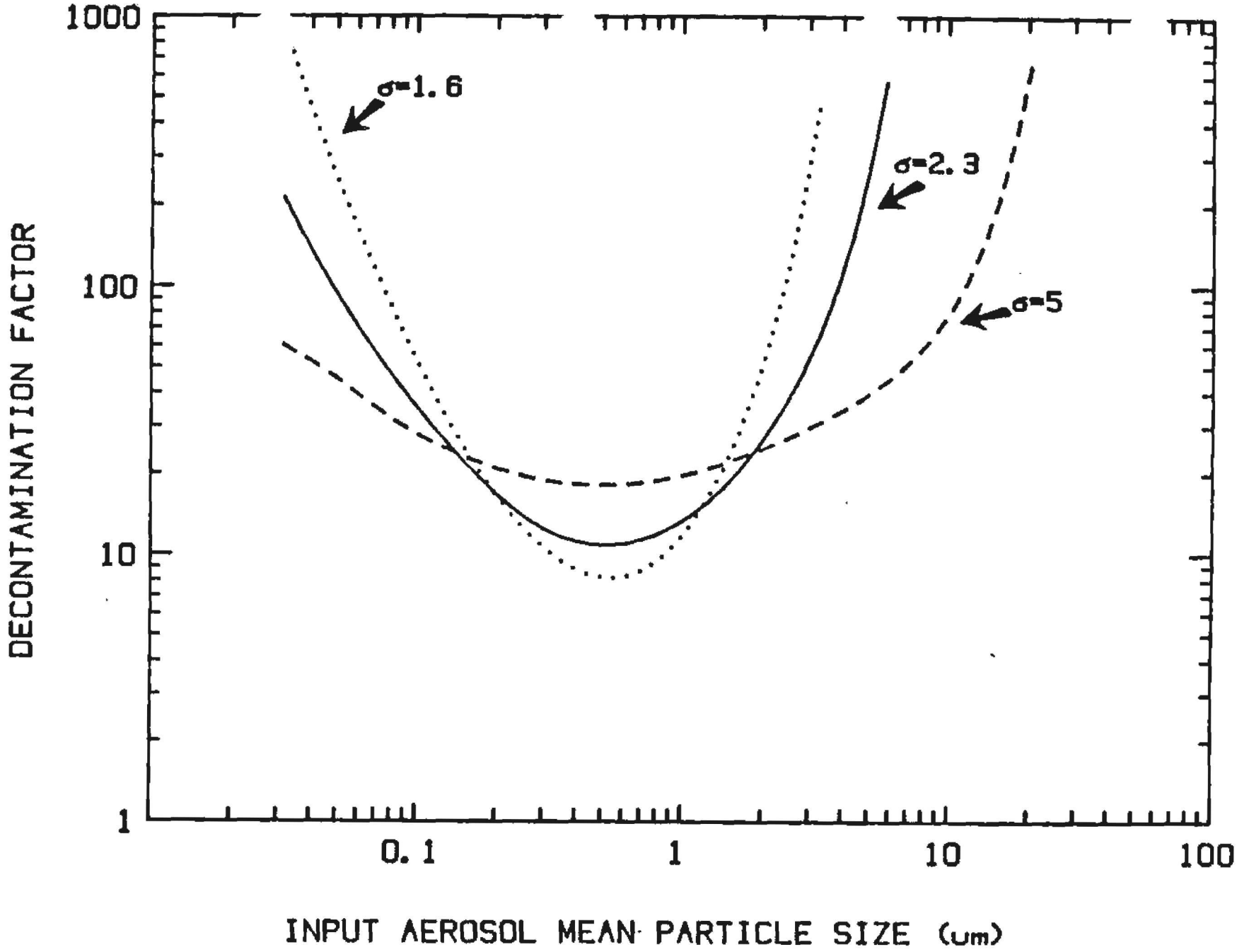

Figure 4.11 Decontamination of Aerosol-laden Gas by a Saturated Water Pool 7 Meters Deep as a Function of Mean Particle Size.

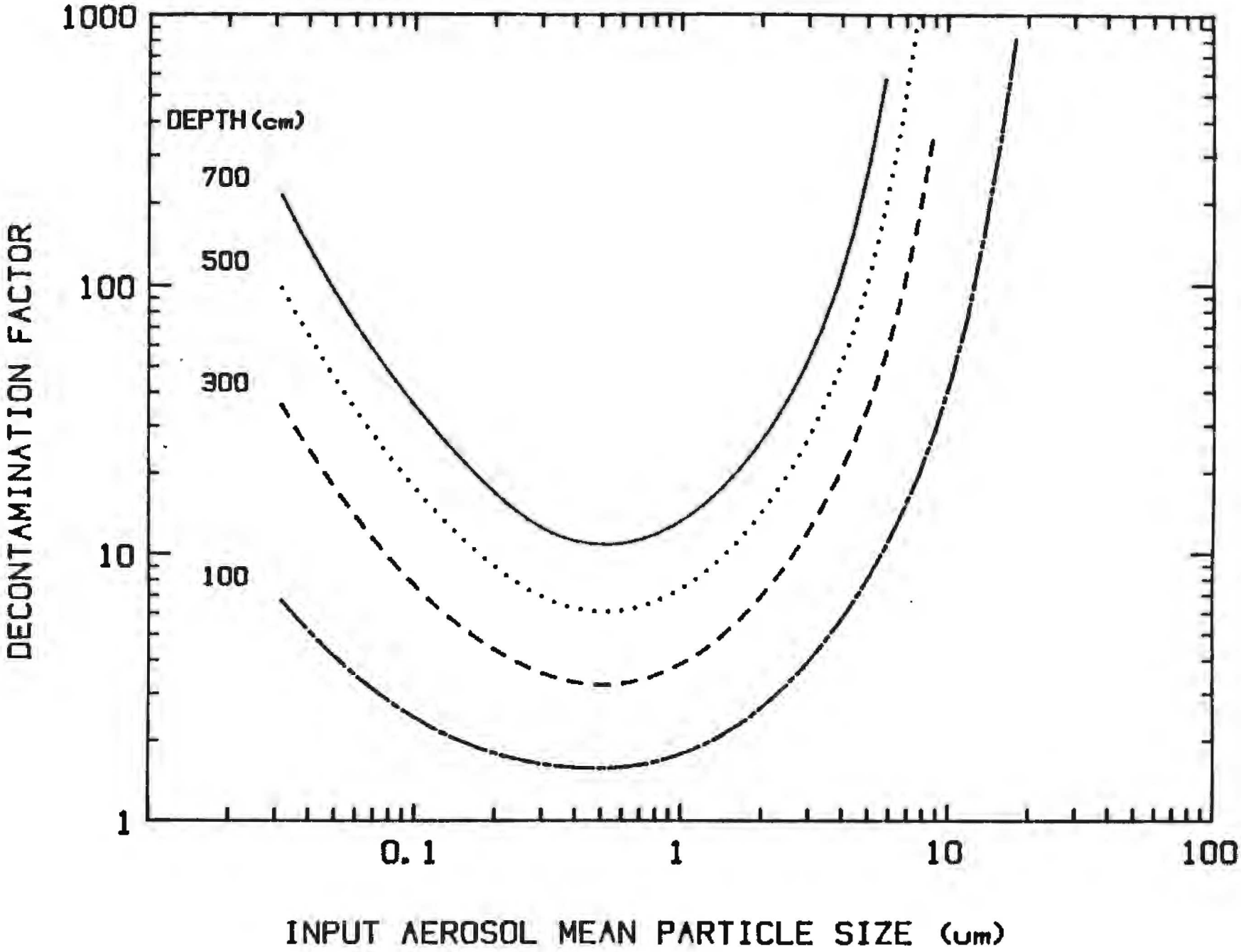

Figure 4.12 Decontamination of Aerosol-laden Gas by a Saturated Water Pool of Various Depths.

Recommendation for the MELCOR Model of the Source Term From Core Debris/Concrete Interactions. At this stage in development, the MELCOR code can use a relatively crude model of the source term associated with core debris interactions with concrete. To this end, the following recommendations are made:

(1) The rate of aerosol mass generation should be obtained from the Powers-Murfin correlation.

(2) The aerosol size distribution can be taken a log-normal with a geometric standard deviation of 2.3 and a mean size given by the Brockmann equation:

$$Dp = 0.266\ (A/\rho)^{1/3}$$

where Dp is the particle diameter in micrometers, A is the aerosol concentration is g/m^3-STP, and p is the material density of the aerosol in g/cm^3.

(3) Aerosol compositions can be provided by the user. Default compositions are shown in Table 6. These compositions change with melt temperature and the time after the start of core debris interactions with concrete. A check will have to be made in the code to assure inventories are not exceeded. Eventually these default compositions will have to be replaced with more smoothly varying functions of the melt properties.

(4) The effect of an overlying water pool can be satisfactorily described by the modified Fuchs model.

D. Fission Product Release by Leaching

The duration of vigorous core debris interactions with concrete is uncertain. Eventually, these interactions must stop and further erosion or thermal decomposition of the concrete cease. If the core debris has eroded through the basemat, when vigorous interactions stops, then the core debris is susceptible to leaching by groundwater. Fission product release by this leaching process* is a long-term, low-level source of radioactivity that is probably much less a threat to the public than the intense, airborne sources discussed above (26).

* Basemat penetration may allow coolant waters containing radioactive material to drain from the plant into the groundwater system. This source of radioactivity is not considered here. It may, however, far exceed in importance to risk the in-plant radioactivity release by leaching.

Table 4.6

Default Compositions for Aerosol from Core Debris Interactions with Concrete

	Early in Time after start of core debris interactions with concrete	Late in Time after start of core debris interactions with concrete
High Melt Temp*		
alkali metals	0.8 w/o as Cs	0
alkaline earths	3.6 w/o as BaO	3.3 w/o as BaO
halogens	0.2 w/o as I	0
chalcogens	0.3 w/o as Te	1.0 w/o as Te
Platinoids	3×10^{-5} w/o as Ru	1×10^{-5} w/o as Ru
early transition	17 w/o as FeO	12.6 w/o as FeO
tetravalents	4 w/o as CeO_2	1.6 w/o as CeO_2
trivalents	2.7 w/o as La_2O_3	1 w/o as La_2O_3
uranium	1.6 w/o as UO_2	0.8 w/o as UO_2
volatile main-group	20 w/o as Cd	0
main group	18 w/o as Sn	16 w/o as Sn
concrete	balance	balance
Low Melt Temp**		
alkali metals	9 w/o as Cs	0
alkaline earths	3.3 w/o as BaO	0.2 w/o as BaO
halogens	8.5 w/o as I	0
chalcogens	0.3 w/o as Te	0.5 w/o as Te
platinoids	0	0
early transition	8.1 w/o as FeO	24 w/o as FeO
tetravalents	0.01 w/o as CeO_2	0.001 w/o as CeO_2
trivalents	4×10^{-6} w/o as La_2O_3	2×10^{-6} w/o as La_2O_3
uranium	0.06 w/o as UO_2	0.04 w/o as UO_2
volatile main group	10 w/o as Cd	0
main group	4 w/o as Sn	9.2 w/o as Sn
concrete	balance	balance

*T > 2200K
**T < 2200K

There have been few systematic studies of leaching of core debris/concrete mixtures expected at this final stage in a severe reactor accident. The core debris is usually considered a single phase solid in analyses of leaching. Recent work by Westrich [35] suggests that this would not be the case. Westrich found that when mixtures of UO_2, ZrO_2 and siliceous materials analogous to concrete were slowly cooled (<2 K/s), phase separation took place. The crystalline precipitates from the melt consisted of UO_2, MgU_2O_5, and ZrO_2, but not $ZrSiO_4$. The silica-rich liquid phase would eventually solidify as a glass. Plagioclase solid solutions ($NaAlSi_3O_8$ - $CaAl_2Si_2O_8$) were observed in high silica content systems.

Westrich examined the partitioning of fission products among the solid phases. He finds the fission products whose oxides favor the cubic fluorite structure, such as cerium and zirconium, preferentially partition into the cubic MgU_2O_5 phase. Alkaline earths remain in the glass phase. Fission products that as oxides form hexagonal structures enter both phases though concentrations are usually higher in the glass.

Braithwaite and Johnson [36] have examined the leaching of cesium and strontium from mixtures of "corium" and basaltic concrete. Leaching was done with distilled water and a saline solution to simulate sea water. Samples were leached for 3 days at 25 and 90°C. Over the leaching period $0.1\text{-}0.8_5$ of the cesium was removed from the corium-concrete mixture and $0.68\text{-}2.5_5$ of the strontium was removed. The temperature dependence of leaching was small, suggesting liquid phase diffusion was the rate controlling process.

Powers [37] conducted scoping studies of Mo, U, Zr, Th, Nb, La, Ce, Sr, and Cs leaching from mixtures composed of 34% UO_2, 5.1% Fe_3O_4, 5.1% Cr_2O_3 and 48% dehydrated basaltic concrete. Samples were leached in bombs for 1.5-200 hours at temperatures of 80-200°C. Leaching solutions of various compositions were used to simulate different groundwater chemistries. Conclusions from this scoping work included:

(1) Cs, La, Ce and U were the most easily leached elements. Only upper bounds on Sr and Th leaching based on the detectability limits could be determined.

(2) Solutions containing NaCl and saturated with CaCO# were not more effective leachants than distilled water.

(3) Solutions containing sodium phosphate were very effective leachants especially for zirconium.

(4) Ferric ion appeared to accentuate leaching. This could be because of the oxidation reaction:

$$UO_2 + 2Fe^{3+} \rightarrow UO_2^{2+} + 2Fe^{2+}$$

or the low pH created by the hydrolysis reaction:

$$Fe^{3+} + 2H_2O \rightarrow FeO(OH) + 3H^+$$

(5) Chromate-containing solutions were not especially effective leachants which suggests that oxidation of the UO_2 to soluble uranyl ions is not the primary leaching mechanism.

(6) Colloidal suspensions were formed during many of the leaching experiments.

(7) The surface area of the solid mixture increased during leaching due to the Zwiebelschale effect [38].

It is apparent, then, that slow leaching of a core debris-concrete mixture that has penetrated the reactor basemat is possible. The leaching may involve subtleties not considered past analyses. It remains to be demonstrated, however, that leached fission products pose a sufficient threat to merit more thorough study of the leaching process.

Recommendations to MELCOR Concerning the Treatment of Ex-vessel Leaching. At this juncture, there appears to be no generally satisfactory model for leaching core debris by groundwater. Nor does there appear to be a critical need to consider this process in MELCOR.

4.3 SECONDARY FISSION PRODUCT RELEASE IN CONTAINMENT

The term "secondary fission product release" is used here to signify the generation of airborne fission product vapors or aerosols by processes not directly connected to the behavior of the core debris. One such process, the combustion of debris to form aerosols in the reactor containment atmosphere, has been discussed above in connection with release associated with pressurized melt ejection. Three other secondary fission product release processes discussed here are:

(1) resuspension of deposited or sedimented aerosols,
(2) vapor partitioning of dissolved fission products, and
(3) mechanical resuspension of fission products trapped in water.

There may be other important, secondary mechanisms of fission product release to the containment atmosphere.

Grouping resuspension of aerosols and vapor partitioning of dissolved fission products under the heading secondary processes is not an assessment of the relative importance of these processes. Resuspension reverses the natural mitigation of the severe reactor accident source term brought on by the agglomeration, deposition and sedimentation of aerosols. Vapor partitioning reverses the natural or engineered mitigation of the source term brought on by water scrubbing of the containment aerosols. The secondary release processes then may play a critical role in determining the severe reactor accident source term. These processes may well undo much of the mitigation expected by many to substantially reduce the severe accident source term to levels well-below those estimated in the Reactor Safety Study.

A. Resuspension of Deposited Aerosols

Detailed, mechanistic treatments of the processes leading to the deposition and sedimentation of aerosols have proliferated in recent years. Treatments of the reverse process, aerosol resuspension, have not been attempted to a similar level of detail. This may be because resuspension involves analysis of both the aerosol particles and the surfaces to which they adhere whereas attention concentrates on only the aerosol particle in the analysis of aerosol deposition. It is likely that in any real situation, a dynamic equilibrium between aerosol deposition and resuspension develops. Throughout most phases of a reactor accident, the rate of resuspension is sufficiently small that it can be neglected or accounted for in an approximate manner as an inefficiency in the deposition process.

There are a few instances in hypothesized nuclear reactor accidents in which wholesale aerosol resuspension must be considered:

(1) blowdown of the reactor coolant system

(2) in-vessel fuel/coolant interactions that lead to high steam generation rates

(3) catastrophic depressurization of the containment building.

In these instances, high gas velocities arise near aerosol-coated surfaces. The surfaces may experience sudden accelerations. High gas velocities and sudden surface acceleration are conducive to efficient particle re-entrainment. Such re-entrainment could reverse temporarily the natural mitigation of the source term produced by aerosol agglomeration, settling and deposition processes.

Aerosol particles are held to surfaces by Van der Walls forces, electrostatic forces, and the surface tension forces of liquid films. It is useful to distinguish between aerosols bound to dry surfaces and aerosols bound to wet surfaces because of the radical differences in adherence forces. The adhesive force between a particle and a surface can be defined as:

$$F_{ps} = H\ Dp$$

where H is a constant and Dp is the particle diameter. For dry aerosols, H is on the order of 1-60 dyne/cm (see Table 4.7). The adherence force does vary over at least 2 orders of magnitude depending on the peculiar nature of the particle and the surface (see Table 4.8). The irregularity of the surface may contribute to some of this variability (see Table 4.9). When the particle is bound to a surface by a liquid film, H is on the order of 400 dyne/cm.

There is a gradation between the extremes posed by the classification of systems as either "dry" or "wet". As shown in Figure 4.13, the adherence of a particle to a surface increases with relative humidity once a critical humidity (.65% relative) is exceeded.

Some data for the resuspension of glass spheres on stainless steel are shown in Figure 4.14. At low velocities (< 5 m/s) some small resuspension occurs. The extent of resuspension does not increase much with gas velocity until a critical velocity is achieved. Then entrainment increases sharply with flow velocity to 40-70%. Once this plateau in the entrainment efficiency is reached, entrainment is again relatively insensitive to gas velocity. It appears then that sudden increases in flow velocity will produce some entrainment, but complete entrainment of all deposited aerosols will be difficult to achieve.

The force on deposited aerosols produced by flowing gas is given by:

$$F = 1/2\ \rho_g\ U_\ell^2\ C\ A_p$$

where ρ_g = gas density

U_ℓ = local gas velocity

$A_p = \pi Dp^2/4$

$C = [2.87 + 1.58\ \log_{10}\ (x/D_p)]^{-2}$ for $10^2 < x/D_p < 10^6$

Table 4.7

Comparison of Air Flow and Acceleration as Mechanisms for Aerosol Removal [40]

Particle Size (μm)	Force (dynes) Required to Achieve 75% Removal by	
	Air Flow	Centrifugation
10.6 - 21.2	0.0195	0.016
21.2 - 31.8	0.056	0.060
31.8 - 42.4	0.11	0.21
42.4 - 53	0.11	0.26

Table 4.8

Effects of Particle Composition and Surface Characteristics on Particle-Surface Adherence [41]

	Force (dynes) Required to Remove 98% of the Particles from a Surface of			
50μ Particles of	Aluminum	Brass	Glass	Enamel
glass	0.5	2.85	1.83	3.63
sand	6.60	0.45	0.06	6.34
charcoal	0.57	0.32	0.94	2.30

Table 4.9

Effect of Surface Roughness on Particle Adherence [39, 42]

Mean Height of Surface Irregularities (Å)	Relative Particle Adhesion
150	100 (a)
1000	79 (a)
4000	51 (a)
100000	0 (a)
2160	100 (b)
2920	67 (b)
3430	59 (b)
4826	45 (b)

(a) Adhesion of glass particles to a glass surface at 100% relative humidity.

(b) Adhesion of quartz particles to Pyrex glass.

figure 13

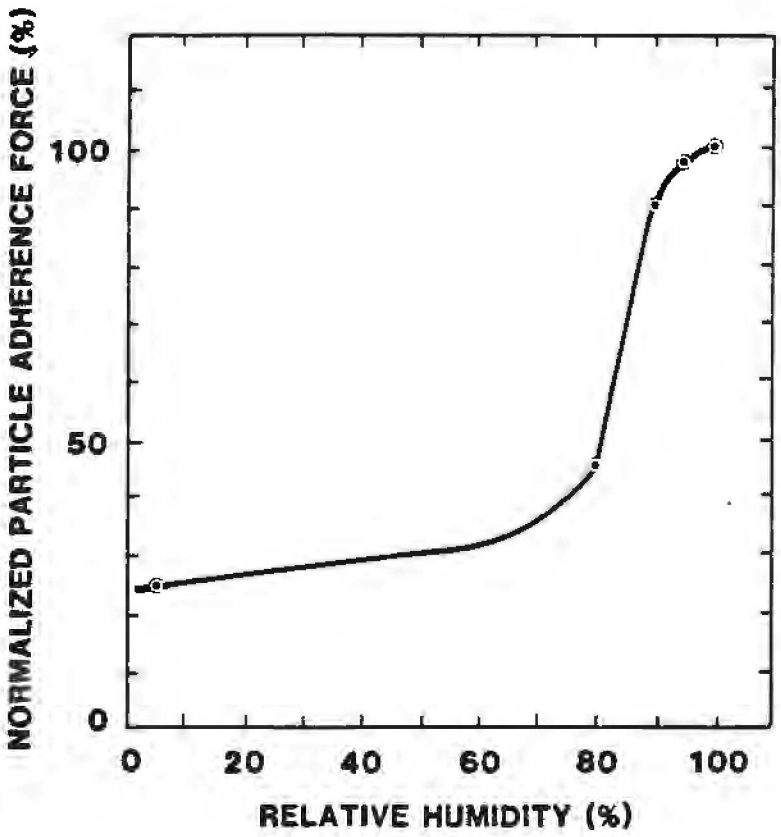
NORMALIZED PARTICLE ADHERENCE FORCE (%)
100
50
0
0
20
40
60
80
100
RELATIVE HUMIDITY (%)

figure 14

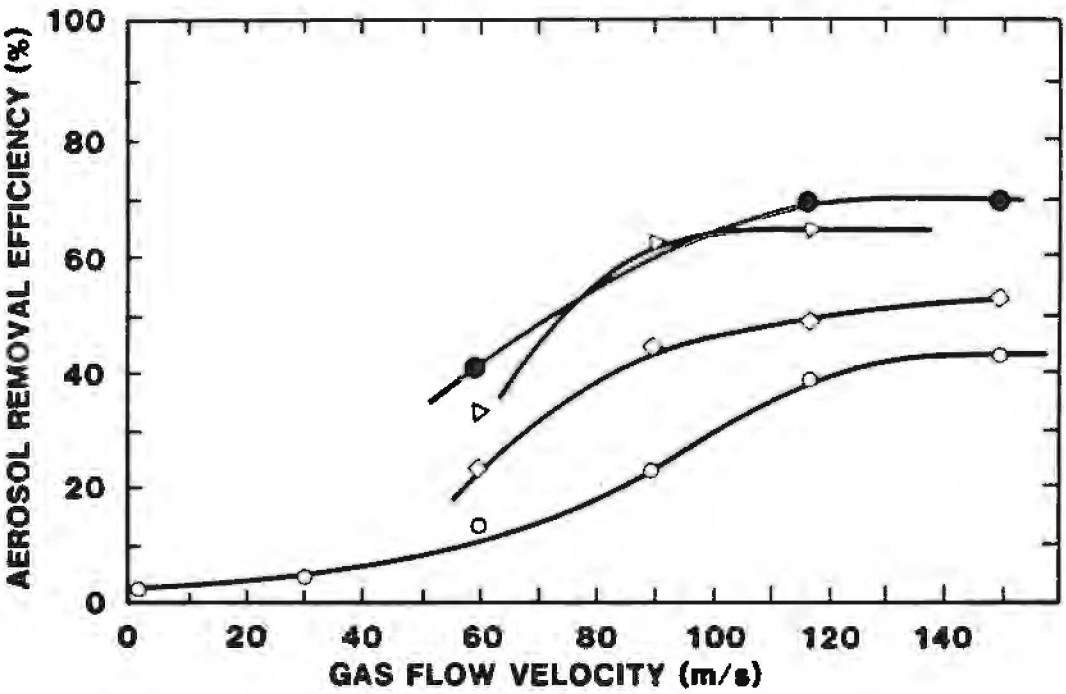
AEROSOL REMOVAL EFFICIENCY (%)
100
80
60
40
20
0
0
20
40
60
80
100
120
140
GAS FLOW VELOCITY (m/s)

x = distance along a surface where re-entrainment begins.

Notice that the local gas velocity, as opposed to the free-stream or bulk velocity is used in this description of the forces. Because this local velocity will depend on both the surface geometry and the aerosol deposit geometry, it is most difficult to estimate for reactor accident situations.

Brockmann [23] has advocated using an equation derived by equating binding forces between the surface and aerosol and the flow forces on the aerosol as a criterion for re-entrainment:

$$U_{Re\text{-}ent} > \frac{8H}{\pi \rho_g D_p C} + \frac{4 f \rho_p g D_p}{3 C \rho_g}$$

where f = friction factor = 0.2; C has a typical value of 0.01 and U is the free stream velocity. This criterion indicates re-entrainment of dry, 1 μm particles occurs at flow velocities of about 2 m/s. Brockmann asserts that once the criterion is met, re-entrainment will be 90% complete. The criterion also indicates that wet aerosols are unlikely to be entrained by gas flows arising in nuclear reactor accidents.

Particle removal by acceleration of surface has received some study in non-nuclear contexts. This mechanism of particle resuspension is often overlooked in the analysis of severe reactor accidents. In view of the many dynamic events postulated to occur during severe reactor accidents, this is likely to be an important process. Where comparisons have been made, the forces to remove particles by gas flow entrainment or by acceleration agree to within about a factor of two (see Table 4.7)

Recommendations to MELCOR Concerning Aerosol Particle Re-entrainment

(1) MELCOR should allow for re-entrainment of aerosol particles during blowdown of the reactor coolant system.

(2) Since particle deposits in the reactor containment are wet it is probably unnecessary to treat particle re-entrainment during pressurization of the containment.

(3) The criterion for re-entrainment during vessel depressurization is:

$$U > \frac{258H}{\rho_g D_p} + \frac{26\rho_p g D_p}{\rho_g}$$

where H is a user supplied force constant with a default value of 1 dyne/cm.

(4) The extent of re-entrainment is also a user supplied constant with a default value of 90%.

(5) No recommendation is made concerning particle resuspension caused by surface acceleration save that it should be noted as a possibility.

B. Secondary Release From Water

One of the most important caused of source term mitigation is the entrapment of radioactive species in water. Mitigation of this sort can arise at many points in a severe reactor accident. Effluent from the core may have to pass over or through water as it is carried through the primary system; thus, an opportunity to partition between the liquid and the vapor is presented. For boiling water reactors, radioactive species may have to pass through the steam suppression pool before they can enter containment. Once in containment, there will very likely be large bodies of water to absorb radioactive species. Operation of containment sprays can sweep the containment atmosphere of suspended vapors or particles.

The mitigation of the source term that can be provided by water depends not only on the efficiency with which water can entrap radioactive species, but also the permanence of the entrapment. In this section, some of the mechanisms available to reverse water entrapment of radioactive materials are described.

Iodine Partitioning. Modern perceptions concerning the severe reactor accident source term hold that fission product iodine is liberated from the core and carried through the reactor primary system as iodide - probably cesium iodide - rather than as iodine gas. With few exceptions, iodides are quite soluble in water. Dissolution of any iodides in water would mitigate possible airborne release of the iodine from containment.

Iodide (I^-) in aqueous solution can be oxidized to volatile iodine (I_2) or to another soluble anion, iodate (IO_3-). Some of the relevant chemical reactions and their associated equilibrium constants at 298K are shown in Table 4.10.

Table 4.10

Some Relevant Solution Phase Equilibria

Reaction	Equilbrium Constant
$2H^+ + 2I^-(aq) + 1/2\ O_2 \rightleftarrows I_2(aq) + H_2O$	$[I_2]/[H^+]\ [I^-]^2\ Po_2^{1/2} = 2.6\times10^{23}$
$2I_2(aq) + 2H_2O + 5O_2 \rightleftarrows 4IO_3^-(aq) + 4H^+$	$[IO_3^-]^4\ [H^+]^4/[I_2]^2\ P_{O_2}^5 = 9.4\times10^{16}$
$I_2(aq) + H_2O \rightleftarrows H^+ + I^-(aq) + HOI\ (aq)$	$[H^+]\ [I^-]\ [HOI]/[I_2] = 4.04\times10^{-13}$
$HOI(aq) \rightleftarrows H^+ + OI^-$	$[OI^-]\ [H^+]/[HOI] = 5\times10^{-13}$
$H_3BO_3 \rightleftarrows H^+ + H_2BO_3^-$	$[H^+]\ [H_2BO_3^-]/[H_3BO_3] = 6.4\times10^{-10}$
$I_2(aq) \rightleftarrows I_2(g)$	$P_{I_2}/[I_2] = 0.303$
$5Ag^+ + 3I_2 + 3H_2O \rightleftarrows 5AgI + IO_3^- + 6H^+$	$[IO_3^-]\ [H^+]^6/[Ag^+]\ [I_2]^3 = 1.68\times10^{33}$
$I_2(aq) + I^- \rightleftarrows I_3^-$	$[I_3^-]/[I_2]\ [I^-] = 710$
$AgI(s) \rightleftarrows Ag^+ + I^-$	$[Ag^+]\ [I^-] = 8.32\times10^{-17}$
$Ca(OH)_2 \rightleftarrows Ca^{2+} + 2OH^-$	$[CaOH^+]\ [OH^-] = 1.7783\times10^{-4}$
$Ca(OH)_2 \rightleftarrows CaOH^+ + OH^-$	

Because there is the potential for iodide in solution to form volatile species, there is the potential for iodide to escape the solution. The tendency for iodine to escape the solution is measured by a partition coefficient which is defined as:

$$\text{Partition Coefficient} = \frac{\text{moles of iodine in solution}}{\text{moles of iodine in vapor}}$$

Estimates of this partition coefficient have appeared in the literature [43].

Quantitative analysis of the hydrolysis and vaporization equilibria listed above leads to the conclusions:

(1) with increasing acidity of the water, the partition coefficient decreases

(2) the partition coefficient increases with dilution of the iodine solution

(3) the variation of the partition coefficient with temperature depends on the acidity and iodine concentration of the aqueous phase.

Equilibrium analysis of the behavior of iodine species and the partitioning of iodine between the aqueous and vapor phases is not likely to be entirely satisfactory because:

(1) radiolysis will affect the partitioning

(2) the gas phase in reactor containment is not at equilibrium especially whenever both O_2 and H_2 are present.

(3) other species dissolved in the water - such as Cd^{2+} or Ag^{+} - can alter the partitioning by reacting with iodide to form insoluble precipitates.

The vapor-liquid partitioning of iodine can be responsible for long-term, low-level release of iodine. This, of course, is quite different than the prompt, intense release of iodine envisaged by the Reactor Safety Study. The radiological consequences of slow iodine release from aqueous solutions are very much mitigated by the rapid radioactive decay of iodine.

Other fission product species, nominally quite soluble in water, will partition between the aqueous and the gas phases. For instance, ruthenium tetroxide engages in such a process:

$$RuO_4(g) \rightleftarrows RuO_4(aq)$$

Quantitative evaluations of the partitioning of these other radionuclides between the aqueous and vapor phases under reactor accident conditions have not been reported.

Recommendation to MELCOR Concerning Iodine Partitioning. It is recommended that MELCOR allow for iodine partitioning between water and the containment atmosphere. The equilibrium partial pressure of I_2 in the atmosphere can be defined as

$$P_{I_2}^{eq} = C_I/K$$

where $P_{I_2}^{eq}$ = equilibrium I_2 partial pressure

C_I = total iodine concentration in water pools (moles/liter)

K = user-supplied partition coefficient with a default value of 1 x 104

The approach to equilibrium can be calculated knowing the surface area of water pools in the containment, A, and a mass transport coefficient, K_m, appropriate for the flow conditions over the water pools:

$$\frac{dN_{I_2}}{dt} = \frac{K_m A}{RT}\left[P_{I_2}^{eq} - P_{I_2}(t)\right]$$

where N_{I_2} = moles of I_2 in the containment atmosphere

R = gas constant

$P_{I_2}(t)$ = I_2 partial pressure in containment at time t

There appears at this time to be no need to recognize partitioning of other fission products between water and the containment atmosphere.

Mechanical Release From Water. Water pools within the containment will contain, for the reasons outlined above, fission products. These fission products will be dissolved or present as particulate. The decay heat from the fission products will tend to keep the water pools at or near the boiling point as the reactor containment pressurizes. Should the containment suddenly depressurize, the superheated water pools will boil spontaneously. If the depressurization is rapid, vigorous boiling will entrain water droplet laden with dissolved and particulate fission products. That is, sudden depressurization can reverse the mitigation of the severe accident source term provided by water entrapment of fission products. The extent of water entrainment by flash boiling depends on (1) the rate at which the containment depressurizes and (2) the geometry of the water pool.

Brockmann [23] has formulated a model of liquid entrainment caused by the boiling of water pool during depressurization of containment. The pressure within the containment during depressurization is given by:

$$\frac{dp}{dt} = -\frac{PQ}{V}$$

where P = pressure
t = time
V = containment volume
Q = volumetric flow rate

The volumetric flow rate depends on the size of the hole in the containment. When the flow is choked:

$$Q = 0.65\, A_o C_D\, (RT/MW)^{1/2}$$

where A_o = hole area
R = universal gas constant
T = absolute temperature of the containment atmosphere
MW = mean molecular weight of the containment atmosphere
C_D = orifice drag coefficient = 0.61

When the flow out of the containment is subcritical:

$$Q = 4.19\ A_o\ C_D\ (RT/MW)^{1/2}\ [(Pa/P)^{1.77} - (Pa/P)^{1.89}]^{1/2}$$

where Pa is the pressure of the atmosphere surrounding the containment.

The temperature of the water is assumed to adjust to the saturation temperature of water throughout the depressurization

$$T(K) = \frac{3576}{11.342 - \ln P(atms)} + 57.8$$

The rate at which mass evaporates from the water pools is given by:

$$m_v = - \frac{Cp}{h_f}\ m_f\ \frac{dT}{dt}$$

where m_v = mass evaporation rate

Cp = specific heat of water

h_f = enthalpy of vaporization of water

m_f = mass of water in the pool

The evaporating water entrains liquid:

$$E = \frac{M_e}{m_v} = 3.8x10^{-5}\ (K^{1/2} + 530K^{2.1})\ [(\rho_f - \rho_g)/\rho_g]^{1/2}$$

where m_e = mass rate of entrainment

ρ_f = density of water

ρ_g = density of water vapor

$K = D_c\ j_c$

$j_c = U_v\ (\rho_g)^{1/2}/[g\sigma(\rho_f - \rho_g)]^{1/4}$

$$D_c = 4U_v \left[n_g \rho_g / g(\rho_f - \rho_g)\right]^{1/3} \left[\sigma / g(\rho_f - \rho_g)\right]^{-1/2}$$

U_v = superficial velocity of water vapor off the pool surface

g = gravitational acceleration

n_g = viscosity of water vapor

σ = surface tension of water

The size distribution of water droplets entrained by evaporating water is assumed by Brockmann to be log-normal with a geometric standard deviation of 2.3 and a geometric mass mean diameter, DGM, of

$$DGM = \begin{cases} D_s/2 & \text{if } D_c > D_s \\ D_c/2.3 & \text{if } D_s > D_c \end{cases}$$

where

$$D_s = 12\sigma / \rho_f U_v^2$$

$$D_c = 4U_v n_g \sigma_g / (\rho_f g)^2$$

Some results for a specific accident at the SURRY reactor obtained with Brockmann's model are shown in Figures 4.15 and 4.16. The mass geometric mean particle size increases with the area of the hole in containment to a plateau of 50-3000 mm for a hole area of about 100 m^2. The entrained mass increases sharply with hole area. Significant entrainment is obtained only when holes sizes are large (10-100 m^2).

Recommendation to MELCOR Concerning Re-entrainment from Water

Re-entrainment during containment depressurization should be recognized by MELCOR. The model developed by Brockmann is sufficiently simple. It can be implemented in MELCOR. The containment hole size may have to be a user-supplied value. A default value of 1 m^2 would allow a rather modest amount of release by re-entrainment from water pools.

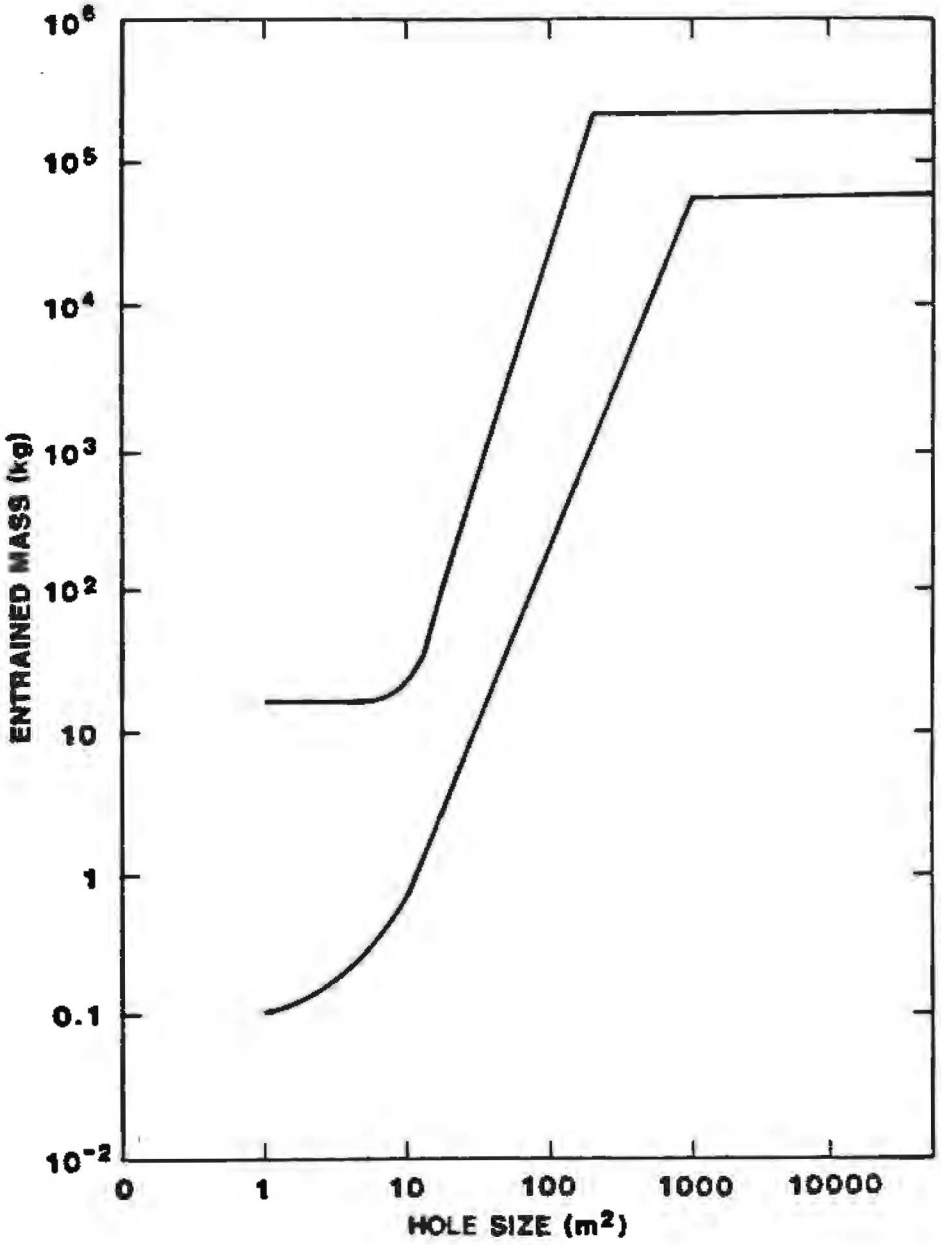

Figure 4.15 Bounding Estimates Obtained with the Brockmann Model of Entrainment of Water During Containment Depressurization as a Function of the Containment Hole Size (23).

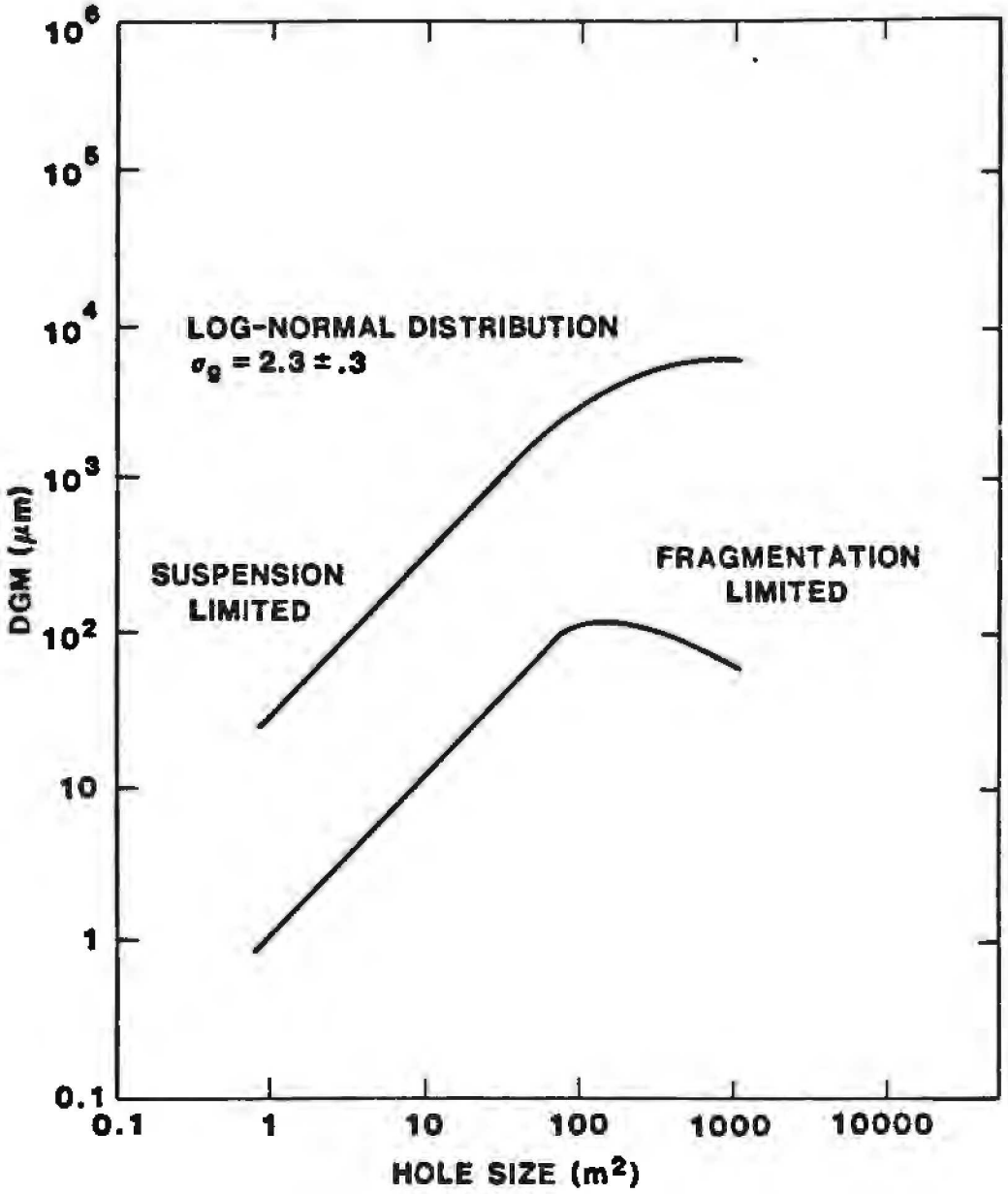

Figure 4.16 Mean particle size predicted with the Brockmann model of entrained water during containment depressurization as a function of the size of the hole in containment [23].

4.4 Conclusions

The ex-vessel sources of fission product release may be categorized as "primary processes" involving the core debris and "secondary processes" that involve resuspension of material that had previously escaped the core debris. Releases of aerosols and fission products associated with melt ejection from the primary system, core debris-coolant interactions, core debris-concrete interactions and groundwater leaching are the most important primary mechanisms. Resuspension of aerosols, vapor partitioning of fission products dissolved in water, and mechanical release of dissolved or suspended material from water are the most important secondary release processes.

Aerosol and fission product release that occurs when a melt is ejected from pressurized primary system was not recognized in the Reactor Safety Study. Recent analyses of the fission product source term associated with steam explosions suggest the Reactor Safety Study estimate of this source may have been too high. Significant improvements have been made in the capabilities to model fission product and aerosol releases during core debris concrete interactions. The effects of coolant waters on this source term can be estimated. Scoping studies support the contention that fission product release by groundwater leaching is not as significant an effect as intense, airborne release of fission products except when very specialized circumstances are present.

Secondary release process can reverse or certainly limit the effectiveness of natural or engineered source term mitigation features of a nuclear power plant. Of the secondary processes, only vapor phase partitioning of dissolved iodide has received great attention. Qualitative indications from a non-nuclear data base suggest there are many instances in a severe reactor accident in which resuspension of deposited or sedimented aerosols would be a serious concern. Data are available to qualitatively assess the likelihood of aerosol resuspension to occur in severe accidents. Similarly, resuspension of dissolved or entrapped material in pools of water by the mechanical action of sparging bubbles or boiling can be quantified. It is apparent that this effect poses a limit to the decontamination that can be achieved with water during a severe accident.

References

1. U. S. Nuclear Regulatory Commission, Reactor Safety Study: An Assessment of Accident Risks in U. S. Commercial Nuclear Power Plants, NUREG 75/014, WASH 1400, Washington, DC, October 1975.

2. R. L. Ritzman, et al., "Release of Radioactivity in Reactor Accidents", Appendix VII to Reactor Safety Study - Reference 1.

3. J. Gieseke, et al., Radionuclide Release Under Specific Accident Conditions, Volume I: A PWR Analysis, BMI-2104 (Draft), Battelle Columbus Laboratory, Columbus, OH, January 1983.

4. T. Y. Chu, et al., Report on a Large-scale UO_2 Melt/MgO Brick Interaction Test, SAND83-1692, NUREG/CR-3438.

5. J. B. Rivard, "Review of In-Vessel Meltdown Models", Sandia National Laboratories, Albuquerque, NM, July 1980.

6. D. Alpert, unpublished results, 1983.

7. R. Henry, Section 3 in Zion Probabilistic Safety Study, Commonwealth Edison Co., 1982.

8. W. W. Tarbell, J. E. Brockmann, M. Pilch, High Pressure Melt Streaming (HIPS) Program Plan, NUREG/CR-3025, SAND82-2477, Sandia National Laboratories, Albuquerque, NM, June 1983.

9. M. Pilch, Advanced Reactor Safety Research Quarterly Report, January-March 1982, NUREG/CR-2679 (1 of 4), SAND82-0904 (1 of 4), SAndia National Laboratories, ALbuquerque, NM.

10. D. A. Powers, Gas Solubility in SPIT Melts.

11. M. Weinstein and J. F. Elliott, Trans. Met. Soc. AIME 227 (1963) 382.

12. M. Blander, W. R. Grimes, N. V. Smith and G. M. Watson, J. Phys. Chem. 63 (1959) 1164.

13. J. Nichols, Contrib. Mineral. Petrol. 74 (1980) 211.

14. W. W. Tarbell, Technical Highlights/Administrative Report for the Nuclear Regulatory Commission Advanced Reactor Safety Reseach Program, March, 1983, Sandia National Laboratories, Albuquerque, NM, May 1983.

15. M. Tomaides and K. T. Whitby, "Generation of Aerosols by Bursting of Single Bubbles" in Fine Particles: Aerosol Generation, Measurements, Sampling, and Analysis, B. Y. U. Liu, Ed., Academic Press, Inc., New York, New York.

16. M. Pilch, unpublished results.

17. K. A. Peakall and J. E. Antill, J. Nucl. Materials 2, (1960) 194.

18. M. Iwasaki, T. Sakukrai, N. Ishikawa, and Y. Kobayashi, J. Nucl. Sci. Tech 5, (1968) 652.

19. J. Bittel, L. H. Sjodahl and J. F. White, J. Am. Ceramic Society 52, (1969) 446.

20. D. Cubicciotti, Nuclear Technology 53, (1981) 5.

21. L. S. Nelson, Pyrodynamics 3, (1965) 121.

22. D.G.C. Robertson and A. E. Jenkens, in Heterogenous Kinetics at Elevated Temperatures, G. R. Belton and W. L. Worrell, eds., Plenum Press, 1970.

23. R. J. Lipinski et al., Uncertainty in Radionuclide Release Under Specific LWR Conditions Volume II: Analyses, SAND84-0410/2, Sandia National Laboratories, Albuquerque, NM.

24. M. Pilch, "Direct Heating of Containment Atmosphere by Airborne Core Debris", contribution to the Containment Loads Working Group final report, dated May 3, 1984.

25. G. W. Parker, et al., ORNL-3319, Oak Ridge National Laboratory, Oak Ridge, TN, August 1962.

26. B. M. Jeffrey, J. Nucl. Materials 22, (1967) 33.

27. M. Corradini, "Hydrogen Generation During Molten-FuelCoolant Interactions", Second Workshop on the Impact of Hydrogen on Water Reactor Safety.

28. D. A. Powers, "A Re-Examination of the Steam Explosion Source Term During Severe Accidents," paper IAEA-SM-281/34, Intl. Symp. on Source Term Evaluation for Accident Conditions, 28 Oct. to 1 Nov., Columbus, OH, IAEA, 1986.

29. D. A. Powers, "Aerosol Generation During Core Debris Interactions with Concrete", 7th International Light Water Reactor Safety Information Exchange, Gaithersburg, MD.

30. W. B. Murfin and D. A. Powers, Report of the Zion Indian Point Study: Volume I, NUREG/CR-1410, SAND80-0617/1, Sandia National Laboratories, Albuquerque, NM.

31. D. A. Powers and J. E. Brockmann, "Release of Fission Products and Generation of Aerosols Outside the Primary System", Appendix C in J. Gieseke et al., Radionuclide Release Under Specific LWR Accident Conditions, Volume 1: PWR Analyses, BMI-2104, Battelle Columbus Laboratory, Columbus, OH, January 1983.

32. J. F. Muir et al., CORCON-MOD1: An Improved Model for Molten/Core Concrete Interactions, SAND80-2415, NUREG/CR-2142, Sandia National Laboratories, Albuquerque, NM, July, 1981.

33. N. A. Fuchs, The Mechanics of Aerosols, Pergamon Press, 1964.

34. Office of Nuclear Reactor Regulation, U. S.Nuclear Regulatory Commission, Liquid Pathways Generic Study, NUREG -0440, February 1978.

35. H. Westrich, J. Nucl. Materials 110, (1982) 324.

36. J. W. Braithwaite and J. K. Johnson, Light Water Reactor Safety Research Quarterly Report, October-December 1977, NUREG/CR-0307, SAND78-0600, Sandia National Laboratories, Albuquerque, NM, June 1978.

37. D. A. Powers, Advanced Reactor Safety Research Quarterly Report, January-March 1980, NUREG/CR-1594 (1 of 4), SAND80-1646 (1 of 4), Sandia National Laboratories, Albuquerque, NM.

38. H. J. Matzke, "Actinide Diffusion in Waste Glasses", Thermodynamics of Nuclear Materials, Vol. 1, IAEA, Vienna, Austria, 1980, p. 311.

39. M. Corn, J. Air Poll. Control Assoc. 11, (1961) 566.

40. M. Corn and F. Stein, Amer. Ind. Hyg. Assoc. J. 26, (1965) 26.

41. M. C. Kordeki and C. Orr, Arch. Env. Health 1, (1960) 1.

42. F. P. Bowden and D. Tabor, The Friction and Lubrication of Solids, Clarendon Press, Oxford (1954).

43. J. T. Bell, et al., "Chemistry of Cesium and Iodine", Chapter 5 in Technical Bases for Estimating Fission Product Behavior During LWR Accidents, NUREG 0772, U. S. Nuclear Regulatory Commission, June 1981.

CHAPTER 5

FISSION PRODUCT TRANSPORT AND DEPOSITION INCLUDING VAPOR CONDENSATION AND AEROSOL AGGLOMERATION

by C. D. Leigh and J. L. Sprung

5.1 Introduction

Fission products are released from degraded core materials by vaporization and mechanical aerosolization. Once gas borne, transport to the location of containment failure allows fission products to escape to the environment. The magnitude of the environmental release (the radiological source term) is not necessarily equal to the magnitude of the release from degraded core materials (the phenomenological source term). The radiological source term can be smaller than the phenomenological source term if, during transport to the containment failure, gas borne fission products are depleted due to the operation of natural processes or Engineered Safety Features (ESFs).

In-vessel release of radioactive materials from degraded core materials was examined in Chapter 3. Ex-vessel release was discussed in Chapter 4. Removal of gas borne radioactive materials by Engineered Safety Features is reviewed in Chapter 6. In this chapter those natural processes that can significantly alter the concentrations or properties of gas borne vapors and aerosols are examined. Vapor processes are discussed first. Then aerosol processes are examined. Finally, numerical methods for solving aerosol rate equations are reviewed, because the solution of those equations is greatly complicated by the need to integrate them over the range of aerosol particle sizes.

5.2 Vapor Processes

After release from degraded core or structural materials, diffusion, condensation, evaporation, and chemical reactions of vapors can change their location, physical state, or chemical form. Concentrations of gas borne vapors are diminished by diffusion of the vapors to surfaces followed by either condensation on or binding to those surfaces. Gas borne vapor concentrations are increased by evaporation of condensed vapors, and the properties of vapors are altered by chemical transformations. All of these phenomena are discussed in this section.

A. Diffusion to Surfaces

Molecular diffusion of a vapor in a bulk gas mixture is well described by Fick's first law of diffusion [1a].

$$J_{k,x} = D_{k,g} \frac{dC_{k,x}}{dx} = N_{k,x} - y_k \sum_i N_{i,x} \qquad (5.1)$$

where $J_{k,x}$ = molar flux of vapor k relative to the flux of the bulk gases

$N_{k,x}$ = molar flux of vapor k relative to stationary coordinates

$C_{k,x}$ = molar concentration of vapor k at the point x

y_k = mole fraction of vapor k

$D_{k,g}$ = molecular diffusion coefficient for vapor k in the bulk gas mixture

$N_{i,x}$ = molar flux of bulk gas component i relative to stationary coordinates

When vapor k is present only in trace quantities, as will be the case for most fission product vapors, $y_k << 1.0$, and Eq. 5.1 reduces to

$$N_{k,x} = D_{k,g} \frac{dC_{k,x}}{dx} \qquad (5.2)$$

Eq. 5.2 accurately describes vapor diffusion only when bulk gases are stationary or in laminar flow. When flow is turbulent, vapor transport by turbulent eddies (eddy diffusion) becomes important. If Prandtl's mixing length hypothesis is used to define the transient concentration gradient produced by a turbulent eddy, a modified form of Eq. 5.2, that incorporates eddy diffusion, can be derived [1b],

$$N_{k,x} = [D_{k,g} + E(x)] \frac{dC_{k,x}}{dx} \qquad (5.3)$$

where E(x) is the eddy diffusion coefficient at point x. For turbulent flows E(x) is much smaller than $D_{k,g}$ in the laminar sublayer, much larger than $D_{k,g}$ next to the well-mixed turbulent core, and of comparable magnitude in the transition region in between. Because the dependence of E(x) on x is generally not known, integration of Eq. 5.3 is possible only after E(x) is replaced with its average value E_{av} within the boundary layer [2]. When this is done the following equation results,

$$N_{k,x} = \frac{1}{\delta} [D_{k,g} + E_{av}][C_{k,g} - C_{k,s}] \qquad (5.4)$$

where $C_{k,g}$ and $C_{k,s}$ are the concentrations of trace vapor k in the turbulent core and at the deposition surface, and δ is the thickness of the boundary layer. Even after this transformation has been made, Eq. 5.4 is rarely useful, because values of E_{av} are only infrequently available. Hence, Eq. 5.4 is usually rewritten [2],

$$N_{k,x} = \frac{1}{A} \frac{dC_{k,g}}{dt} = k_{c,k} [C_{k,g} - C_{k,s}] \qquad (5.5)$$

where $k_{c,k} = [D_{k,g} + E_{av}]/\delta$ is the mass transfer coefficient and A is the area of the deposition surface. The advantage of this transformation is that values of $k_{c,k}$ can be determined experimentally or by mass-transfer/heat-transfer analogies.

Structural Surfaces. Heat transfer to structural surfaces will be modeled in the MELCOR code system using Nusselt number (Nu) heat transfer correlations for forced [Nu = f(Re,Pr)] and natural [Nu = f(Gr,Pr)] convection by laminar and turbulent flows over regular surfaces (e.g., flat plates, cylinders). Therefore, consistency, convenience, and the scarcity of experimental mass transfer correlations all suggest that vapor transport to structural surfaces should be modeled in the MELCOR code system using Sherwood number (Sh) mass transfer correlations constructed by mass-transfer/heat-transfer analogies.

Mass transfer correlations are constructed from heat transfer correlations by substitution of dimensionless groups [1c]. When mass transfer is caused by forced convection, Nusselt number heat transfer correlations [Nu = f(Re,Pr)] are converted to Sherwood number mass transfer correlations by substituting the Sherwood number (Sh) for the Nusselt number (Nu) and the Schmidt number (Sc) for the Prandtl number (Pr). Thus, Nu=f(Re,Pr) becomes Sh=f(Re,Sc), where

Nu = Nusselt number = hL/k
Re = Reynolds number = Lv/ν
Pr = Prandtl number = $\mu c_p/k$
Gr = Grashof heat transfer number = $g\beta L^3\Delta T/\nu^2$
Sh = Sherwood number = $k_{c,k}L/D_{k,g}$
Sc = Schmidt number = $\nu/D_{k,g}$
h = convective heat transfer coefficient
L = characteristic length
k = thermal conductivity

v = velocity
ν = kinematic viscosity = μ/ρ
μ = dynamic viscosity
ρ = mass density
c_p = heat capacity
g = acceleration due to gravity
β = thermal coefficient of volumetric expansion
T = temperature
k_c = mass transfer coefficient
$D_{k,g}$ = diffusion coefficient of vapor k in the bulk gas mixture

When mass transfer is caused by natural convection driven only by density gradients (negligible thermal gradients), Nusselt number heat transfer correlations [Nu = f(Gr,Pr)] are converted to Sherwood number mass transfer correlations by substituting the Sherwood number (Sh) for the Nusselt number (Nu), the mass transfer Grashof number (GrAB) for the heat transfer Grashof number (Gr), and the Schmidt number (Sc) for the Prandtl number (Pr). Thus, Nu = f(Gr,Pr) becomes Sh = f(GrAB,Sc), where

$$\text{GrAB} = \text{Grashof mass transfer number} = g\zeta L^3 \Delta\rho_k/\nu^2$$

ζ = concentration coefficient of volumetric expansion

Conditions where transport of a fission product trace vapor to structural surfaces is driven principally by gradients in the density of the trace vapor are unlikely to be encountered during a severe LWR accident. Instead trace vapor transport to structural surfaces during severe accidents is most likely to be driven principally by temperature gradients in the bulk fluids. When this is the case, how to convert a Nusselt number heat transfer correlation to a Sherwood number mass transfer correlation is not obvious.

Mass transport caused by natural circulation driven by gradients in both temperature (thermal diffusion) and density (mass diffusion) has been examined by Jaluria [3]. Jaluria notes that for systems where $\beta\Delta T$ and $\zeta\Delta\rho_k$ are both $<< 1$, the Boussinesq approximations apply and the buoyancy term in the momentum equation is adequately approximated by:

$$g\Delta\rho = g\beta\Delta T + g\zeta\Delta\rho_k \qquad (5.6)$$

But $g\beta\Delta T = (\nu^2/L^3)\text{Gr}$ and $g\zeta\Delta\rho_k = (\nu^2/L^3)\text{GrAB}$. Therefore, after substitution of Gr and GrAB into Eq. 5.6 the buoyancy term becomes

$$g\Delta\rho = (\rho\nu^2/L^3)(Gr+GrAB) \qquad (5.7)$$

Consequently Jaluria [3] derives Sherwood number mass transfer correlations having the following form

$$Sh = f([Gr + GrAB],Sc) \qquad (5.8)$$

for systems where mass transfer is caused by natural convection driven by gradients in both temperature and density.

For systems where temperature gradients are negligible, Gr << GrAB, and Equation 5.8 reduces to Sh = f(GrAB, Sc), the conventional result for mass transfer driven only by density gradients [3]. Conversely, for systems where density gradients are negligible, GrAB << Gr, and Equation 5.8 reduces to

$$Sh = f(Gr,Sc) \qquad (5.9)$$

This suggests that, when mass transfer is caused by natural circulation driven only by thermal gradients (negligible density gradients), Nusselt number heat transfer correlations [Nu = f(Gr,Pr)] should be converted to Sherwood number mass transfer correlations by substituting the Sherwood number (Sh) for the Nusselt number (Nu) and the Schmidt number (Sc) for the Prandtl number (Pr). Thus, Nu = f(Gr,Pr) becomes Sh = f(Gr,Sc). Since deposition of trace vapors on structural surfaces during severe LWR accidents will usually be driven by large thermal gradients and small density gradients, it is recommended that deposition of trace vapors on structural surfaces be calculated in the MELCOR code system using Eq. 5.9.

Finally, having constructed an appropriate Sherwood number mass transfer correlation from the Nusselt number heat transfer correlation applicable to the existing thermal-hydraulic regime, the mass transfer coefficient $k_{c,k}$ of trace vapor k can then be determined by substituting that Sherwood number correlation into the definition of the Sherwood number and solving for the mass transfer coefficient,

$$k_{c,k} = Sh \frac{D_{k,g}}{L} \qquad (5.10)$$

where L is the characteristic length of the deposition surface.

Vapor Transport to Aerosol Surfaces. Vapor transport from a stagnant fluid to an aerosol particle suspended in that fluid takes place by molecular diffusion only. For a spherical

particle of diameter d_p, both theoretical and experimental results [1d,4] show that

$$\frac{k_{c,k} d_p}{D_{k,g}} = 2.0 \qquad (5.11)$$

where $k_{c,k}$ is the mass transfer coefficient for trace vapor k for transfer from the stagnant fluid (the bulk gases) to a spherical particle (m/s). Accordingly,

$$k_{c,k} = D_{k,g}/r_p \qquad (5.12)$$

where r_p is the equivalent spherical radius of the aerosol particle.

Diffusion Coefficients. In Eqs. 5.10 and 5.12, $D_{k,g}$, the diffusion coefficient for diffusion of vapor k in the bulk gas mixture, should be calculated using the following equation derived by Wilke [1e,5] which closely approximates the general expression developed by Hirschfelder, Curtis, and Bird [6].

$$D_{k,g} = (1 - y_k) \left[\sum_n (y_n/D_{k,n})\right]^{-1} \quad \text{where } 1-y_k \cong 1 \qquad (5.13)$$

where y_k is the mole fraction of trace vapor k, y_n is the mole fraction of bulk gas component n, and $D_{k,n}$ is the binary diffusion coefficient for diffusion of vapor k in bulk gas component n.

Methods for estimating $D_{k,n}$ have been compared by Reid, Prausnitz, and Sherwood [7a]. Their results suggest that the following equation, derived for non-polar gases by Hirschfelder, Bird, and Spotz [7,8], gives results in reasonable agreement with experimental data even for polar gases,

$$D_{k,n} = \frac{0.001858\ T^{3/2} \left(\frac{1}{M_k} + \frac{1}{M_n}\right)^{1/2}}{P\ \sigma_{k,n}^2\ \Omega_D} \qquad (5.14)$$

where T and P are the temperature and pressure of the bulk gases, M_k and M_n are the molecular weights of trace vapor k and

of bulk gas component n, and $\sigma_{k,n}$ and Ω_D, the collision diameter and collision integral, are Leonard-Jones parameters.

When an experimental or calculated value of $D_{k,n}$ is available at temperature and pressure, T_1 and P_1, extrapolation to T_2 and P_2 can be done using the following equation [1f],

$$D_{k,n}(T_2,P_2) = D_{k,n}(T_1,P_1)\left(\frac{P_1}{P_2}\right)\left(\frac{T_2}{T_1}\right)^{3/2}\frac{\Omega_D(T_1)}{\Omega_D(T_2)} \qquad (5.15)$$

In Eqs. 5.14 and 5.15, the Leonard-Jones parameters $\sigma_{k,n}$ and Ω_D can be estimated using the following empirical relations [1f,7]:

$$\Omega_D = \frac{A}{(T^*)^B} + \frac{C}{\exp(DT^*)} + \frac{E}{\exp(FT^*)} + \frac{G}{\exp(HT^*)}$$

A = 1.06036	E = 1.03587
B = 0.15610	F = 1.52996
C = 0.19300	G = 1.76474
D = 0.47635	H = 3.89411

$$T^* = k_B T/\varepsilon_{k,n} \qquad \sigma_{k,n} = \frac{1}{2}(\sigma_k + \sigma_n)$$

$$\varepsilon_{k,n} = (\varepsilon_k \varepsilon_n)^{1/2} \qquad \sigma_i = 1.18\, V_b^{1/3}$$

$$\varepsilon_i/k_B = 0.77\, T_c \qquad \sigma_i = 0.841\, V_c^{1/3}$$

$$\varepsilon_i/k_B = 1.15\, T_b \qquad \sigma_i = 2.44\left(\frac{T_c}{P_c}\right)^{1/3}$$

where V_b is the molecular volume at the normal boiling temperature; T_b, V_c, T_c, and P_c are the critical molecular volume, the critical temperature, and the critical pressure, and k_B is the Boltzmann constant.

B. Condensation and Evaporation.

Vapor condensation and evaporation involve diffusion to or from a surface, a phase change at the surface (gas to liquid or liquid to gas) with release or gain of energy (the heat of vaporization), and possibly a chemical reaction of the vapor with the surface. Release or gain of energy by the condensing or evaporating vapor is important only if the amount of energy released or gained is large enough to significantly alter surface or bulk gas surface temperatures.

During severe reactor accidents, water, and core and structural materials will often be present as vapors. Because water has a high vapor pressure, the masses of steam present in reactor and containment compartments will frequently be large. Thus, when water condenses or evaporates, the amounts of heat released or absorbed will usually be large enough to significantly affect surface and bulk gas temperatures. Therefore, release or gain of heat during the condensation and evaporation of steam should be modeled in the MELCOR code system. Steam condensation onto and evaporation from structures will be modeled in the thermal hydraulic portions of the MELCOR code system. Steam condensation onto and evaporation from aerosols is discussed below in Section 5.2.

Most vapors that contain core or structural materials will have low vapor pressures at reactor accident temperatures. Therefore, vapors formed from core or structural materials will rarely be present during severe reactor accidents in quantities large enough to release significant amounts of heat upon condensation or evaporation (CsOH and CsI may be exceptions at upper plenum temperatures). This suggests that MELCOR need not model heat release or gain during the condensation or evaporation of trace vapors (core or structural material vapors).

Given that the release or gain of heat upon change of phase by trace vapors can be neglected, the rate of mass transfer of a trace vapor from one phase to another (gas phase to surface state or the converse) may be modeled as the product of the mass transfer rate constant and the mass of material available for transfer. Thus,

$$\frac{dm_{k,g}}{dt} = - k_{c,k} \frac{A}{V} (m_{k,g} - m_{k,sat}^{Ts}) \qquad (5.16)$$

where $k_{c,k}$ = the mass transfer coefficient (deposition velocity) for trace vapor k (m/s)

A = the area of the deposition surface (m^2)

V = the volume of the compartment gas space (m^3)

$m_{k,g}$ = the mass of trace vapor k in the compartment gas space (kg)

$m_{k,sat}^{Ts}$ = the mass of trace vapor k that would saturate that gas space at the temperature of the condensing surface, Ts (kg)

Ts = the temperature of the condensing surface (K)

As it should, Eq. 5.16 predicts that supersaturation, $m_{k,g} > m_{k,sat}^{Ts}$ will cause vapor k to condense onto surfaces, and subsaturation, $m_{k,g} < m_{k,sat}^{Ts}$, will cause vapor k to evaporate from surfaces. Equation 5.16 may be expanded to include both structural and aerosol surfaces as follows:

$$\frac{m_{k,g}}{dt} = -\left[m_{k,g} - m_{k,sat}^{Tg}\right] k_{c,k,a} \frac{A_a}{V} \qquad (5.17)$$

$$+ \sum_s \left[m_{k,g} - m_{k,sat}^{Ts}\right] k_{c,k,s} \frac{A_s}{V}$$

where $m_{k,sat}^{Ts}$ = the saturation mass of trace vapor k at the temperature of the structural surfaces (kg)

$m_{k,sat}^{Tg}$ = the saturation mass (kg) of trace vapor k at the temperature (Tg) of the bulk gases (since gas borne aerosols are assumed to be in thermal equilibrium with bulk gases)

Tg = the temperature (K) of the bulk gases

Ts = the temperature (K) of structural surface, s

A_a = the surface area of the gas borne aerosol mass mass in the compartment (m^2)

A_s = the area (m^2) of the structural surface, s

$k_{c,k,a}$ = the gas phase mass transfer coefficient to the aerosol surfaces for trace vapor k (m/s)

$k_{c,k,s}$ = the gas phase mass transfer coefficient to structural surface, s for trace vapor k (m/s)

Vapor Pressure. In Equations 5.16 and 5.17, the mass of trace vapor k, $m_{k,sat}^{Ts}$, that would saturate the compartment bulk gas space at the temperature of the condensation/evaporation surface, Ts, can be related to the vapor pressure of trace vapor k at that temperature, $P_{k,sat}^{Ts}$, by an equation of state such as the ideal gas equation.

$$P_{k,sat}^{Ts} V = \frac{m_{k,sat}^{Ts}}{MW_k} R\ Ts \qquad (5.18)$$

where V = the volume of the compartment gas space (m^3)

R = the universal gas constant (J/mol K)

MW_k = the molecular weight of trace vapor k (kg/kgmole)

Thus, $m_{k,sat}^{Ts}$ can be calculated if $P_{k,sat}^{Ts}$ can be calculated.

For single component systems, the dependence of P_{sat} on the temperature of the condensed phase is usually expressed using some integral form of the Clausius-Clapeyron equation [9-11] with parameter values derived from experimental data or thermodynamic calculations. For narrow temperature ranges over which the latent heat of vaporization may be taken as a constant, the following expression is adequate:

$$\text{Log } (P_{sat}) = - a/T + b \qquad (5.19)$$

For broader temperature ranges, over which the latent heat of vaporization may not be taken as a constant, data is frequently correlated using the following equation [11].

$$\text{Log } (P_{sat}) = - a/T + b + c \text{ Log } T \qquad (5.20)$$

Values for the parameters a, b, and c in Eqs. 5.19 and 5.20 are available from standard reference documents and literature reviews [9, 10]. Parameter values for Eq. 5.20 for a number of vapor species that are expected to be formed during severe reactor accident sequences are presented in Table 5.1.

TABLE 5.1

Coefficients for Equation 5.20 [12]

$$\text{Log } P \text{ (mm Hg)} = - a/T + b + c \text{ Log } T(K)$$

Compound	A	B	C	Temperature Range, K
I_2	3578	17.72	-2.51	298-387
	3205	23.65	-5.18	387-457
CsI	10420	19.70	-3.02	600-894
	9678	20.35	-3.52	894-1553
RbI	8979	8.07	--	1348-1598
HI	Critical temperature = 424 K (always gaseous)			
Br_2	2048	8.65	0.958	266-331
CsBr	10950	20.02	-3.02	700-909
	10080	20.56	-3.52	909-1573
HBr	Critical temperature = 363 K (always gaseous)			
Cs	4075	11.38	-1.45	280-1000
CsOH[(a)]	--	--	--	--
Cs_2O	33880	11.62	--	298-1800
Rb	4560	12.00	-1.45	312-952
RbOH[(a)]	--	--	--	--
Rb_2O	26011	11.62	--	298-2000
Te_2	9320	19.85	-2.71	298-723
TeO_2	13940	23.51	-3.52	298-mpt
Se_2	4990	8.09	--	493-958
SeO_2	6170	21.40	-3.02	298-588
Sb_4	11560	22.40	-3.52	298-903
Sb_4O_6	9625	11.31	--	742-914
	3900	5.14	--	929-1073

(a) No data located. Vapor pressure can be estimated by assuming the hydroxide vapor pressure equals the iodide vapor pressure.

vapor species that are expected to be formed during severe reactor accident sequences are presented in Table 5.1.

In a system where a vapor is in equilibrium with its condensed (liquid or solid) phase, the equilibrium pressure of the vapor is its saturation pressure at the system temperature. Thus, equilibrium vapor pressures can be estimated by performing equilibrium thermodynamic calculations on systems that contain both the vapor and one of its condensed phases.

Equilibrium thermodynamic calculations are performed by minimizing the Gibbs free energy of the system of equilibrium thermodynamic equations that describes the chemical reactions and changes of phase that the species that comprise the system can undergo at the system temperature. Equilibrium thermodynamic calculations may be expected to yield reasonably accurate equilibrium concentrations for dilute gaseous systems (no condensed phases) that behave ideally (fugasities = 1.0), provided that the following conditions are met:

(1) accurate values for important input parameters are available,

(2) the set of chemical reactions used is complete (omits no reaction that contributes significantly to the interconversion of two species), and

(3) the calculation is performed for a system temperature sufficiently high to cause equilibrium conditions to be rapidly established.

For heterogeneous systems less accurate results are expected since condensed phases (liquids and solids) rarely behave ideally and activities (correction factors for non-ideal behavior) for all the important condensed phase species are rarely available.

Equilibrium thermodynamic calculations for a number of heterogeneous chemical systems expected to exist during severe reactor accidents have been performed over the temperature range 600 to 3000 K by Cubicciotti and Sehgal [13,14]. From the equilibrium results, vapor pressure expressions were developed for five elements (Cs, I, Te, Ru, and Sr) at two system pressures (3 and 170 atm) and three hydrogen/steam pressure ratios (0.01, 1.0, and 9). Specifically, the logarithm of the equilibrium vapor pressure of the element (sum of the equilibrium vapor pressures of all gaseous forms of the element) divided by the sum of the pressures of steam and hydrogen (the system pressure) was found to be linearly dependent on the reciprocal of the system temperature, as would be expected if the equilibrium pressures of the gaseous species of the element were principally controlled by vapor phase/condensed phase equilibria. Thus,

where a and b are constants that vary with temperature, total system pressure, and hydrogen/steam pressure ratio. Table 5.2 presents values for the constants a and b and indicates the system conditions where they apply.

Although availability of parameter values may automatically select among Eqs. 5.19, 5.20, and 5.21, any selection should reflect the following facts: (1) Eq. 5.19 will be inaccurate if applied to a broad temperature range; (2) Eqs. 5.19 and 5.20 apply to one component systems (vapor in equlibrium with its condensed phase); and (3) Eq. 5.21 may be significantly in error due to the assumption of unit activities for condensed phase species. Selection among Eqs. 5.19, 5.20, and 5.21 can be avoided by implementing the following equation in MELCOR,

$$\text{Log } P_{sat} = - a/T + b + c \text{ Log } T + d \text{ Log } (P_{H_2} + P_{H_2O}) \qquad (5.22)$$

since this equation reduces to Eq. 5.19 when c = d = 0, to Eq. 5.20 when d = 0, and to Eq. 5.21 when c = 0 and d = 1.

C. Surface Chemistry.

Fission product vapors can bind to structural and aerosol surfaces by adsorption, chemisorption, or chemical reaction. If the vapor has already been removed from the gas phase by condensation, these processes serve only to enhance its retention on the surface. However, if the vapor is non-condensible or if it is condensible but below its saturation pressure, these processes permit vapor removal in the absence of condensation.

The significance of fission product binding to surfaces depends first on whether the binding occurs to an aerosol or a structural surface and second on whether the binding is irreversible. Irreversible binding of a vapor to a structural (i.e. stationary) surface terminates transport and thus precludes release to the biosphere should the containment fail. Reversible binding to a structural surface interrupts transport, which will delay release to the biosphere, when binding is not reversed until after the containment fails. In addition, when binding is only slowly reversed, the release characteristics of the bound material will be changed from those of a puff to those of a plume.

Since flows of bulk fluids transport vapors and aerosols at nearly identical rates (drag forces alter only slightly the rates of transport of fluid borne aerosols compared to those of fluid borne vapors), the irreversible binding of a vapor to a gas borne aerosol will not appreciably change its bulk transport

TABLE 5.2

Constants for Equation 5.21 [14]

Element	Constants		Systems Conditions	
	a	b	Temp. (K)	P_{H_2}/P_{H_2O} Ratios
Total Pressure = 170 atm				
Ruthenium	-34885	6.98	1500 - 3000	9, 1.0,
Tellurium	-15790	8.37	600 - 1100	9, 1.0,
Iodine	-8770	2.98	700 - 1300	9, 1.0, 0.01
Cesium	-5400	2.05	700 - 1200	9, 1.0, 0.01
Strontium	-18520	3.52	600 - 2000	9, 1.0,
Total Pressure = 3 atm				
Ruthenium	-33330	7.66	1500 - 3000	9, 1.0,
Tellurium	-12195	6.10	600 - 1200	9, 1.0,
Iodine	-8570	4.71	600 - 1000	9, 1.0, 0.01,
Cesium	-4515	2.53	600 - 1000	9, 1.0, 0.01,
Strontium	-18405	2.02	600 - 2000	9, 1.0,

characteristics. However, its deposition and resuspension characteristics will be changed from those of a vapor to those of an aerosol. Thus, irreversible binding to a gas borne aerosol can prevent release of a vapor, if the aerosol deposits prior to containment failure and does not resuspend. Reversible binding to an aerosol also changes vapor deposition characteristics, since while bound to the aerosol the deposition will occur by aerosol rather than vapor processes.

When binding energies are small, as is usually the case when binding takes place by adsorption or chemisorption, binding will be easily reversed by small increases in the temperature of the binding surface. Conversely, when binding energies are large, as is usually the case when a vapor reacts chemically with a surface (large exothermicity or large activation energy), binding will be reversible only by large increases in the temperature of the binding surface. Therefore, chemical reactions of a vapor with a surface will usually substantially alter its transport and/or deposition characteristics, while adsorption and chemisorption are unlikely to appreciably affect either transport or deposition. Accordingly, since treatment of a reversible surface state will add an equation to MELCOR's set of fission product behavior equations, unless experimental results indicate atypically large binding energies, MELCOR should probably neglect vapor adsorption and chemisorption in routine calculations. In addition, in order to minimize growth of MELCOR's fission product equation set, surface chemistry should be addressed only for species that are significantly radiotoxic, that is species that contain significant quantities of Cs, I, or Te.

The surface chemistry of Cs, I, and Te has been reviewed by Taig et al. [15]. Experimental results indicate that CsI reacts with boric acids (which can be formed by oxidation of boron carbide, a constituent of BWR control rods) to form a borate and liberate an iodine containing compound, possibly HI. The available data suggests that this is a surface reaction. No significant reactions of CsI with stainless steel or Inconel surfaces have been identified. CsI does react very slowly with unoxidized Inconel surfaces to bind Cs and release I. However, the reaction is too slow to significantly affect the behavior of CsI during severe reactor accidents. Accordingly, the deposition of CsI onto structural and aerosol surfaces may be adequately described by condensation and evaporation alone.

Like CsI, CsOH can condense onto and evaporate from surfaces. However, CsOH also binds chemically to unoxidized steel surfaces, forming silicates and other products. This reaction appears to be relatively slow and slowly reversible. Because it is slow and reversible, it may not have a significant effect upon the behavior of CsOH during severe reactor accidents.

Te reacts rapidly with unoxidized, moderately reactive metals, such as Zr, Ni, Ag, and Sn, to form tellurides. Scavenging of Te by cladding was discussed in Chapter 3, where a correction term for reaction with unoxidized or partially oxidized clad was added to the release equation recommended for Te. Te also reacts with unoxidized Ni atoms at surface sites in stainless steels to form tellurides. Since Te also forms tellurides with Sn and Ag, it is expected that Te will react with the large amounts of Sn and Ag expected to be present in the aerosols formed during severe reactor accidents. Although telluride formation is not irreversible, reversal seems to require a substantial rise in temperature. Thus, it may be reasonable to assume that any Te that escapes reaction with clad will bind irreversibly either to structural or aerosol surfaces in proportion to their surface areas.

Removal Rates. A non-condensible vapor or a condensible vapor that is subsaturated can be removed from the gas phase by diffusion to a surface followed by reaction with the surface. If the surface reaction is reversible and the vapor concentration at the surface is assumed to attain a steady state, the following rate expression can be derived,

$$\frac{dM_{k,g}}{dt} = - \frac{k_{c,k}}{k_{c,k} + k_{f,k}} \frac{A}{V} \left[k_{f,k} M_{k,g} - k_{b,k} M_{k,s} \right] \qquad (5.23)$$

where A = the area of the deposition surface

V = the compartment volume

$M_{k,g}$ = the gas borne mass of vapor k in the volume V

$M_{k,s}$ = the mass of vapor k bound by reaction to the deposition surface

$k_{c,k}$ = the mass transfer rate constant for vapor k in the bulk gases (see Sect. 5.1 above)

$k_{f,k}(A/V)$ = the forward rate constant for reaction of vapor k with the surface

$k_{b,k}(A/V)$ = the backward rate constant for reaction of vapor k with the surface

As defined here, $k_{c,k}$, $k_{f,k}$, and $k_{b,k}$ all have the dimensions of a velocity (L/t). Thus, $k_{f,k}$ is a deposition velocity and in effect $k_{b,k}$ is a resuspension velocity.

As it should, for an irreversible reaction [$k_{b,k} = 0$], Eq. 5.23 reduces to

$$\frac{dM_{k,g}}{dt} = - k_{c,k} \frac{A}{V} M_{k,g} \qquad (5.24)$$

when deposition is mass transfer rate limited [$k_{f,k} >> k_{c,k}$], and to

$$\frac{dM_{k,g}}{dt} = - k_{f,k} \frac{A}{V} M_{k,g} \qquad (5.25)$$

when deposition is reaction rate limited [$k_{c,k} >> k_{f,k}$].

Equation 5.23 is strictly valid only when the rate of the surface reaction is either much faster or much slower than the mass transfer rate. However, even when these two rates are comparable, Eq 5.23 should still provide a reasonable estimate of vapor removal rates.

If vapor deposition occurs not by transient adsorption but by condensation, then the rate of the surface reaction will be much increased because the surface concentration of the condensed vapor will be much greater than that of the transiently adsorbed vapor. Thus, when surface reaction is preceded by condensation, the overall removal rate of the vapor from the gas phase is likely to be mass transfer rate limited, and Eq. 5.16 should be used (see vapor condensation above),

$$\frac{dM_{k,g}}{dt} = - k_{c,k} \frac{A}{V} \left[M_{k,g} - M_{k,sat}^{Ts} \right] \qquad (5.16)$$

The mass of vapor k that can react with a surface is limited by the availability of reactive sites on or near the surface. If reactive sites account for a fraction F_{rx} of the total (microscopic) surface area A_m and diffusion into the surface does not occur, then the maximum vapor mass that can be bound to the reaction surface may be estimated as follows:

$$M_{max} = \frac{4\ MW\ F_{rx}}{N_o \pi\ \sigma^2} \frac{A_m}{A_g} A_g \qquad (5.26)$$

where MW is the molecular weight and σ the collision diameter of vapor k, N_o is Avogadro's number, A_g is the geometric area of the reaction surface, which may be signficantly smaller than the microscopic area of that surface A_m, and F_{rx} and A_m/A_g may be poorly known. Even if the entire surface is reactive, F_{rx} will still be less than one, because $4A_m/\pi\sigma^2$ is an overestimate of the number of molecules in a monolayer. Conversely, if diffusion of vapor k into the surface increases the number of available reactive sites, then F_{rx} can be greater than one.

Although Eq. 5.23 provides a way to model simple reaction schemes in MELCOR, such as irreversible

A(g) ----> B(s)

or reversible

A(g) <===> B(s)

reaction with a surface, more complicated schemes may need to be addressed. For example, the reaction of CsI with steel surfaces to form CsOH which upon rise in surface temperature can desorb,

CsI(g) ----> CsOH(c) + HI(g) and CsOH(c) <====> CsOH(g)

or the following general reaction scheme,

$$A(g) \overset{k_c}{\Longleftrightarrow} A(c) \underset{k_b}{\overset{k_f}{\Longleftrightarrow}} B(c) \overset{k_c}{\Longleftrightarrow} B(g)$$

In principle, complicated reaction mechanisms could be examined in MELCOR by adding an ODE for each rate process in the reaction mechanism to MELCOR's set of fission product behavior ODEs. For the general reaction scheme just presented this would entail adding the following set of ODEs:

$$d/dt[A(g)] = - k_c [A(g) - A(c)]$$

$$d/dt[A(c)] = - k_c [A(c) + A(g)] - k_f[A(c)] + k_b[B(c)]$$

$$d/dt[B(c)] = - k_c [B(c) + B(g)] - k_b[B(c)] + k_f[A(c)]$$

$$d/dt[B(g)] = - k_c [B(g) - B(c)]$$

In practice, this would increase computational times unacceptably. So an alternative approach is needed that allows chemical transformations and their timing to be qualitatively captured.

Any specie individually tracked in MELCOR (e.g., CsI, CsOH, HI) must have its mass assigned to a unique chemical class. Therefore, the effect of a chemical reaction can be captured by transferring mass from the class of the reactant to the class of the product, and the timing of the transfer can be captured by making the transfer occur instantly or at a specified rate, once some specified condition has been met. For example, the reaction of CsI(g) with a steel surface releasing HI(g) and forming CsOH(c) which desorbs when surface temperatures exceed some specified temperature, can be treated by transferring mass (corrected for stoichiometry) from the CsI class to the CsOH and HI classes instantly upon deposition of CsI, and applying a temperature constraint to the vapor pressure limited desorption of CsOH.

Deposition Velocities. In Eq. 5.23, values for $k_{f,k}$ and $k_{b,k}$ must either be supplied as input or calculated using the Arrhenius equation:

$$k = A \exp(-E/RT) \qquad (5.27)$$

where A and E, the preexponential factor and activation energy for the surface reaction, are Arrhenius constants supplied as input, R is the universal gas constant, and T is the temperature of the surface. Deposition velocities for some surface reactions of interest have been measured [16-18]. Their values are presented in Table 5.3.

D. Condensation and Evaporation of Steam.

When a condensible vapor represents a significant fraction of the mass of the bulk gases in a control volume, the temperature of the bulk gases will be significantly affected by the heat released by condensation of that vapor onto, or absorbed by evaporation of that vapor from gas borne aerosols. Therefore, because steam will frequently be a major component of primary system or containment bulk gases during a severe reactor accident, steam condensation and evaporation can not be adequately modeled using a representation such as Eq. 5.16 that neglects the impact of the heat of vaporization on bulk gas temperatures.

Wagner [19] has developed a first order treatment of droplet growth that quantitatively accounts for heat and mass transport at the droplet surface, and for the effect of droplet size on these two fluxes (transition regime correction factors). Wagner derives expressions for the heat and mass fluxes at the surface of a single droplet, and for the temperature of the droplet

Table 5.3
Deposition Velocities for Some Surface Reactions

Vapor	Surface	Temperature (K)	Bulk Gases	Deposition Velocity (m/s)	Arrhenius Constants A (m/s)	E (cal/mole-deg)	Ref.
CsOH	304 SS	973	H_2,H_2O	1.3×10^{-5}			16
	304 SS	1123	H_2,H_2O	2.6×10^{-6}			16
	304 SS	1273	H_2,H_2O	3.5×10^{-6}			16
	Inconel 600	1273	H_2,H_2O	9.8×10^{-6}			16
CsI	304 SS	1273	H_2,H_2O	$\leq 5\times10^{-5}$			16
	304 SS	823-1313	H_2O		1.65×10^{-9}	-21600	18
	Inconel 600	1273	H_2,H_2O	1.2×10^{-5}			16
	Inconel 600	1088-1313	H_2O		6.36×10^{-8}	-13670	18
I_2	304 SS	388-823	air,H_2O		9.08×10^{-8}	-8100	17
	304 SS	673-1403	H_2O		7.42×10^{-3}	8500	18
	304 SS	673-1403	air,H_2O		2.53×10^{-3}	6670	18
	Inconel 600	673-1173	H_2O		3.49×10^{-6}	-3940	18
HI	304 SS	423-823	air,H_2O		5.5×10^{-5}	-5950	17
Te	Ag	773	Ar	$\geq 10^{-1}$			16
	Sn	900-1170	Ar,H_2	$\geq 10^{-3}$			16
	Zircaloy	773	Ar	$< 10^{-6}$			16
	Zircaloy	1060	Ar	2×10^{-5}			16
	304 SS	773-1073	Ar	10^{-2} to 10^{-3}			16

surface. Because these expressions can only be solved numerically by computational methods that are quite lengthy, Wagner also presents an analytical solution for these expressions that is based on an approximate expression (derived by integrating the Clausius-Clapeyron equation) for the saturation pressure of the vapor (in this case, steam).

The following equations present the analytical solution derived by Wagner:

$$\frac{dm}{dt} = 4\pi r \frac{S-S_r}{A+B} \tag{5.28}$$

$$A = \frac{1}{\beta_t F_t} \frac{L}{KT} \left[\frac{LM}{RT} - 1\right] \tag{5.29}$$

$$B = \frac{1}{\beta_m F_m} \frac{RT}{DMP_s} \tag{5.30}$$

$$\beta_t = \left\{1 + \left[\Lambda_t - \frac{4}{3} + \frac{4}{3\alpha_t}\right] Kn_t\right\}^{-1} \tag{5.31}$$

$$\beta_m = \left\{1 + \left[\Lambda_m - \frac{4}{3} - \frac{4}{3\alpha_m}\right] Kn_m\right\}^{-1} \tag{5.32}$$

$$F_t = 1 - \left[\frac{1}{L} - (1 + \alpha) \frac{D\rho}{KT}\right] \left[h + \alpha \frac{RT}{M}\right] \tag{5.33}$$

$$F_m = \left[1 - (1 + \alpha) \frac{\rho LD}{KT}\right] \left[\frac{P_o}{P_o - P}\right] \tag{5.34}$$

where m = mass of water that condenses onto or evaporates from the droplet
r = the droplet radius
S = P/P_S = the saturation ratio of steam [$H_2O(g)$] in the bulk gases
S_r = the saturation ratio of steam at the droplet surface
P = the partial pressure of the steam in the bulk gases
P_S = the saturation pressure of steam at the bulk gas temperature T
R = the Gas Constant
K = the thermal conductivity of the bulk gases
L = the specific heat of vaporization of water
M = molecular weight of water
D = the diffusivity of steam in the bulk gases
α_m = mass accommodation coefficient
α_t = thermal accommodation coefficient
Kn_m = Knudsen number for steam, the bulk gas component that transports mass to the droplet surface
Kn_t = Knudsen number for the bulk gas components that transport heat to the droplet surface
ρ = density of steam, the condensible vapor
h = specific enthalpy of steam, the condensible vapor
α = thermal diffusion factor
P_o = total pressure

In Eqs. 5.29 through 5.34, β_t and β_m are correction factors that convert continuum regime fluxes of heat and mass to transition regime fluxes, and F_t and F_m are first order corrections to the zeroth order expressions for the dependence of the heat flux on the temperature gradient at the droplet surface, and for the dependence of the mass flux on the density gradient at the droplet surface.

Wagner compared the droplet growth curves predicted by Eqs. 5.28 through 5.34 to experimental data and found that the predicted growth curves agreed well with the experimental data (the predicted growth curves exceeded the experimental data points by about 10 percent). Based on these comparisons and on a review of previous experimental and theoretical studies, Wagner concluded that for water the thermal diffusion factor (α) and the thermal and mass accommodation coefficients (α_t and α_m) have the following values:

$$\alpha < 0.01, \text{ and } \alpha_t = \alpha_m = 1$$

Accordingly, Eqs. 5.31 through 5.34 reduce to:

$$\beta_t = 1 + \Lambda_t Kn_t \tag{5.35}$$

$$\beta_m = 1 + \Lambda_m Kn_m \tag{5.36}$$

$$F_t = 1 - h\left\{\frac{1}{L} - \frac{D\rho}{KT}\right\} \tag{5.37}$$

$$F_m = 1 - \frac{\rho LD}{KT}\left\{\frac{P_o}{P_o - P}\right\} \tag{5.38}$$

In Eqs. 5.31, 5.32, 5.35, and 5.36, values for Λ_t and Λ_m can be determined using the following equation, which is an interpolation formula developed by Fuch's [20] for data derived by Sahni [21]:

$$Z_i = (\tfrac{4}{3} Kn_i + 0.710)/(Kn_i + 1) \tag{5.39}$$

and Kn_t and Kn_m can be calculated using the following expressions:

$$Kn_i = 2_i/r \tag{5.40}$$

$$2_i = 3D_i/\bar{c}_i \tag{5.41}$$

or

$$2_i = 3K_i/\rho_i c_{v_i} \bar{c}_i \tag{5.42}$$

and

$$\bar{c}_i = (8kT/\pi_i m_i)^{1/2} \tag{5.43}$$

where r is the drop radius, D_i is the diffusion coefficient, K_i the thermal conductivity, P_i the mass density, and c_{v_i} the specific heat capacity at constant volume of gas i; λ_i is the mean

free path and $\bar{c}_i$ is the average absolute velocity and m_i is the molecular mass of gas i molecules; k is Boltzmann's constant, and i distinguishes between the gas molecules that carry mass and those that carry heat to the drop surface.

For bulk gas atmospheres in which the condensible vapor is a minor component, Kn_t and Kn_m will not be identical, because mass will be transported to the droplet surface by molecules of the condensible vapor, while heat will be transported to the droplet surface principally by molecules of the non-condensible components of the bulk gases. However, when the condensible vapor is the major component of the bulk gases, as it frequently will be during a severe reactor accident, Kn_t and Kn_m will be approximately equal, and thus $\beta_t = \beta_m$.

For atmospheric conditions (e.g., T = 20°C, P = 15 torr, P_o = 760 torr) Wagner calculates values for F_t and F_m that are somewhat smaller than one. However, for severe accident conditions (substantial steam partial pressures, e.g., 5 to 10 atm.), F_t and F_m can differ substantially from one.

For large droplets (continuum regime where $Kn_t = Kn_m = 0$) suspended in a well-mixed control volume characterized by small steam supersaturations (small values of S), S_r, β_t, and β_m will all have values of unity. If F_t and F_m are also set equal to unity, then Wagner's analytical solution (Eqs. 5.28 through 5.34) reduces to the Mason equation [22]. Moreover, because for water L is large and thus at moderate temperatures LM/RT >> 1, if β_t, β_m, F_t, F_m, and S_r are all set equal to unity, then Wagner's analytical solution is also identical to the solution derived by Byers [23].

The special case of condensation of steam onto a gas borne aerosol suspended in the atmosphere of a well mixed compartment, due to cooling of that atmosphere by heat transfer to the compartment walls, has been examined by Clements [24]. When suspended aerosol concentrations are everywhere large enough to keep steam supersaturations small throughout the compartment, the following equations provide good estimates of the rate of steam condensation onto the suspended aerosol (I_c), the rate of steam condensation onto the compartment walls (I_p), and the ratio of I_c to I_p:

$$I_c = \frac{Q_c}{L(T_w)Cn(T_w)}\left[\frac{Cn(T_w) - \Delta - \delta}{1 + \Delta}\right] \qquad (5.44)$$

$$I_p = \frac{Q_c}{[L(T_w)Cn(T_w)]} \tag{5.45}$$

$$\frac{I_c}{I_p} = \frac{Cn(T_w) - \Delta - \delta}{1 + \Delta} \tag{5.46}$$

$$\Delta = Cn(T_b)/Le(T_b) \tag{5.47}$$

$$\delta = c_{pv}(T_b)[T_b - T_w]/L(T_b) \tag{5.48}$$

$$Le(T) = \frac{k(T)}{[D(T)c_p(T)\rho(T)]} \tag{5.49}$$

$$Cn(T) = \frac{k(T)}{L(T)D(T)\frac{d}{dt}[\rho_{ve}(T)]} \tag{5.50}$$

$$\frac{d}{dt}[\rho_{ve}(T)] = \frac{\rho_{ve}(T)}{T}\left[\frac{M_v L(T)}{RT} - 1\right] \tag{5.51}$$

$$c_p(T)\rho(T) = c_{pg}(T)\rho_g(T) + c_{pv}(T)\rho_v(T) + c_{pa}(T)\rho_a(T) \tag{5.52}$$

where Cn is the condensation number, Le is the Lewis number, T_b and T_w are the temperatures of the compartment bulk gases and walls, Q_c is the rate of transfer of sensible heat from the compartment bulk gases to the compartment walls, M_v and L(T) are the molecular weight and the latent heat of vaporization of water, k(T) is the thermal conductivity of the mixture of noncondensible gases and steam, D(T) is the diffusivity of that mixture, ρ_{ve} is the equilibrium density of steam, R is the gas constant, and c_p, ρ, c_{pg}, ρ_g, c_{pv}, ρ_v, c_{pa}, and ρ_a are the specific heat (c_p) and density (ρ) of the mixture, the non-condensible gases (g), steam (v), and aerosol (a), respectively.

A Mason equation that does not contain the term $(S-S_r)$ may be developed from Eq. 5.44 by noting that

$$I_c = \frac{dM_a}{dt} \tag{5.53}$$

$$M_a/V = \int \frac{4}{3} \pi \rho_\ell r^3 n(r) dr \tag{5.54}$$

and thus $$\frac{I_c}{V} = \frac{d}{dt} \left[\int \frac{4}{3} \pi \rho_\ell r^3 \{n(r)dr\} \right] \tag{5.55}$$

where V is the volume of the compartment, M_a is the aerosol mass in that volume, ρ_ℓ is the density of water, r is the radius of an aerosol particle, and n(r)dr is the number of aerosol particles per unit volume having radii between r and r + dr.

Since the rate of increase of total aerosol mass due to steam condensation may be approximated as the product of the rate of increase of the mass of aerosol particles of a given size times the number of particles of that size integrated over all sizes, when differentiating Eq. 5.55 with respect to time, {n(r)dr} should be treated as time independent. Therefore

$$\frac{I_c}{V} = \int \frac{4}{3} \pi \rho_\ell \{n(r)dr\} \frac{dr^3}{dt} = \int 4\pi \rho_\ell \left[r \frac{dr}{dt} \right] r \{n(r)dr\} \tag{5.56}$$

But substitution of Eq. 5.28 into

$$\frac{dm}{dt} = 4\pi \rho_\ell r \left[r \frac{dr}{dt} \right] \tag{5.57}$$

yields

$$r \frac{dr}{dt} = \frac{S - S_r}{\rho_\ell (A+B)} \tag{5.58}$$

which shows that $r \frac{dr}{dt}$ has no dependence on r. Therefore, Eq. 5.56 can be rewritten as follows:

$$\frac{I_c}{V} = 4\pi \rho_\ell \left[r \frac{dr}{dt} \right] \int r n(r) dr \tag{5.59}$$

Finally, combination of this equation with Eq. 5.57 yields

$$\frac{dm}{dt} = I_c \frac{r}{\int rn(r)dr} \tag{5.60}$$

from which I_c may be eliminated using Eq. 5.44, thereby obtaining

$$\frac{dm}{dt} = \frac{r}{\int rn(r)dr} \frac{Q_c}{L(T_w)Cn(T_w)} \frac{Cn(T_w) - \Delta - \delta}{1 + \Delta} \tag{5.61}$$

which does not depend on supersaturation ratios (S or S_r).

In Eq. 5.61 the integral may be evaluated using either mean properties of the aerosol distribution or by division of that distribution into sections. Evaluation using mean properties is accomplished by noting that $N_{av}r_{av} = rn(r)dr$, where N_{av} is the mean aerosol number density and r_{av} is the mean radius of the aerosol particle distribution. Alternatively, when using a sectional aerosol code, if an expression for n(r)dr is available for each aerosol section (e.g., $N_{av_i} r_{av_i}$ where i is the aerosol size section), then the integral can be reformulated and evaluated as a sum of integrals, one integral for each aerosol size section.

The MELCOR code system will determine the mass of water, that condenses onto or evaporates from aerosols, from thermodynamic calculations implemented in MELCOR's thermal-hydraulic modules. Thus, the fission product behavior modules of the MELCOR code system need to use a Mason equation (Eq. 5.28 or Eq. 5.61) only to determine the fraction, F_i, of the condensed or evaporated water mass that should be added to or removed from aerosol section i, where

$$F_i = \frac{\left(\frac{dm}{dt}\right)_i}{\sum_i \left(\frac{dm}{dt}\right)_i} \tag{5.62}$$

Since in this ratio all dependencies on bulk gas properties will cancel, F_i will depend only on aerosol properties [Kn_i if Eq. 5.28 is used; $r_i n(r_i)dr_i$ if Eq. 5.61 is used].

5.3 Aerosol Processes

After formation by heterogeneous nucleation of supersaturated vapors (gas-to-particle conversion) or mechanical aerosolization, aerosol particles increase in size by agglomeration and are depleted by the operation of natural deposition processes or Engineered Safety Features (ESFs). In this section aerosol agglomeration and deposition mechanisms expected to be significant during severe reactor accidents are discussed. Removal of aerosols by ESFs is discussed in the next chapter.

Aerosol agglomeration and deposition are rate processes, which are modeled by selecting an expression for the process rate coefficient. Selection of rate coefficient expressions is complicated by the fact that aerosol rate coefficients have functional forms that vary with particle size. The functional form of aerosol rate coefficients varies with particle size because for large particles rate coefficients are derived assuming that the surrounding bulk gases can be treated as a continuum, while for very small particles coefficients are derived assuming that gas molecule trajectories (and therefore collisions between gas molecules and very small particles) are not perturbed by the presence of those particles.

A. Knudsen Number Regimes [25a]

The Knudsen number (Kn_i) is a dimensionless parameter that equals the ratio of the mean free path of the bulk gas molecules (λ) to the radius of the aerosol particle (r_i)

$$Kn_i = \frac{\lambda}{r_i} = 2\,\frac{\lambda}{d_i} \tag{5.63}$$

$$\lambda = \frac{1}{2\,\pi n \sigma^2} \tag{5.64}$$

where d_i is the particle diameter, and n and σ are the number density and collision diameter of the bulk gas molecules. Since $P = nkT$, where k is Boltzman's constant, and P and T are the bulk gas pressure and temperature

$$Kn_i = \frac{2\ kT}{\pi P \sigma^2 d_i} \tag{5.65}$$

Bulk gas molecules appear to be a continuum to particles with very small Knudsen numbers (Kn_i --> 0, continuum regime). Gas molecule trajectories are not significantly perturbed by particles having very large Knudsen numbers (Kn_i --> infinity, free-molecule regime). Between these two extremes neither approximation is valid. When $0.1 < Kn_i < 0.25$ (slip-flow regime), rate coefficients may be derived using continuum analysis with a slip-flow boundary condition [25b]. For the Knudsen number range $0.25 < Kn_i < 10$ (transition regime), suitable expressions for rate coefficients are often lacking.

An estimate of the range of Knudsen numbers that might occur during severe reactor accidents can be obtained by substituting bounding parameter values into Eq. 5.63. Representative values of T and P for several PWR severe accident sequences are presented in Table 5.4. Hydrogen, oxygen, nitrogen, and water molecules have collision diameters of 2.8, 3.4, 3.7 and 2.6 Å, respectively [7b]. Since agglomeration of small particles is rapid, and large particles are rapidly deposited by sedimentation, the diameters of gas borne particles will fall within the range, $0.1\ \mu m < d_i < 100\ \mu m$.

Kn_i values will be large when sequence conditions simultaneously produce high temperatures, moderate pressures, and small particles in bulk gases that have small diameters. Examination of Table 5.4 suggests that such conditions will occur in the upper plenum soon after core melting begins during a large break accident such as the ABHL sequence. Assuming T = 2400 K, $P = 1.72 \times 10^5$ Pa, bulk gases composed principally of hydrogen (d = 2.8 Å), and small particles ($d_i = 0.1\ \mu m$) gives $Kn_i = 10.3$.

Kn_i values will be small when sequence conditions simultaneously yield moderate temperatures, elevated pressures, and large particles in bulk gases that have large diameters. Such conditions are likely to be encountered in containment late in the accident after substantial agglomeration of particles has occured. Assuming T = 350 K, $P = 6.89 \times 10^5$ Pa, bulk gases composed principally of air (d = 3.6 Å), and large particles ($d_i = 100\ \mu m$) gives $Kn_i = 2.85 \times 10^{-4}$.

Because Knudsen numbers as small as 0.0003 and as large as 10 may occur during at least some severe reactor accidents, whenever available, models of aerosol rate coefficient should be implemented in MELCOR that are appropriate for the continuum, slip-flow, and transition Knudsen number regimes. Models appropriate for the free-molecule regime appear to be needed only when Brownian diffusion causes agglomeration or deposition of very small particles ($d_i \leq 0.1\ \mu m$).

B. Aerosol Deposition

Aerosol deposition is caused by particle transport to surfaces. Since severe accidents normally do not involve

Table 5.4

Bulk Gas Pressures and Temperatures for Four PWR Sequences*

Volume	ABHL		TMLB'		V		S2D	
	T (K)	P (Pa)	T (K)	P (Pa)	T (K)	P (Pa)	T (K)	P (Pa)
Core (exit gas)	700-2400	- 1.72E5	700-2400	- 1.72E7	1000-2400	- 6.89E5	1300-2300	- 4.14E6
Grid Plate	700-2400	- 1.72E5	700-1800	- 1.72E7	1000-2400	- 6.89E5	1300-2300	- 4.14E6
Upper Plenum	700-2400	- 1.72E5	700-1000	- 1.72E7	800-1800	- 6.89E5	700-1800	- 4.14E6
Hot Leg	- -	- -	~700 -	- 1.72E7	~700 -	- -	~700 -	- -
Sparge Line	- -	- -	~700 -	- 1.72E7	- -	- -	- -	- -
Pres-surizer	- -	- -	- -	- -	- -	- -	- -	- -
SG Piping	- -	- -	- -	- -	~700 -	- 6.89E5	- -	- -
Contain-ment	350-450	2.76E5-6.89E5	350-450	1.72E7-6.89E5	- -	- -	- -	- -

* Taken from Radionuclide Release Under Specific LWR Accident Conditions (BMI-2104)[Gi83]

external fields (e.g., electric or magnetic), and charged particles are discharged by radiation, particle transport to surfaces during severe accidents will be caused by Brownian and eddy diffusion, by inertial transport across bulk gas streamlines, by transport down thermal (thermophoresis) or concentration (diffusiophoresis) gradients, and by sedimentation.

The rate of removal of particle mass for particles of mass i is given by

$$\frac{dM_i}{dt} = \sum_j R_{i,j} M_i = \sum_j k_{i,j} \frac{A_j}{V} M_i \qquad (5.66)$$

where $R_{i,j}$ and $k_{i,j}$ are the rate coefficient and mass transfer coefficient (deposition velocity) for deposition of particles of mass M_i by deposition process j, A_j is the area of the deposition surface for deposition process j, and V is the volume of the compartment.

Diffusive Deposition. By analogy to vapor diffusion (see Section 5.1A above), when particle deposition is caused by diffusion, $k_{i,j}$ in Eq. 5.66 represents the combined effects of Brownian and eddy diffusion. Thus, the mass transfer coefficient for diffusive deposition ($k_{i,Df}$) is given by

$$k_{i,Df} = (D_i + E_i)/\delta_D \qquad (5.67)$$

$$D_i = B_i kT \qquad (5.68)$$

$$B_i = \frac{C_i}{3\pi\mu_g d_i \chi} \qquad (5.69)$$

where D_i and E_i are Brownian and eddy diffusivities for diffusion of particles of mass i, δ_D is the diffusive boundary layer thickness (the thickness within which the particle concentration gradient is appreciable), B_i is the Stokes law mobility for spherical particles of mass i corrected for slip and for nonspherical shape, C_i is the slip correction factor, χ is the dynamic shape factor, d_i is the particle diameter, u_g and T are the dynamic viscosity and temperature of the bulk gases, and k is Boltzman's constant.

When bulk gases are stagnant or in laminar flow (an unlikely situation during a severe reactor accident), $E_i = 0$ and Eq. 5.67 reduces to

$$k_{i,Df} = \frac{D_i}{\delta_D} \tag{5.70}$$

When the bulk gas flow over the deposition surface is turbulent, Eq. 5.67 will again reduce to Eq. 5.70, provided that the rate of diffusive deposition is limited by Brownian diffusive transport through a laminar sublayer (i.e., rapid eddy transport from the turbulent core where $D_i << E_i$, across the buffer layer where $D_i \approx E_i$, to the laminar sublayer where $D_i >> E_i$).

Diffusive deposition from turbulent flows has been examined theoretically by Fuchs [a7b]. Fuchs showed that if turbulence is assumed to die out completely at the outer edge of the laminar sublayer, then

$$k_{i,Df} = \frac{D_i}{\delta_L} \tag{5.71}$$

where δ_L is the thickness of the laminar sublayer. This result shows that the rate of diffusive deposition does not depend on the rate of transport from the turbulent core through the buffer layer, which means that eddy transport is much faster than transport by Brownian diffusion. Therefore, Eq. 5.70 also applies to diffusive deposition from turbulent flows.

Experimental determinations of the boundary layer thickness for diffusive particle deposition in well-stirred compartments have been reviewed by Van de Vate [26]. Much of the avaliable data had to be discarded, because significant contributions to the total deposition rate by deposition mechanisms other than diffusion had not been considered. Correlation of the remaining data gave

$$\delta_D = 4.8\ D_i^{0.274} \tag{5.72}$$

which when substituted in Eq. 5.71 gives

$$k_{i,Df} = 0.21\ D_i^{0.76} \tag{5.73}$$

Despite the simplicity of this relationship, because it was derived from a minimal experimental data base, it may be preferable in MELCOR to calculate mass transfer coefficients for diffusive deposition of particles using Sherwood number mass-transfer/heat-transfer analogies,

$$k_{i,Df} = Sh \frac{D_i}{L} \tag{5.74}$$

where D_i is the particle diffusion coefficient and L is the characteristic length of the deposition surface.

Slip Correction Factor. Expressions for C_i, the slip correction factor (see Eq. 5.69 above), have been developed by Knudsen and Weber [27], Millikan [28], and Phillips [29]. The Knudsen-Weber and Millikan correction factors have the following functional form:

$$C_i = 1 + AKn_i + QKn_i \exp(-b/Kn_i) \tag{5.75}$$

where values for the constants A, Q, and b are derived from experimental data. Fuchs [30a] recommends use of Millikan's oil drop data [28] which yields A = 1.246, Q = 0.42, and b = 0.87, when interpreted using σ = 0.499 in the following relation between viscosity and mean free path

$$\eta = \sigma n_g m_g v_g \lambda_g \tag{5.76}$$

where η is the bulk gas dynamic viscosity, and n_g, m_g, v_g, and λ_g are the number concentration, mass, mean velocity, and mean free path of the bulk gas molecules. Using the same value for σ in Eq. 5.71, Davies [31] derived values of A = 1.257, Q = 0.400, and b = 1.1 from an analysis of experimental data from several sources [27,28,32,33].

Using a method of moments solution to the Boltzmann equation, Phillips [29] derived the following expression for the slip correction factor

$$C_i = \frac{5 + 4Kn_i + 6Kn_i^2 + 18Kn_i^3}{5 - Kn_i + (8+\pi)Kn_i^2} \tag{5.77}$$

Using this equation, Phillips showed that drag forces on falling oil spheres corrected for slip, agreed well with experimental data including the oil drop data of Millikan.

Inertial Deposition. Substitution of Eq. 5.69 into Eq. 5.68 shows that D_i, the particle diffusion coefficient, is inversely proportional to particle diameter. Therefore, diffusive deposition of particles will decrease as particle diameter increases. The dependence of particle diffusive deposition velocity on particle diameter has been examined by Davies [34], who calculates that diffusive deposition should be negligible for particles with diameters of 0.1 μm or larger.

This conclusion is at varience both with the observation that large particles accumulate on the inside surfaces of vertical sections of pipes and ducts, and with the laboratory experiments of Friedlander and Johnstone [35]. Friedlander and Johnstone studied the deposition of electrically neutral particles with diameters greater than 0.5 μm onto the walls of straight sections of vertical glass or brass tubes from isothermal turbulent flows of dry gases. Even though their experimental conditions precluded significant deposition by electrostatic, diffusive, gravitational, or phoretic processes, particle deposition was still substantial. Since the tube sections were straight, the deposition was not caused by the inability of large particles to follow bulk gas streamlines at tube bends. Therefore, Friedlander and Johnstone concluded that some other inertial effect must have been operative.

Friedlander and Johnstone explained their experimental results by noting that a particle moving through a fluid with a velocity v_o will not come to rest in that fluid until it has traversed a distance $s = v_o\tau$ where $\tau = mB$, and s, τ, m, and B are the particle stopping distance, relaxation time, mass, and mobility (see Eq. 5.69 above). Thus, if a turbulent eddy imparts a velocity v_o to a particle located at the outer edge of the laminar sublayer, the velocity will carry the particle across that sublayer provided that the distance to the wall in the direction the particle is moving is less than or equal to the sum of the particle radius plus the particle stopping distance.

Friedlander and Johnstone [35] used the concept of a particle launching velocity v_o and a free flight distance s to develop a model of inertial deposition. Varients of that model have subsequently been developed by Owen [36], Davies [34,37,38], Wells and Chamberlain [39], Beal [40], Liu and Ilori [41], and Browne [42]. The development of all of these "free flight" models proceeds as follows.

Development begins with the following equation for the particle flux (N_i) produced by diffusive transport of particles

$$N_i = kc_b = (D_i + E_i)\frac{dc_i}{dy} \tag{5.78}$$

where k is the particle mass transfer coefficient, c_i and c_b are the local and bulk particle number concentrations, and D_i and E_i are the local Brownian and eddy particle diffusivities. Substitution of the following dimensionless ratios into Eq. 5.78

$$k^+ = \frac{k}{u_*} \qquad c^+ = \frac{c}{c_b} \qquad y^+ = \frac{yu_*}{\nu}$$

produces the following dimensionless equation

$$k^+ = \left[\frac{D}{\nu} + \frac{E}{\nu}\right]\frac{dc^+}{dy^+} \tag{5.79}$$

where $u_* = (\tau/\rho)^{1/2}$ and u_*, τ, ρ, and ν are the friction velocity, shear stress at the deposition surface, density, and kinematic viscosity of the bulk gases. Solutions for Eq. 5.79 are then developed as follows. First, Eq. 5.79 is expressed in integral form

$$\frac{1}{k^+}\int_{c_{y_o^+}}^{c_{y_3^+}} dc^+ = \int_{y_o^+}^{y_3^+}\frac{dy^+}{\frac{D}{\nu} + \frac{E}{\nu}} \tag{5.80}$$

Second, because E/ν will have a different functional dependence on y^+ in the laminar sublayer $[f_1(y^+)]$, the buffer layer $[f_2(y^+)]$, and the turbulent core $[f_3(y^+)]$, the integral over y^+ is split into three integrals

$$\frac{1}{k^+}\int_{c_{y_o^+}}^{c_{y_3^+}} dc^+ = \int_{y_o^+}^{y_1^+}\frac{dy^+}{\frac{D}{\nu} + f_1(y^+)} + \int_{y_1^+}^{y_2^+}\frac{dy^+}{\frac{D}{\nu} + f_2(y^+)} + \int_{y_2^+}^{y_3^+}\frac{dy^+}{\frac{D}{\nu} + f_3(y^+)} \tag{5.81}$$

where $0 < y_o^+ = r^+ + s^+$

$$r^+ = r_p \frac{u_*}{\nu} \qquad s^+ = s \frac{u_*}{\nu} \qquad s = \frac{2\rho_p r_p^2 v_o}{9\mu}$$

y_1^+, y_2^+, and y_3^+ are the dimensionless distances from the deposition surface at which the buffer layer, the turbulent core, and the well-mixed portion of the turbulent core begin; μ is the dynamic viscosity of the bulk gases; r_p and ρ_p are the particle radius and density; and s is the stopping distance of the particle when a velocity v_o has been imparted to it. Third, expressions for v_o and for the functions $f_1(y^+)$, $f_2(y^+)$, and $f_3(y^+)$ and values for the limits of integration are chosen. And last Eq. 5.81 is integrated and solved for k^+ with the constraint that solutions for integrals match at shared integration limits.

Although all of the free flight models follow this general development, they differ in their selection of integration limits, functional forms for the dependence of E/ν on y^+, expressions for v_o, and treatment of Brownian diffusion. For example, Friedlander and Johnstone, Wells and Chamberlain, Beal, and Owen evaluate only the first two integrals in Eq. 5.81, and calculate c^+ at y_2^+ using the Reynolds analogy. Davies, Browne, and Liu and Ilori use R^+, the dimensionless pipe radius, as the upper limit of integration and consequently use $c^+ = 1$ at $y^+ = R^+$.

Friedlander and Johnstone, and Liu and Ilori neglect Brownian diffusion ($D/\nu = 0$). Wells and Chamberlain assume that the deposition velocities for Brownian and eddy diffusion are separable and additive, and calculate the deposition velocity for Brownian diffusion using the Colburn analogy. All the other authors assume $D = BkT$ (see Eq. 5.68).

Friedlander and Johnstone, Wells and Chamberlain, and Beal assume that $y_o^+ = s^+ = v_o^+\tau^+$. Davies, and Liu and Ilori assume that $y_o^+ = s^+ + r^+$. Browne assumes that $s^+ + r^+ \sigma^+$ where σ^+ is the dimensionless surface roughness height. Owen's assumption for y_o^+ is not clear (Sehmel states [43] that Owen assumes $y_o^+ = 1.6$ for all particle sizes).

Friedlander and Johnstone, and Wells and Chamberlain assume a constant launching velocity $v_o^+ = 0.9$. Davies, Browne, and Liu and Ilori assume that $v_o^+ = v_{f+}(s^+ + r^+)$, where $v_{f+}(s^+ + r^+)$ is the value of v_{f+} at $y^+ = s^+ + r^+$, and v_f is the rms fluctuating velocity of the bulk gases normal to the deposition surface. Beal assumes that

$$v_o^+ = v_B^+ + \frac{1}{4} v_f^+(r^+) + v_f^+(s^+) \qquad (5.82)$$

where $v_B = (kT/2\pi m_p)^{1/2}$ is the particle velocity caused by Brownian motion. Beal, Davies, Browne, and Liu and Ilori all calculate v_{f+} from the data of Laufer [44].

Liu and Ilori assume that the eddy diffusivities for particles (E_p) and air (E) are not equal, and are related by

$$E_p^+ = E^+ + (v_f^+)^2 \tau^+ \qquad (5.83)$$

In all the other models it is assumed that $E_p = E$. Finally, all of the models including the model of Liu and Ilori calculate the the dependence of the eddy diffusivity of air on y^+ using either the equations of Lin et al. [45]

$$\frac{E}{\nu} = \left[\frac{y^+}{14.5}\right]^3 \qquad y^+ \leq 5 \qquad (5.84)$$

$$\frac{E}{\nu} = \frac{y^+}{5} - 0.959 \qquad 5 < y^+ \leq 30$$

of Owen [36]

$$\frac{E}{\nu} = \left[\frac{y^+}{10}\right]^3 \qquad y^+ \leq 5 \qquad (5.85)$$

$$\frac{E}{\nu} = 0.012(y^+ - 1.6)^2 \qquad 5 < y^+ \leq 20$$

$$\frac{E}{\nu} = 0.4(y^+ - 10) \qquad y^+ > 20$$

or of Davies [34,38]

$$\frac{E}{\nu} = \frac{(y^+)^A}{10^3(2.5\times10^7 Re^{-1})^B} \qquad (5.86)$$

$$A = 4 - (y^+)^{0.08}$$

$$B = (y^+)/(400 + y^+)$$

Specifically, Friedlander and Johnstone, Wells and Chamberlain, and Beal use Eq. 5.84, Owen uses Eq. 5.85, and Davies, Browne, and Liu and Ilori use Eq. 5.86 which agrees well with either Eq. 5.84 or 5.85.

The predictions of the free flight models of Friedlander and Johnstone, Beal, Davies, and Liu and Ilori have been compared to experimental data by Montgomery and Corn [46], Liu and Agarwal [47], Wildi and Thomann [48], and Gieseke et al. [49]. Plots of k^+ vs τ^+ show that inertial deposition becomes comparable to deposition due to Brownian diffusion only for particles which have dimensionless relaxation times $\tau^+ > 0.1$. Measured rates of inertial deposition rise steadily from $\tau^+ = 0.1$ to $\tau^+ = 10$, peak at $\tau^+ = 30$, and then remain essentially constant (or decline slightly) from $\tau^+ = 30$ to $\tau^+ = 10{,}000$.

The peaking of inertial deposition rates at $\tau^+ = 30$ has been explained by Reeks and Skyrme who developed a stochastic model of inertial deposition [50]. The stochastic model of Reeks and Skyrme assumes that deposition of large particles from turbulent flows is controlled by two processes, eddy transport to the viscous boundary layer, and inertial projection (free flight) through that boundary layer. Although increasing particle size increases the chance of inertial projection through the boundary layer, above some critical particle size, rates of eddy transport from the turbulent core to the boundary layer begin to fall off. Consequently, rates of inertial deposition are predicted to rise rapidly to a peak, and then to decline slowly.

As Figures 5.1 and 5.2 illustrate, comparison of model predictions to experimental data shows that, when $0.1 < \tau^+ < 10$, the model of Davies underpredicts the experimental data while the models of Friedlander and Johnstone, Beal, and Liu and Ilori agree well with the data. In this range both the data and the models are well approximated by the following relation [47]

$$k^+ = 6 \times 10^{-4} (\tau^+)^2 \qquad (5.87)$$

For $\tau^+ > 10$, the experimental results are well represented by

$$k^+ = 0.1 \qquad (5.88)$$

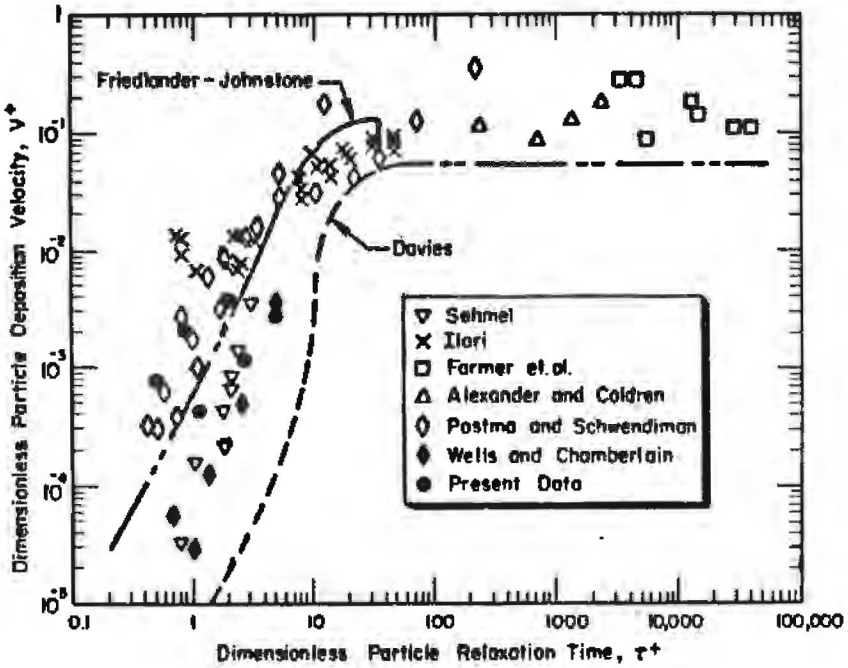

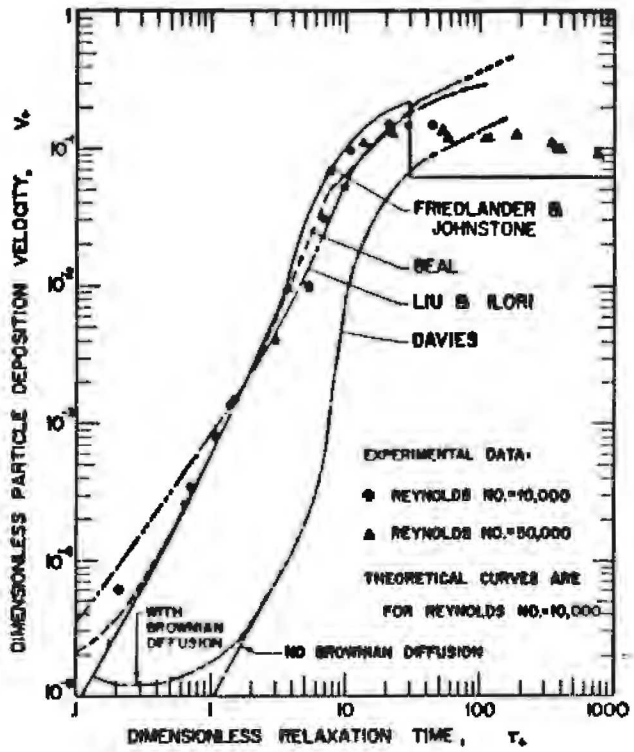

Figures 5.1 and 5.2. Comparison of Free Flight Models to Experimental data (Fig. 5.1 from Gieseke et al. [49], Fig. 5.2 from Liu and Agarwal [47]).

Implementation in MELCOR of an inertial deposition model (a free flight model or perhaps Eqs. 5.87 and 5.88) requires conversion of the deposition velocity from dimensionless to dimensioned form. Since $k^+ = k/u_*$ and $u_* = (\tau_o/\rho)^{1/2}$ where u_* is the friction velocity, ρ is the bulk gas density, and τ_o is the shear stress at the deposition surface, conversion of k^+ to k depends on being able to calculate a value for the surface shear stress τ_o.

When flow over a vertical flat plate is turbulent [1g]

$$\tau_o = 0.0225\rho u_g^2 \left[\frac{\nu}{u_g \delta}\right]^{1/4} \tag{5.89}$$

$$\frac{\delta}{x} = \frac{0.376}{Re_x^{1/5}} = \frac{0.376}{\left[\frac{u_g x}{\nu}\right]^{1/5}} \tag{5.90}$$

and when laminar [1h]

$$\tau_o = 0.332\ \mu u_g \left[\frac{u_g}{\nu x}\right]^{1/2} \tag{5.91}$$

where ρ, ν, and u_g are the density, the kinematic viscosity, and the free stream velocity of the bulk gases, and δ is the thickness of the hydrodynamic (velocity) boundary layer.

Eqs. 5.89 through 5.91 require a value for u_g, the free stream velocity over the deposition surface. The thermal-hydraulic portions of MELCOR will develop a reasonable estimate for the free stream velocity u_g, when the flow over the deposition surface is driven by forced convection, when the flow is driven by a natural circulation loop that involves several (at least three) control volumes, but not when the flow is driven by natural circulation within a single control volume.

Ostrach [51] has solved the boundary layer equations for laminar free convective flow over an isothermal vertical plate. Ostrach's analysis develops dimensionless velocity and temperature profiles as functions of Pohlhausen's similarity parameter. For fluids with Prandtl numbers between 0.72 and 1.0 (Prandtl numbers for air, steam, and hydrogen fall in this range), Ostrach predicts that the maximum in the dimensionless velocity profile occurs when

$$\frac{\frac{u_g x}{\upsilon}}{\frac{1}{2} Gr_x^{1/2}} \simeq 0.25 \qquad (5.92)$$

which suggests that for free convection $4Re_x^2 = Gr_x$. Therefore, since Gr_x will always be known for free convective regimes, an estimate or Re_x and thus of u_g can be made.

Inertial Impaction. Because of inertia, gas borne particles are not able to exactly follow nonlinear bulk gas stream lines. Consequently, large particles are efficiently removed from flowing gases by inertial impaction, when the gases flow past surfaces with substantial curvature. Inertial impaction onto spheres, cylinders, or flat plates placed in rectilinear gas flows can be described theoretically [30b]. However, theoretical descriptions of inertial deposition from turbulent flows through pipe bends or over baffles are not available, even for spherical particles that obey Stokes law. Thus, deposition of particles due to inertial impaction during flow through a pipe network (e.g., at pipe bends) or through a baffle (e.g., in a steam dryer) can not be modeled in MELCOR.

Gravitational Settling. A considerable amount of research has centered on the movement of particles in a gravitational force field where Newton's equation of motion for the particle is solved based on a given set of initial conditions. In most cases, the downward gravitational forces and the upward buoyancy and drag forces come quickly into balance and a constant settling velocity is reached. This settling velocity is related to the drag coefficient, C_D, by Equation 5.93 and is commonly used to represent the gravitational deposition velocity in aerosol calculations.

$$C_D = \frac{4}{3} \frac{d_P \; g \; \rho_P}{\rho \; V_s^2} \qquad (5.93)$$

where d_p is the particle diameter, ρ_p is the particle density, ρ is the fluid density, g is the acceleration due to gravity and V_s is the particle settling velocity. If the drag force on the particle is known, the particle settling velocity can be found by solving Equation 5.93, although in some cases the drag coefficient is a complex function of the settling velocity and an explicit expression for the settling velocity be found. Fluid dynamic correlations that relate the drag coefficient to the particle Reynolds number have been developed for various

Reynolds number regimes. The most common correlation is Stoke's law where $C_D = 24/Re$ when $Re<<1$ and the settling velocity is

$$V_s = \frac{g\, d_p^2\, (\rho_P - \rho)}{18\, \mu} \qquad (5.94)$$

This Stoke's law settling velocity is generally valid for Reynolds numbers less than two and is commonly used for LWR containment applications since the Reynolds numbers in LWR containments are expected to be small. When large convection currents exist in the containment or the reactor coolant circuit, Stokes law settling velocities will most likely not be valid. Alternate expressions for the drag coefficient for larger Reynolds numbers are available and, when substituted into Equation 5.93, lead to more accurate estimates of the settling velocities for particles outside of the Stokes regime. Several correlations for the particle drag coefficient and the corresponding settling velocities developed for large Reynolds numbers regimes are listed in Table 5.5.

All of the equations discussed so far are strictly correct only for spherical particles. If the particles are not spherical, a volume equivalent diameter d_e is substituted for the spherical diameter d_p, and a dynamic shape factor is included to account for increased fluid resistance. In addition, the slip correction factor C is needed for particles less than a tenth micron. As a result, the settling velocity for the spherical particle $V_s(d_p)$ is multiplied by a correction factor as follows,

$$V_s(d_e) = V_s(d_p)C/\chi \qquad (5.95)$$

where $V_s(d_e)$ is the settling velocity for a nonspherical particle with an equivalent diameter d_e.

For MELCOR, both the Stokes settling velocity and the non-Stokesian settling velocity developed by Abraham given in Table 5.4 should be available. The proper settling velocity to use will depend on the particle Reynolds number.

A subject of ongoing controversy is the correct way to treat the effect of vertical components of fliud flow velocities on gravitational settling rates. Upward flowing gases may exist because gases can flow off the core or off boiling pools of water and because natural convection currents may have upward components. In general, fluid flow will only affect settling

Table 5.5

Drag Coefficients and Settling Velocities for Non-Stokesian Settling

Oseen [52]

$Re < 3$	$C_D = 24/Re + 4.5$	$V_s = \dfrac{4\rho_p g}{\frac{72\mu}{d_p^2} + \frac{13.5\rho}{d_p}}$

Klyachko [53]

$3 < Re < 400$	$C_D = 24/Re + 4/Re^{1/3}$	no explicit solution

Abraham [54]

$0 < Re < 5000$

$$CD = \frac{24}{9.06^2}\left\{1 + \left[\frac{9.06}{Re^{1/2}}\right]\right\}^2$$

$$V_s = \frac{\upsilon}{4d_p}\left[\left(82 + 9.06\left[\frac{64\rho_p \rho\, d_p^3\, g}{72\mu^2}\right]^{1/2}\right)^{1/2} - 9.06\right]^2$$

Note: A good summary of the correlations available for the particle drag coefficient for various Reynolds numbers is given by Clift et al. [55]. However, the correlations given by Clift et al. do not yield explicit solutions for the particle settling velocity, and therefore are not amenable to this application.

C_D = drag coefficient
V_s = particle settling velocity
d_p = particle diameter
μ = fluid viscosity
ρ = fluid density
ρ_p = particle density
g = acceleration of gravity
Re = particle Reynolds number
υ = dynamic viscosity

rates if, at the plane across which settling occurs, there is a net upward component of fluid velocity normal to that plane. For settling from a fluid onto a solid surface, it is impossible to have a net normal component of fluid velocity at the plane without altering the fluid pressure at the plane, and therefore, no correction to the settling rate is required. However, when settling takes place across a gas boundary (i.e. aerosol transport between control volumes), there can be a component of fluid velocity normal to the plane of interest. In this case, the net upward velocity of the fluid should be subtracted from the particle settling velocity. In addition, when settling takes place on a liquid surface where evaporation or boiling of the liquid produces a net flux of fluid away from the liquid surface, a velocity correction must be made. The correction for this particular case is discussed with diffusiophoresis later in this section.

Thermophoresis. Observations indicate that a particle suspended in a gas with an existing temperature gradient experiences a thermal force moving it toward regions of lower temperature. For small particles, this force results mainly from the fact that molecules of higher temperature on one side of the particle hit harder and more frequently than cooler molecules on the other side. For larger particles, the difference between the thermal conductivity of the particle and that of the gas becomes important because a temperature gradient is induced within the particle, which in turn induces differences in the slip forces around it. As a result, models for the thermal force acting on a particle vary according to particle size as discussed below.

For a particle in the free-molecule regime, the magnitude of the thermal force is estimated by integrating, over the particle surface, the net momentum transferred to the surface by the colliding gas molecules. This momentum transfer approach is used both by Waldman [56] and by Deryaguin and Bakanov [57] to obtain the thermophoretic deposition velocity in the free molecule regime. The results reported by both authors are the same except for slightly different numerical coefficients. The Waldman expression is given in Table 5.6.

In the transition regime, Brock [58] derives an expression for the thermophoretic deposition velocity by assuming a velocity distribution for the molecules surrounding the particle and applying the momentum transfer approach. The assumed velocity distribution is derived by solving an approximate form of the Boltzman equation which follows from the BGK model [59]. The resulting expression is given in Table 5.6. Previous research indicted that an empirical representation of the thermal force in the transition regime could be formulated by multiplying the free molecule thermal force by an exponential correction factor involving τ, a constant that must be determined for a particular aerosol system, and the Knudsen number [60]. This empirical formulation is given in Table 5.6. Brock's equation for the

Table 5.6

Thermophoretic Deposition Velocities
for Different Knudsen Number Regimes

Free Molecule Regime

Waldman [56] $$v_t = \frac{3\,\mu\,\nabla T}{4\rho(1 + \pi\,\alpha/8)\,T}$$

Transition Regime

Jacobsen and Brock [60] $$v_t = \frac{3\,\mu\,\nabla T}{4\rho(1 + \pi\,\alpha/8)\,T}\,\exp(-T/Kn)$$

Brock [58] $$v_t = \frac{3\,\mu\,\nabla T}{4\rho(1 + \pi\,\alpha/8)\,T}\left[1 - 0.06 + 0.09a + 0.28a\,\left(1 - \frac{ak_f}{2k_p}\right)\frac{1}{Kn}\right]$$

Slip-Flow Regime

Epstein [61] $$v_t = \frac{3}{2}\,\frac{k_f}{(2k_f + k_p)}\,\frac{\mu}{\rho\,T}\,\nabla T$$

Brock [62] $$v_t = \frac{3\,\mu\,C(c_t Kn + k_f/k_p)\,\nabla T}{2\,\chi\,\rho\,T(1+3C_m Kn)(1+2C_t Kn+2k_f/k_p)}$$

Deryaguin et al. [63] $$v_t = \frac{(4k_f + 0.5k_p)}{(2k_f + k_p)}\,\frac{\mu}{\rho\,T}\,\nabla T$$

v_t = thermophoretic deposition velocity
μ = fluid viscosity
∇T = temperature gradient
T = temperature
ρ = fluid density
α = thermal diffusivity (m^2/s)
Kn = Knudsen number
k_f = fluid thermal conductivity
k_p = particle thermal conductivity
χ = dynamic shape factor
C = particle slip coefficient
c_m = constant derived from the accommodation coefficient
c_t = constant derived from the thermal accommodation coefficient

thermal deposition velocity in the transition region can be viewed in the same way, namely it is the free-molecule expression multiplied by an exponential correction factor (the terms in parentheses in Table 5.6 represent the first and second terms in the expansion of the exponential function).

In the slip-flow regime, the macroscopic conservation equations are used to calculate the thermal force with non-continuum effects close to the particle accounted for by slip flow boundary conditions. The models shown in Table 5.6 that are derived by Epstein [61] and by Brock [62] are the result of such slip flow calculations. Deryaguin, Bakanov, and Rabinovich [63] obtain similar results for the thermophoretic deposition velocity in the slip-flow regime with a thermodynamic calculation using the third order Chapman-Enskog theory and Onsager's principle of symmetry of kinetic coefficients.

The thermophoretic force vanishes in the continuum regime. A good review of the thermal deposition models for all Knudsen number regimes is given in Talbot [64].

The thermal force models given in Table 5.6 all involve complex size dependencies and, in order to be applied to specific systems, usually involve the fitting of certain of their parameters to experimental data. Some sources of experimental values for the thermal force and the thermophoretic deposition velocity are given in Table 5.7.

Prodi et al. [65] conclude that Waldman's model for small particles most reasonably approximates experimental data in the free-molecule regime while several authors agree that the Brock transition expression most closely predicts experimental results for medium sized particles. For larger particles, $Kn < 0.3$ and at $Kn = 1.0$, the results obtained by using the expressions presented by various authors show large discrepancies among themselves and, in general, do not agree with experimental data [64].

The expression derived by Brock for the slip-flow regime is used in current aerosol codes (i.e. MAEROS [66], QUICK [67], and HAARM-3 [68]) for the thermophoretic deposition velocity. Although Brock's slip-flow expression is not strictly valid for small particles, it has successfully fit a wide range of experimental data and is believed to estimate the thermophoretic deposition velocity in all Knudsen number regimes within 20% [64]. As a result, the following formulation is recommended for MELCOR.

$$V_d = \frac{3\mu C(C_t Kn + k_f/k_p)\nabla T}{2x\rho T(1 + 3C_m Kn)(1 + 2\,C_t Kn + 2\,k_f/k_p)} \qquad (5.96)$$

Table 5.7

Experimental Data on the Thermophoretic Deposition of Particles

Tobacco smoke in air [62]
Oil fog in helium [69]
Steric acid aerosol in helium; MgO smoke and NaCl in air [70]
Tobacco smoke in air [61]
Spherical NaCl aerosols in argon [60]
Sodium oxide in argon [71]
NaCl in air [65]
Tricresyl phosphate in air [72]
M 300 oil aerosols and Ph 300 oil aerosols in argon [73]
NaCl in air [74]
Transformer oil in air [75]
Oil and NaCl in air [76]

where μ is the fluid viscosity, C is the particle slip coefficient, C_t is a constant derived from the thermal accommodation coefficient, Kn is the Knudsen number, k_f is the fluid thermal conductivity, k_p is the particle thermal conductivity, ∇T is the thermal gradient, χ is the dynamic shape factor, ρ is the fluid density, T is the temperature, and C_m is a constant derived from the thermal accommodation coefficient.

It is important to note that, according to Jacobson and Brock [60] none of the models discussed thus far gives reasonable results for particles with large thermal conductivities. The inability of such models to account for non-equilibrium conditions around highly conductive particles is given as the cause. For particles with large thermal conductivities, they suggest

$$F_t = \frac{-12\pi m r^2 (C_{tm} Kn)(k_f/k_p + C_t Kn)(1 + \frac{4}{3} a_3 C_m K_n) - \frac{4}{3} a_3 C_m Kn}{(1 + 3C_m Kn)(1 + 2\, k_f/k_p + 2\, C_t Kn)} \quad (5.97)$$

where F_t is the thermal force and m is the mass of the particle (all other symbols are as defined for Eq. 5.96).

They note that Equation 5.97 is best used as a curve fitting equation in combination with empirical results. This expression should be available for use in MELCOR when the user believes large differences between the gas and particle thermal conductivities will arise in his calculation.

Diffusiophoresis. Diffusiophoresis is the enhanced transport of aerosols that ocurs as a result of vapor movement down a concentration gradient. Mechanistically, thermophoresis and diffusiophoresis are very similar. For instance, in a binary gas mixture of A and B where A and B are diffusing in opposite directions, more A molecules will strike the particle on the side with the higher A concentration and more B molecules will strike the particle on the side with the higher B concentration. The net result, if the flux of A and B are equal, is movement of the particle in the direction that the heavier molecules are moving (i.e. heavier molecules transfer more momentum to the particle). In most systems, however, the fluxes of the two components will not be equal, and the particle will move in the direction of the net vapor flux at a rate that is reduced by the effect of the collisions by the opposing molecules.

Experiments [77-79] show that the diffusiophoretic velocity for particles falls somewhere between the mean mass and mean molar velocity of the gas mixture where the mean mass velocity is defined as:

$$\bar{v} = \frac{\sum_{i=1}^{n} \rho_i V_i}{\rho} = \frac{\sum_{i=1}^{n} MW_i N_i}{\overline{MW}\, c} \qquad (5.98)$$

where ρ_i is the mass density of specie i, ρ is the fluid density, MW_i is the molecular weight of specie i, N_i is molar flux of specie i, and V_i is the velocity of i, and the mean molar velocity is defined as:

$$\bar{V} = \frac{\sum_{i=1}^{n} C_i V_i}{C} = \frac{\sum_{i=1}^{n} N_i}{C} \qquad (5.99)$$

where C_i is the molar concentration of specie i and C is the molar concentration of the fluid.

Whitmore and Meisen [77], in particular, use these expressions to fit their experimental data. Both Schmitt and Waldman [78] and Derjaguin and Bakanov [79] calculate the diffusiophoretic deposition velocity for small particles by balancing velocity of the Stefan flow (velocity of the flow of bulk gases toward the condensing surface) against the velocity that arises from the unequal momentum exchanges on the sides of the particle. The resulting expression for the diffusiophoretic deposition velocity in a binary system is:

$$V_d = \frac{MW_1^{1/2}}{\gamma_1 MW_1^{1/2} + \gamma_2 MW_2^{1/2}} U \qquad (5.100)$$

$$U = \frac{D_{12}}{\gamma_2} \nabla\gamma_1 = \frac{MW_2}{MW_1} \frac{W_1}{\rho_2}$$

where V_d is the diffusiophoretic deposition velocity, V is the velocity of the Stefan flow, D_{12} is the diffusion coefficient of the condensing fluid 1 in the non-condensible bulk fluids 2, W_1 is the mass condensation rate of the condensing fluid (e.g., steam), ρ_2 is the density of the non-condensible bulk gases, and MW_i and γ_i are the molecular weight and mass fraction of fluid i.

In general, velocities calculated using Equation 5.100 fall between the mean molar and the mean mass velocity of the flow and compare well with exprimental data in the free molecule regime. In the slip-flow regime, Schmidt and Waldman [78] solve the hydrodynamic problem of the particle in the gas accounting for a finite gas velocity at the particle surface due to diffusion slip to obtain:

$$V_d = - (1 + \sigma_{12} \gamma_2) \frac{D_{12}}{\gamma_2} \nabla \gamma_1 \qquad (5.101)$$

$$\sigma_{12} = 0.95 \left[\frac{m_1 - m_2}{m_1 + m_2} \right] - 1.05 \left[\frac{d_1 - d_2}{d_1 + d_2} \right] \qquad (5.102)$$

where σ_{12} is a numerical constant derived empirically and m_i is the particle mass. In addition, Derjagiun, Yalomov, and Storozhilova [70] use thermodynamic calculations to obtain:

$$V_d = - \frac{\rho_1}{\rho} \frac{D_{12}}{\gamma_1} \nabla \gamma_1 \qquad (5.103)$$

where ρ_1 is the density of specie 1, ρ is the fluid density, D_{12} is the diffusion coefficient, γ_1 is the mass fraction of specie 1 and $\nabla \gamma_1$ is the gradient in the mass fraction of 1 for the diffusiophoretic deposition velocity in the slip-flow regime. Very little work is published on the effects of diffusiophoresis in the transition regime.

None of the slip-flow formulations agree well with experimental results without the use of fitting parameters [80]. Although it is not entirely clear that the free-molecule expression will be valid over the full range of Knudsen numbers, its agreement with experimental results [81] indicates that it should be used to model diffusiophoresis in MELCOR.

In the containment, steam condensing on cool surfaces induces diffusiophoretic forces too large to neglect, and they should be modeled as described above. It is interesting to note that for conditions similar to those expected in an LWR containment the thermophoretic deposition velocity is about two orders of magnitude smaller than the diffusiophoretic deposition velocity.

In the reactor coolant system, diffusiophoresis is not expected to be an important phenomenon to model in its own right. This is because, for the situations involving steam condensation in the coolant system (e.g., flow through a steam generator with auxiliary feed), all the aerosols will be removed from the condensing medium into the condensate. A more important effect of diffusiophoresis under such conditions may be the modification of thermophoretic forces in the primary system. Several authors have derived expressions for the coupling term introduced when thermophoresis and diffusiophoresis are considered together. In particular, a good reference in this area is Annis and Mason [82]. The term is significant when components of a gas mixture are present in comparable amounts, even if none of those components undergo condensation or evaporation. Consideration of the coupling term is believed to be beyond the scope of MELCOR.

C. Aerosol Agglomeration

Estimates of particle growth rates due to agglomeration require estimates of the probability of particle collisions. In general, only binary collisions are considered. A collision probability is calculated for each process that causes significant particle motion. In particular, Brownian, turbulent, and gravitational processes are usually considered. Then, the collision probability is converted to a collision rate called the collision kernel or coagulation coefficient.

The Brownian Agglomeration Kernel. When two particles in the same proximity are subject to Brownian forces (diffusion), there is a probability that their induced relative motion will result in a collision. For a large number of particles in a volume, many such collisions occur resulting in aerosol particle growth. Growth by Brownian agglomeration is most important for small particles (Kn > 10) since their movement is induced primarily by Brownian forces. As particle size increases, such movement decreases, and Brownian agglomeration becomes less important.

Expressions for the Brownian agglomeration kernel are different for each of the four Knudsen number regimes identified earlier (the free-molecule regime, the transition regime, the slip-flow regime, and the continuum regime). In the limits of large and small particle size, the coagulation coefficient expressions (derived from continuum theory and the kinetic theory of gases respectively) are well established. The continuum expression is [83]

$$k_{ij} = 4\pi(D_i + D_j)(r_i + r_j) \qquad Kn \ll 1 \tag{5.104a}$$

$$D_i = k_b T/6\pi r_i \mu \tag{5.104b}$$

where D_i is the particle diffusion coefficient, r_i is the radius of particle i, k_b is Boltzman's constant, T is the temperature, and μ is the fluid viscosity. The free-molecule expression is

$$k_{ij} = \pi(r_i + r_j)^2(\bar{c}_i^{\,2} + \bar{c}_j^{\,2}) \qquad Kn > 10 \qquad (5.105a)$$

$$\bar{c}_i = (8k_bT/\pi m_i)^{1/2} \qquad (5.105b)$$

where m_i is the mass of particle i.

For the slip-flow and transition regimes, modifications of the continuum and free-molecule expressions are used. The continuum formulation is extended into the slip-flow regime by modifying the particle diffusion coefficient with the slip correction factor, C. The resulting formulation is [84]

$$k_{ij} = 4\pi(D_i + D_j)(r_i + r_j) \quad Kn < 0.25 \qquad (5.106a)$$

$$D = \frac{k_bTC}{6\pi r_i\mu} \qquad (5.106b)$$

A semiempirical expression that embodies the free-molecule and continuum limits was developed by Fuchs [30c] for the transition regime.

$$k_{ij} = \frac{4\pi\,(D_i + D_j)(r_i + r_j)}{F} \qquad 0.1 < Kn < 10 \qquad (5.107a)$$

$$F = \frac{(r_i + r_j)}{(r_i + r_j + g_{ij})} + \frac{4(D_i + D_j)}{(\bar{c}_i^{\,2} + \bar{c}_j^{\,2})(r_i + r_j)} \qquad (5.107b)$$

$$g_{ij} = (g_i^2 + g_j^2) \tag{5.107c}$$

$$g_i = \frac{(2r_i + \lambda_i)^3 - [4r_i^2 + \lambda_i^2]^{3/2} - 2r_i}{6r_i \lambda_i} \tag{5.107d}$$

$$\lambda_i = 8D_i/\pi\bar{c}_i \tag{5.107e}$$

$$\bar{c}_i = [8k_bT/\pi m_i]^{1/2} \tag{5.107f}$$

The correction factor, F, above accounts for distortion of the isotropic nature of the gas between the particles as they move together.

Recently, Sitarski and Seinfeld [85] solved the Fokker-Planck equation to obtain the following fully analytical expression for the Brownian coagulation coefficient applicable to the full range of particle radii:

$$k_{ij} = 4\pi A(r_i + r_j) \tag{5.108a}$$

$$A = (D_iQ_i + D_jQ_j) \tag{5.108b}$$

$$Q_i = \frac{1 + 0.2\alpha_i}{(0.188\alpha_i^2 + 0.994\alpha_i + 1)} \tag{5.108c}$$

$$\alpha_i = \frac{40\ \pi^{1/2}\ r_i^3\ \rho_p}{3\ \ 2\ k_bT\ \ (r_i+r_j)} \tag{5.108d}$$

where ρ_p is the density of the particle.

Examination of this expression shows that for large values of r it reduces identically to the expression for Brownian agglomeration in the continuum range (Eq. 5.104), for small values of r it differs from the free-molecule expression for

Brownian agglomeration (Eq. 5.104) by a multiplicative factor of 2/3, and between these limits it predicts values that agree well with the predictions of the Fuchs expression (Eq. 5.107). Furthermore, predictions of this expression and the Fuchs expression both agree reasonably with experimental results for Brownian agglomeration of a diethylhexylsebacate aerosol (86). Accordingly, either the Fuchs formulation or the formulation of Sitarski and Seinfeld could be used in MELCOR. The Fuchs formulation is recommended because it is in use in several aerosol codes including the MAEROS code which implements the approach to aerosol behavior recommended in this report for use in MELCOR.

The Gravitational Agglomeration Kernel. The force of gravity acting on an aerosol particle induces a settling velocity that depends on the particle size and the material density. As a result, in a volume containing particles of different sizes, the larger ones tend to catch up with the smaller ones, and collisions occur. This phenomenon is known as gravitational agglomeration. Gravitational agglomeration is most important for large particles that, because of their mass, feel the influence of gravity more than small particles.

Most sources agree on the general formulation of the gravitational collision kernel.

$$k = \frac{2\pi g \rho_p \gamma^2 \varepsilon r_1}{9\mu\chi} \left| Cr_1^{2\prime} - Cr_1^{2\prime} \right| (r_1' + r_2')^2 \qquad (5.109)$$

where g is the acceleration of gravity, ρ_p is the particle density, γ is the agglomeration shape factor, ε is the collision efficienty, r is the particle radius, μ is the fluid viscosity, χ is the dynamic shape factor and C is the slip coefficient.

The major source of controversy, however, is the definition of the collision efficiency, ε. The collision efficiency implied in Eq. 5.109 is an overall efficiency that accounts for collection by impaction, interception, and diffusion and can be calculated by combining individual collision efficiencies for these three mechanisms additively as recommended by Fuchs [30d]:

$$\varepsilon = 1 - (1 - \varepsilon_{im})(1 - \varepsilon_{diff}) + \Delta\varepsilon_{in} \qquad (5.110)$$

where ε_{im}, ε_{diff}, and ε_{in} are the collision efficiencies due to impaction, diffusion and interception, respectively.

The most widely used expression for collision efficiency for interception is the viscous flow expression attributed to Fuchs.

$$\epsilon = \frac{3}{2}\frac{r_i^2}{(r_i + r_j)^2} \simeq \frac{3}{2}\frac{r_i^2}{r_j^2} \quad \begin{cases} r_i << r_j \\ Re_j << 1 \end{cases} \tag{5.111}$$

where Re_j is the Reynolds number associated with the larger particle.

The Fuchs formulation was developed for a stationary spherical collector and does not account for the curvilinear path taken by small particles traveling around large particles. As a result, the calculated efficiencies are artificially high. Alternative expressions for the collision efficiency due to interception are recommended (1) by Lee and Gieseke [87] where

$$\epsilon_{in} = 1.5(r_i/r_j)^2/(1+r_i/r_j)^{1/3} \quad \begin{cases} r_i << r_j \\ Re_j << 1 \end{cases} \tag{5.112}$$

(2) by Pruppacher and Klett [88] where

$$\epsilon_{in} = \left[\frac{1}{2}\frac{r_i}{r_i + r_j}\right]^2 \quad \begin{cases} r_i < r_j \\ Re_j << 1 \end{cases} \tag{5.113}$$

and (3) by Hidy and Brock [89] where

$$\epsilon = \frac{r_i^2\,(2r_i/r_j + 3)}{2r_j^2\,(1 + r_i/r_j)} \quad \begin{cases} r_i < r_j \\ Re_j << 1 \end{cases} \tag{5.114}$$

For potential flow, Fuchs[30f] recommends

$$\epsilon_{in} = 3(r_i/r_j) \quad \begin{cases} Re_j > 1 \\ r_i << r_j \end{cases} \tag{5.115}$$

For collection due to impaction the Fuchs [30g] expressions in the viscous flow regime are

$$\varepsilon_{im} = 1 + \left[\frac{0.75\ \ln(2Stk)}{Stk - 1.214}\right]^{-2} \qquad Stk > 1.214 \qquad (5.116a)$$

$$\varepsilon_{im} = 0 \qquad Stk < 1.214 \qquad (5.116b)$$

where

$$Stk = 2\tau_i/(\gamma_i Dp_j)(V_{si} - V_{sj}) \qquad Dp_i < Dp_j \qquad (5.116c)$$

and

$$\tau_i = \rho_{pi}\ C_i\ r_i^2/\chi \qquad (5.116d)$$

γ_i is the agglomeration shape factor, V_{si} is the particle settling velocity, and χ is the dynamic shape factor. For potential flow, Fuchs [30g] recommends

$$\varepsilon_{im} = 0 \qquad Stk < 1/12 \qquad (5.117a)$$

$$\varepsilon_{im} = \frac{Stk^2/(Stk + 0.5)^2(12Stk - 1)}{1.4} \qquad \frac{1}{12} < Stk < 0.2 \qquad (5.117b)$$

$$\varepsilon_{im} = Stk^2/(Stk + 0.5)^2 \qquad Stk > 0.2 \qquad (5.117c)$$

Alternate expressions for the impaction collection efficiency for potential flow are given by Langmuir [90]

$$\varepsilon_{im} = Stk^2/(Stk + 0.125)^2 \qquad (5.118)$$

and Hetsroni [91] where

$$\varepsilon_{im} = Stk^2/(Stk + 0.35)^2 \qquad (5.119)$$

For the impaction effect only, Langmuir [90] suggests an interpolation formula for intermediate values of Re_j

$$\varepsilon_{im} = \frac{60\ \varepsilon_{im,vis} + Re_j\ \varepsilon_{im,pot}}{60 + Re_j} \qquad (5.120)$$

where $\epsilon_{im,vis}$ is the viscous flow expression for collection efficiency, and $\epsilon_{im,pot}$ is the potential flow expression. The diffusion collision efficiency is given by Lee and Gieseke [92] as:

$$\epsilon_{diff} = 3.5Pe^{-2/3} \tag{5.121a}$$

$$Pe_i = \frac{(Vs_i - Vs_j)Dp_i}{k_b\ T\ B(Dp_i)} \qquad Dp_i < Dp_j \tag{5.121b}$$

$$B(dp_i) = C_i/3\pi\ \mu\ Dp_i\ \chi \tag{5.121c}$$

and by Rimberg and Peng [93] as:

$$\epsilon_{diff} = (4/Pe_i)(2 + 0.557\ Re_j^{1/2}\ Sc_i^{3/8}) \tag{5.121d}$$

where Sc_i is the particle Schmidt number.

Most codes used today employ the Fuchs viscous flow expression for the overall gravitational collection efficiency. Code authors do, however, question its adequacy. Jordan, Schumacher, and Gieseke, authors of the QUICK [67] aerosol code, compare the calculated collision efficiencies with experimental efficiencies reported by Pertmer and Loyalka [94] concluding that the calculated results are accurate enough for their application. Other aerosol code authors have incorporated various combinations of the expressions given above. The expressions used in the recent BMI-2104 study [95] and in the CONTAIN code [96] are summarized in Table 5.8. Further investigation is required before sanctioning the use of either of these approaches in MELCOR.

The Turbulent Agglomeration Kernel. Collisions between particles can occur because of a relative motion induced by two distinct turbulent mechanisms. The first type of collision is due to fluid shear. Because of the variable fluid velocity field, a particle entrained in one streamline may travel faster than a particle entrained in an adjacent streamline, and a collision results. The second type of collision is due to particle inertia. Since the degree to which a particle can be accelerated by a force is related to its mass, particles of varying masses react differently to fluid accelerations. Large particles are often thrown across fluid streamlines because of

such accelerations resulting in an increased probability of collisions. Obviously, the first collision mechanism is important for small particles while the second is important for large particles. Turbulent agglomeration is probably more important in the primary system, where turbulent flow fields are expected, than in containment.

Quantifying turbulent effects is often very difficult because of the indeterminate character of the turbulence itself. The two approaches commonly used for the derivation of turbulent-collision kernels are the stochastic treatment of Saffman and Turner [97] and the diffusion equation solution of Levich [98]. Both methods give expressions with the same functional form but with different leading coefficients. For the shear term, the general form is

$$k = \frac{A\, E_T^{1/2}}{\nu^{1/2}}\, B\, (r_i + r_j)^3 \qquad (5.122)$$

where E_T is the turbulent energy dissipation rate and ν is the kinematic viscosity. The values of A and B vary. The general form of the inertial term is

$$k = \frac{\rho^{1/4}\, E_T^{3/4}}{\mu^{5/4}}\, \gamma^2\, (r_i + r_j)^2\, |\, \tau_i - \tau_j\, | \qquad (5.123)$$

$$\tau_i = \rho_{pi}\, C_i\, r_i^2\, /\chi \qquad (5.124)$$

The Saffman and Turner formulations outlined above are the basis of the turbulent agglomeration modeling in most state-of-the-art aerosol codes. However, it involves physical approximations that may fail under certain reactor accident conditions, most probably in cases where there is high turbulence and large particles (in this context > 5μm). These approximations include: 1) Saffman and Turner assume that Stokes Law can be used to obtain the particle relaxation time, 2) the Saffman and Turner analysis is valid only when the particle relaxation time is small compared to the time scale characteristic of the smallest eddies of the turbulence, and 3) Saffman and Turner assume unit collision efficiencies for both the turbulent shear and the turbulent inertial mechanisms. All three of these assumptions can lead to large uncertainties in the magnitude of particle growth due to turbulent agglomeration. These uncertainties have been studied

Table 5.8

Summary of the Expressions Used for the Overall Collision Efficiency In BMI-2104 [95] and CONTAIN [96]

BMI-2104

$$\varepsilon = \varepsilon_{im} + \varepsilon_{in} + \varepsilon_{diff}$$

$$\varepsilon_{im} = Stk^2/(Stk + 0.35)^2$$

$$\varepsilon_{in} = 1.5(r_i/r_j)^2/(1 + r_i/r_j)^{1/3}$$

$$\varepsilon_{diff} = 3.5\ Pe^{-2/3}$$

CONTAIN

$$\varepsilon = \varepsilon_{in}$$

$$\varepsilon_{in} = 1 \qquad \text{for } r_i/r_j < 2$$

$$\varepsilon_{in} = -\frac{5}{3}\ \frac{r_i/r_j}{3} + \frac{1.5r_i^2\ (r_i/r_j - 2)}{3\ (r_i + r_j)^2} \qquad \text{for } 2 < r_i/r_j < 5$$

$$\varepsilon_{in} = \frac{1.5\ r_i}{(r_i - r_j)^2} \qquad \text{for } r_i/r_j > 5$$

recently by Williams as part of the QUEST [99] program and further as part of the program on "Localized Deposition from Wet Plumes" [100] where he suggests some corrections to the Saffman and Turner formulations for systems where their assumptions are not believed to be valid. For MELCOR 1.0 the Saffman and Turner formulations are adequate, but William's corrections should be considered for later versions of the code.

One of the largest uncertainties reflected in the turbulent agglomeration coefficients is the uncertainty in the calculation of E_T, the rate of energy dissipation per unit mass of gas. Uncertainties in E_T reflect uncertainties in the hydrodynamics of the turbulence itself. Estimates of the energy dissipation rate are available for a buoyant plume, for a turbulent jet, for turbulent pipe flow, and for a LWR containment. In a plume, the turbulent energy dissipation rate is estimated by Tennekes and Hales [101] as:

$$E_T = U^3/L \tag{5.125}$$

where U is a turbulent velocity scale and L is an eddy length scale. Typical values for the energy dissipation rate given by this expression are 1000 cm^2/sec^3 at 1 meter above the ground and 5 cm^2/sec^3 at 100 meters above the ground. For turbulent pipe flow, Friedlander [35] (based on Laufer [44]) gives

$$E_T = \frac{4}{d}\left[\frac{f}{2}\right]^{3/2} U^3 \tag{5.126}$$

where f is the Fanning friction factor and d is the diameter of the pipe. Friedlander calculates a dissipation rate of 2E4 cm^2/sec^3 for 20° C air with Re = 50,000. Typical values of the turbulent energy dissipation rates used in containment aerosol codes are of the order of 10 cm^2/sec^3. Williams [99] estimates an upper bound for the energy dissipation rate due to convection currents in a LWR containment with the expression

$$E_T = 0.065(\alpha/Pr)^{1/3}(g\beta\Delta T_{wb})^{4/3} H_e S_e/V_e \tag{5.127}$$

where
- α = thermal diffusivity = $k/\rho C_p$
- P_r = Prandtl number
- H_c = effective height of convective pattern (m)
- S_e = effective heat-tranfer surface area (m^2)
- V_e = effective volume (m^3)
- β = gas volumetric coefficient of expansion (m^3/k)

This expression is developed by equating the energy dissipation forces to the thermal buoyancy forces driving natural circulation. The upper limit obtained using this expression is 200 cm^2/sec^3.

Since the turbulent energy dissipation rate is still highly uncertain, it should be available as an input parameter in MELCOR. Default calculations for E_T can be based on the expressions given above for turbulent pipe flow (in the RCS) and for an LWR containment.

Combination of Agglomeration Coefficients. The appropriateness of any particular method for combining the individual agglomeration kernels into an overall kernel is not clear. The most common approach is to assume that the mechanisms act independently and add the individual kernels. Some authors have argued, however, that the agglomeration mechanisms do not act independently, and a strict addition of the individual kernels is not appropriate, particularly for the turbulent kernels. Other functional combinations have been proposed, but evidence supporting them is sparse. A brief summary of the combination schemes currently used in several state-of-the-art aerosol codes is given in Table 5.9.

Table 5.9

The Combination of Kernels in Current Aerosol Codes

QUICK	$k_b + (k_{T1}^2 + k_{T2}^2 + k_g^2)^{1/2}$
MAEROS	$k_b + k_G + (k_{T1}^2 + k_{T2}^2)^{1/2}$
HAARM-3	$k_b + k_g + k_{T1} + k_{T2}$
NAUA-4	$k_b + k_g$

Recommendations for MELCOR. Formulations for the coagulation coefficients to be used in the coagulation equation are outlined in the discussion above. The various state-of-the-art aerosol codes employ these formulations except as noted above with only minor variations, for example in numerical coefficients. The exact representations used in any one code do not appear to be any better than any other. Therefore, mostly as a convienience, the expressions used in the MAEROS code are recommended for MELCOR-1. These representations are documented in the MAEROS User's Manual [66].

Calculation of Agglomeration Coefficients in the Context of a Sectional Technique. In the context of a sectional solution technique to the particle growth rate equation, calculation of the agglomeration coefficients involves integration of the collision frquency expressions above over a range of particle sizes (a size section). Naturally, when a complex intergration is involved, the calculation of the agglomeration coefficeints is time consuming. Typically, to save computing time, codes that use a sectional technique (e.g. MAEROS) precalculate the values of the collison kernels for a given set of thermal hydraulic conditions (usually temperature and pressure pairs) and obtain kernel values for other sets of thermal hydraulic conditions by linear interpolation between the precalculated values. For LWR containment applications, this technique has proven to be adequate since the temperature and pressure variations seen in the containment during a severe accident are not large.

The method of linear interpolation between the values calculated for a given set of temperature and pressure pairs may not be adequate for primary system conditions where temperature and pressure ranges are broad and other thermal hydraulic parameter values (e.g., bulk gas collision cross section, viscosity, and thermal conductivity assumed constant when precalculating kernel values) vary significantly with changing bulk gas composition. The significance of any errors introduced by using this linear interpolation technique in the primary system needs to be assessed.

If precalculation of kernel values for sets of temperature/pressure pairs is shown to be inadequate in the primary system, it may be possible to obtain better kernel values and still minimize computing time by using an alternate interpolation technique. For instance, if the collision kernel can be separated into a simple multiplicative factor (containing the thermal hydraulic parameters) in front of the integrand (containing the aerosol parameters), an interpolation table can be established for the integrand, and the integrand can be scaled by the multiplicative factor appropriate for the current thermal hydraulic conditions.

Inspection of the kernel formulations shows that this separation technique is possible for all agglomeration kernels except those that contain the Knudsen number (i.e., the Brownian, gravitational and turbulent shear agglomeration kernels). For these kernels it may be necessary to precalculate values of the inseparable kernel residue using sets of temperature/pressure pairs and appropriate values of other thermal hydraulic variables that do not separate. For example, since the collision cross sections for water, hydrogen, and air are 2.6, 2.8, and 3.7 angstroms respectively, an average value of 3.0 angstroms may yield acceptable results when combined with an appropriate set of temperature/pressure pairs.

Further, if linear interpolation proves inadequate, nonlinear interpolation may yield improved accuracy.

5.4 Numerics

All of the rate processes described in Chapters 3 thru 6 of this report may be represented as zeroeth, first, or second order equations of the form

$$\begin{aligned} d/dt(M) &= k && \text{zero order} \\ d/dt(M) &= k\,(M) && \text{first order} \\ d/dt(M) &= k\,(M)(M') && \text{second order} \end{aligned}$$

Implementing this set of rate equations poses two problems: how to interface the fission product behavior rate equations to the thermal-hydraulic portions of MELCOR; and how to treat aerosol particle size distributions.

A. Thermal-Hydraulic Interface.

The first question, how to interface the fission product behavior rate equations to the thermal-hydraulic portions of MELCOR, arises because the fission product behavior rate equations require thermal-hydraulic data as input, and generate decay heat data that is required by the thermal-hydraulic portions of the code. Since simultaneous solution of both thermal-hydraulic and fission product behavior phenomena would be computationally intractable, this feedback dictates an ordered calculation.

Although recommendation of an order for the calculational sequence in MELCOR is beyond the scope of this review, several cautionary points should be noted. For many severe accident sequences decay heat emitted by fission products released from degraded core materials will constitute a significant portion of the total energy driving thermal-hydraulic behavior. For these sequences bulk gas temperatures and pressures will be strongly

influenced by the amount and location of the decay heat emitted by fission products that have been released from core materials. But bulk gas temperatures and pressures strongly influence bulk gas turbulence, intercompartment bulk gas flow rates, and vapor saturation pressures. Thus, turbulent agglomeration and deposition processes, vapor condensation and evaporation, diffusiophoretic and thermophoretic deposition, and intercompartment transport of fission products will all be sensitive to bulk gas thermal-hydraulic conditions and thus to the amount and location of decay heat release. So fission product behavior and thermal-hydraulic conditions will be tightly coupled, and therefore the order of their calculation is likely to be important.

B. Solution of the Aerosol Equation.

The form of and solution methods for the integrodifferential equation that describes the evolution with time of the size distribution of a gas borne aerosol size distribution has been reviewed by Drake [102] in the context of atmospheric physics, and by Loyalka [103] and Dunbar et al. [104] in the context of nuclear reactor safety. In a well mixed compartment (spatially homogeneous size distribution) the integrodifferential equation has the following form

$$\frac{\partial n(v,t)}{\partial t} = \frac{1}{2}\int_0^v \beta(u,v-u)n(u,t)n(v-u,t)du - n(v,t)\int_0^\infty \beta(u,v)n(u,t)du$$

$$+ G(v,t)n(v,t) - R(v,t)n(v,t) + S(v,t) \qquad (5.128)$$

where u and v are particle masses;

$\beta(u,v)$ = the rate coefficient for agglomeration of particles of mass u with particles of mass v

$G(v,t)$ = the rate coefficient for particle growth due to vapor condensation

$R(v,t)$ = the rate coefficient for removal of particles due to natural processes or Engineered Safety Features (ESFs)

$S(v,t)$ = the rate coefficient for particle production by sources

and $n(v,t)$, the particle number density function, is defined such that $n(v,t)dv$ is the number concentration of particles in the size range $[v,v+dv]$ at time t.

In Eq. 5.128 the first integral represents creation of particles of mass v by agglomeration of particles of mass v-u with particles of mass u; the second integral represents depletion of particles of mass v due to agglomeration with other particles; and $\beta(u,v)$, $G(v,t)$, $R(v,t)$, and $S(v,t)$ are compound functions constructed by combining individual rate coefficients for contributing processes. For example $\beta(u,v)$ usually represents the overall agglomeration rate coefficient for gravitational, turbulent, and Brownian agglomeration, and $R(v,t)$ is the overall removal rate coefficient for particle removal caused by natural deposition mechanisms (e.g., sedimentation, diffusiophoretic deposition) and engineered safety features (e.g., sprays, suppression pool). Despite the likelihood that different mechanisms reinforce each other, most often individual rate processes are assumed to be independent and overall rate coefficients are expressed as the sum of the rate coefficients of the individual processes. Thus $R(v,t) = \sum_i R_i(v,t)$.

For simple forms of $\beta(u,v)$, $G(v,t)$, $R(v,t)$, and $S(v,t)$, analytical solutions can be obtained for Eq. 5.128 [98]. Since none of the simple forms are realistic for reactor accidents, if the complicated coefficients recommended in Chapters 3 through 6 of this report are to be used in the MELCOR code system, the equations that result from their substitution into Eq. 5.128 is usually solved by assuming some functional form for the particle number density function $n(v,t)$, which reduces Eq. 5.128 to a set of ordinary differential equations. In the context of reactor safety, usually $n(v,t)$ has been assumed either to have a well defined form over its entire range (Method of Moments Approach) or a well defined form in each section of its range (Sectional Approach).

Method of Moments. Using the method of moments [68], Eq. 5.128 is transformed into a set of ordinary differential equations by multiplication by v^k and integration over v, thereby obtaining after some manipulation the following expression for the time derivative of X_k

$$\frac{dX_k}{dt} = \frac{1}{2}\int_0^\infty\int_0^\infty [(u+v)^k - v^k - u^k]\beta(u,v)n(u,t)n(v,t)dudv$$

$$+ \int_0^\infty v^k G(v,t)n(v,t)dv - \int_0^\infty v^k R(v,t)n(v,t)dv$$

$$+ \int_0^\infty v^k S(v,t)dv \qquad (5.129)$$

where

$$X_k(t) = \int_0^\infty v^k \, n(v,t)dv \tag{5.130}$$

is the kth moment of the density function n(v,t).

To solve Eq. 5.130 some functional form must be assumed for n(v,t). Since atmospheric aerosols are observed to have log-normal size distibutions, several aerosol codes [68, 105-108] assign a log-normal distribution to n(v,t). Thus,

$$n(v,t) = \frac{1}{v} \frac{N(t)}{(2\pi)^{1/2}\sigma(t)} \exp\left\{ - \frac{\ell n\, v - \ell n\, \bar{v}(t)}{2\sigma(t)^2} \right\} \tag{5.131}$$

where N(t) = the number concentration of particles

$\bar{v}(t)$ = the geometric expected value for particle mass, i.e., $\bar{v} = \exp \mu$, where $\mu = E(\ell n\, v)$ and E denotes expected value,

$\sigma(t)$ = the logarithmic variance for particle mass, i.e., $\sigma(t)^2 = E[(\ell n\, v - \mu)^2]$,

which leads to [99]

$$X_k = N(t)\, v(t)^k \exp\left\{ \frac{1}{2} k^2 \, v(t) \right\} \tag{5.132}$$

and therefore

$$N(t) = X_o(t) \tag{5.133}$$

$$\bar{v}(t) = X_1(t)^2 \Big/ X_o(t)\, X_2(t)^{1/2} \tag{5.134}$$

$$\sigma(t)^2 = \ln \left[X_o(t)\, X_2(t) \Big/ X_1(t)^2 \right] \tag{5.135}$$

Accordingly, $N(t)$, $\bar{v}(t)$, and $\sigma(t)$, and thus the log-normal form of $n(v,t)$ can be determined at any time t by simultaneous solution of the time derivatives of the first three moments of the density function (Eq. 5.129).

Sectional Techniques. Imposition of a fixed functional form on $n(v,t)$, the particle number density function, can be avoided by integration over v, discretization of the range of $n(v,t)$ into sections, and assignment of some functional form to $n(v,t)$ within each section. When this is done $n(v,t)$ becomes a histogram of unconstrained form; and Eq. 5.128 transforms to,

$$\frac{dN_\ell}{dt} = \frac{1}{2}\sum_{i=1}^{\ell}\sum_{j=1}^{i}\int_{v_{i-1}}^{v_i}\int_{v_{j-1}}^{v_j}\theta\,\beta(u,v)n(u,t)n(v,t)dudv$$

$$-\sum_{i=1}^{m}\int_{v_{i-1}}^{v_i}\int_{v_{\ell-1}}^{v_\ell}\phi\,\beta(u,v)n(u,t)n(v,t)dudv$$

$$+\int_{v_{\ell-1}}^{v_\ell}G(v,t)n(v,t)dv - \int_{v_{\ell-1}}^{v_\ell}R(v,t)n(v,t)dv$$

$$+\int_{v_{\ell-1}}^{v_\ell}S(v,t)dv \qquad (5.136)$$

where N_ℓ is the number concentration of particles in section ℓ, $\ell = 1,2,....m$, m is the number of sections, and θ and ϕ are partitioning functions with the following properties

$\theta = 1$ if $v_{\ell-1} < u+v < v_\ell$ and 0 otherwise; and
$\phi = 1$ if $u+v > v_\ell$ and 0 otherwise

Assignment of a functional form to $n(v,t)$ within each section can be done in at least two different ways. The simplest approach assigns the same properties to all particles in a section (QUICK Approach). Alternatively, some particle property can be assumed to have a known distribution over the range of each section (MAEROS Approach).

QUICK Approach. In the QUICK code [67] Eq. 5.136 is further simplified by assignment of the same properties to all particles in a section (characteristic particle approximation). The use of charateristic particles has two effects. First, because all particles in section i have mass v_i and all particles in section j have mass v_j, $B(v_i,v_j)$ = constant; and second, N_ℓ the number concentration of particles in section ℓ is now given by

$$N_\ell = n(\bar{v}_\ell,t)(v_\ell - v_{\ell-1}) = \int_{v_{\ell-1}}^{v_\ell} n(v,t)dv$$

Together these two transformations eliminate the integrals in Eq. 5.136 yielding

$$\frac{dN_\ell}{dt} = \frac{1}{2} \sum_{i=1}^{\ell} \sum_{j=1}^{i} \theta B(\bar{v}_i,\bar{v}_j)N_i(\bar{v}_i,t)N_j(\bar{v},t)$$

$$- \sum_{i=1}^{m} \phi\, B(\bar{v}_i,\bar{v}_j)N_i(\bar{v}_i,t)N_\ell(\bar{v}_\ell,t) + G(\bar{v}_\ell,t)N_\ell(\bar{v}_\ell,t)$$

$$- R(\bar{v}_\ell,t)N_\ell(\bar{v}_\ell,t) + S(\bar{v}_\ell,t) \qquad (5.137)$$

Although the characteristic particle approximation greatly simplifies Eq. 5.136 by eliminating all integrals, this simplification complicates the form of θ and ϕ. The form of θ and ϕ becomes more complicated because for most sets of characteristic particle masses, the sum of two characteristic particle masses does not equal the mass of any other characteristic particle. Consequently, the partitioning functions θ and ϕ, when not equal to zero, can have fractional values,

$$\theta = f_\ell \text{ if } \bar{v}_{\ell-1} < \bar{v}_i+\bar{v}_j \leq \bar{v}_\ell \text{ and 0 otherwise; and}$$

$$\phi = f_\ell \text{ if } \bar{v}_i+\bar{v}_\ell > v_\ell \text{ and 0 otherwise}$$

and some expression must be selected to calculate the fraction, f_ℓ.

When section boundaries increase monotonically, it is easy to show [67] that the sum of any two characteristic particle masses needs to be apportioned over at most three consecutive sections, and into only two consequtive sections, if section boundaries are equispaced on the logarithm of particle mass. If section boundaries are chosen so that the mass $v = v_i + v_j$ of the agglomerated chacteristic particles $\bar{v}i$ and $\bar{v}j$ needs to be apportioned only over two consecutive sections, the value of the partitioning fraction f_ℓ can be determined by solving the following two equations

$$f_\ell \bar{v}_\ell + f_{\ell+1}\bar{v}_{\ell+1} = v \quad \text{where } \bar{v}_\ell < v < \bar{v}_{\ell+1}$$

and

$$f_\ell + f_{\ell+1} = 1$$

where the first equation conserves mass and the second conserves the number of agglomerated particles. When this is done, the following expression is obtained for f_ℓ,

$$f_\ell = \frac{\bar{v}_{\ell+1} - v}{\bar{v}_{\ell+1} - \bar{v}_\ell}$$

Griesmeyer et al. [109] have shown that this partitioning scheme leads to an artificial migration of mass toward larger sections that increases in magnitude as the spacing between characteristic particle masses increases. To avoid this artificial migration of mass, Griesmeyer et al. recommend that both the first and second moments of the distribution of particle mass be conserved, which means that f_ℓ is determined by solving

$$f_\ell \bar{v}_\ell + f_{\ell+1}\bar{v}_{\ell+1} = v \quad \text{where } \bar{v}_\ell < v < \bar{v}_{\ell+1}$$

and

$$f_\ell \bar{v}_\ell^{\,2} + f_{\ell+1}\bar{v}_{\ell+1}^{\,2} = v^2$$

where the second equation conserves the mean mass of the distribution. When this is done, the following expression is obtained for f_ℓ,

$$f_p = \frac{v}{\bar{v}_\ell} \frac{\bar{v}_{\ell+1} - v}{\bar{v}_{\ell+1} - \bar{v}_\ell}$$

When this second partioning scheme is used, Griesmeyer et al. [109] have shown that the time evolution of the particle distribution is not sensitive to the spacing of the characteristic particle masses. Alternatively, if one wishes to conserve the number of agglomerated particles ($f_\ell + f_{\ell+1} = 1$), many narrow sections can be used, which will suppress artificial mass migration but sacrifice computational speed.

Besides questions about how to partition agglomerate masses over size sections, the characteristic particle approach has one additional shortcoming. Because all particles in a section have the same properties, intrasectional agglomeration of particles driven by differences in particle velocities (i.e., gravitational and turbulent inertial agglomeration) can not be modeled by a characteristic particle approach. Therefore, for small numbers of sections, agglomeration may be significantly underestimated. Again, as was the case with partitioning factors, if many narrow sections are used, the problem can be suppressed by sacrificing computational speed.

MAEROS Approach. An alternative implementation of Eq. 5.136 has been formulated by Gelbard and Seinfeld [110], which allows tracking of aerosol components (aerosol mass having an identifiable composition). Two assumptions are made. First, that within any section ℓ of the aerosol distribution, v_k the mass of component k in any particle is given by

$$v_k = v \frac{Q_{\ell,k}}{Q_\ell}$$

where Q_ℓ is the total aerosol mass in section ℓ and $Q_{\ell,k}$ is the mass of aerosol component k in section ℓ. Second, that there is some aerosol property x, which has a known functional dependence $x = f(v)$ on particle mass v, where the form of f(v) is such that $vn(v)/f'(v)$ is a constant in each aerosol section ℓ. Accordingly,

$$f'(v)dv = dx$$

and, since $dQ = vn(v)dv$,

$$n(v)/f'(v) = Q_\ell/v(x_\ell - x_{\ell-1})$$

Given the preceding, Eq. 5.136 is now transformed as follows. All terms on the right hand side of the equation are multiplied by mass weighting factors ($u_k \cdot v_k$, v_k, or v'_k, where v'_k is the mass of a molecule of vapor k), second order terms are multiplied

by $f'(u)f'(v)/f'(u)f'(v)$ and first order terms by $f'(v)/f'(v)$, the following substitutions are made

u_k and v_k are replaced by $uQ_{j,k}/Q_j$ and $vQ_{i,k}/Q_i$

$f'(u)du$ and $f'(v)dv$ by dy and dx

$n(u)/f'(u)$ and $n(v)/f'(v)$ by $Q_j/u(x_j - x_{j-1})$

and $Q_i/v(y_i - y_{i-1})$

and the limits of integration are changed to $f(v_{i-1})$ to $f(v_i)$, thereby obtaining

$$\frac{dQ_{P,k}}{dt} = \frac{1}{2}\sum_{i=1}^{\ell}\sum_{j=1}^{i}\int_{f(v_{i-1})}^{f(v_i)}\int_{f(v_{j-1})}^{f(v_j)}(uQ_{j,k}Q_i + vQ_{i,k}Q_j)$$

$$\times \theta\beta(u,v)\frac{dydx}{uv(x_i - x_{i-1})(x_j - x_{j-1})}$$

$$-\sum_{i=1}^{m}\int_{f(v_{i-1})}^{f(v_i)}\int_{f(v_{P-1})}^{f(v_\ell)} Q_{\ell,k}Q_i\phi\beta(u,v)\frac{dydx}{uv(x_i-x_{i-1})(x_\ell-x_{\ell-1})}$$

$$+\int_{f(v_{\ell-1})}^{f(v_\ell)} v_k' Q_\ell G(v,t)\frac{dx}{u(x_\ell-x_{\ell-1})}$$

$$-\int_{f(v_{\ell-1})}^{f(v_\ell)} Q_{\ell,k} R(v,t)\frac{dx}{x_\ell-x_{\ell-1}} + \int_{f_{\ell-1}}^{v_\ell}\bar{v}_k S(v,t)dv \quad (5.138)$$

Eq. 5.138 can be further simplified by imposing a geometric constraint ($v_{\ell+1} \geq 2v_\ell$) on section boundaries, whereupon the partitioning factors θ and ϕ become single valued (0 or 1) and Eq. 5.138 reduces to the final form of the multicomponent sectional equations developed in Gelbard and Seinfeld [110],

$$\frac{dQ_{\ell,k}}{dt} = \frac{1}{2}\sum_{i=1}^{\ell-1}\sum_{j=1}^{\ell-1} {}^{1a}\tilde{\beta}_{i,j,\ell}Q_{j,k}Q_i + {}^{1b}\tilde{\beta}_{i,j,\ell}Q_{i,k}Q_j$$

$$- \sum_{i=1}^{\ell-1} {}^{2a}\bar{\beta}_{i,\ell} Q_i Q_{\ell,k} - {}^{2b}\bar{\beta}_{i,\ell} Q_\ell Q_{i,k} - \frac{1}{2} {}^{3}\bar{\beta}_{\ell,\ell} Q_\ell Q_{\ell,k}$$

$$- Q_{\ell,k} \sum_{i=\ell+1}^{m} {}^{4}\bar{\beta}_{i,\ell} Q_i + \bar{F}_{\ell,k} Q_\ell + {}^{1}\bar{G}_{\ell,k} Q_\ell \qquad (5.139)$$

$$- \sum_{i=1}^{s} {}^{2}\bar{G}_{\ell,i} Q_{\ell,k} - {}^{2}\bar{G}_{\ell-1,i} Q_{\ell-1,k} + {}^{3}\bar{G}_{\ell-1,k} Q_{\ell-1} + \bar{S}_{\ell,k} - \bar{R}_{\ell,k},$$

where the coefficients β, G, R, and S are given in Table 5.10.

Recommendations for MELCOR. Benchmark calculations [104] and comparisons to experiments [111] suggest that the method of moments approach is inferior to sectional approaches whenever agglomeration rates are rapid or sources or sinks (deposition processes) are important. Accordingly, MELCOR should use a sectional approach.

A basis for choosing either the QUICK approach [67] or the MAEROS approach [66,110] is less obvious. Both approaches allow multicomponent aerosols to be treated (the QUICK approach has been adapted in the MSPEC code [112] to treat multicomponent aerosols), which is essential if important aerosol components (e.g., CsI) are to be modeled. If the QUICK approach is selected, a scheme for partitioning agglomerate masses between characteristic particle masses must be selected. If the MAEROS approach is selected, when temperature and pressure ranges are broad, the suitability of linearly interpolating between precalculated values of single and double integrals should be examined. Although the QUICK approach can not directly treat intrasectional gravitational and turbulent inertial agglomeration, this shortcoming does not seem to necessitate the use of many narrow aerosol sections. Therefore, at least in principle, the QUICK approach should be more rapid than the MAEROS approach, because evaluation of single and double integrals is avoided. However, sensitivity studies using the MAEROS code indicate that its computational speed is adequate for MELCOR [113, 114]. Accordingly, either the multicomponent QUICK approach implemented in the MSPEC code or the MAEROS approach should be suitable for use in MELCOR. Because the MAEROS approach is well documented [110], and because the MAEROS code was developed at Sandia National Laboratories, availability of information and familiarity suggest that the MAEROS approach be used in MELCOR.

TABLE 5.10

Sectional Coefficients with Geometric Constraint [110]
$(v_{i+1} > 2v_i, i = 0,1,2,\ldots,m-1)$

Symbol	Remarks	Coefficient[a]
1. Coagulation		
$^{1a}\beta_{i,j,k}$	$i < k-1$ $j < k-1$	0
$^{1a}\beta_{i,k-1,k} - {}^{1b}\beta_{k-1,i,k}$	$1 < k \le m$ $i < k-1$	$\int_{x_{i-k}}^{x_i}\int_{f(v_{k-1}-v)}^{x_{k-1}} \frac{u\beta(u,v)}{uv(x_i - x_{i-1})(x_{k-1} - x_{k-2})}\,dydx$
	$1 < k \le m$ $i = k-1$	$\int_{x_{i-1}}^{f(v_i-v_{i-1})}\int_{f(v_{k-1}-v)}^{x_{k-1}} \frac{u\beta(u,v)}{uv(x_{k-1} - x_{k-2})^2}\,dydx + \int_{f(v_i-v_{i-1})}^{x_i}\int_{x_{k-2}}^{x_{k-1}} \frac{u\beta(u,v)}{uv(x_{k-1} - x_{k-2})^2}\,dydx$
$^{1b}\beta_{i,k-1,k} - {}^{1a}\beta_{k-1,i,k}$	$1 < k \le m$ $i < k-1$	$\int_{x_{i-1}}^{x_i}\int_{f(v_{k-1}-v)}^{x_{k-1}} \frac{v\beta(u,v)}{uv(x_i - x_{i-1})(x_{k-1} - x_{k-2})}\,dydx$
$^{2a}\beta_{i,k} - {}^{1a}\beta_{i,k,k+1}$	$1 < k \le m$ $1 \le i < k$	$\int_{x_{i-1}}^{x_i}\int_{f(v_k-v)}^{x_k} \frac{u\beta(u,v)}{uv(x_i - x_{i-1})(x_k - x_{k-1})}\,dydx$
$^{2b}\beta_{i,k}$	$1 < k \le m$ $1 \le i < k$	$\int_{x_{i-1}}^{x_i}\int_{x_{k-1}}^{f(v_k-v)} \frac{v\beta(u,v)}{uv(x_i - x_{i-1})(x_k - x_{k-1})}\,dydx$
$^{3}\beta_{k,k} - {}^{2}\beta_{k,k,k+1}$	$1 \le k \le m$	$\int_{x_{i-1}}^{f(v_k-v_{k-1})}\int_{f(v_k-v)}^{x_k} \frac{(u+v)\beta((u,v)}{uv(x_k - x_{k-1})^2}\,dydx + \int_{f(v_k-v_{k-1})}^{x_k}\int_{x_{k-1}}^{x_k} \frac{(u+v)\beta(u,v)}{uv(x_k - x_{k-1})^2}\,dydx$
$^{4}\beta_{i,k}$	$1 \le k < m$	$\int_{x_{i-1}}^{x_i}\int_{x_{k-1}}^{x_k} \frac{u\beta(u,v)}{uv(x_i - x_{i-1})(x_k - x_{k-1})}\,dydx$
2. Gas-to-particle conversion		
$^{1}G_{k,k}$	$1 \le k \le m$	$\int_{x_{k-1}}^{f(v_k-v_k^i)} \frac{v_k^i G_k(\bar{v}_1,\ldots,\bar{v}_6)}{v(x_k - x_{k-1})}\,dx$
$^{2}G_{k,i}$	$1 \le k \le m$	$\int_{f(v_k-v_i^i)}^{x_k} \frac{G_i(\bar{v}_1,\ldots,\bar{v}_6)}{(x_k - x_{k-1})}\,dx$
$^{3}G_{k,k}$	$1 \le k \le m$	$\int_{f(v_k-v_k^i)}^{x_k} \frac{v_k^i G_k(\bar{v}_1,\ldots,\bar{v}_6)}{v(x_k - x_{k-1})}\,dx$
3. Sources and removal mechanisms		
$S_{k,k}$	$1 \le k \le m$	$\int_{v_{k-1}}^{v_k} \bar{v}_k S(v,t)dv$
$R_{k,k}$	$1 \le k \le m$	$Q_{k,k}\int_{x_{k-1}}^{x_k} \frac{\bar{R}(v,t)}{(x_k - x_{k-1})}\,dx$

[a] $x_i = f(v_i)$. $u = f^{-1}(y), v = f^{-1}(x), \bar{v}_i = vQ_{k,i}/Q_k, n(v,t) = Q_k f'(v)/[v(x_k - x_{k-1})]$.

References

1. J. R. Welty, C. E. Wicks, and R. E. Wilson, Fundamentals of Momentum, Heat and Mass Transfer, John Wiley and Sons, 1984: a. p.478; b. p. 608; c. p. 592; d. p. 650; e. p. 492; f. p. 487; g. p. 196; h. p. 175.

2. C. J. Geankoplis, Mass Transport Phenomena, Ohio State University, Columbus, Ohio, p. 252, 1972.

3. Y. Jaluria, HMT The Science and Applications of Heat and Mass Transfer, Reports Reviews and Computer Programs, Vol. 5: Natural Convection Heat and Mass Transfer, Pergamon Press, p. 290, 1980.

4. T. K. Sherwood, R. L. Pigford, and C. R. Wilke, Mass Transfer, McGraw Hill Book Company, p. 215, 1975.

5. C. R. Wilke, Chem. Eng. Prog., 46, 95 (1950).

6. J. O. Hirschfelder, C. F. Curtis, and R. B. Bird, Molecular Theory of Gases and Liquids, Wiley, New York, p. 718, 1964.

7. C. R. Reid, J. M. Prausnitz and T. K. Sherwood, The Properties of Gases and Liquids, Third Ed., McGraw-Hill 1977: a. p. 548, b. p. 678.

8. J. O. Hirschfelder, R. B. Bird, and E. L. Spotz, "The Transport Properties of Gases and Gaseous Mixtures," Chem. Revs., 44, 205, (1949).

9. J. A. Dean, Ed., Lange's Handbook of Chemistry, McGraw-Hill, New York, p. 10-28, 1979.

10. T. R. Morrow and E. A. Mason, J. Phys. Chem. Ref. Data, 1, 3 (1972).

11. K. Denbigh, The Principals of Chemical Equilibrium, Cambridge University Press, Cambridge, p. 197, 1966.

12. Impell Corporation, Fission Product Transport in Degraded Core Accidents IDCOR 11.3 Report, Draft, p. 15, Nov. 1983.

13. D. Cubicciotti and B. R. Sehgal, "Vapor Transport of Fission Products in Postulated Severe Light Water Reactor Accidents," Nucl. Technol., 65, 266 (1984).

14. EPRI, Estimation of Fission Product and Core-Material Characteristics, IDCOR Technical Report 11.1, 11.4, and 11.5, p. 4-141, Draft Oct. 1983.

15. A. R. Taig, et al., "Interpretations of Experimental Results on the Interactions of Fission Product Vapours with Reactor Materials," Draft, 1984.

16. R. M. Elrick and R. A. Sallach, "Fission Product Chemistry in the Primary System," Proceed. Intl. Mtg., on Light Water Reactor Severe Accident Evaluation, Vol. 1, Cambridge, MA, Aug. 28-Sept. 1, 1983, p. 4.6 - 1, American Nuclear Society, LaGrange Park, IL, p. 4.6 - 1, 1983.

17. J. M. Genco, et al., Fission Product Deposition and Its Enhancement under Reactor Accident Conditions: Deposition on Primary System Surfaces, BMI-1863, March 1969.

18. S. L. Nicolose and P. Baybutt, Vapor Deposition Velocity Measurements and Correlations for I_2 and C_sI, NUREG/CR-2713, BMI-2091, Battelle Columbus Laboratories, Columbus, OH, May 1982.

19. P. E. Wagner, "Aerosol Growth by Condensation," in Aerosol Microphysics II, Chemical Physics of Microparticles, W. H. Marlow, Ed., Springer-Verlag, New York, NY, 1985, p. 129.

20. N. A. Fuchs in Proceedings of the 7th Int. Conf. on Condensation and Ice Nuclai, Prague and Vienna, J. Podzimek Ed., Academia, Prague, 1969, p. 10.

21. D. C. Sahni, J. Nucl. Energy A/B, 20, 915 (1966).

22. B. J. Mason, The Physics of Clouds, Clarendon, Oxford, 1971, p. 24.

23. H. R. Byers, Elements of Cloud Physics, Univ. Chicago, Chicago, 1965, p. 109.

24. C. F. Clements, Aerosol Growth in Vapour-Gas Mixtures Cooled Through Surfaces, AERE-TP-897, UKAEA, Atomic Energy Establishment, Harwell, England, May 1982.

25. J. R. Hidy and G. M. Brock, The Dynamics of Aerocolloidal Systems, Pergamon Press, 1970: a. p. 15; b. p. 147, c. p. 341.

26. J. F. van de Vate and H. M. ter Brink, "The Boundary Layer for Diffusive Aerosol Deposition onto Walls." Proceedings of the CSNI Specialists Meeting on Nuclear Aerosols in Reactor Safety, NUREG/CR-1724, ORNL/NUREG/TM-404, CSNI-45, October 1980.

27. M. Knudsen and S. Weber, Ann. Physik, 36, 982 (1911).

28. R. A Millikan, Phys. Rev., 22, 1 (1923).

29. W. F. Phillips, Phys. Fluids, 18, 1089 (1975).

30. N. A. Fuchs, Mechanics of Aerosols, Pergamon, New York, 1964: a. p. 27; b. p. 159; c. p. xxx; d. p. xxx; e. p. xxx; f. p. xxx; g. p. xxx;

31. C. N. Davies, Proc. Phys. Soc., 57, 18 (1945).

32. J. Mattanch, Z. Phys, 32, 439 (1925).

33. G. Monch, Phys. Z., 34, 77 (1933).

34. C. N. Davies, Aerosol Science, Academic Press, New York, 1966, p. 417.

35. S. K. Friedlander, Smoke, Dust and Haze: Fundamentals of Aerosol Behavior, John Wiley and Sons, 1977.

36. P. R. Owen, "Dust Deposition from a Turbulent Air Stream." Air-Water Pollut., 3, 8 (1960).

37. C. N. Davies, Ann. Occup. Hyg., 8, 239 (1965).

38. C. N. Davies, Proc. Roy. Soc. London, A289, 235 (1966).

39. A. C. Wells and A. C. Chamberlain, "Transport of Small Particles to Vertical Surfaces." Brit. J. Appl. Phys., 18, 1793 (1967).

40. S. K. Beal, "Deposition of Particles in Turbulent Flow on Channel or Pipes." Nucl. Sci. Eng., 40, 1 (1970).

41. B. Y. H. Liu and T. A. Ilori, "Inertial Deposition of Aerosol Particles in Turbulent Pipe Flow." ASME Symposium on Flow Studies in Air and Water Pollution, Atlanta, Georgia, June 20-22, 1973, p. 103.

42. L. W. B. Browne, Atmos. Environ., 8, 801 (1974).

43 G. A. Sehmel, "Particle Deposition from Turbulent Airflow," J. Geophys. Res.., 75, 1766 (1970)

44. J. Laufer, The Structure of Turbulence in Fully Developed Pipe Flow, NACA Report 1174, 1954.

45. C. S. Lin et al., Ind. Eng. Chem., 45, 636 (1953).

46. T. L Montgomery and M. Corn, "Aerosol Deposition in a Pipe with Turbulent Air Flow." Aerosol Sci., 1, 185 (1970).

47. B. Y. H. Liu and J. K. Agarwal, "Experimental Observation of Aerosol Deposition in Turbulent Flow." J. Aerosol Sci., 5 (1974).

48. J. Wildi and H. Thomann, J. Aerosol Sci., 14, 615 (1983).

49. J. A. Gieseke et al., Measurement of Aeosol Deposition Rates in Turbulent Flows, NUREG/CR-1264, BMI-2041, Battelle Columbus Laboratories, Columbus, OH, 1980.

50. M. W. Reeks and G. Skyrme, "The Dependence of Particle Deposition Velocity on Particle Inertia in Turbulent Pipe Flow." J. Aerosol Sci., 7, 485 (1976).

51. S. Ostrach, "Laminar Flows with Body Forces," in Theory of Laminar Flows, F. K. Moore, Ed., Princeton Uniersity Press, Princeton, NJ, 1964, p. 528.

52. C. W. Oseen, "Neuere Methoden Und Ergebnisse in der Hydrodynamik." Liepzig, Vol. 16, 1927.

53. L. Kylachko, Otopl. i ventil., 4, (Page) (1934).

54. F. F. Abraham, "Functional Dependence of Drag Coefficient of a Sphere on Reynolds Number." Phys. Fluids, 3, 194 (1970).

55. Clift, Grace and Weber, Bubbles, Drops and Particles, Academic Pr., 1978.

56. L. Waldmann, "Uber die Kraft eines in homogen Gases aufkleine suspendierte kugeln," Z. Naturforsch, 14a, __ 1959.

57. B. V. Deryaguin and S. P. Bakanov, Koll. Zh., 21, 377 (1959).

58. J. R. Brock, "The Thermal Force in the Transition Region." Colloid Interface Sci., 23, 448 (1967).

59. P. L. Bhatnagar, E. P. Gross, and M. Krook, "A Model for Collision Processes in Gases. I. Small Amplitude Processes in Charged and Neutral One-Component Systems," Phys. Rev., 94, 511 (1954).

60. S. Jacobsen and J. R. Brock, "The Thermal Force on Spherical Sodium Chloride Aerosols." J. Colloid Sci., 20, 544, (1965).

61. P. S. Epstein, "Zur Theorie des Radiometers," Z. Physik, 54, 537, (1929).

62. J. R. Brock, "On the Theory of Thermal Forces Acting on Aerosol Particles." Colliod Sci., 17, 768 (1962).

63. B. V. Deryaguin, S. P. Bakanov and J. I. Rabinovich, "Theory of Thermophoresis of Aerosol Particles and Its Verification", Proc. Natl. Conf. Aerosols, 1st, Liblice near Prague, 1962

64. L. Talbot, "Thermophoresis - A Review." Proceedings from the Twelfth International Symposium on Rarefied Gas Dynamics, Charlottesville, VA., July 7-11, 1980.

65. F. Prodi, G. Santachiara, and V. Prodi, "Measurements of Thermophoretic Velocities of Aerosol Particles in the Transition Region." J. Aerosol Sci., 10, 421 (1979).

66. F. Gelbard, MAEROS User's Manual, SAND80-0822, NUREG/CR-1391, Sandia National Laboratories, December 1982.

67 H. Jordan, P. M. Schumacher, and J. A. Gieseke, QUICK User's Manual, NUREG/CR-2105, BMI-2082:R7, Battelle Columbus Laboratories, May 1981.

68. J. A. Gieseke, K. W. Lee, L. D. Reed, Haarm-3 User's Manual, BMI-NUREG-1991, Battelle Columbus Laboratories, January 1978.

69. C. Y. Cha and B. J. McCoy, "Thermal Force on Aerosol Particles," Phys. Fluids, 17, (1974).

70. B. V. Deryaguin, Y. I. Yalamov, and R. J. Storozhilova, "Diffusiophoresis of Large Aerosol Particles." J. Colloid Interface Sci., 22, 117, (1966).

71. G. Nishio, S. Kotani and K. Takahashi, "Thermophoretic Deposition of Aerosols in a Heat Exchanger Pipe," Ind. Eng. Chem. Process Design Develop., 13, ___ (1974).

72. P. Rosenblatt and V. K. LaMer, "Motion of a Particle in a Temperature Gradient: Thermal Repulsion as a Radiometer Phenomenon," Phys. Rev., 70, , (1946).

73. K. H. Schmitt, Z. Naturforsch, Vol. 14a, No. 870, 1959.

74. C. F. Schadt and R. D. Cadle, "Thermal Forces on Aerosol Particles," Journal of Physical Chemistry, Vol. 65, 1961.

75. A. I. Storozhilova and G. I. Scherbina, "Measuring the Rate of Thermophoresis for Large Aerosol Particles and Use of the Results for Determining the Coefficient of Thermal Glide of a Gas," Academy of Sciences (USSR) Proceedings Physical Chemistry Sections Translated from Doklady Akademii Nauk SSSR, 217, 386 (July).

76. L. Talbot, R. K. Cheng, R. W. Schefer, and D. R. Willis, "Thermophoresis of Particles in a Heated Boundary Layer," J. Fluid Mechanics, Vol. 101, No. 4, pp. 737-758, 1980.

77. P. J. Whitmore and A. Meisen, "Diffusiophoretic Particle Collection Under Turbulent Conditions." J. Aerosol Sci., 9, 135 (1978).

78. K. H. Schmitt and L. Waldmann, "Untersuchungen an Schwebstoffteilchen im Diffundierenden Gasen." Z. Naturforsch., 15a, 843 (1960).

79. B. V. Deryaguin and S. P. Bakanov, "The Theory of the Motion of Small Particles in a Diffusion Field," Dokl. Akad. Nauk. SSSR, 117, 959 (1957).

80. T. W. Horst, "A Review of Particle Transport in a Condensing Steam Environment," BNWL-848, UC-80, Reactor Technology, (page) June 1968.

81. I. H. Dunbar, "The Role of Diffusiophoresis in LWR Accidents", Proceedings from the International Meeting on Light Water Reactor Severe Accident Evaluation, Cambridge, MA, 1983.

82. B. K. Annis and E. A. Mason, "Theory of Thermo diffusiophoresis of Spherical Aerosol Particles." Aerosol Sci., 6, 105 (1975).

83. M. V. Smoluchowski, Phys. Chem., 92, 144 (1918).

84. R. A. Millikan, "Coefficients of Slip in Gases and the Law of Reflection of Molecules from the Surfaces of Solids and Liquids." Phys. Rev., 21, 217 (1923).

85. M. Sitarski and J. H. Seinfeld, "Brownian Coagulation in the Transition Regime", J. of Colloid and Interface Science, Vol. 61, No.2, p. 261, September 1977.

86. A. Chatterjee, M. Kerker and D. D. Cooke, "Brownian Coagulation of Aerosols in the Transition Regime," J. Colloid Interface Sci., 53., 71 (1975).

87. K. W. Lee and J. A. Gieseke, "Note on the Approximation of Interceptional Collection Efficiencies," J. Aerosol Sci., 11, 335 (1980).

88. H. R. Pruppacher and J. D. Klett, Microphysics of Cloud Precipitation, D. Reidel, 1978.

89 G. M. Hidy and J. R. Brock, The Dynamics of Aerocolloidal Systems, Pergamon Press, 1970, p. 318.

90. I. Langmuir, "The Production of Rain by a Chain Reaction in Cumulus Clouds at Temperatures above Freezing." J. Meteor., 5, 175 (1948).

91. G. Hetsroni, Handbook of Multiphase Systems, Mcgraw Hill Book Company and Hemisphere Pub. Co., 1982.

92. K. W. Lee and J. A. Gieseke, "Collection of Aerosol Particles by Packed Beds," Environ. Sci. Technol., 13, 466 (1979).

93. D. Rimberg and Y.M. Peng, "Aerosol Collection by Falling Droplets." Air Pollution Control and Design Handbook, Part 2, incomplete.

94. G. Pertmer and S. K. Loyalka, Gravitational Collision Efficiency of POST-HCDA LMFBR Aerosols, to be published as an NRC report.

95. J. A. Gieseke, et al., Radionuclide Release Under Specific LWR Accident Conditions: Vol. 1, BMI-2104, Battelle Columbus Laboratories, July 1983.

96. K. D. Bergeron, et al., User's Manual for CONTAIN 1.0: A Computer Code for Severe Nuclear Reactor Accident Containment Analysis, SAND84-1204, NUREG/CR-4085, January 1985.

97. P.G. Saffman and J.S. Turner, "On the Collision of Drops in a Turbulent Cloud." J. Fluid Mechanics, Vol. 1, p. 16, 1956.

98. V. G. Levich, Physiochemical Hydrodynamics, Prentice-Hall, Inc., Englewood Cliffs, NJ, 1962.

99. R. J. Lipinski et al., Uncertainty in Radionuclide Release Under Specific LWR Accident Conditions: Vol. 2, SAND84-0410, Sandia National Laboratories, Febuary 1985.

100. C. D. Leigh, et al., Analyses of Plume Formation, Aerosol Agglomeration and Rainout Following Containment Failure, SAND84-2581, NUREG/CR-4222, Sandia National Laboratories, Albuquerque, New Mexico, March, 1985.

101. H. Tennekes and J.M. Hales, A First Course in Turbulence, 6th Ed., MIT Press, Cambridge, Mass., 1980.

102. R. L. Drake, "A General Mathematical Survey of the Coagulation Equation," International Reviews in Aerosol Physics and Chemistry, Volume 3, Topics in Current Aerosol Research (Part 2), G. M. Hidy and J. R. Brock, Eds., Pergamon, New York, 1972, p. 201.

103. S. K. Loyalka, "Mechanics of Aerosols in Nuclear Reactor Safety: A Review," Prog. Nucl. Energy, 12, 1 (1983).

104. I. H. Dunbar, et al., Comparison of Sodium Aerosol Codes, Commission of European Communities: Nuclear Science and Technology, EUR 9172 En, 1984.

105. Castleman, Horn, and Lindaauer;1969(TRAP)

106. Hubner, Vaughan, and Baurinosh; 1973 (HAA-3)

107. H. J. Jordan, et al., TRAP-MELT User's Manual, NUREG/CR-0632, BMI-2017, R3, 4, February, 1979.

108. Nishio, Kitani, and Takada;1975 (ABC-3)

109. J. M. Griesmeyer, et al., "A Dynamic Intragranular Fission Gas Behavior Model." Nucl. Engineer. Design, 55, 69 (1979).

110. F. Gelbard and J. H. Seinfeld, "Simulation of Multicomponent Aerosol Dynamics." J. Colloid Interface Sci., 78, (1980).

111. Hilliard

112. Jo82

113. J. C. Helton et al., Uncertainty and Sensitivity Analysis of a Upper Plenum Test Problem for the MAEROS Aerosol Model, NUREG/CR-4460, SAND85-2196, Sandia National Laboratories, Albuquerque, NM, June 1986.

114. J. C. Helton et al., Uncertainty and Sensitivity Analysis of a Dry Containment Test Problem for the MAEROS Aerosol Model, NUREG/CR-4487, SAND-2795, Sandia National Laboratories, Albuquerque, NM, June 1986.

CHAPTER 6

ENGINEERED SAFETY FEATURES

J. L. Sprung

6.1 Introduction

All Light Water Reactors are equipped with a variety of engineered safety features (ESFs), which are designed to mitigate the consequences of a severe accident. Although all ESFs, if operable and not bypassed, will influence fission product behavior indirectly due to their impacts on thermal-hydraulic conditions, the following five ESFs can have major direct impacts on the concentrations of gas borne fission products, both vapors and aerosols: filters, fan coolers, ice condensers, scrubbing pools, and sprays. Therefore, MELCOR should model the effects of these ESFs on fission product behavior.

The way an ESF is modeled by the thermal-hydraulic modules of the MELCOR code system will determine how that ESF is modeled by the fission product behavior modules of MELCOR. MELCOR's thermal-hydraulic modules will model an ESF either as a node in a flow path or as one or more control volumes. If MELCOR's thermal-hydraulic modules model an ESF as a node in a flow path, then a decontamination factor should be used to model the impact of the ESF on fission product behavior. Alternatively, if MELCOR's thermal hydraulic modules model an ESF as one or more control volumes, then the impact of that ESF on fission product behavior should be modeled mechanistically.

Mechanistic modeling of fission product behavior within the control volumes used to represent an ESF can be accomplished in two ways. If the fission product processes operable within the ESF are adequately modeled by MELCOR's standard set of fission product behavior models (the models described in chapters 2 through 5 of this report), then these models can be applied to the ESF control volumes just as they would be applied to any other control volume. However, if ESF operation introduces a new process (e.g., bubble transport through a pool during pool scrubbing) or substantially alters a modeled process (e.g., gravitational agglomeration and deposition during spray operation), then additional mechanistic fission product models will be needed to describe the new or altered processes.

6.2 Decontamination Factor Models.

The Decontamination Factor of an ESF is defined as follows:

$$DF_{k,ESF} = \frac{\text{mass species k leaving ESF}}{\text{mass species k entering ESF}}$$

The decontamination factor of an ESF for species k is related to the removal efficiency of the ESF for species k as follows:

$$\eta_{k,ESF} = 1 - \frac{1}{DF_{k,ESF}} \qquad 6.1$$

where

$$\eta_{k,ESF} = \frac{\text{mass species k removed ESF}}{\text{mass species k entering ESF}}$$

Thus, given flow from control volume i through an ESF to control volume j, the mass loss rate of fission product species k from control volume i due to operation of the ESF is given by:

$$\frac{dM_{k,i}}{dt} = - \frac{F_{ESF}}{V_i} M_{r,i} \qquad 6.2$$

The rate of deposition of species k mass in the ESF is given by:

$$\frac{dM_{k,ESF}}{dt} = \eta_{k,ESF} \frac{F_{ESF}}{V_i} M_{k,i} \qquad 6.3$$

And the rate of gain of mass of species k in the downstream control volume j is given by:

$$\frac{dM_{k,j}}{dt} = (1-\eta_{k,ESF}) \frac{F_{ESF}}{V_i} M_{k,i} \qquad 6.4$$

where

F_{ESF} = volumetric flow rate through the ESF

V_i = volume of control volume i

$M_{k,i}$ = gas borne mass of species k in control volume i

and $M_{k,ESF}$ = mass of species k deposited in the ESF

If the ESF exhausts to the same control volume from which it takes flow, then the mass loss rate of species k from that control volume due to operation of the ESF is given by:

$$\frac{dM_{k,i}}{dt} = - \eta_{k,ESF} \frac{F_{ESF}}{V_i} M_{k,i} \qquad 6.5$$

6.3 Filters

Because passage of containment atmosphere through a filter does not remove significant amounts of heat or cause significant amounts of steam to condense from that atmosphere, filters can be modeled as a node in a flow path in the thermal-hydraulic portions of the MELCOR code system. Accordingly, the fission product modules of MELCOR should model filters using the decontamination factor approach described above.

When fission product removal by a filter is modeled by a decontamination factor, release of decay heat by filter deposits and the flow resistance of deposits also need to be modeled. Because MELCOR's thermal-hydraulic modules will not add or remove heat from a flow path, heat generated by decay of fission products deposited on a filter in a flow path should be added to the bulk gases in the downstream control volume at a rate consistent with the flow rate of bulk gases through the filter.

For low filter mass loadings, filter flow rates and efficiencies will generally be available from manufacturer's specifications. However, as filter mass loadings increase, bulk gas flow through the filter will decrease and filter efficiency will increase. Although filter efficiency increases as filter loadings increase, this effect can probably be neglected, since it is likely to be significant only for loadings large enough to cause flow through the filter to be negligible.

Decrease of filter flow rates with increase of filter mass loadings is not negligible. Moreover, for large mass loadings the functional dependence of flow rate on filter mass loading is generally not available from the filter manufacturer's specifications, and is unlikely to be linear. Therefore, the dependence of flow rate on mass loading will have to be provided by the user as input to the code, and the effect of changing the form of the dependence examined during sensitivity studies.

6.4 Fan Coolers

A fan cooler both removes heat and condenses steam from the bulk gases flowing though it. If the steam condensation rate within the fan cooler is high, diffusiophoretic deposition of

vapors or aerosols transported with the bulk gas flow will be significant. Removal of vapors and aerosols by other deposition mechanisms may also be significant, if the fan cooler has a large internal surface area.

When a fan cooler has a large internal surface area, heat removal and steam condensation may not be modeled adequately, unless the fan cooler is modeled as a control volume containing a heat slab, rather than as a node on a flow path. A large internal volume, one comparable to the volumes of other compartments, is also likely to require modeling as a control volume.

When thermal-hydraulic processes require that a fan cooler be represented by a control volume, fission product removal within the fan cooler should be modeled mechanistically. Since the fission product processes operable within a fan cooler are not likely to differ in kind or degree from those operable within a general control volume (diffusiophoretic deposition will be enhanced, but still adequately modeled by the equations recommended in Chapter 5), adequate mechanistic modeling can be attained by application of the standard set of fission product behavior models (the models described in Chapter 5 of this report) to the fan cooler control volume. Degradation of cooler efficiency due to build-up of deposits on cooling surfaces should be modeled in the thermal-hydraulic portions of MELCOR using cooler mass loadings calculated by the fission product portions of the code.

When thermal-hydraulic processes permit modeling of a fan cooler as a node on a flow path, fission product behavior within the fan cooler should be modeled using a decontamination factor approach. Because MELCOR's thermal-hydraulic modules will not add or remove heat from a flow path, when a fan cooler is modeled as a node on a flow path, the steam and heat that would in actuality be removed within the fan cooler should in MELCOR be removed from the downstream control volume, decay heat from fission products deposited within the fan cooler should be added to the downstream control volume, the water that condenses in the fan cooler should be added to those control volumes to which condensate flows from the fan cooler, and the rate of removal of heat from the downstream control volume should depend on the mass of fission products deposited within the fan cooler.

When a decontamination factor approach is used to model a fan cooler, the efficiency of the fan cooler must either be supplied as input to the code or be calculated assuming that fission product removal in the fan cooler is dominated by diffusiophoretic deposition due to steam condensation within the cooler. If the latter approach is taken, then the following equations may be used to approximate the removal efficiency of fission product species k:

$$\eta_{k,ESF} = \text{factor} \times \frac{W_s}{F_{ESF}\ \rho_g} \qquad 6.6$$

$$\text{factor} = \frac{M_s^{1/2}}{X_s M_s^{1/2} + X_g M_g^{1/2}} \quad \text{for aerosol species}$$

$$\text{factor} = \frac{k_{rx}}{k_{rx} + k_{tr}} \quad \text{for non-condensible vapors}$$

$$\text{factor} = 1 - \frac{p_{v,sat}}{\rho_v} \quad \text{for non-reactive, condensable vapors}$$

$$k_{trans} = \frac{W_s}{V_{ESF}\ \rho_g}$$

where M_s and M_g, X_s and X_g, and ρ_g are the molecular weights (M), mole fractions (X), and mass density (ρ) of the steam (s) and non-condensible gases (g) in the gas stream flowing through the fan cooler; V_{ESF}, F_{ESF}, and W_s are the volume of the cooler, the volumetric flow rate of the gas stream, and the removal rate of steam mass due to condensation from that gas stream; and $\rho_{k,sat}$ and ρ_k, and $k_{rx,k}$ and $k_{tr,k}$ are the saturated and actual mass densities, and the reaction and transport rate constants of fission produce vapor k, which is being transported through the cooler by the gas stream.

6.5 Ice Condensers

Should a severe accident occur at a PWR equipped with an ice condenser, until its ice has melted, the ice condenser will remove substantial amounts of steam and heat from the ice condenser containment of the PWR. Therefore, an ice condenser will be modeled as one or more control volumes by MELCOR's thermal-hydraulic modules, and thus should be modeled mechanistically by the fission product behavior portions of MELCOR.

A mechanistic model of fission product removal by an ice condenser has recently been developed and implemented in the computer code ICEDF by Winegardner et al. [1,2]. ICEDF treats removal of aerosols and molecular iodine (I_2).

Removal of molecular iodine is assumed to occur predominantly by partitioning of iodine vapor between the gas phase and liquid water (i.e., deposition to dry surfaces is thought to be relatively unimportant). The partition coefficient H for molecular iodine is determined by simultaneous solution of the following four equilibria,

$$I_2(g) = I_2(aq) \qquad K_1 = [I_2(aq)]/[I_2(g)]$$

$$I_2(aq) + I^- = I_3^- \qquad K_2 = [I_3^-]/([I_2(aq)][I^-])$$

$$I_2(aq) + H_2O = H^+ + I^- + HOI \qquad K_3 = [H^+][I^-][HOI]/[I_2(aq)]$$

$$I_2(aq) + H_2O = H_2OI^+ + I^- \qquad K_4 = [H_2OI^+][I^-]/[I_2(aq)]$$

using the following values for the equilibrium constants K_1 through K_4.

Constant	Value	
	at 25°C	at 100°C
K_1	83	91
K_2	768	305
K_3	4.0×10^{-13}	5.0×10^{-11}
K_4	1.2×10^{-11}	3.9×10^{-11}

Mechanisms for aerosol removal due to deposition driven by gravitational settling, diffusiophoresis, thermophoresis, diffusion (both Brownian and eddy), turbulence, inertial impaction, and interception are implemented in ICEDF. The equations used to model deposition due to gravitational settling, diffusiophoresis, and thermophoresis [1-3] are essentially identical to those recommended in Chapter 5 for the modeling of aerosol deposition in a general control volume. First order rate constants (k_i) for deposition due to diffusion, turbulence, inertial impaction, and interception are expressed as the product of the process collection efficiency (E_i), deposition velocity (v_i), and deposition surface area (A_i) divided by the compartment volume (V)

$$k_i = (E_i v_i A_i)/V \qquad 6.7$$

Collection Efficiencies. For particle impaction onto ice basket strips, ICEDF uses an empirical fit to experimental data for the dependence of the collection efficiency of cylinders upon Stokes number (Stk):

$$E_i = \left[\frac{Stk}{Stk + 0.5}\right]^2 - 0.04 \qquad 6.8$$

For particle interception by basket stripts, ICEDF uses the following theoretical expression for the collection efficiency for particle interception by cylinders [4]:

$$E_i = 2\, d_p/d_c \qquad 6.9$$

where d_p is the particle diameter and d_c the cylinder diameter. For deposition onto basket strips due to diffusion in gas flows around the strips, ICEDF uses the following expression for E_i,

$$E_i = Pe^{-1} + 1.727\, Re^{1/6}\, Pe^{-2/3} \qquad 6.10$$

In this expression, which was developed from a heat transfer/mass transfer analogy applicable to filter fibers [1,5], Pe is the Peclet number and Re is the Reynolds number. For all other deposition processes, unit collection efficiencies are assumed.

Deposition Velocities. ICEDF contains no expressions for deposition velocities for impaction or interception. For scoping calculations, the authors of ICEDF estimated impaction and interception deposition velocities, from forced and naturally convected gas flows, to be about 0.3 m/s. For deposition due to diffusion in forced or naturally convected gas flows over flat surfaces or through ice channels, the authors of ICEDF recommend that deposition velocities be calculated using mass transfer/heat transfer analogies for flat plates [6-8a] or packed beds [8b]. For deposition to ice surfaces due to turbulent transport through ice channels, ICEDF calculates a deposition velocity using the following empirical correlation for vertical tubes developed by Sehmel [9]:

$$v_i/U^* = 1.47 \times 10^{-16}\, \rho_p^{1.01}\, R^{2.10}\, Re^{3.02}$$

where U* is the friction velocity, ρ_p is the particle density, R is the ratio of the particle diameter to the tube diameter, and Re is the Reynolds number.

Structural Surface Areas. The following table [1] presents typical structural surface areas for an ice condenser:

Structure	Area (m^2)
Compartment Walls and Heavy Support Structures	
Vertical surfaces	3.98×10^3
Upward-facing horizontal surfaces	6.46×10^2
Downward-facing horizontal surfaces	6.46×10^2
Ice Basket Support Frames	
Vertical surfaces	1.33×10^4
Upward-facing horizontal surfaces	2.95×10^2
Downward-facing horizontal surfaces	2.95×10^2
Ice Baskets	
Outer walls, vertical surfaces	1.04×10^4
Inner walls, vertical surfaces	1.04×10^4
Hole edges, vertical surfaces	2.48×10^3
Hole edges, upward-facing horizontal surfaces	1.24×10^3
Hole edges, downward-facing horizontal surfaces	1.24×10^3

Surface Area of Ice. From the surface to volume ratio of ice flakes (0.625 cm^{-1} when first formed), the packing fraction of the ice baskets (0.6 at filling), and the total volume of the baskets (2.0×10^5 m^2), the surface area of the ice in a freshly filled ice condenser may be estimated [1] to be 7.6×10^5 m^2. From filling to the time of accident initiation this surface area changes slowly due to glaciation and sublimation. After accident initiation the ice surface area changes rapidly due to melting. Accordingly, the surface area of ice basket ice is not easy to calculate.

Deposition Areas. Provided that flow rates do not prevent gravitational settling, deposition driven by gravitational settling will occur onto all upward-facing surfaces including upward-facing ice surfaces. Diffusiophoretic deposition will occur onto all ice surfaces on which steam is condensing. Thermophoretic deposition will occur principally to ice surfaces, because temperature gradients will be largest next to these surfaces. Impaction and interception will occur principally onto surfaces that are perpendicular to gas flows (e.g., the edges of ice basket lattice strips). Diffusive deposition will take place onto all available surfaces.

Relative Importance of Deposition Mechanisms. Scoping calculations and sensitivity studies performed with ICEDF [1,2,10] suggest

(1) when compared to other deposition mechanisms, turbulent deposition is negligible under all conditions, thermophoretic deposition is important

only when inlet gas temperatures are unusually high, and deposition due to impaction and interception is generally unimportant;

(2) sedimentation controls deposition for particles with radii larger that 2 μ; when steam condensation is significant, diffusiophoresis dominates deposition for particles with radii less than 2 μ; and diffusive deposition is always important for particles with radii smaller that 0.1 μ;

(3) the large structural surface areas of an ice condenser cause deposition due to sedimentation and diffusion to be substantial (even after all of the ice has melted).

Because inertial impaction and interception are generally unimportant, these conclusions suggest that the removal mechanisms recommended in Chapter 5 for modeling particle deposition in a general control volume will be quite adequate for the treatment of deposition in an ice condenser.

6.6 Water Pool Scrubbing

During a severe LWR accident, if bulk gases are transported through water pools, vapors and aerosols will be removed from the bulk gases by pool scrubbing. Pool scrubbing would occur during PWR accidents, if bulk gases were transported through the quench tank, or through the pressurizer surge line (as happened at TMI-2). By design, in BWRs bulk gases are vented to the suppression pool in order to condense steam and to remove fission product vapors and aerosols by pool scrubbing. Pool scrubbing will also occur when bulk gases flow through water lutes in reactor piping.

Depending on the amounts of steam and heat removed during the transport of bulk gases through a water pool, the thermal-hydraulic modules in MELCOR will model a structure that contains a water pool either as a control volume or as a node in a flow path. Small structures that contain either small pools (e.g., pipes with water lutes) or shallow pools (short flow paths for bulk gases) will be modeled as nodes in flow paths. Structures that contain large pools with long gas flow paths through the pool will be modeled as control volumes.

If a structure, that contains a small or shallow water pool, is modeled as a node in a flow path, removal of vapors and aerosols during transport through that flow path should be modeled using the decontamination factor approach described

above with the value for the decontamination factor specified via code input. If a structure, that contains a large water pool with a long gas transport path through that pool (e.g., a BWR suppression pool), is modeled as a control volume, then fission product behavior within that control volume should be modeled mechanistically.

Mechanistic modeling of fission product behavior within a control volume that contains a large water pool may be divided into two parts: fission product behavior in the bulk gas space above the pool, and fission product behavior in the bulk gas stream during transport through the pool. Mechanistic treatment of fission product behavior in the bulk gas space should be adequately represented using the standard set of models described in Chapters 3 through 5. Additional models are required to mechanistically treat fission product behavior in the gas stream during transport through the pool.

Removal of aerosols from gas streams by bubbling through water pools has been examined theoretically [11-17] and experimentally [18,19], and in order to develop the SPARC [20] and SUPRA [21,22] models of fission product scrubbing in BWR suppression pools. Review of this literature suggests that fission product removal by bubbling involves four phenomenological regimes: an injection regime, a breakup regime, a bubble rise regime, and an exit regime. Within the injection regime, steam and non-condensable gases enter the water pool either as a jet that sheds globules, or by sequential formation on and detachment of globules from the inlet vent. Within the breakup regime, detached globules shatter into bubble swarms. Within the bubble rise regime, bubbles in the swarm grow by coallescence to unstable sizes that shatter into smaller bubbles. And within the exit regime, bubbles burst from the surface into the gas space above the pool.

Pool Hydrodynamics. The hydrodynamics of bubbling is too complicated to be modeled exactly. Some simplifying assumptions are required. In the SPARC [20] and SUPRA [21,22] codes, fission product behavior during transport through the pool is assumed to depend upon but not affect pool hydrodynamics. Pool hydrodynamics is modeled in three stages: entrance effects, bubble rise, and exit effects. The hydrodynamic behavior of the stream of steam and non-condensable gases upon entrance into the water pool is modeled using empirical data. Bubble rise is modeled assuming (1) that bubbles do not interact, (2) that the water pool is stationary, and (3) that there is no circulation of water in the bubble/pool interface (stationary film model). Heat and mass transfer (steam condensation and evaporation) at the bubble/pool interface is modeled using dimensionless heat and mass transfer correlations. Transfer of water to the gas space above the pool due to bubble breaking or evaporation upon bubble exit from the pool is neglected.

Injection Regime. Pool scrubbing experiments [14] conducted at Battelle Columbus Laboratories suggest that gas entrance into a water pool as a jet or by formation of a gas globule on the inlet vent depends upon the Weber number of the inlet vent, We_I, where,

$$We_I = U_g^2 \rho_\ell D_I / \sigma_\ell \qquad 6.11$$

U_g = velocity of the inlet gas stream

ρ_ℓ = density of the water

σ_ℓ = surface tension of the water

D_I = diameter of the inlet

In these experiments jets were observed when $We_I \geq 10^5$, while globule formation on the inlet vent occured when $We_I \leq 10^5$. When globules formed on the inlet vent, their normalized volume at detachment, V_N, showed the following dependence on We_I,

$$V_N = 3.45\ We_I^{0.46} \qquad 6.12$$

$$V_N = \frac{V_g}{A_I} \frac{\sigma_\ell}{(\rho_\ell - \rho_g)g} \qquad 6.13$$

$$V_G = \frac{1}{6} \pi D_G^3 \qquad 6.14$$

V_G = globule volume at detachment

A_I = inlet cross sectional area

ρ_g = density of the gas stream

g = gravitational constant

D_G = equivalent sphere diameter of the globule at detachment

The SUPRA code [21,22] contains four options for specifying initial globule volume: user input; calculation by balancing surface tension and buoyancy; calculation by the procedure of Ramakrishnan et al. [23]; and use of Reynolds number correlations proposed by Leibson et al. [24]. Except for very low inlet flow rates, SUPRA predictions give better agreement with experimental data when the forth option is used. Therefore, SUPRA calculations are generally performed using Leibson's Reynolds number correlations at all but the lowest of inlet gas flow rates. Thus, for turbulent flow regimes, $Re_{g,I} > 10{,}000$, the following correlation is used:

$$D_G = 0.28\ Re_{g,I}^{-0.05} \qquad 6.15$$

For laminar flow regimes, $Re_{g,I} < 1000$, the following correlation is used:

$$D_G = 0.18\ D_I^{0.5}\ Re_{g,I}^{0.33} \qquad 6.16$$

Between $Re_{g,I} = 1000$ and $Re_{g,I} = 10{,}000$, a linear interpolation between Eqs. 15 and 16 is used. Finally, at very low flow rates, the following equation, derived by balancing globule surface tension and buoyancy, is used

$$V_G = \pi\ D_I\ \frac{\sigma_\ell}{(\rho_\ell - \rho_g)g} \qquad 6.17$$

so long as the diameter of the equivalent sphere corresponding to V_G is larger than the equivalent sphere diameter, D_G, predicted by Eq. 16.

During severe accidents at BWRs, suppression pool inlet vent gas stream velocities, U_g are expected [14] to range from 5 to 150 ft/sec. Therefore, values of $Re_{g,I}$ for suppression pool inlet vents should range from about 700 to 20,000 with values at the high end of this range applying to large pipe break accidents. Accordingly, for most BWR accidents initial globule sizes would be calculated with Eq. 16. Since $\rho_\ell >> \rho_g$, combination of Eqs. 11 thru 13 yields

$$V_G = k_{We}\ D_I^{5/2}\ U_g \qquad k_{We} = 0.088$$

while substitution of $Re_{g,I} = \rho_{gI} U_g D_I/\mu_g$ into Eq. 16 and calculation of the volume of the equivalent sphere yields

$$V_G = k_{Re} D_I^{5/2} U_g \qquad k_{Re} = 0.024$$

where $k_{Re} = 0.001\pi\rho_g/\mu_g$. Accordingly, the Battelle Weber number correlation and the SUPRA Reynolds number correlation applicable to moderate gas flow rates should yield similar estimates of initial globule volume for most BWR accident senarios. Finally, because the density and viscosity of the gas mixture in the vent inlet stream will not be constant, the Reynolds number correlations used in the SUPRA code may be preferable to the Battelle Weber number correlation.

In the injection regime aerosol particles are removed by inertial deposition from the inlet gas stream or from circulation currents within gas globules. In the SPARC code [20] neither of these deposition mechanisms is treated. In the SUPRA code [21,22] inertial deposition from the inlet gas stream is modeled using single orifice impactor correlations [25] and inertial deposition from circulation currents within globules is modeled using a spherical bubble model developed by Fuchs [11].

For single stage impactors both theoretical and experimental results [25] show that particle collection efficiency (ϵ) correlates with the square root of the Stokes number (Stk), where

$$Stk = \frac{1}{9} \frac{\rho_p d_p^2 U_g C_p}{\mu_g D_I} \qquad 6.18$$

and ρ_p, d_p, and C_p are the density, diameter, and Cunningham slip correction factor for the aerosol particles, U_g and μ_g are the velocity and viscosity of the inlet gases, and D_I is the diameter of the inlet vent. For impactors with round orifices, ϵ vs $Stk^{0.5}$ correlations exhibit [25,26] little dependence on the ratio of orifice throat length, x_I, to orifice diameter, D_I, and as Fig 1 shows only a weak dependence on the ratio of impaction surface distance, x_S, to orifice diameter, D_I, for $x_S/D_I \leq 5$. Fig 1 shows that, for $x_S/D_I \leq 5$, $\epsilon = 0$ when $Stk^{0.5} \leq 0.35$ and $\epsilon = 1$ when $Stk^{0.5} = 0.5$ to 0.6. Therefore, since x_S/D_I should be ≤ 5 for both globules and jets, it seems reasonable to model particle collection during injection of a gas stream from a vent into a water pool by setting $\epsilon = 0$ for $Stk^{0.5} \leq 0.35$, $\epsilon = 1.0$ for $Stk^{0.5} \geq 0.55$, and interpolating linearly between these bounds.

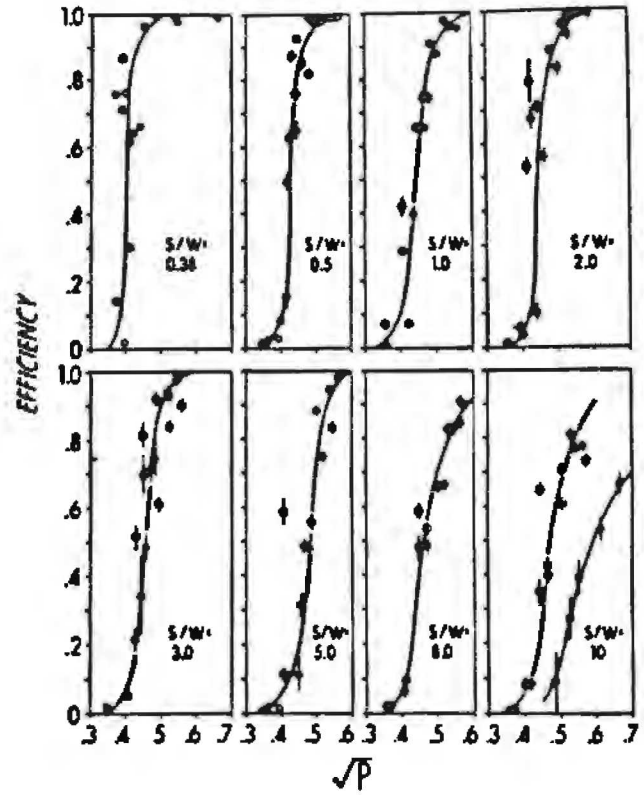

Figure 6.1 Experimental characteristics of round impactors ($S=X_S$, $W=D_I$, $P=Stk$) [7].

SUPRA calculates particle deposition from globules due to centrifugal forces using the Fuchs model [11] with the gas velocity at the globule surface, v_c, approximated by

$$v_c = U_g \sin \theta \qquad 6.19$$

which gives

$$DF_{c,G} = \exp \left\{ 12 \frac{U_g^2 \sin^2\theta}{D_G^2} \right\} t_G \tau \qquad 6.20$$

$$\tau = \frac{2}{9} \frac{\rho_p r_p^2 C_p}{\mu_g} \qquad 6.21$$

where θ is the angle between globule radius vector that points toward the particle and the globule velocity vector, $DF_{c,G}$ is the decontamination factor for particle deposition in globules caused by centrifugal forces, U_g and μ_g are the velocity and viscosity of the inlet gas stream, t_G and D_G are the detachment time and diameter of the gas globule, and ρ_p, r_p, and C_p and the density, radius, and Cunningham slip correction factor for the aerosol particles.

Substitution of reasonable parameter values into Eqs. 18 and 20 shows that particle removal from the inlet gas stream due to impaction will be negligible for particles with radii less than about 30 μ, and that particle removal from circulatory gas flows within a globule will have DF values little greater than 1.0. Therefore, it seems reasonable to neglect aerosol removal due to inertial deposition within detached globules.

Breakup Regime. In the breakup regime globule shattering produces bubbles with surface to volume ratios, large enough to allow efficient transfer of heat between bubble atmospheres and the pool. Consequently, the bubbles initially formed by globule shattering rise only a few centimeters before attaining thermal equilibrium with the pool [15]. If at these depths the pool is subcooled, as thermal equilibrium is approached, bubbles with pure steam atmospheres will collapse completely because steam condensation will be complete, and the partial pressures of steam in bubbles that contain non-condensible gases will increase or decrease until they become equal to the saturation pressure of steam at the pool temperature.

The relatively small size of the bubbles initially produced by globule shattering also means (1) that the total surface area of aerosol particles suspended in the bubble atmospheres will be less than or comparable to the surface areas of the bubbles which contain them; and (2) that the bubble atmospheres will be poor heat sinks for heat released by condensation of steam on aerosol particles. Therefore, both surface area and heat transfer constraints indicate that steam condensation on aerosol surfaces will be negligible within bubbles.

Rapid cooling of hot steam laden bubbles also produces rapid condensation of steam. Because steam condensation is rapid, particle deposition in the globule breakup regime will be dominated by diffusiophoresis. If only diffusiophoretic deposition (see Chap. 5) is important during globule breakup, then the mass of particles removed during breakup can be calculated as follows:

$$\frac{dMp}{dt} = - \frac{A}{V} v_p M_p \qquad 6.22$$

$$v_p = - v_s F \qquad 6.23$$

$$v_s = J_s/C_g = \frac{V}{A} \frac{MW_g}{MW_s} M_g \frac{dM_s}{dt} \qquad 6.24$$

$$F = \left[X_s + X_g \frac{MW_g}{MW_s} \right]^{-1} \qquad 6.25$$

where M_p and v_p are the particle mass and diffusiophoretic particle deposition velocity, A/V is the surface to volume ratio of the bubble, v_s is the velocity of the Stefan flow, J_s is the molar flux of the condensing steam, C_g, M_g, MW_g, and X_g are the concentration, mass, molecular weight, and mole fraction of the non-condensible gases in the bubble, and M_s, MW_s and X_s are the mass, molecular weight, and mole fraction of steam in the bubble. Combination of Eqs. 22 thru 25 now yields

$$\frac{dM_p}{M_p} = \frac{MW_g F}{MW_s M_g} dM_s \qquad 6.26$$

Since MW_g and MW_s are constants, M_g is invarient because adsoption of non-condensible gases by the pool is negligible, and F though not constant varies slowly and thus may be treated as constant, Eq. 26 may easily be integrated to yield

$$\frac{M_{p,i}}{M_{p,f}} = \exp \left[\frac{MW_g F}{MW_s M_g} \left(M_{s,i} - M_{s,f} \right) \right] \qquad 6.27$$

where i and f indicate conditions in the bubble when first formed by globule breakup and after attainment of equilibrium with the pool (i.e., before and after the condensation of steam).

An alternative treatment of particle removal due to steam condensation during globule breakup is implemented in the SPARC code [20]. In the SPARC code the fraction of particles removed due to steam condensation during globule breakup (i.e., the removal efficiency ϵ for particles) is assumed to be the same as the mole fraction of condensed inlet gas. Thus,

$$\begin{aligned} \epsilon = (n_i - n_f)/n_i &= 1 - (n_f/n_i) \\ &= 1 - (X_{g,i}/X_{g,f}) \\ &= 1 - (1/DF) \end{aligned} \qquad 6.28$$

where n_f and n_i are the final and initial moles of inlet gas, $X_{g,i}$ and $X_{g,f}$ are the initial and final mole fractions of non-

condensible gases, and DF is the decontamination factor due to steam condensation during globule breakup. Accordingly,

$$DF = X_{g,f}/X_{g,i} \qquad 6.29$$

which is the expression used in SPARC to model particle removal during globule breakup. Comparison of Eq. 29 to Eq. 27 shows that they are quite dissimilar. Therefore, Eq. 29 can be at best only an approximation to particle removal by diffusiophoresis.

Because bubble rise is minimal during globule breakup, temperature and pressure will be nearly constant throughout the breakup regime. Accordingly,

$$V_i/V_f = n_i/n_f \qquad 6.30$$

which suggests that Eq. 29 represents particle collection due to impaction on the bubble wall as the bubble shrinks due to steam condensation. However, because of the inertia of the water mass surrounding the bubble, bubble collapse is unlikely to be rapid enough to produce significant particle collection by impaction.

Bubble Rise Regime. Globule breakup produces a swarm of bubbles that entrains water in it as it rises toward the surface of the pool. The rate of removal of particle mass from the atmosphere of a bubble in the swarm due to deposition onto the wall of the bubble is

$$\frac{dM_p}{dt} = \frac{dM_p}{dz}\frac{dz}{dt} = -\frac{A_d}{V} v_p M_p \qquad 6.31$$

where M_p is the mass of particles in the bubble, $dz/dt = U_S$ is the rise velocity of the bubble swarm, A_d and V are the particle deposition surface area and volume of the bubble, and v_p is the particle velocity normal to the bubble wall. Substitution of U_S for dz/dt and rearrangement now yields

$$-\frac{1}{M_p}\frac{dM_p}{dz} = \frac{A_d}{V}\frac{v_p}{U_s} \qquad 6.32$$

Because hydrostatic pressure depends on submergence depth, bubble pressures decrease and bubble volumes increase as bubbles

rise toward the surface of the pool. Since pool temperatures in pools stirred by bubbling will be quite uniform, as bubble volume increases, water must evaporate from the bubble wall in order to keep the partial pressure of steam in the bubble equal to the saturation pressure of steam at the temperature of the pool.

Evaporation of water in rising bubbles has been examined by Moody and Nagy [15]. Their calculations suggest that bubble wall temperatures differ little from bulk water temperatures, that bubble steam partial pressures differ little from pool steam saturation pressures, and consequently that water vapor evaporation velocities, v_s, are adequately expressed by

$$v_s = \frac{V}{A}\left[\frac{\rho_w U_s}{P_{atm} - P_{sat,T} + \rho_w(h-U_s t)}\right] \qquad 6.33$$

where ρ_w is the density of water, U_s is the rise velocity of the bubble swarm, V, A, and h are the volume, total surface area, and submergence depth of the bubble, P_{atm} and $P_{sat,T}$ are the total pressure of the atmosphere above the pool and the saturation pressure of steam at the pool temperature, and t is time.

Because particles suspended in the atmosphere of a rising bubble are subject to several forces, v_p should be expressed as a sum of deposition velocities, $v_{p,i}$, one velocity for each deposition mechanism acting on the particles, minus the velocity of the water evaporating from the bubble wall. Thus,

$$v_p = (\Sigma\, v_{p,i}) - v_s \qquad 6.34$$

Two deposition mechanisms, diffusiophoresis and thermophoresis, significant in a large control volume may be neglected in rising bubbles. Diffusiophoresis may be neglected in the bubble rise regime, because the bubbles have already attained thermal equilibrium with the pool and therefore steam condensation does not occur. Thermophoresis may be neglected because thermal equilibrium and small bubble size causes temperature gradients within the bubbles to be negligible. Therefore, only three deposition mechanisms need be considered: inertial impaction caused by circulation currents within the bubble, sedimentation, and diffusive deposition.

Theoretical expressions for

$$\frac{A_d\, v_{p,i}}{V\, U_s} = \alpha_{p,i} \qquad 6.35$$

the particle absorption coefficient due to deposition mechanism i, were first developd by Fuchs [11] for deposition in spherical bubbles due to inertial impaction, sedimentation, and Brownian diffusion. Table 6.1 presents these expressions and compares them to the corresponding expressions derived for elliptical bubbles by Demitrack and Moody [16].

Velocities normal to the bubble wall for particle deposition caused by inertial impaction, v_I, sedimentation, v_S, and Brownian diffusion, v_D, are given by [11,15]

$$v_S = - g\tau \cos \theta \qquad 6.36$$

$$v_D = 2\left(\frac{D_p}{\pi t_e}\right)^{1/2} \qquad 6.37$$

$$v_I = G\tau \qquad 6.38$$

$$\tau = \frac{2}{9} \frac{\rho_p r^2 C_p}{\mu_g} \qquad 6.39$$

$$t_e = 2R_B/U_B \qquad 6.40$$

$$G = U_g^2/R_B \qquad 6.41$$

$$U_g = \frac{3}{2} U_B \sin\theta \qquad 6.42$$

where theta is the angle between the vertical and the bubble radius vector directed toward the gas borne particle, g is the acceleration due to gravity, μ_g is the viscosity of the bubble atmosphere, U_g is the circulation velocity of the bubble atmosphere next to the bubble wall, t_e is the approximate transit time for circulation of gas around the bubble [15,27-29], D_p, ρ_p, r_p, and C_p are the particle diffusion coefficient, density, radius, and Cunningham slip correction factor, and R_B and U_B are the bubble radius and the rise velocity of the bubble relative to the water in which it is entrained.

Table 6.1

Absorption Coefficients

	PLANETARY ELLIPSOID	SPHERICAL
INERTIAL IMPACTION	$\frac{3}{2}\ \frac{U\tau}{b^2}\ \frac{\left\{\left(\frac{a}{b}\right)^2-1\right\}+\left\{\left(\frac{a}{b}\right)^2-1\right\}^{3/2}\ \left\{\left(\frac{a}{b}\right)^2-2\right\}\ \tan^{-1}\sqrt{\left(\frac{a}{b}\right)^2-1}}{\left(\sqrt{\left(\frac{a}{b}\right)^2-1}\ -\ \left(\frac{a}{b}\right)^2\ \tan^{-1}\sqrt{\left(\frac{a}{b}\right)^2-1}\right)^2}$	$\frac{9}{2}\ \frac{U\tau}{R^2}$
SEDIMENTATION	$\frac{3}{4}\ \frac{g\tau}{bU}$	$\frac{3}{4}\ \frac{g\tau}{RU}$
BROWNIAN DIFFUSION	$\sqrt[6]{\frac{D}{Ua^2b\ \pi}}\ \frac{\left\{\left(\frac{a}{b}\right)^2-1\right\}}{\left[1+\sqrt{4+2\left\{\left(\frac{a}{b}\right)^2-1\right\}}\right]}\ \sqrt{\frac{\frac{1.76\left(\frac{a}{b}\right)^2}{\frac{a}{b}^2-1}-\sqrt{2}}{\frac{\left(\frac{a}{b}\right)^2\ \tan^{-1}\sqrt{\left(\frac{a}{b}\right)^2-1}}{\sqrt{\left(\frac{a}{b}\right)^2-1}}-1}}$	$1.8\sqrt{\frac{D}{UR^3}}$

U - Bubble velocity

$\tau = \frac{2}{9}\ \frac{\rho_p}{\mu_g}\ r_p^2\ C_m$

τ - Stokes' characteristic time

g - Acceleration due to gravity

μ_g - Gas viscosity

ρ_p - Particle density

r_p - Particle radius

C_m - Cunningham's slip factor

Since

$$v_p = v_S + v_D + v_I - v_s \quad . \qquad 6.43$$

may not be greater than zero for all values of theta (at all points on the surface of the bubble), particle deposition may occur on only part of the total surface of the bubble. Therefore, when solving Eq. 32, A_d must first be expressed as an integral over a differential surface element, dA. Thus,

$$A_d = \int dA \qquad 6.44$$

where

$$dA = 2\pi R_B^2 \sin\theta d\theta \qquad 6.45$$

for spherical bubbles,

$$dA = \frac{2\pi a^2}{e} (e^2-1)^{1/2} \left[(e^2-1)^{-1} + \cos^2\theta\right]^{1/2} \sin\theta d\theta \qquad 6.46$$

for elliptical bubbles [30], and the limits of integration for Eq. 44 are obtained by solving Eqs. 33 and 36 through 43 with v_p in Eq. 43 set equal to zero.

Combination of Eqs. 32, 33, 36 through 44, and either 45 or 46 produces an equation which has the following functional form

$$-\frac{dM_p}{M_p} = (U_s V)^{-1} \iint v_p dA dz \qquad 6.47$$

where the inner integral has an analytic solution [31] for both dA(sphere) and dA(ellipse). Therefore Eq. 47 can be integrated to yield

$$DF = \frac{M_i}{M_f} = \exp\left[h(U_s V)^{-1} \int v_p dA\right] \qquad 6.48$$

since $z_f - z_i = h$, the submergence depth (i.e., the bubble rise distance).

Values of h, the bubble rise distance, V, the bubble volume, U_S, the rise velocity of the bubble swarm, and U_B, the bubble rise velocity relative to the water in which it is entrained (see Eqs. 40 and 42 above), are required before M_i/M_f can be calculated using Eq. 48. If bubble swarm characteristics are relatively constant, average values of h, V, U_S, and U_B can be used. If not, discretization over bubble sizes will be required.

Pool scrubbing experiments [14] conducted at Battelle Columbus Laboratories show that shattering of large bubbles in bubble swarms limits the size to which bubbles grow by coalescence. Consequently, although the characteristics of individual bubbles varied rapidly, swarm characteristics were quite stable. Although several non-condensible gases were employed and experimental conditions (inlet gas flow rates, inlet gas steam volume fractions, orifice submergence depths, orifice diameters, inlet gas temperatures, pool temperatures) were varied, the equivalent spherical diameters of bubbles in swarms were always observed to be log-normally distributed. Whenever steam volume fractions in the inlet gases were less that 0.8, the distributions of bubble diameters had mean and maximum (99.8 percentile) values of approximately 5 and 19 mm, with 19 mm representing the largest stable bubble size observed. As steam volume fractions increased from 0.8 to 0.95, bubble mean diameters decreased from approximately 5 to approximately 3.5 mm. Thus, bubble swarm characteristics should be well represented by an average bubble that has an equivalent spherical diameter of approximately 5 mm.

The diameters reported in the Battelle study were derived by assuming that the equivalent spherical bubble had a volume equal to that of the experimentally observed elliptical bubble. Had equal surface areas rather than equal volumes been assumed, different equivalent spherical diameters would have been calculated. Because the experimental data was distributed log normally, the mean equivalent spherical diameter based on equal volumes, d_V, and the mean equivalent spherical diameter based on equal areas, d_A, are related by [32].

$$\ln d_V = \ln d_A + (\ln \sigma)^2 \qquad 6.49$$

where σ is the standard deviation of the log-normal distribution. Since the Battelle study determined d_V and σ, mean values of surface area and volume can be calculated. Then, using these values and the equations for the surface area and volume of an ellipsoid, the aspect ratio of an elliptical bubble having a surface area and volume equal to the mean values calculated from the Battelle data can be shown to be about 1.5.

Because low levels of contamination greatly increase surface tension, elliptical bubbles are not observed to have high aspect

ratios in contaminated liquids. Specifically, air bubbles with equivalent spherical diameters of 5 mm are predicted [33] to have aspect ratios of 1.5 in contaminated water; and experimental data for the terminal rise velocities of air bubbles in tap water [34] are fit well by correlations for solid spheres [35]. Accordingly, because small bubbles will rapidly attain terminal velocities, U_B in Eqs. 40 and 42 should be calculated using either the data for air bubbles in tap water of Haberman and Morton [34] or the solid sphere correlations of Wallis [35].

Experimental values for U_S, the swarm rise velocity, were determined during the GE Fission Product Scrubbing Program [19]. The following table presents the limited data reported in that study:

Reactor	Vent	Swarm Diameter (ft)	Swarm Rise Velocity (ft/sec)
BWR/6	X-Quencher	1.8	3.8
	Full Scale Horizontal	2.4	4.2
		1.0	2.6

These data suggest that swarm rise velocity is linearly related to swarm diameter. Therefore, if swarm diameter may be approximated by globule diameter at detachment, then swarm rise velocity can be estimated using the following equation:

$$U_S = 0.7\ D_G + 2.6 \qquad 6.50$$

The distance that detached globules rise before they shatter into bubble swarms decreases h, the bubble rise distance (scrubbing height). Both dimensionless analysis [12] and experimental observations [13,36] suggest that initial globule breakup requires a rise distance of about one globule diameter, although up to ten globule diameters [14] are required to establish stable bubble swarm characteristics. Accordingly, since scrubbing is expected to become effective upon initial globule breakup [36], scrubbing heights (vertical length of the bubble rise regime) should be calculated in MELCOR as the difference between the vent submergence distance minus the globule diameter upon detachment, D_G, where the latter is calculated using either Eqs. 11 thru 14 or Eqs. 15 thru 17.

Finally, so long as bubble aspect ratios are not large (less than 2), the effects of elliptical shape on particle removal in the bubble rise regime may be approximated [17] by multiplying deposition velocities for spherical bubbles by corrections factors, which have the following form

$$F_i = \alpha_{E,i}/\alpha_{s,i} \qquad 6.51$$

where $\alpha_{E,i}$ is the absorbtion coefficient for deposition process i in an elliptical bubble, $\alpha_{s,i}$ is the absorbtion coefficient for deposition process i in a spherical bubble, and the expressions for $a_{E,i}$ and $\alpha_{s,i}$ are taken from Table 6.1. Substitution of these correction factors into Eq. 43 then yields

$$v_p = F_S v_S + F_D v_D + F_I v_I - v_s \qquad 6.52$$

where the spherical bubble deposition velocities for gravitational, v_S, diffusive, v_D, and inertial, v_I, deposition are given by Eqs. 36 through 42, and Figure 6.2 presents plots of F_i versus aspect ratio a/b. Figure 6.2 shows that bubbles with aspect ratios of 1.5 and equivalent spherical diameters of 5 mm, have values of F_S, F_D, and F_I of 1.3, 1.05, and 1.7, which suggests that elliptical shape principally affects inertial deposition.

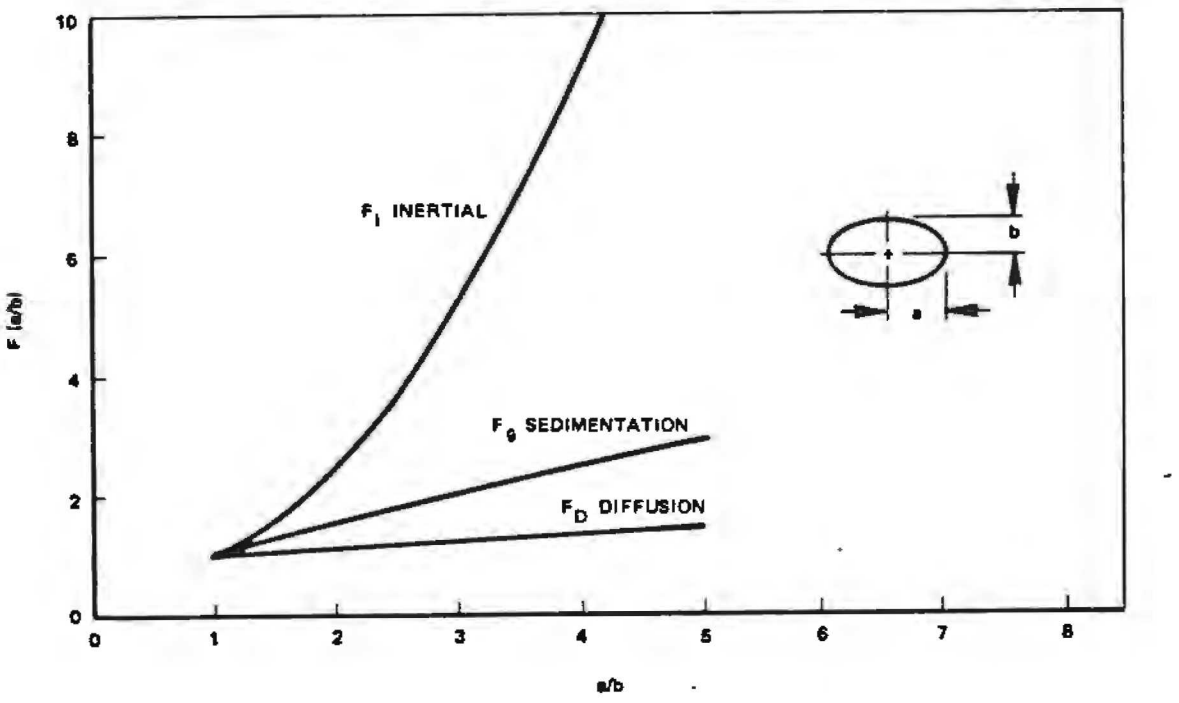

Figure 6.2. Bubble Scrubbing Shape Factors [12]

Exit Regime. After bursting from the surface, evaporation of bubbles transfers materials dissolved or suspended in bubble walls to the atmosphere above the pool [37]. Although this mechanism is important for the production of salt aerosols above oceans, unless dissolved and suspended materials are concentrated in bubble walls (at the bubble/water interface), it may be unimportant for pool scrubbing. Since experimental data are lacking, this process should be qualitatively captured by limiting overall pool scrubbing DFs to 10^5, as is done in the SPARC code [20].

6.7 Sprays

During a severe accident, operation of the spray system installed in PWR containments, or the fire sprays installed in BWR reactor buildings, would (1) reduce compartment temperatures and pressures by condensing steam on spray droplets; and (2) remove fission products by adsorption of vapors at and deposition of aerosols onto droplet surfaces. Because the impact of spray operation on compartment thermal hydraulic conditions (temperature, pressure, masses of steam and liquid water) will usually be substantial, spray operation will be modeled mechanistically in MELCOR's thermal-hydraulic modules. Accordingly, the removal of fission products by spray droplets should be mechanistically modeled by MELCOR's fission product behavior modules.

The removal of vapors and aerosols by spray droplets has generally been modeled as a first order rate process [38-40].

$$\frac{dM_k}{dt} = \lambda_{k,i} M_k \qquad 6.53$$

where M_k is the mass of fission product species k in the compartment (control volume) in which the sprays are operating and $\lambda_{k,i}$ is the rate constant for the removal of fission product species k by spray droplets of size i. Because vapors and aerosols are removed by spray droplets by different mechanisms, vapors and aerosols require different formulations for $\lambda_{k,i}$.

An expression for the time rate of change of the gas borne mass of fission product vapor k due to its adsorption into spray droplets may be derived [38,41,42] by constructing a mass balance for the vapor for the time interval dt. Thus,

$$dM_{k,g} = - F_i dt \, (\rho_{k,fn} - \rho_{k,in}) \qquad 6.54$$

where $M_{k,g}$ is the gas borne mass of fission product vapor k in the control volume in which the sprays are operating, F_i is

the volumetric flow rate of spray drops of size i, and $\rho_{k,in}$ and $\rho_{k,fn}$ are the initial (before fall) and final (after fall) mass densities of the vapor in the spray water. Substitution of the following expressions (Eqs. 55 and 56) for the adsorption efficiency $E_{k,i}$ for the vapor in spray water and the equilibrium value of the partition coefficient H for partition of the vapor between the gas phase and spray water

$$E_{k,i} = \frac{\rho_{k,fn} - \rho_{k,in}}{\rho_{k,eq} - \rho_{k,in}} \qquad 6.55$$

$$H = \frac{\rho_{k,eq}}{\rho_{k,g}} \qquad 6.56$$

into Eq. 54 yields

$$\frac{dM_{k,g}}{dt} = - F_i E_{k,i} (H\rho_{k,g} - \rho_{k,in}) \qquad 6.57$$

which is appropriate for spray operation in the recirculation mode where $\rho_{k,in}$ has a non zero value. When the sprays are operating in the injection mode, $\rho_{k,in} = 0$, and Eq. 57 reduces to

$$\frac{dM_{k,g}}{dt} = - F_i E_{k,i} H\rho_{k,g} \qquad 6.58$$

Since $\rho_{k,g} = M_{k,g}/V$, where V is the volume of the control volume gas space, substitution of $M_{k,g}/V$ for $\rho_{k,g}$ and comparison of the resulting equation to the general equation for fission product removal by spray droplets (Eq. 53) shows that, for vapor adsorption by spray droplets when the sprays are operating in the injection mode, the proportionality constant $\lambda_{k,i}$ in the Eq. 53 is given by

$$\lambda_{k,i} = F_i E_{k,i} H/V \qquad 6.59$$

A formulation for $\lambda_{k,i}$ for removal of aerosol particles by spray drops may be derived [40] by assuming that falling drops do not interact and that each falling drop removes aerosol particles from the volume that it traverses during its fall with

an efficiency $E_{i,j}$ that depends on the collision mechanisms operating. Accordingly,

$$\frac{dM_{k,j}}{dt} = \frac{N_i A_i g E_{i,j}}{V} M_{k,j} \qquad 6.60$$

where $M_{k,j}$ is the mass of aerosol particles of composition k in aerosol size section j. N_i is the number of drops of size i sprayed into the compartment per unit time. A_i is the cross sectional area of drops of size i, h is the fall height of the drops. $E_{i,j}$ is the efficiency of collection of particles in size class j by drops of size i, and V is the compartment volume. Since

$$N_i = \frac{F_i}{\frac{4}{3}\pi r_i^3} \qquad 6.61$$

and

$$A_i = \pi r_1^2 \qquad 6.62$$

where F_i is the volumetric flow rate and r_i the radius of spray droplets of size i, substitution of Eqs. 61 and 62 into Eq. 60 yields

$$\frac{dM_{k,j}}{dt} = \frac{3F_i h E_{i,j}}{4Vr_i} M_{k,j} \qquad 6.63$$

Comparision of Eq. 63 to Eq. 53 shows that

$$\lambda_{k,i} = \frac{3F_i h E_{i,j}}{4Vr_i} \qquad 6.64$$

Spray Droplet Size Distribution. Because the removal rates for vapors and aerosols depend on droplet size, the constancy of the size distribution of spray droplets needs to be examined. Spray nozzles do not produce droplets of a uniform size. Instead a distribution of droplet sizes is produced, which is approximately log-normal [43,44]. Figure 6.3 presents a typical distribution (range approx. 100 μ to 2000 μ; median diam. approx. 600 μ).

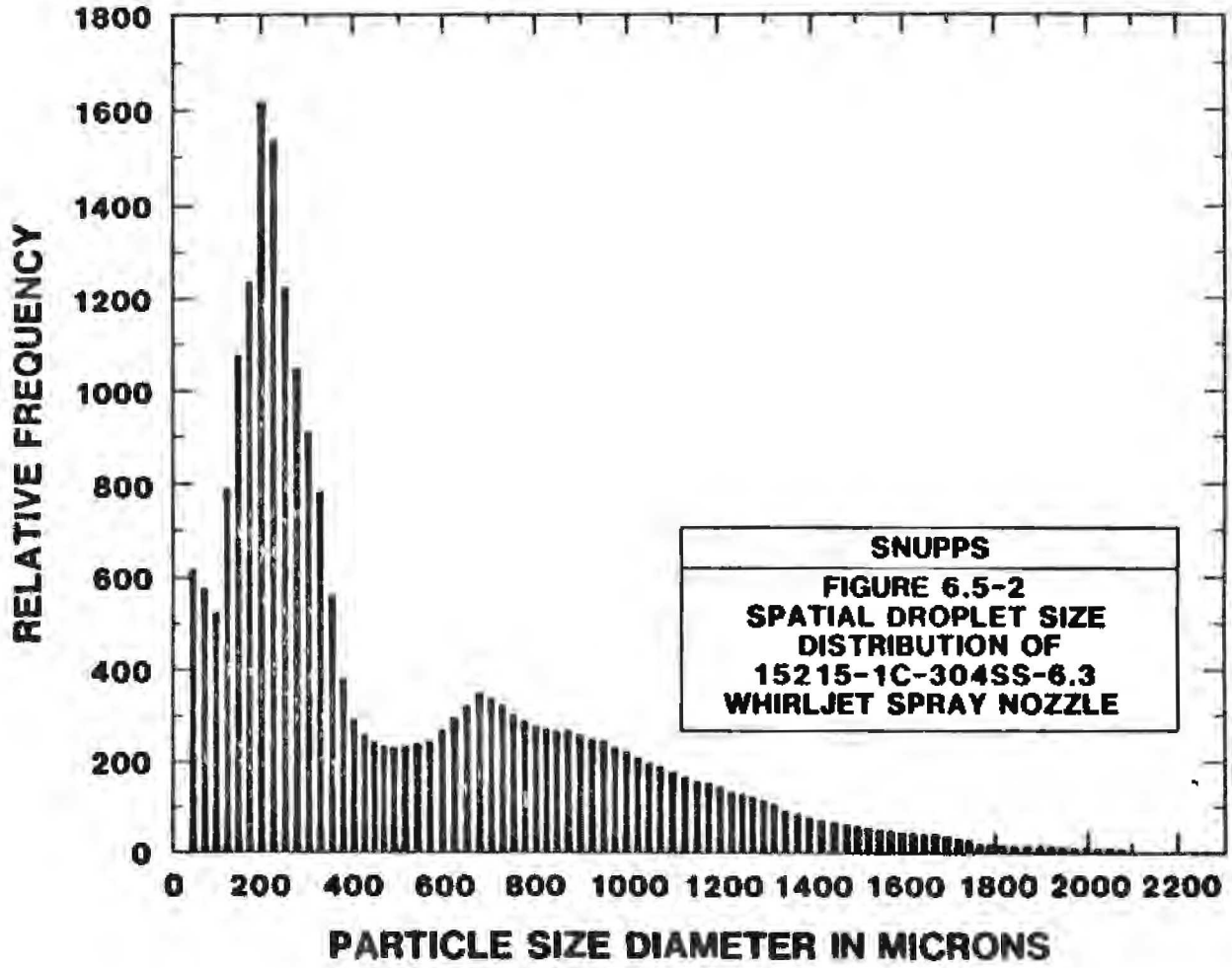

Figure 6.3 Particle Size Diameter in Microns

An initial spray droplet size distribution can be altered during droplet fall by vapor condensation onto or evaporation from droplets, and by agglomeration of droplets. Because the gas borne mass of a fission product vapor, when compared to the total mass of spray droplets, will always be small, condensation or evaporation of fission product vapors will have no appreciable effect upon the droplet size distribution. Because steam can be present in the containment atmosphere in large amounts, steam condensation and evaporation could appreciably alter the droplet size distribution.

When operated in either the injection or the recirculation mode, spray water is likely to be at a temperature lower than that of the containment atmosphere. Since both experimental [45] and theoretical [46] studies show that spray droplets will attain thermal equilibrium with the containment atmosphere after falling only a few meters (< 4 m for atmos. T > 100°C), a simple heat balance can be used [40,47] to bound the increase in size of the droplets due to steam condensation. Thus,

$$\frac{4}{3}\pi(r_f^3 - r_i^3)\rho L = \frac{4}{3}\pi_i r^3 \rho s \Delta T \qquad 6.65$$

which upon solution for r_f/r_i yields

$$\frac{r_f}{r_i} = \left[1 + s\,\frac{\Delta T}{L}\right]^{1/3} \qquad 6.66$$

where r_i and r_f are the initial and final drop radii, ρ is the density of the drops, L is the latent heat of steam, s is the specific heat of water, and ΔT is the temperature rise of the drops due to condensation of steam. Substitution of an upper bound temperature for the containment atmosphere (250°C), a lower bound temperature for spray water (37°C), and appropriate values for L (2×10^6 Jkg^{-1}) and s (4.18 $J\ g^{-1}\ °C^{-1}$ at 37°C) yields $r_f/r_i = 1.13$, which suggests that the growth of spray droplets due to steam condensation can probably be neglected.

Once spray droplets have attained thermal equilibrium with the containment atmosphere, unless a hydrogen burn occurs, significant changes in the size distribution of the spray droplets due to condensation or evaporation of steam are unlikely, since large deviations of the containment atmosphere from saturation with respect to steam are also unlikely. If a hydrogen burn occurs, spray droplets will rapidly evaporate during the burn. After the burn, if the containment atmosphere cools rapidly, droplet growth due to steam condensation may also be rapid.

Droplet agglomeration during fall has been examined during several studies [47-49]. Postma and Pasedag found [47] that particle washout rates during the CSE experiments were not appreciably affected by agglomeration of spray droplets. For adsorption of molecular iodine, Pasedag and Gallager found [48] that the mass transfer surface area of a typical spray droplet size distribution was reduced about 10% by agglomeration of spray droplets. Walker et al. found [49] that agglomeration increased the median diameter of a typical droplet size distribution from about 600 μ to about 700 μ. Together these results suggest that droplet agglomeration during droplet fall does not appreciably alter the character of the initial droplet size distribution, and thus can probably be neglected. Alternatively, Postma and Pasedag have suggested [47] that the impact of droplet agglomeration can be approximated by increasing the median diameter of the initial droplet distribution by about 25 percent.

Vapor Adsorption Efficiency. Vapor adsorption by spray droplets can be represented using a well mixed drop model, a stagnant film model, or a rigid drop model [41,47,50,51]. The well-mixed drop model assumes that the entire liquid volume of the drop is in equilibrium with the gas boundary layer that surrounds the drop. Consequently, the rate of vapor adsorption by the drop is limited only by mass transport through the gas boundary layer. The stagnant film model divides that the drop into two layers, a well-mixed interior and a stagnant boundary layer next to the drop's surface. Thus, for the stagnant film model vapor adsorption by the drop is limited by mass transfer through both a gas and a liquid boundary layer. Finally, the rigid drop model assumes that the entire liquid volume of the drop is stagnant. Thus, vapor transport into the drop is mass transfer limited throughout the entire drop.

Because each of these models assumes a different drop structure, each model will have a different vapor adsorption efficiency, $E_{k,i}$. Postma and Pasedag [47] have derived the following expressions for $E_{k,i}$ for the well-mixed, stagnant film, and rigid drop models.

Well Mixed Drop Model.

$$E_{k,i} = 1 - \left[\exp - \frac{6k_g t_e}{2r_i H}\right] \qquad 6.67$$

Stagnant Film Drop Model.

$$E_{k,i} = 1 - \exp\left[-\frac{6k_g t_e}{2r_i H + \frac{k_g}{k_\ell}}\right] \qquad 6.68$$

Rigid Drop Model.

$$E_{k,i} = 1 - \sum_{n=1}^{\infty} \frac{6\ Sh^2\ \exp\{\alpha_n^2 \theta\}}{\alpha_n^2\left[\alpha_n^2 + Sh(Sh - 1)\right]} \qquad 6.69$$

where k_g, the gas boundary layer mass transfer coefficient, is calculated using the Ranz and Marshall approximation [52] to the Frossling equation [53].

$$k_g = \frac{D_{k,gas}}{2r_i}\ 2.0 + 0.60\ Re^{1/2}Sc^{1/3} \qquad 6.70$$

k_ℓ, the liquid boundary layer mass transfer coefficient, is calculated using the Griffith's approximation for diffusion in a rigid drop [50].

$$k_\ell = \frac{\pi^2\ D_{k,H_2O}}{3r_i} \qquad 6.71$$

$D_{k,gas}$, the diffusion constant for vapor k in the gas phase, is calculated using the approximation of Wilke [54,55].

$$D_{k,gas} = \left[\sum_n \frac{X_n}{D_{k,n}}\right]^{-1} \qquad 6.72$$

D_{k,H_2O}, the diffusion constant for vapor k in H_2O, is calculated using the approximation of Wilke and Change [56,57].

$$D_{k,H_2O} = \frac{7.4 \times 10^{-8} (ZM)^{1/2} T}{\mu V_k^{0.6}} \qquad 6.73$$

and r_i = the drop radius

t_e = the drop exposure time

$$Sh = \frac{k_g r_i}{H D_{k,H_2O}}$$

$$\theta = \frac{D_{k,H_2O} t_e}{r_i^2}$$

α_n = nth root of $\alpha_n[\cot \alpha_n] + (Sh-1) = 0$

H = the equilibrium value of the solvent/gas partition coefficient for vapor k

Re = Reynolds Number

Sc = Schmidt Number

X_n = the mole fraction of bulk gas component n, where n is air, steam, hydrogen,...

$D_{k,n}$ = the diffusion coefficient of vapor k in bulk gas component n, which is calculated using equation 5.13.

Z = the solvent association parameter

= 2.26 for H_2O

M = the molecular weight of the solvent = 18 for H_2O

T = the temperature of the solvent

μ = the viscosity of the solvent

V_k = the molal volume of the vapor k at its normal boiling point

= 71.5 cm^3/g-mole for molecular iodine, I_2

For liquid water μ may be calculated using the following equation [58].

$$\frac{100}{\mu} = 2.1482(T-281.615) + \left[8078.4 + (T-218.615)^2\right]^{1/2} - 120 \qquad 6.74$$

where the units of μ are cp and T is in °K.

Postma and Pasedag [41,47] have compared the vapor removal efficiencies of the well-mixed, stagnant film, and rigid drop models. For drops falling 28 m through a 120 °C atmosphere, they found that, for values of H between 10^2 and 10^6, the three models predicted essentially identical vapor removal efficiencies for 500 μ drops. However, for larger drops (1000 and 1500 μ) and values of H between 10^2 and 10^4, removal efficiencies differed by up to factors of 2 and were ordered as follows: well-mixed drop efficiency > rigid drop efficiency > stagnant film drop efficiency. Because the well mixed drop model probably overestimates vapor removal by large drops, that model seems inappropriate for use in MELCOR. Because the stagnant film model predicts somewhat lower removal efficiencies than does the rigid drop model (E stagnant film/E rigid drop > 0.7), and because it is a much simpler mathematical function, the stagnant film removal efficiency is recommended for use in MELCOR.

For molecular iodine in steam/air mixtures,

$$D_{I_2,steam} \text{ and } D_{I_2,air}$$

can be calculated using the following equations developed for the Reactor Safety Study [39] using data and equations from Knudsen [58].

$$D_{I_2,steam} = 3.24\times10^{-5}\,\frac{T^{3/2}}{P\omega_{steam}} \qquad 6.75$$

$$D_{I_2,air} = 2.03\times10^{-5}\,\frac{T^{3/2}}{P\omega_{air}} \qquad 6.76$$

$$\omega_{steam} = 0.7075 + 454.72/T \qquad 6.77$$

$$\omega_{air} = 0.7075 + 141.73/T \qquad 6.78$$

where T and P are the temperature (°K) and pressure (atm) of the steam/air mixture, and ω_{steam} and ω_{air} are collision integrals for mass diffusivity. For I_2 absorption from steam/air mixtures, values of

$$D_{I_2,steam/air},\ D_{I_2,H_2O},\ K_{steam/air},\ K_{H_2O},\ E_{I_2,i},\ \text{and}\ K_{I_2,i}$$

have been calculated by Grist [40] for a range of temperatures (100° to 250°C), drops sizes (100 to 1000 μ), and partition coefficient values ($500 < H < 100{,}000$), using the stagnant film drop model (Eq. 68 with Eqs. 59 and 70-78). For T > 100°C, H > 2500, and drops of radius > 100 μ, the stagnant film drop model predicts I_2 removal rate constant values [$K_{I_2,i}$ values] of at least 50 hr^{-1}, which means that spray operation for only a few minutes (< 5 min.) should produce at least 100-fold reductions in gas borne I_2 concentrations ($C_{in}/C_{fn} > 100$).

Partition Coefficient Values. During severe reactor accidents, containment bulk gas temperatures in excess of 300 °C are unlikely. Therefore, because of their low vapor pressures [59], most materials (e.g., CsI), vaporized due to the melting of the core in-vessel or due to core-concrete reactions ex-vessel, will exist in the containment atmosphere as aerosols rather than as vapors. Only a few compounds of iodine (I_2, HI, and organic iodides) are likely to exist in the containment atmosphere as vapors for time periods long enought to warrent treatment as vapors.

Since organic iodides are only minimally soluble in spray solutions (very small removal rate constants [38,40,60]), and would only be formed during severe reactor accidents in small quantities (I_2 does not react rapidly with those organic materials present in large quantities in reactor containments, e.g., paints), if treated by MELCOR, organic iodides probably should be modeled as though they were non-reactive, non-condensable gases (i.e., rare gases). Because HI is highly soluble in water, if produced in quantities sufficient to require modeling, spray operation should be assumed to instantly and quantitatively

remove HI from the containment atmosphere. Therefore, partition coefficient values would appear to be needed only for I_2.

I_2 partition coefficient values have recently been reviewed by Grist [40]. Table 6.2 presents the values of H recommended by Grist for use when modeling spray removal of gas borne I_2 by sprays containing various additives. Because the solubility of I_2 in water is affected by the pH of the spray solution, and by reaction of I_2 with spray additives and trace impurities, H values for I_2 are not truly constants [40,42]. Accordingly, Table 6.2 presents "conservative" and "best estimate" values for H for several spray solutions. For each spray solution Table 6.2 also contains "cut off" values expressed as a percent of the initial gas borne I_2 concentration. Whenever spray operation reduces gas borne I_2 concentrations to the listed cut-off value, Grist recommends (as has been done previously [39,41]) that I_2 adsorption by droplets be treated using an equilibrium model [39] rather than a droplet adsorption model (e.g., the stagnant film model). Because Grist's recommended cut-off values are so low, unless iodine is shown, during some severe reactor accidents, to be present principally as I_2 rather than as CsI, it is recommended that MELCOR neglect this shift from the stagnant film model to the equilibrium model.

Aerosol Removal Efficiency. A falling spray drop will not collide with all of the aerosol particles contained in the volume that the drop sweeps out during its fall. Some fraction of the aerosol particles in that volume will flow past the drop by following the streamlines that delineate bulk gas flow around the drop. Particles that follow streamlines that lie at a distance from the surface of the drop less than or equal to one particle radius will be intercepted by the drop. Particles that follow streamlines that lie more than one particle radius away from the drop will collide with the drop only if some process transports the particle across streamlines towards the drop.

Five transport processes can cause particle trajectories to deviate from bulk gas streamlines: Brownian diffusion, turbulent diffusion, inertial impaction, diffusiophoresis, and thermophoresis. Collection efficiencies for interception and for all of these transport processes except turbulent diffusion have been examined by several studies [40,61-65]. When diffusiophoresis and thermophoresis are negligible, these studies find that particles with radii $< 0.1\ \mu$ are collected principally by Brownian diffusion, that particles with radii $> 0.1\ \mu$ but $< 10\ \mu$ are collected principally by interception, and that particles with radii $> 10\ \mu$ are collected by both interception and inertial impaction. Since collection by Brownian diffusion decreases with increasing particle diameter, while collection by interception and inertial impaction increases with increasing particle

Table 6.2

PARTITION COEFFICIENTS AND CUT-OFF VALUES

FOR MOLECULAR IODINE, I_2. [40]

1. Sodium hydroxide sprays

   H = 2000 for conservative analysis

   H = 5000 for best estimate analysis

   Cut-off value = 0.1% of initial I_2 concentration

2. Sodium thiosulphate sprays

   H = 100,000

   Cut-off value = 0.05% of initial I_2 concentration

3. Hydrazine sprays

   H = 5000

   Cut-off value = 0.1% of initial I_2 concentration

4. Boric acid sprays

   H = 500 for conservative analysis

   H = 2500 for best estimate analysis

   Cut-off value = 0.1% of initial I_2 concentration

diameter, as is shown in Figure 6.4, total collection efficiency has a minimum at about 0.1 μ. These studies also find that diffusiophoresis and thermophoresis principally influence the collection efficiencies of particles with radii > 0.01 μ but < 1 μ, enhancing collection when heat and water vapor are being transported to the surface of the drop, and diminishing collection when transport is away from the drop surface.

The relative importance of diffusiophoresis and thermophoresis has been examined by Pilat and Prem [65] and by Horst [66]. For below-cloud scavenging of particles by rain drops, the modeling study of Pilat and Prem indicates that, when both diffusiophoresis and thermophoresis are enhancing particle collection, diffusiophoretic collection should exceed thermophoretic collection by about a factor of three for particles with radii between 0.01 and 10 μ. For severe accident conditions, when steam condensation is occurring, Horst concludes that thermophoretic collection will be negligible compared to diffusiophoretic collection.

These results suggest that particle collection by spray drops can probably be adequately represented as the sum of the collection efficiencies for inertial impaction and interception, as is recommended in NUREG-0772 [67]. However, when the rate of steam condensation on drops or the rate of droplet evaporation is appreciable, collection by diffusiophoresis should be investigated by sensitivity calculations. And should the range of the particle size distribution used extend significantly below 0.1 μ, the lower bound recomended for use in MELCOR (see Chap. 7), then the impact of collection by Brownian diffusion should also be investigated. Accordingly, collection efficiencies for each of these four processes are developed in the following paragraphs.

Lee and Gieseke have shown [68] that the following expression

$$\varepsilon_{In,Vis} = \frac{3I^2}{2(1+I)^{1/3}} \qquad 6.79$$

is an excellent approximation to the interceptional collection efficiency for viscous flow around a sphere derived by Fuchs [69,70a]

$$\varepsilon_{In,Vis} = (1+I)^2\left[1 - \frac{3}{2(1+I)} + \frac{1}{2(1+I)^3}\right] \simeq \frac{3}{2} I^2 \qquad 6.80$$

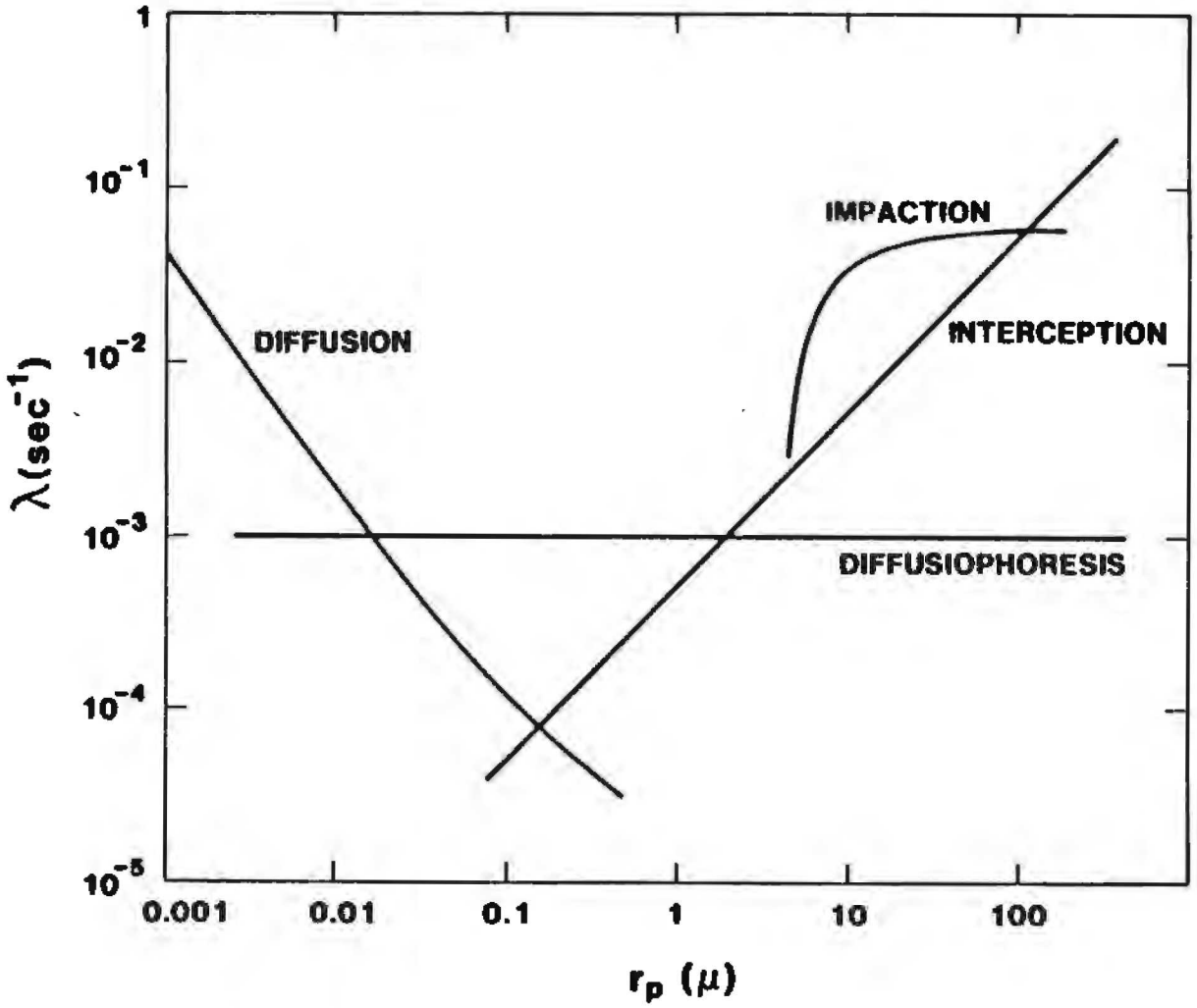

Figure 6.4 Contributing Removal Rate Constants - 300 μ Spray Droplets

when $1 >> I = r_p/r_d$, the ratio of the particle radius to the drop radius. For potential flow around a sphere, Fuchs [70] derived the following expression for the efficiency of collection by interception:

$$\epsilon_{In,Pot} = (1 + I)^2 - (1 + I)^{-1} \qquad 6.81$$

Empirical collection efficiencies for inertial impaction of particles with spheres under conditions of potential or viscous flow have been developed by Langmuir [71] and Fuchs [72]. Langmuir's collection efficiency for inertial impaction from potential flow is

$$\epsilon_{Im,Pot} = \left[\frac{Stk}{Stk + 0.5}\right]^2 \qquad 6.82$$

while the Fuchs' collection efficiency for inertial impaction from viscous flow is

$$\epsilon_{Im,Vis} = \left[1 + \frac{0.75\ \ln(2Stk)}{Stk - 1.214}\right]^{-2} \qquad 6.83$$

where

Stk = Stokes' number = $\dfrac{2r_p^2\ \rho_p(v_d - v_p)}{9\mu r_d}$

r_p = particle radius

r_d = drop radius

μ = bulk gas viscosity

v_d = drop terminal settling velocity = $\dfrac{2\rho_d\ gr_d^2}{9\mu}$

v_p = particle terminal settling velocity = $\dfrac{2\rho_d\ gr_p^2}{9\mu\chi\gamma^2}$

ρ_p = particle mass density

ρ_d = drop mass density

g = gravitational constant

χ = particle agglomeration dynamic shape factor

γ = particle agglomeration collision shape factor

Inspection of Eqs. 79 through 83 shows that for the same Stokes' number, lower values of ε are predicted for viscous flow than are predicted for potential flow. Since for severe accident conditions flow around spray drops is likely to be intermediate in character between potential and viscous flow [38,45], a way to select either the viscous or the potential flow collection efficiency, or to interpolate between them is required.

The following selection/interpolation scheme proposed by Williams [73] for use in the CONTAIN code, is recommended for MELCOR.

$$\varepsilon_{Im,Pot} = 0 \qquad \text{for } Stk \leq Stk_{Cr} = 0.0834 \qquad 6.84$$

$$\varepsilon_{Im,Pot} = \frac{Stk - 0.834}{0.2 - 0.0834} \text{ (Eq. 82)} \qquad \text{for } 0.0834 < Stk < 0.2 \qquad 6.85$$

$$\varepsilon_{Im,Pot} = \text{Eq. 82} \qquad \text{for } Stk \geq 0.2 \qquad 6.86$$

$$\varepsilon_{Im,Vis} = 0 \qquad \text{for } Stk \leq Stk_{Cr} = 1.214 \qquad 6.87$$

$$\varepsilon_{Im,Vis} = \text{Eq. 83} \qquad \text{for } Stk > 1.214 \qquad 6.88$$

$$\varepsilon_{x,Pot} + \varepsilon_{x,Vis} = \frac{\varepsilon_{x,Vis} + \varepsilon_{x,Pot}\,(Re/60)}{1 + (Re/60)} \qquad 6.89$$

where Eq. 88 is an interpolation formula proposed by Langmuir [71]. Stk_{Cr} is the critical Stokes number, and Re is the drop Reynolds number.

The collection efficiency for particles by spray drops under LOCA conditions due to Brownian diffusion can be estimated using the following equation developed by Postma et al. [38]:

$$\epsilon_{BrDiff} = 3.02\ Re^{1/6}Pe^{-2/3} + 1.14(Re/Pe)^{1/3}I + 0.57Re^{1/3}I^2 \qquad 6.90$$

where

$I = r_p/r_d$

Re = Reynolds number = $2r_d\rho/\mu$

Pe = Peclet number = $2r_d(v_d-v_p)/D$

r_p = particle radius

r_d = drop radius

ρ = bulk gas mass density

μ = bulk gas viscosity

v_p = particle terminal settling velocity

v_d = drop terminal settling velocity

and D, the particle diffusion coefficient, is calculated using equations presented in Chapter 5. Since $I = r_p/r_d$ will usually be small, Eq. 90 will be well approximated by its first term

$$\epsilon_{BrDiff} = 3.02\ Re^{1/6}\ Pe^{-2/3} \qquad 6.91$$

The collection efficiency for particles due to diffusiophoresis is obtained as follows. First, the general expression for the rate constant for particle removal by sprays (see Eq. 6.64) is set equal to the rate constant for particle removel by diffusiophoresis, $k_{diffusio} = v_{diffusio}(A_{diffusio}/V)$ where $v_{diffusio}$ and $A_{diffusio}$ are the diffusiophoretic deposition velocity and deposition surface in the volume V. Then, the resulting expression is solved for the diffusiophoretic collection efficiency, $\epsilon_{diffusio}$, thereby obtaining:

$$e_{diffusio} = \frac{4}{3}\ \frac{r_d}{Fh}\ \frac{M_s^{1/2}}{X_s M_s^{1/2} + X_g M_g^{1/2}}\ \frac{M_g}{M_s}\ \frac{R_s}{\rho_g} \qquad 6.92$$

where

R_s = mass condensation rate of steam on drops

r_d = drop radius

F = volumetric flow rate of spray drops

h = drop fall height

M_s = molecular weight of steam

M_g = molecular weight of the non-condensible bulk gases

X_s = mole fraction of steam

X_g = mole fraction of the non-condensible bulk gases = $1-X_s$

ρ_g = density of the non-condensible bulk gases

This approach could also be used to develop collection efficiencies for thermophoresis and turbulent diffusion.

Finally, collection efficiencies for different processes are combined using the following expression

$$\varepsilon_{ij} = 1 - \prod_k (1-\varepsilon_{ijk}) \qquad 6.93$$

where ε_{ij} is the total collection efficiency of drops of size i for aerosol particles of size j by collection process k, and $\varepsilon_{ijk} \leq 1$.

REFERENCES

1. W. K. Winegardner et al., Studies of Fission Product Scrubbing within Ice Compartments, NUREG/CR-3248, PNL-4691, Battelle Pacific Northwest Laboratory, Richland, WA, May 1983.

2. W. K. Winegardner and A. K. Postma, "Fission Product Scrubbing in Ice Compartments," Proceed. Intl. Meeting on Light Water Reactor Severe Accident Evaluation, Cambridge, MA, Aug. 28 to Sept. 1, 1983, Vol. 2, p. 11.6-1.

3. J. A. Gieseke et al., Radionuclide Release under Specific Accident Conditions, Vol. IV, PWR, Ice Condenser Containment Design, BMI-2104, Battelle Columbus Laboratories, Columbus, OH, July 1984, p. 5-19.

4. N. A. Fuchs, The Mechanics of Aerosols, MacMillan, New York, 1964, p. 164.

5. J. Pich, "Theory of Aerosol Filtration by Fibrores and Membrane Filters," in Aerosol Science, C. N. Davies, ed., Academic Press, London, 1966, p. 231.

6. J. G. Knudsen and R. K. Hilliard, Fission Product Transport by Natural Processes in Containment Vessels, BNWL-943. Pacific Northwest Laboratory, Richland, Washington, 1969.

7. R. B. Bird et al., Transport Phenomena, pp. 644-658, John Wiley and Sons, Inc., New York, 1966.

8. T. K. Sherwood et al., Mass Transfer, pp. 201, McGraw-Hill Book Company, New York, 1975; a. p. 201; b. p. 241.

9. G. A. Sehmel, "Particle Deposition from Turbulent Air Flow," J. Geophys. Research, 75, 1766 (1970).

10. P. C. Owczarski, "Particle Retention in PWR Ice Compartments," Proc. Fission Product Behavior and Source Term Research, ANS Topical Mtg., July 15-18, 1984, Snowbird, Utah, July 1985, p. 35-1.

11. N. A. Fuchs, The Mechanics of Aerosols, Pergamon Press, New York, 1964, p. 240.

12. F. J. Moody et al., "Aspects of Modeling Fission Product Scrubbing in Suppression Pools," Proceed. Fission Product Behavior and Source Term Research, ANS Topical Meeting., July 15-18, 1984, Snowbird, Utah, EPRI Rept. NP-4113-SR, July 1985, p. 32-1.

13. W. J. Marble et al., "Retention of Fission Products by BWR Suppression Pools during Severe Reactor Accidents," International Thermal Nuclear Reactor Safety Conference, Chicago, 1982.

14. D. D. Paul et al., "Radionuclide Scrubbing in Water Pools-Gas-Liquid Hydrodynamics, Proceed. Fission Product Behavior and Source Term Research, ANS Topical Meeting, July 15-18, Snowbird, UT, EPRI Rept. NP-4113-Sr, July 1985, p. 30-1.

15. F. J. Moody and S. G. Nagy, "Estimated Effects of Interfacial Vaporization on Fission Product Scrubbing, Proceed. International Meeting on Light Water Reactor Severe Accident Evaluation, Aug. 28-Sept. 1, Cambridge, MA, 1983.

16. T. Demitrack and F. J Moody, "Planetary Ellipsoid Bubble Model for Fission Product Scrubbing, ANS Trans., 45, 483, (1983).

17. F. J. Moody et al., "Aspects of Modeling Fission Product Scrubbing in Suppression Pools," Proceed. Fission Product Behavior and Source Term Research, ANS Topical Meeting, July 15-18, Snowbird, UT, EPRI Rept. NP-4113-Sr, July 1985, p. 32-1.

18. J. C. Cunnane et al., "The Scrubbing of Fission Product Aerosols in LWR Water Pools under Severe Accident Conditions/Experimental Results," Proceed. Fission Product Behavior and Source Term Research, ANS Topical Meeting, July 15-18, 1984, Snowbird, UT, EPRI Rept. NP-4113-SR, July 1985, p. 31-1.

19. W. J. Marble, et al., Preliminary Report on the Fission Product Scrubbing Program, General Electric Report No. NEDO-330017, January 1983.

20. P. O. Owczarski et al., Technical Basis and Users' Manual for SPARC--A Suppression Pool Aerosol Removel Code, NUREG/CR-3317, May 1983.

21. A. T. Wassel, et al., "Analyses of Radionuclide Aerosol Retention in Water Pools," submitted for publication to Nucl. Design Eng.

22. A. T. Wassell et al., "Scrubbing of Radionuclide Aerosols in Water Pools," Proceed. Fission Product Behavior and Source Term Research, ANS Topical Meeting, July 15-18, Snowbird, UT, EPRI Rept. NP-4113-Sr, July 1985, p. .

23. S. Ramakrishnan et al., "Studies in Bubble Formation I: Bubble Formation under Constant Flow Conditions," Chem. Engr. Sci, 24 731 (1969).

24. I. Leibson et al., "Rate of Flow and Mechanics of Bubble Formation from Single Submerged Orifices," A.I.Ch.E. Journal, 2 296 (1956).

25. D. T. Shaw, ed., Fundamentals of Aerosol Science, John Wiley and Sons, New York, 1978, p. 22.

26. T. T. Mercer and R. G. Stafford, Ann. Occup. Hyg., 12, 41 (1969).

27. R. W. Higbie, Trans. Am. Inst Chem. Engrs., 31, 365 (1935).

28. P. Li et al., "Unsteady State Mass Transfer from Gas Bubbles - Liquid Phase Resistance," AICHE Journal, 11 581 (1965).

29. R. B. Bird et al., Transport Phenomena, John Wiley and Sons, Inc., New York, 1966, p. 541.

30 F. J. Moody, personal communication, 1985.

31. S. Webb, personal communication, 1985.

32. R. Dennis, Ed., Handbook on Aerosols, TID-26608, Technical Information Center, ERDA, Washington, DC, 1978, p. 113.

33. J. E. Brockmann, App. E., "Uncertainties in Aerosol Removal by Suppression Pool Scrubbing," in Uncertainty in Radionuclide Release under Specific LWR Accident Conditions, Vol. IV: TC Analysis, P. K. Mast et al., SAND84-0410/4, Sandia National Laboratories, Albuquerque, NM, p. E-9, to be published.

34. W. L. Haberman and R. K. Morton, David W. Taylor Basin Model, An Experimental Investigation of the Drag and Shape of Air Bubbles Rising in Various Liquids, DTMB-802, 1953.

35. G. B. Wallis, Int. J. Multiphase Flow, 1, 491 (1974).

36. D. D. Paul, personal communication, 1985.

37. F. Knelman et al., Nature, 173, 261, (1954).

38. A. K. Postma et al., Models for Predicting the Removal of Airborne Contaminants by Reactor Containment Sprays, BNWL-B-417 (1975).

39. U. S. Nuclear Regulatory Commission, Reactor Safety Study, WASH-1400, App. VII, Sect. 3, (1975).

40. D. R. Grist, Spray Removal of Fission Products in PWR Containments, Report SRD R267, Safety and Reliability Directorate, UKAEA, England (1982).

41. A. K. Postma et al., Technological Bases for Models of Spray Washout of Airborne Contaminants in Containment Vessels, NUREG/CR-0009 (1978).

42. A. E. J. Eggleton, Theoretical Examination of Iodine-Water Partition Coefficients, AERE-R-4887 (1967).

43. T. B. Powers and D. L. Reid, Size Distribution of Drops from Containment Spray Nozzels, PB-293-653 (1979).

44. L. F. Parsly, Removal of Radioactive Particles by Sprays, ORNL-4671 (1971).

45. L. F. Parsly, Design Consideration of Reactor Containment Spray Systems - Part VI. The Heating of Spray Drops in Air-Stream Atmospheres, ORN-TM-2412, Part VI (1970).

46. M. Tanka et al., "Performance of Containment Sprays for Light Water Reactors and Evaluation of the Heat Transfer," Nucl. Technol., 54, 54 (1981).

47. A. K. Postma and W. F. Pasedag, A Review of Mathematical Models for Predicting Spray Removal of Fission Products in Reactor Containment Vessels, WASH-1329 (1973).

48. W. F. Pasedag and J. L. Gallagher, "Drop Size Distribution and Spray Effectiveness," Nucl. Technol., 10, 412 (1971)

49. B. C. Walker et al., Discretization and Integration of the Equation Governing Aerosol Behavior, UKAEA Report SRD R98 (1978).

50. V. Griffiths, The Removal of Iodine from the Atmosphere by Sprays, Report No. AHSB(S)R45, UKAEA, London (1963).

51. P. V. Danckwerts, "Absorption by Simultaneous Diffusion and Chemical Reaction into Particles of Various Shapes and into Falling Drops," Trans. Farad. Soc., 47 1914 (1951).

52. W. E. Ranz and W. R. Marshall, "Evaporation from Drops," Chem. Eng. Prog., 48, No. 3, 141 and 48, No. 173 (1952).

53. N. Frossling, Gerlands Beitr. Geophys., 52, p. 170 (1938), as referenced by R. B. Bird, W. E. Stewart, and E. N. Lightfoot, Transport Phenomena, John Wiley and Sons Inc., New York, 1960, p. 409.

54. C. R. Wilke, Chem. Engr. Prog., 46, 95 (1950).

55. J. R. Welty et al., Fundamentals of Momentum, Heat, and Momentum Transfer, 3rd Ed., Wiley, New York, 1984, p.492.

56. C. R. Wilke and P. Chang, A.I. Ch. E.Journal, 1, 264 (1955).

57. Ref. 55, p. 494.

58. J. G. Knudsen, Properties of Air-Stem Mixtures Containing Small Amounts of Iodine, BNWL-1326, Battelle-Northwest Laboratories (1970).

59. EPRI, IDCOR Technical Report 11.1, 11.4 and 11.5: Estimation of Fission Product and Core-Material Characteristics, Atomic and Industrial Forum, Bethesda, MD, October 1983.

60. L. C. Schwendimann, The Washout of Methyl Iodide by Hydrazine Sprays, BNWL-935 (1968).

61. M. J. Pilat and A. Prem, Atmos. Environ., 10, 13 (1976).

62. M. J. Pilat and A. Prem, J. Air Pollut. Contr. Assoc., 27, 982 (1977).

63. P. K. Wang et al., "A Theoretical and Experimental Determination of the Efficiency with which Aerosol Particles are Collected by Water Drops in Air Due to Brownian Motion, Phoretic Forces, Inertial Impaction, and Electric Forces, 4th Joint Conference on Sensing Environmental Pollutants, New Orleans, LA, Nov. 6-11, 1977, American Chemical Society, Washington, DC, 1978.

64. S. N. Grover and H. R. Pruppacher, J. Atmos. Sci., 34, 1655 (1977).

65. K. H. Leong et al., J. Atmos. Sci., 39, 1130 (1982).

66. T. W. Horst, A Review of Particle Transport in a Condensing Steam Environment, BNWL-848, Battelle Pacific Northwest Laboratories, Richland, WA, 1968.

67. "Appendix E, Transport Models for Containment Transport Analysis," in Technical Bases for Estimating Fission Product Behavior During LWR Accidents, NUREG-0772 (1981).

68. K. W. Lee and J. A. Gieseke, "Note of Interceptional Collision Efficiency," J. Aerosol Sci., 11, 335 (1980).

69. N. A. Fuchs, Kokl. Akad. Nauk. USSR, 81, 1043 (1951).

70. Ref. 4, p. 164.

71. I. Langmuir, J. Meteor., 5, 175 (1948).

72. Ref. 4, p. 162.

73. D. C. Williams, "Spray Efficiency Sensitivity Studies," Appendix C in Uncertainty in Radionuclide Release Under Specific LWR Accident Conditions, Vol. III, S_2D Analyses, R. J. Lipinski et al., SAND84-0410, Sandia National Laboratories, Albuquerque, NM 87185, April 1985.

CHAPTER 7

SIZE OF THE FISSION PRODUCT BEHAVIOR ODE SET

J. L. Sprung

7.1 Introduction

During the analysis of hypothetical severe accidents at Light Water Reactors, Fission Product Behavior is modeled in order to determine the amounts and chemical and physical forms of the species that would be released to the biosphere (the ex-plant source term) should the accident lead to containment failure. The preceding chapters of this report have (1) identified the rate processes that control the amounts and forms of these species, and (2) reviewed and recommended representations for each process. Not addressed in the preceding chapters was the question of the size of the set of ordinary differential equations that would result from the implementation of these processes for all of the chemical classes defined in Chapter 2.

The rate of change with time of the mass of a species (vapor or aerosol) in a state (location within a control volume; i.e., gas borne, deposited or condensed on surfaces, suspended or dissolved in water) can be appropriately represented by an ordinary differential equation comprised of terms which give the contribution of individual rate processes (e.g., aerosol agglomeration, deposition, or resuspension) to the total rate of change of the species. Accordingly, the MELCOR fission product behavior equations will consist of a set of ordinary differential equations (ODEs)

Because a separate ODE is required to describe each species in each state that it can exist, detailed descriptions of fission product behavior (descriptions that involve many species and many states) can very easily produce fission product behavior ODE sets that are very large (~500 ODEs). Since routine MELCOR calculations probably will be unacceptably slow if the fission product ODE set can not be held to about 50 ODEs, this chapter will present the technical basis for adequately modeling fission product behavior using a number of species and states that produces an ODE set of approximately 50 ODEs (as few as 25 for scoping calculations; as many as 100 for sensitivity calculations). Thus, this chapter will discuss the species and states that must be treated in order to develop source terms adequate for the calculation of ex-plant consequences.

7.2 Species Released from Fuel and Structural Materials

An LWR accident that produces a significant ex-plant source term will always involve the melting of fuel, and may involve the melting of control rods and core support structures, high pressure melt ejection from the failed reactor pressure vessel, in-and ex-vessel steam explosions, and attack of molten materials on concrete structures, for example in the reactor cavity. Melting of fuel, control rods, and core support structures causes volatile constituents of these originally solid materials to be released as vapors that may condense to aerosols upon transport to locations cooler than the location of their release. Aerosols can also be produced by ejection of molten materials from the pressure vessel while at high pressure, provided that the melt stream is unstable, and by sparging of melts by gases. Melt sparging and conversion of non-volatile melt constituents to volatile oxides during steam explosions can also lead to the formation of vapors.

Because reactor fuel, cladding, core support structures, and concrete contain many trace constituents in addition to their bulk components, the vapors and aerosols released from these structures during severe LWR accident sequences can have many different isotopic and chemical compositions, far too many to be all simultaneously modeled by MELCOR. Therefore, wherever possible, the MELCOR fission product behavior model should neglect trace species and combine important species into groups.

Combining species released from fuel, control rod, or structural materials was examined in Chapter 2 of this report. Chapter 2 concluded that isotopic effects do not significantly effect release processes and recommended that, as was done in the Reactor Safety Study [1], elements with similar chemical properties be grouped into chemical classes, which are assigned properties similar to those of the most important element in the class, where importance is based upon released mass (determines impact on aerosol agglomeration), thermal power (determines impact on decay heating), and activity (determines impact on health and economic consequences). However, unlike the Reactor Safety Study, which used eight chemical classes, Chapter 2 recommended the use of fourteen classes, in order to better reflect chemical differences among the more important fission product, structural, and control rod elements. Because aerosol behavior is strongly influenced by particle mass, a fourteenth class containing only water is required in order to follow steam condensation onto and evaporation from aerosols. Table 7.1 lists the fifteen chemical classes recommended for use in MELCOR, and presents the more important elements assigned to each class and the suggested representative element.

A. Vapor Species

Vapors released from overheated or molten core or structural materials can be divided into three groups: non-condensable vapors (i.e., Noble Gases), relatively volatile condensable vapors (e.g., CsI), and relatively involatile condensable vapors (e.g., Uranium and its oxides). Because they are chemically inert and non-condensable, Noble Gas fission products (Xe, Kr, Rn) need not be treated within the fission product ODE set. Instead, they should be followed as trace constituents of the bulk gases.

MERGE [2] and PSTAC [3] calculations suggest that for many severe accident sequences relatively involatile vapors (materials with minimal vapor pressures at temperatures of ~1000° C) released in the pressure vessel will encounter temperatures low enough to cause them to condense (undergo gas-to-particle conversion) either in the upper regions of the core or in the upper plenum. Similarly, relatively involatile vapors, released in the reactor cavity from a pool of molten corium due to core-concrete interactions, are expected to condense quite near to the surface of that pool. Therefore, relatively involatile vapors (vapors of elements in chemical classes 7 through 10 in Table 7.1) probably can be treated in MELCOR as though they condense to aerosols immediately upon volatilization.

Table 7.1
Chemical Classes

Class Name	Members (with suggested representive element underlined)
1. Noble Gases	Xe, Kr, Rn
2. Alkali Metals	Cs, Rb, Li
3. Alkaline Earths	Ba, Sr
4. Halogens	I, Br
5. Chalcogens	Te, Se, S
6. Platinoids	Ru, Pd, Rh, Ni
7. Early Transition Elements	Mo, Tc, Nb, Fe, Cr, Mn
8. Tetravalents	Ce, Zr, Th, Np
9. Trivalents	La, Pm, Sm, Pu, Y
10. Uranium	U
11. More Volatile Main Group Metals	Cd, Hg, Pb
12. Less Volatile Main Group Metals	Sn, Ag, In, Ga
13. Boron	B, Si, P
14. Water	H2O
15. Concrete	Concrete

Table 7.1 includes Ag, Cd, and In (control rod materials); Fe, Cr, Ni, and Mn (constituents of stainless steel); Zr and Sn (cladding constituents); and U (major constituent of fuel), because each can be a significant contributor to aerosol mass. Cs, Rb, Ba, Sr, I, Te, Nb, Zr, La, and Y are included because each is an important contributor to decay heat. And Cs, Ba, Sr, I, Te, Ru, and Ce are included because together they largely determine health and economic consequences.

Most volatile vapors can probably be assumed to condense to aerosols immediately upon volatilization without introducing significant errors into MELCOR calculations. This may not be true (1) if the volatile vapor (e.g., Cd) is released in amounts sufficiently large so that treatment as an aerosol would significantly (and artificially) enhance aerosol agglomeration and thus gravitational deposition of aerosols; (2) if the volatile vapor (e.g., CsI) is an important contributor to decay heat; or (3) if the volatile vapor (e.g., Te) has a significant impact upon health or economic consequences.

Experimental [4-6] and calculated [7] vapor pressure data indicate that during at least some severe accident sequences the following materials are likely to transport through much of the reactor coolant system as vapors rather than as aerosols: CsI, CsOH, I_2, and Cd. Accordingly, chemical classes 2, 4, and 11 in Table 7.1 ought not to be assumed in MELCOR calculations to exist only as aerosols or, if this assumption is made during production calculations, then it ought to be examined during sensitivity calculations. The same data suggest that during sequences characterized by very high temperatures $Sr(OH)_2$, $Ru(OH)_2$, $Sn(OH)_2$, Ag, and $In(OH)_2$ will transport through at least part of the upper plenum as vapors. Therefore, for high temperature sequences transport of chemical classes 3, 6, and 12 as vapors probably should be examined during sensitivity studies.

Because boron from control rods can be oxidized to B_2O_3 and then converted to volatile boric acids (HBO_2 and H_3BO_3) by reaction with water, chemical class 13 may transport as a vapor during some severe accident sequences. Finally, because Te reacts with stainless steel surfaces and with aerosols that contain control rod elements to form tellurides, if Te is released from fuel as a metal vapor, then reaction with structural or aerosol surfaces to form tellurides will make transport as a vapor unlikely. Transport as an aerosol would also result if Te is initially released from fuel as a telluride. Transport as a vapor appears possible, only if Te is released as H_2Te. Accordingly, it seems reasonable to assume that chemical class 5 transports as an aerosol.

B. Aerosol Species

Aerosol species can be produced indirectly by vaporization of fuel or structural materials followed by vapor condensation to aerosols (gas-to particle conversion), or by mechanical aerosolization of these solid materials (for example during high pressure melt ejection). Because of the complexity of these processes, aerosols of quite differing sizes (particle diameters) are produced. The resulting aerosol size distribution is further perturbed by agglomeration and deposition processes. Thus, the distribution is not constant with time, and some numerical approach must be adopted to follow its time evolution.

The number of aerosol species that a fission product behavior code must treat depends strongly upon the numerical method adopted to follow the time evolution of the aerosol size distribution. Two approaches are widely used. The first approach assumes that the distribution has a constant form, typically log-normal, and follows, using some appropriate numerical method, for example a method of moments technique, the variation with time of the values of the parameters that specify the exact shape of the distribution. The second approach divides the size distribution into sections and then follows the variation with time of the mass in each section by integrating a set of ODEs, one for each section. If the aerosol can have several distinguishable compositions, one ODE is written for each composition in each section. Thus, the total number of ODEs written equals the number of sections times the number of distinguishable compositions.

In blind comparisons to experiment, fission product behavior codes that use the sectional approach predict experimental results substantially better than do codes that assume a log-normal distribution and implement it using a methods of moments technique [8]. Therefore, a sectional approach for the treatment of aerosol processes is recommended for MELCOR.

Sectional Aerosol Codes. Sectional aerosol behavior codes represent aerosol properties within a section using either a characteristic particle (particle diameter equal to the arithmetic or geometric mean of the section boundaries) [9], or a distribution of particle masses within each section [10]. If distributions are used, then aerosol behavior rate coefficients must be represented as integrals over the distribution, double integrals when the rate process involves two distributions (e.g., second order rate processes such as agglomeration). Because double integrals are time consuming to evaluate, sectional codes that evaluate rate coefficients using double integrals, typically do so only at a selected set of temperatures and pressures, obtaining coefficient values at other temperatures and pressures by interpolation.

When aerosol properties within a section are represented by a characteristic particle, rate coefficients can be evaluated without using integrals. Because integrals are not needed, evaluation of rate coefficients is rapid and can be performed at every time step. Therefore, interpolation between precalculated values is not necessary. However, because each section is represented by only one mass, aerosol agglomeration due to gravitational settling, which involves a collision between two particles of different masses, can not be directly treated within a single section. Therefore, unless corrected for in some ad hoc fashion [11], in order to adequately treat gravitational agglomeration, sectional codes that use characteristic particles generally must use many more sections than do sectional codes that evaluate rate coefficients using integrals (particle distributions). Because more sections means more ODEs, it is recommended that MELCOR use the integral approach (particle distribution within each section) for the calculation of rate coefficients rather than the characteristic particle approach.

Number of Sections. The number of sections and thus the number of ODEs required by a sectional aerosol code can be limited first by applying a geometric constraint to the selection of section boundaries, and second by limiting the range of the aerosol size distribution that is treated by the code. When the geometric constraint [10] is used, the upper section boundary is chosen to be at least twice the lower section boundary. This causes the width of sections to increase steadily by factors of at least two and thus decreases the number of sections that span a given aerosol size distribution. In addition, use of the geometric constraint minimizes the number of agglomeration coefficients that need to be calculated, because particle collisions can produce a new particle only in two sections, in the section of the larger of the two collision particles or in the section just above that section.

The range of an aerosol size distribution is determined by the smallest size at which particles are formed and by the largest size at which particles can remain airborne for a significant length of time. A sensitivity study of aerosol agglomeration and deposition using the MAEROS code [12] showed that calculations that use 10 sections spanning the range 0.1 to 50 microns give results essentially indistinguishable from those obtained using 20 sections spanning the range from 0.01 to 400 microns. The same study showed that use of only 5 sections produced results not substantially different form those obtained using 10 sections. Two aerosol processes, gas-to-particle conversion and gravitational settling of large particles, explain the first result.

The smallest particles in an aerosol size distribution are usually formed by gas-to-particle conversion. Gas-to-particle conversion typically forms large numbers of very small particles (diam. ~0.01μ), which rapidly agglomerate to form larger particles. Because this process is very rapid, if modeled, it will make the fission product ODE set stiff whenever it occurs. Thus, it is recommended that rapid agglomeration of small particles be neglected, and that it be assumed that gas-to-particle conversion yields particles of diameter about 0.1 micron.

The largest particles in an aerosol size distribution are most efficiently removed from the distribution by gravitational settling (sedimentation). For particles of diameter 100 microns or larger, sedimentation is quite rapid. Therefore, it is recommended that collisions between particles of diameter about 100 microns or larger be assumed to produce a particle on the floor (instant sedimentation).

Confining the aerosol size distribution treated by MELCOR to the range 0.1 to 100 microns and division of this range into only 10 sections may be adequate for most calculations, but it is unlikely to be appropriate for all severe accident sequences or for all sensitivity or uncertainty calculations. Therefore, it is recommended that the lower and upper bounds of the aerosol size distribution used in MELCOR and the number of sections used to span that range be variably dimensioned to permit easy use of other bounds and numbers of sections.

Size Distribution of Deposited Aerosols. Deposition of an aerosol particle onto a previously deposited aerosol layer causes the deposited particle to agglomerate with the layer. Because agglomeration takes place upon deposition, the size distribution of the gasborne aerosol particles is not preserved in the deposit. Deposition of an aerosol particle onto a water layer (film or pool) causes the particle to become suspended in the water layer. Because aerosol particles suspended in water do not agglomerate, the size distribution of the gas borne aerosol particles is preserved in the suspension (agglomeration will occur if the suspension becomes highly concentrated due to evaporation of water). However, should the water layer flash to gas borne water droplets, each droplet will contain an unknown number of aerosol particles that will agglomerate as the droplet evaporates, thereby destroying the original size distribution of the particles. Accordingly, it is recommended that MELCOR not try to track the size distribution of aerosol particles deposited on dry surfaces or suspended in water layers.

Resuspension of Deposited Aerosols. Because short duration energetic events, that produce high surface flow rates or pool flashing (e.g., rapid compartment depressurization, hydrogen

burn, steam explosion), may cause significant amounts of deposited aerosols to become resuspended, a size distribution for the resuspended aerosol material must be supplied as input to or calculated by MELCOR. Because current knowledge does not seem adequate to support the development of a simple mechanistic model of aerosol resuspension, it is recommended that the size distribution of resuspended aerosol deposits be supplied to MELCOR as user input. Further, because energetic events will generally be of quite short duration, it is recommended that resuspension of deposited aerosols be treated outside of the fission product ODE set (between time steps), as a correction to the gas borne aerosol size distribution existing at the end of the time step during which the energetic event occurred.

7.3. Species Formed by Chemical Transformations

Fission product species initially formed within the fuel matrix can undergo numerous transformations by reacting chemically with other species, which they encounter within or after release from that matrix. In general, a chemical transformation will be important only if the transformation changes the physical state of a fission product (e.g., conversion of a condensed species to a gaseous species), and thus its transport characteristics and the likelihood of its release to the biosphere.

Each of the following processes can transform existing fission product species into new species: (a) nuclear transformations, (b) reactions along the tracks of recoil atoms, (c) reactions in fog lines above the surface of degraded fuel, (d) transformations induced by the interactions of molten corium with concrete, (e) oxidation during steam explosions (e.g., conversion of Ruthenium to its oxides), (f) reactions initiated by combustion events, (g) interactions of deposited fission product vapors with surfaces (adsorption, chemisorption, and reactions), (h) chemical transformations induced by radiolysis of bulk materials, and (i) the solution chemistry of water soluble fission products, particularly molecular iodine and its disproportionation products, iodide and iodate ions. Because complex reaction mechanisms are expressed mathematically by large sets of ordinary differential equations, which are time consuming to implement numerically, wherever possible explicit modeling of complex chemistry should be avoided in the MELCOR code system.

Since the isotopic inventory of a reactor at scram can be determined by ORIGEN [13] calculations and provided to MELCOR as input data, nuclear transformations need not be modeled in MELCOR. Reactions of fission product atoms along recoil tracks and at fuel lattice sites determine the chemical (molecular)

form of stabilized fission product atoms. These processes are not well characterized and should not .be modeled in MELCOR. Instead the influence of chemical form upon the rates of release of fission products from fuel should be captured using empirical fits to experimental data (see Chapters 3 and 4 for recommended models for release mechanisms).

Chemistry in fog lines above fuel surfaces principally affects the chemical compositions of aerosol particles formed by gas-to-particle conversion processes. Since MELCOR's aerosol models depend only on particle mass and not on particle composition, fog line chemistry can be neglected in MELCOR as long as the gross features of aerosol composition are captured by use of some suitable set of aerosol components.

The chemical reactions that occur in core-concrete melts release amounts of heat that are negligible compared to the amounts generated by decay of fission products in the melt, produce significant amounts of combustible gases (H_2 and CO), and determine the chemical forms of fission products released from corium during core-concrete reactions. Generation of combustible gases in core-concrete melts will be treated in MELCOR's thermal-hydraulics modules. The effects of chemical reactions in core-concrete melts upon release of fission products are captured using the core-concrete fission product release model described in Chapter 4.

Oxidation of fission product species during steam explosions was discussed in Chapter 5. Because of rapid settling rates for particles ejected into the atmosphere by the steam explosion and kinetic limits on heat transfer to the particles and on oxygen availability, it was concluded in Chapter 5 that significant oxidation of fission product species during steam explosions was unlikely.

Reactions of fission product species with combustion intermediates (O, OH, H) will most often be unimportant either because the reactions occur only to a limited degree or because they do not produce a change in the physical state of the fission product and thus do not alter its transport characteristics or probability of release to the biosphere. For example, the large heat sink capacities of walls will prevent fission products condensed on wall surfaces from reacting extensively; fission products condensed on wet aerosol particles will not react until the condensed water evaporates; and vaporization of fission products species from dry aerosols followed by oxidative reactions with combustion intermediates will generally yield products less volatile than the vaporized reactant, which will therefore rapidly condense after passage of the flame front [e.g., conversion of Te(s) to TeO_2(s)]. Thus, only reactions that convert a condensed fission product to a gas [e.g., conversion of CsI(s) to CsOH(s) + I(g) with I(g) forming principally HI(g)

when H_2 is in excess, and $HI(g) + I_2(g)$ when H_2 is limited], or a gaseous fission product to an aerosol [e.g., conversion of $H_2Te(g)$ to $TeO_2(s)$] need be considered during MELCOR analyses. Furthermore, since combustion events will be of short duration, it should be adequate to assume that these conversions are instantaneous, and therefore can be modeled outside the fission product ODE set.

Reactions of deposited fission products with surfaces were discussed in Chapter 5 where it was concluded that adsorption and chemisorption should be neglected because they are easily reversed, and that irreversible reaction could be treated without adding any rate equations to the fission product ODE set by modifying the deposition rate constant of the irreversibly bound specie. However, treatment of reversible reactions requires addition of rate equations to the fission product ODE set and thus should be done only for important fission products (e.g., compounds of Cs, I, Te). Reversible surface reactions probably should be investigated during sensitivity calculations for at least two compounds, CsOH and $ZrTe_2$.

Radiolysis of media that do not contain easily ionizable bulk constituents [e.g., air, H_2O] typically culminates in the ionization of the more easily ionizable trace species present in the media. Accordingly, radiolysis is not expected to significantly transform metal oxides or hydroxides, but may convert iodide ions to iodine atoms which can then form molecular iodine. Although G-values (radiolytic conversion rates) for the conversion of iodide ion to iodine atom are not available for reactor accident conditions, rapid radiolytic conversion of iodide ions to iodine atoms does not seem likely either in solution or in the gas phase.

Because most fission product species are insoluble in water at acidities characteristic of severe reactor accident conditions (e.g., most fission product oxides or hydroxides), few fission products are likely to have significant solution phase chemistries. Of those fission product species that are soluble in water, most have no significant solution chemistries because of the stability of their ionic forms (e.g., Cs^{+}, Ba^{+2}, Sr^{+2}, La^{+3}), because of sparing solubility (e.g., MoO_4^{-2}), or because their masses are negligible (e.g., Br^{-}). Thus, only the solution phase chemistry of iodine seems capable of significantly affecting the consequences of a severe reactor accident.

The solution chemistry of iodine under accident conditions has been extensively reviewed [14,15]. Since iodide ion is stable in solution, iodine solution phase chemistry will be significant only if iodide ion can be efficiently converted to molecular iodine either by radiolysis or oxidation. Radiolytic conversion is unlikely to be efficient, and oxidation is

efficient only under strongly acidic conditions, a situation unlikely to develop during a severe reactor accident. Thus, for routine MELCOR analyses, iodine solution chemistry probably need not be modeled although the code system should be structured to allow iodine solution phase chemistry to be examined during sensitivity studies.

The preceding summary review suggests that, although fission products can experience complicated chemical transformations during severe accident sequences, in general these transformations can either be neglected (chemistry in fog lines), encompassed using simple models (release from fuel), or treated without the addition of rate equations (combustion events). Thus, excepting atypical conditions, fission product chemistry will not necessitate significantly increasing the size of the fission product ODE set.

7.4. States

Within a control volume aerosols and vapors can be located in the gas phase or on surfaces. Because the gas phase is assumed to be well mixed, it constitutes a single state. Because surfaces may be distinguished by many properties (e.g., aerosol or structural, wet or dry, horizontal or vertical, high or low thermal conductivity), many surface states are possible. To minimize the number of surface states, surface states should be defined only for properties that significantly affect the transport or deposition of fission product species.

Because aerosols can be transported from one control volume to another by flows of bulk gases, aerosol surfaces must be distinguished from structural surfaces. Because water can flow from one compartment to another and within a compartment from one location to another, wet and dry surfaces must be distinguished. Because geometric orientation and thermal properties affect deposition rates, surfaces may also need to be distinguished with regard to these properties.

Geometric Orientation. Experiments show that surface deposition velocities vary with surface orientation [16]. For particles with diameters larger than 0.1 micron, the combined deposition velocity resulting from Brownian diffusion, turbulent diffusion, and gravitational settling is largest for deposition to floors, is somewhat smaller for deposition to walls, and is much smaller for deposition to ceilings. Differences were decreased by increased bulk gas flow rates (i.e., increased friction velocities, increased Renolds numbers). For particles with diameters greater than 40 microns, gravitational settling causes deposition velocities to floors to be significantly greater than deposition velocities to walls or ceilings.

Therefore, because most of the mass of an aerosol size distribution is in the larger particles, and because water flows from walls and ceilings to floors, and from floors to other control volumes, floors need to be distinguished from walls and ceilings. Conversely, despite the fact that wall deposition velocities are generally larger than ceiling deposition velocities, because non-rectangular compartments (e.g., containment domes, pipes) have poorly defined ceilings, and because water pools don't collect on ceilings, it may not be necessary to distinguish walls from ceilings in MELCOR control volumes.

Surface Thermal Conductivities. Diffusional, diffusiophoretic, and thermophoretic deposition velocities all depend upon boundary layer temperature gradients and thus on surface thermal conductivities. Despite this, to avoid multiplying surface states, it may be advisable in MELCOR to avoid distinguishing surfaces within the same control volume according to their thermal properties.

7.5. Size of the MELCOR Fission Product Behavior ODE Set.

The number of ODEs needed to describe aerosol species equals the sum of the number needed to treat gasborne aerosol species plus the number needed to treat deposited aerosols. The number of ODEs needed to treat gasborne aerosols equals the product of the number of sections used to describe the size distribution of the gasborne aerosol species times the number of distinguishable aerosol compositions being tracked. Because specification of the size distribution of an aerosol deposit is not possible (and possibly is not meaningful), the number of ODEs required to describe an aerosol deposit is equal to the number of distinguishable compositions in the deposit times the number of deposition surfaces (no sectional information is needed). Therefore, if for scoping calculations 4 compositions (water, primary system, high pressure melt ejection, and core-concrete aerosol compositions) distributed over 5 size sections are used to specify gasborne aerosols, and 4 surface states (wet and dry walls and floors) and the same 4 compositions are used to characterize deposited aerosols, then 36 ODEs will be required to describe aerosol species [(4x5)+(4x4)].

If for production calculations 10 aerosol size sections are used and CsOH and CsI are treated as a fifth composition which can transport both as an aerosol and as a vapor, then the number of ODEs increases to 71 = [(5x10)+(5x4)]+1. Finally, a sensitivity calculation that examined the impact on production calculation results, of treating Cd and Te (chemical classes 5 and 11) as species that transport through high temperature compartments as vapors (i.e., 7 compositions), will require 101 = [(7x10)+(7x4)]+3 ODEs.

REFERENCES

1. U. S. Nuclear Regulatory Commission, "Release of Radioactivity in Reactor Accidents," Appendix VII of the Reactor Safety Study, WASH-1400, October 1975.

2. J. A. Giescke et al., Radionuclide Release Under Specific LNR Accident Conditions, Vols. I and II, BMI-2104, Battelle Columbus Laboratories, Columbus, OH, July 1983.

3. M. S. Hoseyni et al., "Estimate of Primary-System Temperatures in Severe Reactor Accidents," NP-3120, EPRI, Palo Alto, CA, May 1983.

4. D. R. Stull, Ind. Eng. Chem., 39, 517 (1947).

5. C. J. Smithells, "Metal Reference Book," Butterworths, Boston, 1962, p. 655.

6. M. W. Chase et al., "JANAF Thermochemical Tables - 1974 Supplement," Reprint No. 50 from J. Phys, and Chem. Ref. Data, 3, 311 (1974).

7. D. Cubicciotti and B. R. Sehgal, Nucl. Technol., 65, 266 (1984).

8. R. K. Hilliard et al., "Results and Code Predictions for ABCOVE Aerosol Code Validation - Test AB5," HEDL-TME 83-16, Hanford Engineering Development Laboratory, Richland, WA, November 1983.

9. H. Jordan et al., "QUICK Users' Manual," NUREG/CR-2105, BMI-2082, Battelle Columbus Laboratories, Columbus, OH, May 1981.

10. F. Gelbard and J. H. Sciseteld, J. Colloid Interface Sci., 78, 485 (1980).

11. H. Jordon, private communication.

12. J. C. Helton et al., "Uncertainty and Sensitivity Study of a Model for Multicomponents Aerosol Dynamics," SAND84-1307, Sandia National Laboratories, Albuquerque, NM, in press.

13. D. E. Bennett, SANDIA-ORIGEN User's Manual, NUREG/CR-0987, Sandia National Laboratories, Albuquerque, NM 87185, October 1979.

14. R. J. Lemire et al., "Assessment of Iodine Behavior in Reactor Containment Buildings from a Chemical Perspective," AECL-6812, Atomic Energy Canada Ltd., Pinawa, Manitoba, Canada, June 1981.

15. P. N. Clough and H. C. Starkie, "EEC Study Contract on the Aqueous Chemistry and Partitioning of Inorganic Iodine under LWR Severe Accident Conditions," SINDOC(84)220, OECD, Paris, France, October 1984.

16. G. A. Schmel, Aerosol Sci., 4, 125 (1973).

DISTRIBUTION

Email—Internal

Name	Org.	Sandia Email Address
Humphries, Larry	8852	llhumph@sandia.gov
Phillips, Jesse	8852	jphill@sandia.gov
Technical Library	9536	libref@sandia.gov

This page left blank

This page left blank

Sandia National Laboratories

Sandia National Laboratories is a multimission laboratory managed and operated by National Technology & Engineering Solutions of Sandia LLC, a wholly owned subsidiary of Honeywell International Inc. for the U.S. Department of Energy's National Nuclear Security Administration under contract DE-NA0003525.